Morphogenesis of the early post-implantation mouse embryo

Christos Kyprianou

Girton College

University of Cambridge

This dissertation is submitted for the degree of Doctor of Philosophy

September 2018

Declaration

This dissertation is the result of my own work and includes nothing which is the outcome of work done in collaboration except when specified in the text. It does not exceed the Degree Committee's prescribed word limit.

Christos Kyprianou

Acknowledgements

I would like to thank my supervisor Prof. Magdalena Zernicka-Goetz for all her guidance and support throughout the course of my PhD. I am very thankful for her trust in me and for providing me with both the knowledge and freedom to pursue the research I was most interested in.

I am also most grateful and thankful for my friend and lab partner Dr. Neophytos Christodoulou with whom I have collaborated throughout my PhD and has contributed to the work presented in this dissertation. Him and I share the same passion for morphogenesis and all processes that give shape to the developing embryo. His help, guidance and friendship have been instrumental in my PhD journey.

I would also like to thank my collaborators outside the lab that have contributed to my PhD project. Specifically, Dr. Naihe Jiang and Dr. Ran Wang for generating the spatial transcriptome and analysis as well as Dr. Isabelle Migeotte for providing the visceral endoderm-deleted RhoA mouse embryos.

I also wish to thank all past and current members of the MZG lab as well as Prof. David Glover for all the constructive discussions, support and technical guidance. I am also particularly thankful to Charlotte Handford and Gianluca Amadei of the MZG lab for taking the time to give me their own feedback on the dissertation manuscript.

Finally, I would like to thank and dedicate this thesis to my loving parents Antonis and Stevie Kyprianou for their unconditional love and support throughout my whole life. None of this would be possible without them.

Abstract

Candidate's name: Christos Kyprianou
Thesis title: Morphogenesis of the early post-implantation mouse embryo

The morphogenetic events that give rise to the early post-implantation mouse embryo (egg cylinder) have not been thoroughly studied and our knowledge is restricted to "snap-shot" descriptions of embryos recovered at different stages of implantation from the mother. A central feature of the egg cylinder is the pro-amniotic cavity, which spans the embryo and participates in formation of the extraembryonic membranes. The major aims of my PhD studies have been to reveal how this cavity is formed (Aim 1) and then how the egg cylinder grows (Aim 2).

In order to address how the pro-amniotic cavity forms (Aim 1), I first characterised in detail development of the architecture of the extra-embryonic ectoderm (ExE), which has to be remodelled to permit cavity formation. My findings indicate that the ExE comprises cells in direct contact with a basement membrane and cells that lie deeper in the tissue. The ExE originates in the polar trophectoderm, a monolayer covering the epiblast of the blastocyst, which expands and undergoes invagination to form a slit-like cavity. By carrying out analyses of fixed specimens and live imaging of cultured embryos, I have found that the epiblast and ExE cavity extend towards each other through the formation and resolution of multiple rosette structures. This leads to the fusion of the ExE and epiblast cavities to form the unified pro-amniotic cavity. I show that this process is dependent on signalling cues stemming from the underlying basement membrane that activate the β1-integrin signalling pathway to regulate cell polarity, ExE tissue architecture and rosette formation.

In addition to the basement membrane's role in β1-integrin signalling, it also has physical functions that I characterise in the second part of my study (Aim 2). High resolution imaging revealed that the basement membrane underlying the epiblast is highly perforated during the implantation stages. These perforations are initially evenly distributed and then accumulate asymmetrically at the future posterior part of the embryo, just prior to gastrulation. Finally, I demonstrate that remodelling of the basement membrane requires the expression of matrix metalloproteinases (MMPs) in the epiblast under the control of Nodal. The anterior visceral endoderm inhibits Nodal signalling and hence MMP inhibition in the anterior. I demonstrate that activity of the MMPs and perforations in the basement membrane are essential for embryo growth. The domain of posterior basement membrane perforations persists beyond gastrulation suggesting a potential role for these perforations in primitive streak formation and extension.

Together, my studies bring new important insights into the understanding of early mouse embryo morphogenesis.

TABLE OF CONTENTS

LIST OF FIGURES

LIST OF ABBREVIATIONS

Amot = angiomotin

Anxa2 = annexin A2

AP = anterior-posterrior

aPKC = atypical protein kinase C

APS = anterior primitive streak

AVE = anterior visceral endoderm

BM = basement membrane

BMP4 = bone morphongenetic protein 4

BSA = bovine serum albumin

c-Casp = cleaved caspase

CARM1 = coactivator associated arginine methyltransferase 1

Cdx2 = caudal type homeobox 2

COLIV = collagenase IV

Dkk1 = dickkopf 1

DVE = distal visceral endoderm

DVL2 = dishevelled 2

ECM = extracellular matrix

EDTA = ethylenediaminetetraacetic acid

Elf5 = E74-like factor 5

Em-Ab = embryonic-abembryonic

Em-ExEm = embryonic-extraembryonic

emVE = embryonic visceral endoderm

Eomes = eomesodermin

Epi = epiblast

EpiLC = Epiblast-like cells

ESC = embryonic stem cells

Esrrb = estrogen related receptor beta

ETS = embryonic and trophoblast stem cell structures

Ets2 = E26 avian leukemia oncogene 2, 3' domain

ExE = extraembryonic ectoderm

exVE = extraembryonic visceral endoderm

FC = feeder cells

FCS = fetal calf serum

FGF = fibroblast growth factor

Gata3 = GATA binding protein 3

GSK3 = glycogen synthase kinase 3

Hex = hematopoietically expressed homeobox

HRP = horseradish peroxidase

HSPG2 = heparan sulphate proteoglycan 2

ICM = inner cell mass

ITS-X = insulin-transferrin-selenium-ethanolamine

IVC = *in vitro* culture

KO = knockout

LIF = leukemia inhibitor factor

MDCK = Madine – Darby canine kidney

MEK = MAP kinase-ERK kinase

MMP = matrix metalloproteinase

NAC = N Acetyl-L-Cysteine

Nckap1 = NCK associated protein 1

OCT = optimal cutting temperature

Oct4 = organic cation/carnitine transporter 4

Otx2 = orthodenticle homeobox 2

PAC = proamniotic cavity

Pard6b = par-6 family cell polarity regulator beta

PBS = phosphate buffered saline

PCP = planar cell polarity

PD = proximal-distal

PE = primitive endoderm

Pen/Strep = penicillin/streptomycin

PIP = phosphotidyl inositol

pMLC = phosphor-myosin light chain

Podxl = podocalyxin

PTEN = phosphatase and tensin homolog

qPCR = quantitative polymerase chain reaction

Rab11a = RAB11A, member RAS oncogene family

Rac1 = Rac family small GTPase 1

RhoA = ras homolog family member A

RV = renal vesicle

Sh3pxd2a = SH3 and PX domains 2A

Snx18 = sorting nexin 18

Sox2 = SRY-box 2

Stx3 = syntaxin 3

T = brachyury

Tead4 = TEA domain transcription factor 4

Tfap2c = transcription factor AP-2 gamma

TSC = trophoblast stem cells

TTR = transthyretin

UB = ureteric bud

VE = visceral endoderm

Wnt = wingless-type MMTV integration site family

Yap = Yes associated protein

ZFP42 = zinc finger protein 42

ZO-1/Tjp1 = tight junction protein 1

1 INTRODUCTION

1.1 MOUSE EMBRYO DEVELOPMENT OUTLINE

Early mouse embryo development is divided into three major phases during which a fertilised zygote grows into a patterned collection of tissues, both embryonic and extraembryonic, that generate the three germ layers; the material for further development. Development subsequently progresses through the successive pre-, peri- and post-implantation phases (Bedzhov et al., 2014a) (**Figure 1.1**).

Pre-implantation development begins upon fertilisation of the egg and zygote formation. The zygote starts to divide to first reach the 8-cell stage. Up to this point the blastomeres appear loosely in contact with each other. However, during the transition from the 8 to 16-cell embryo the cells increase their area of contact and appear to flatten giving the embryo a smooth and spherical appearance; this is also considered the first morphogenetic event in embryo development as this is the first time the shape is actively altered and is also associated with the first polarisation event of the blastomeres (Kojima et al., 2014; Maitre, 2017; Sutherland and Calarco-Gillam, 1983); (Ziomek and Johnson, 1980) (**Figure 1.2**).

Following this, as the embryo progresses to the 32-cell stage, fluid starts to be pumped into the intercellular region of the compacted embryo giving rise to an emerging cavity known as the blastocoel. This is another critical feature of early embryo development as at this point the asymmetry of the cavity localisation determines the first identifiable axis; the embryonic-abembryonic axis (Em-Ab) (Garbutt et al., 1987). The embryo at this point has transformed from a spherical collection of blastomeres to a hollow spheroid made up of flattened cells and a clump of cells on the inside called the inner cell mass (ICM); the cells that will give rise to both the yolk sac and the embryo proper (Bedzhov et al., 2014a; Maitre, 2017) (**Figure 1.3**).

The polarised outside cells of the blastocyst are called the trophectoderm and will later give rise to the placenta. The trophectoderm cells away from the ICM are called the mural trophectoderm, important in embryo implantation and its integration to the uterine environment, while the trophectoderm cells directly abutting the ICM are termed the polar trophectoderm and give rise to the post-implantation extraembryonic ectoderm (ExE) which then goes on to become the chorion (Copp, 1978; Gardner, 2000; Pereira et al., 2011) (**Figure 1.1**).

The ICM segregates into two populations of cells; the primitive endoderm (PE) and the epiblast (Epi). These two populations sort out so that the PE lines the Epi cells (thus separating the blastocoel from the Epi) and start to expand sideways, away from the ICM, to also line the mural trophectoderm, forming the parietal endoderm; this will become the yolk sac. The PE, will give rise to the post-implantation visceral endoderm (VE) whereas the Epi will eventually give rise to the embryo proper (Bedzhov et al., 2014a; Bedzhov and Zernicka-Goetz, 2014).

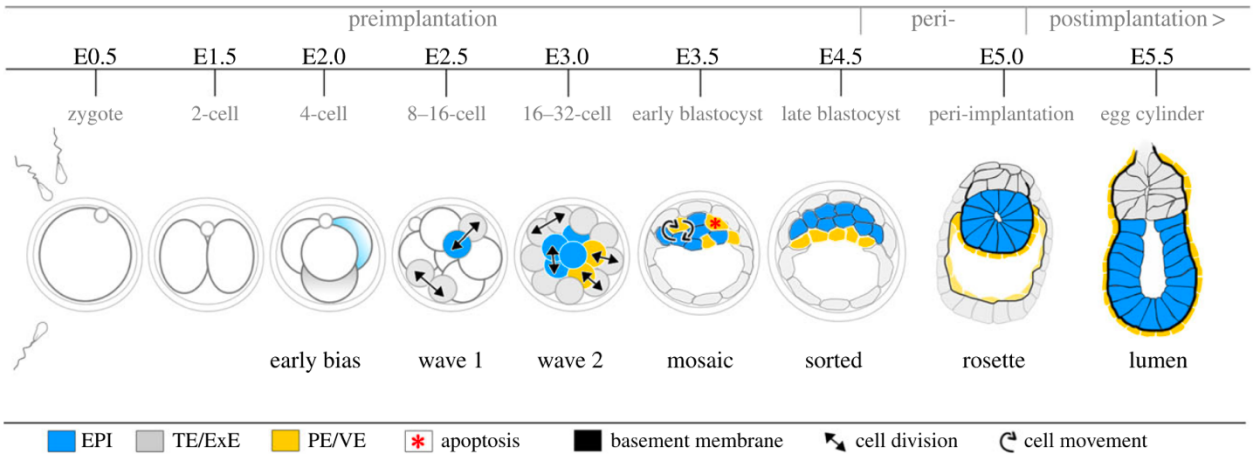

FIGURE 1.1: THE THREE PHASES OF EARLY POST-IMPLANTATION DEVELOPMENT.

Transition of the pre-implantation blastocyst into an egg cylinder through peri-implantation development during which the Epi lumen is established. EPI = Epiblast; TE = trophectoderm; ExE = extraembryonic ectoderm; PE/VE = primitive endoderm / visceral endoderm (Bedzhov et al., 2014a).

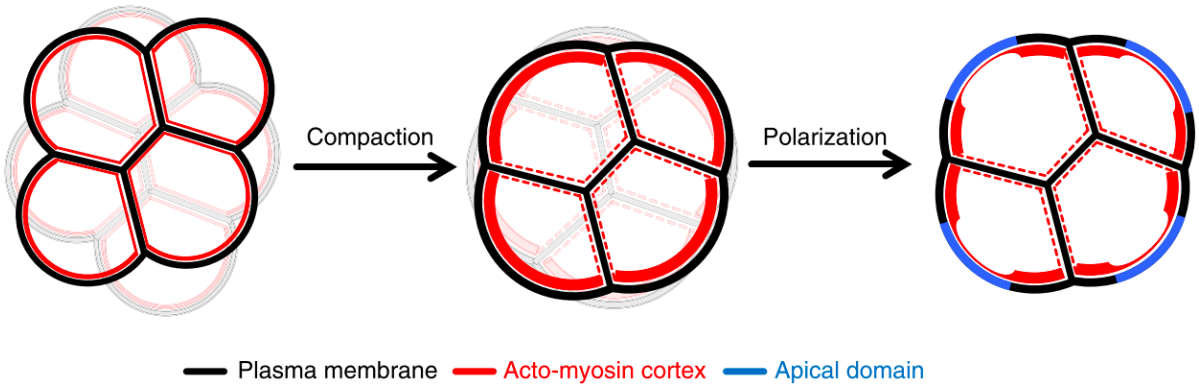

FIGURE 1.2: MOUSE EMBRYO COMPACTION

Representation of the 8-cell stage embryo compacting by increasing the cell contact surface area between adjacent blastomeres. This results in an increased angle of contact at the cell interphases and a smooth embryo appearance. Compaction is followed by polarisation and the emergence of an apical domain on the cell contact-free region of each blastomere. Thickness of red line corresponds to enrichment of acto-myosin cortex; dashed line shows inhibited acto-myosin cortex in the cell-contact areas (Maitre, 2017).

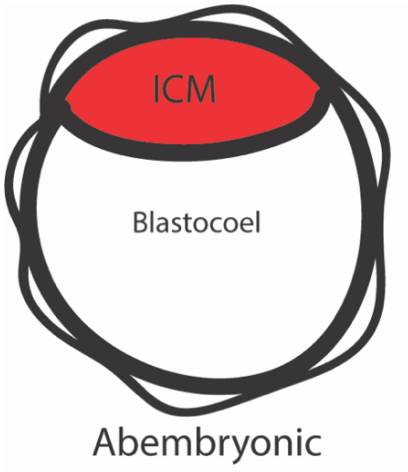

FIGURE 1.3: BLASTOCYST APPEARANCE AND THE FIRST AXIS

A E3.5 embryo is a hollow spheroid of trophectoderm cells with a clump of cells inside (inner cell mass; ICM) which also dictates the site of embryonic pole. The cavity that fills the blastocyst is called the blastocoel and dictates the side of embryonic pole.

Once these lineages are in place the embryo enters the peri-implantation stage of development. Here, the mural trophectoderm becomes invasive to allow for embryo implantation into the endometrium and decidualisation initiates to form a decidua around the implanting embryo; a tissue that cushions the embryo at the site of implantation (Bergstrom, 1971; McRae and Church, 1990) (**Figure 1.4**). The parietal endoderm and the invading mural trophectoderm are now separated by a specialised basement membrane (BM) called the Reichert's membrane (Inoue et al., 1983; Smith and Strickland, 1981) .

The polar trophectoderm during this period completely transforms from a flattened epithelium to a columnar architecture expanding along the Em-Ab axis. The Epi at this stage undergoes a very dramatic change in its organisation. Prior to implantation, the Epi consists of a collection of apolar cells with a disorganised and round appearance, however, during implantation the Epi cells become columnar and form a rosette structure that undergoes hollowing at its centre (Bedzhov and Zernicka-Goetz, 2014; Shahbazi et al., 2017) (**Figure 1.5**). The cavity that forms between the Epi cells is called Epi cavity and constitutes the first morphogenetic

feature associated with post-implantation development (Rivera-Perez and Hadjantonakis, 2014). The PE does not undergo major changes at this stage but is already transitioning to VE based on the changes of GATA6 expression (Cai et al., 2008).

Upon entering the post-implantation stage of development, the embryo has an expanded polar trophectoderm and a hollowed Epi and from here onwards the embryo assumes an egg cylinder structure. At this point the embryo has established an axis aligned to the earlier Em-Ab axis called the proximal-distal axis (PD) with the proximal pole on the expanded polar trophectoderm site and the distal pole at the tip of the Epi (Frankenberg et al., 2007; Rodriguez et al., 2005). As the ExE emerges from the expanded polar trophectoderm a slit-like cavity appears at the proximal-most tip of the embryo and the VE extends from only covering the Epi to also cover the ExE (Bedzhov and Zernicka-Goetz, 2014). The VE appearance is visibly different between the part covering the Epi and the part covering the ExE (Epi VE cells are squamous whereas the ExE VE cells are cuboidal) (**Figure 1.6A**) and shortly after this, the VE cells at the distal-most part become visibly more columnar (Rivera-Perez et al., 2003; Sozen et al., 2018; Trichas et al., 2012). This part of the VE is called the distal VE (DVE) and the morphogenetic transformation associated with the columnar appearance of these cells is termed the VE thickening (Rivera-Perez et al., 2003) (**Figure 1.6B**).

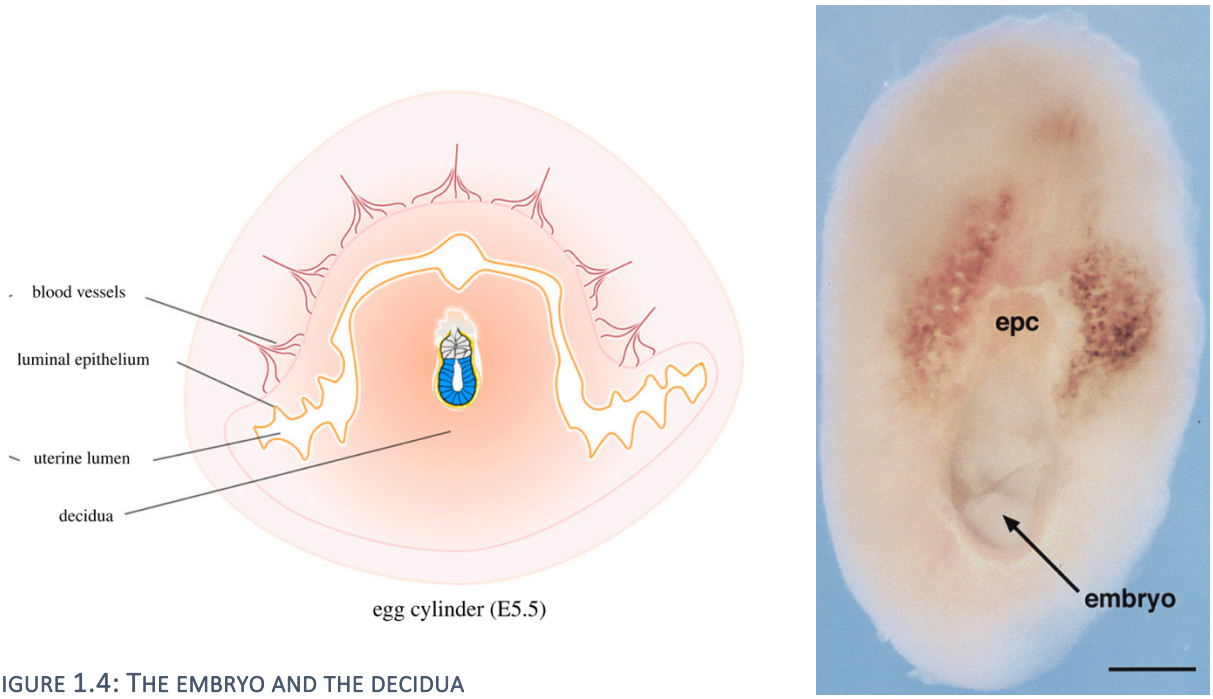

FIGURE 1.4: THE EMBRYO AND THE DECIDUA

After implantation of the embryo, the decidua forms around the embryo from the anti-mesometrial side of the uterus and cushions it. A schematic of relative position of embryo, decidua and uterus. A sectioned decidua with a E7.5 embryo in it (Bedzhov et al., 2014a; Passey et al., 1999).

The DVE then starts to migrate to one side of the Epi VE which goes on to become the future anterior of the embryo. The migrating DVE becomes the anterior VE (AVE) as it is the population of cells that establishes the anterior-posterior axis (AP), which is perpendicular to the PD axis (Thomas et al., 1998). The AVE is a signalling centre for anteriorising signals and restricts posteriorising signals to the opposite side (Tam and Loebel, 2007) (Figure 1.7).

At the same time of AP establishment, the two cavities in the Epi and ExE are no longer discernible and, in their place, a single cavity appears that spans both the Epi and ExE giving the egg cylinder its hollowed appearance. This cavity is called the proamniotic cavity and after gastrulation it becomes divided up by the two extraembryonic membranes, the amnion and the chorion to give rise to the amniotic, chorionic and ectoplacental cavity (Pereira et al., 2011).

Finally, in the last part of early post-implantation development, gastrulation ensues. Here, there is mesendodermal specification in the cells of the proximo-posterior site of the Epi which is followed by their loss of polarity (aPKC), loss of adherens junctions (E-cadherin) and ingression to the space between the Epi and the VE upon breakage of the separating BM that lines the basal site of Epi and VE (Fujiwara et al., 2007; Williams et al., 2012). These cells will form the three germ layers, namely the ectoderm, mesoderm and endoderm that give rise to all the tissues of the adult mouse (Tam and Behringer, 1997) (Figure 1.8). Additionally, these cells also give rise to the extraembryonic mesoderm involved in the formation of the allantois which goes on to establish a connection with the chorion and the maternal tissues for nutrient exchange (Downs and Gardner, 1995; Jin et al., 2016; Lawson et al., 1999)

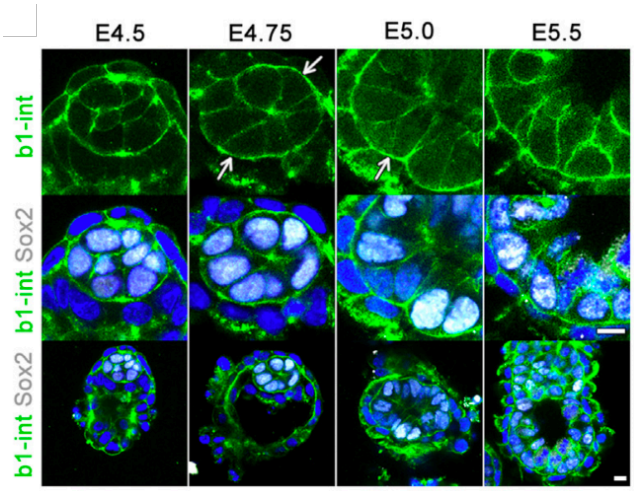

FIGURE 1.5: EPITHELIALISATION OF EPI CELLS

Epi from pre- to post-implantation stages. Initially cells are round and apolar. They then become polar and acquire a columnar shape which culminates in the formation of a rosette structure. Membrane separation at the centre of the rosette leads to cavity formation. The embryo here is stained with b1-integrin showing enriched localisation on the basal side (white arrows) relaying integrin signalling from the underlying basement membrane; Sox2 = epiblast marker (Bedzhov and Zernicka-Goetz, 2014).

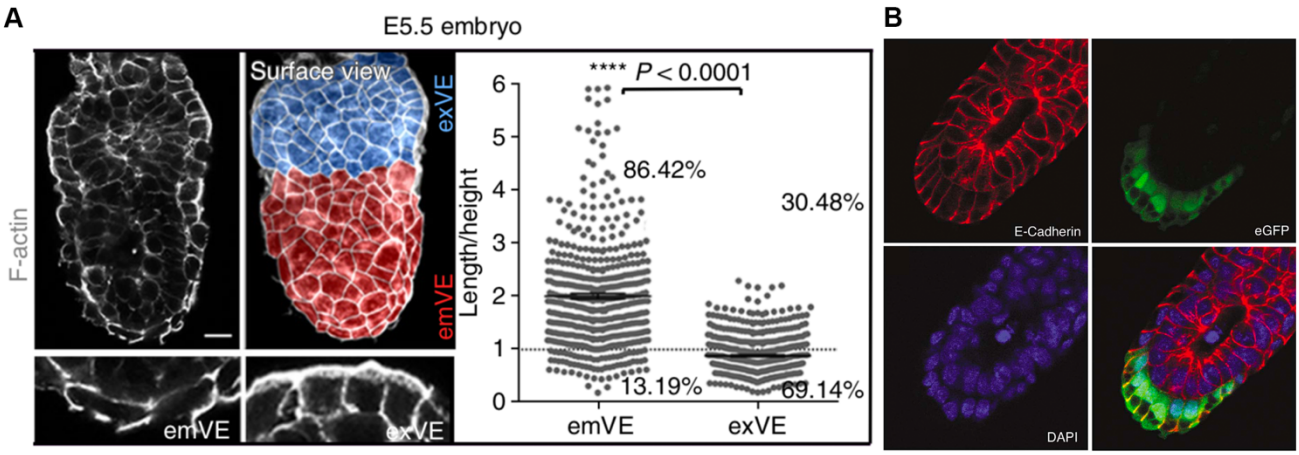

FIGURE 1.6: MORPHOLOGICAL CHARACTERISTICS OF THE VISCERAL ENDODERM

(A) The embryonic VE (emVE) and extraembryonic VE (exVE) are markedly different in their shape with the emVE being more columnar when compared to exVE during early post-implantation development; % = percentage of cells with Length/height value that are either <1 or >1; values <1 indicate predominantly cuboidal shape whereas >1 predominantly squamous shape (Sozen et al., 2018). (B) Established distal visceral endoderm appears more columnar in shape (visceral endoderm thickening; VET) when compared to the rest of the embryonic VE. eGFP is *Tg(Hex-eGFP)ARbe* transgene marking the distal VE (Rivera-Perez et al., 2003).

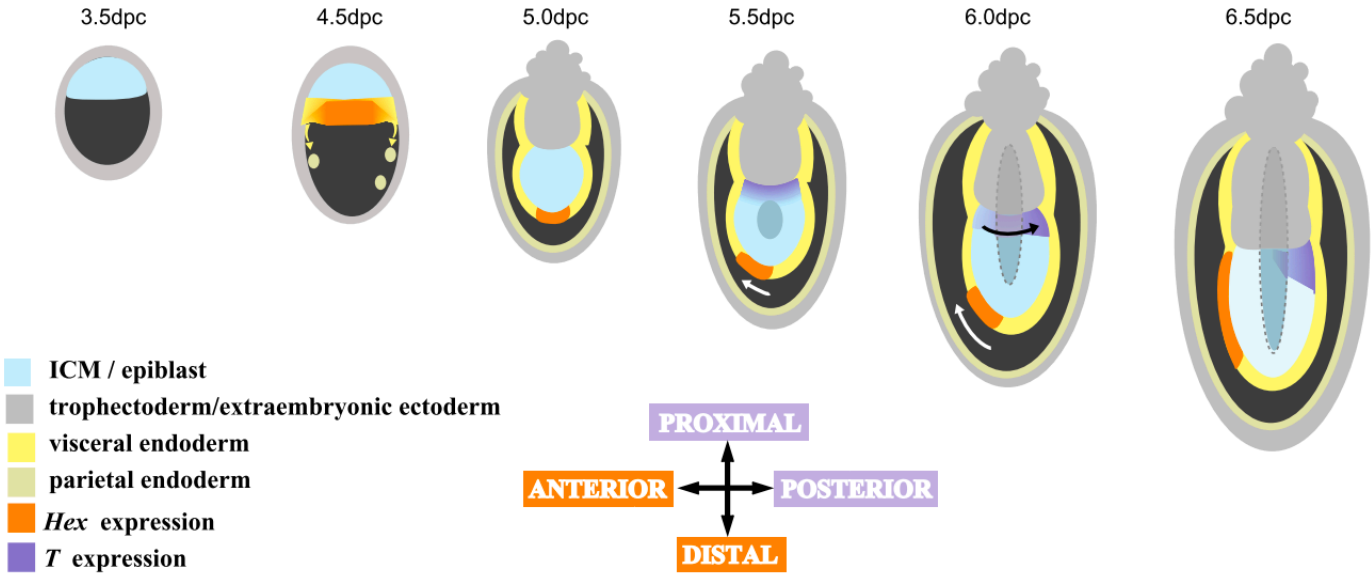

FIGURE 1.7: DVE ESTABLISHMENT AND AVE MIGRATION

Schematic of the establishment of the Hex (a homeobox gene)-expressing DVE at the distal tip of the embryo and its progressive migration to one side restricting the mesendoderm-specifying factor T (Brachyury) expression to the opposite side where gastrulation will take place (Thomas et al., 1998).

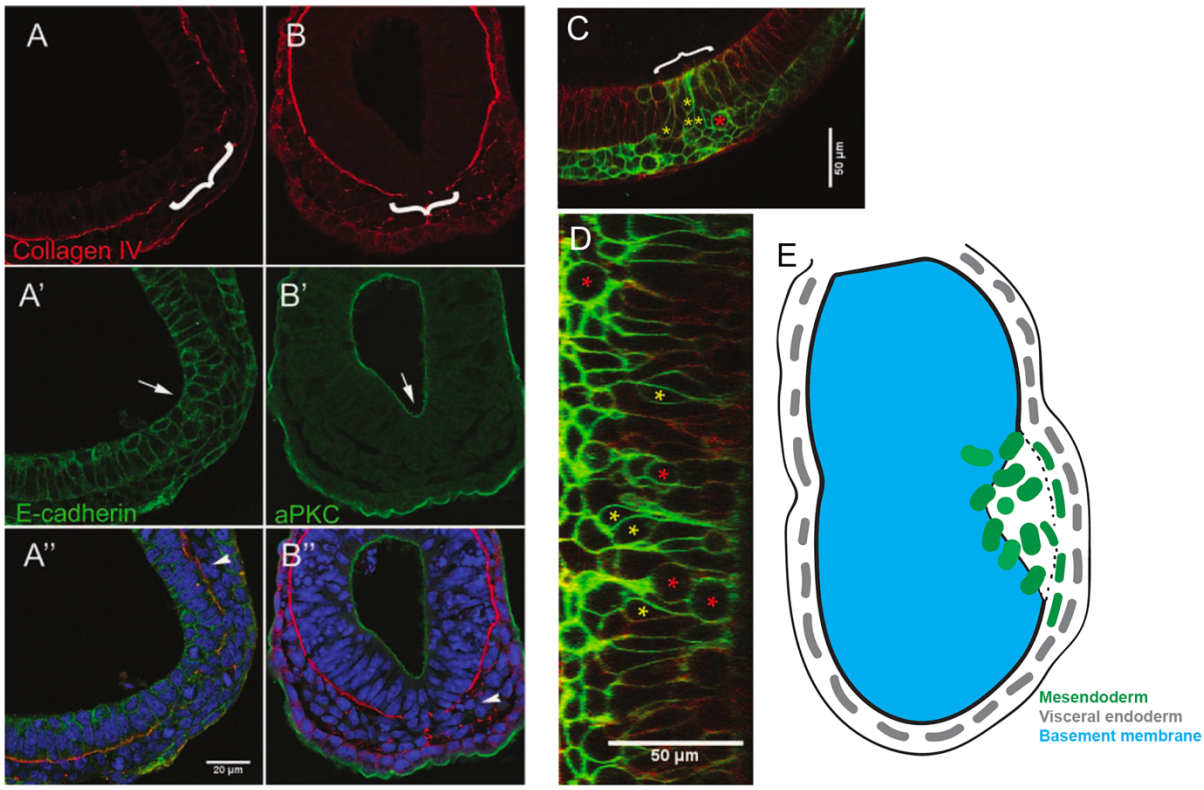

FIGURE 1.8: GASTRULATION

(A-B) Collagen staining of a transversely sectioned E6.75 embryo at the time of gastrulation; white bracket = primitive streak. (A'-B') Staining for E-cadherin and aPKC showing increased E-cadherin in the and persistence of aPKC in the epiblast at the site of primitive streak (white arrow). (A''-B'') Merge images with white arrowheads showing absence of E-cadherin and aPKC in the mesodermal layer. (C-D) Ingression of mesendodermal cells (yellow astersks; T:Cre; mTmG) at the site of primitive streak and rounded cells undergoing division (red asterisks). (E) Schematic of gastrulating embryo showing basement membrane breakdown and ingression of mesendodermal cells (Williams et al., 2012).

1.2 MORPHOGENETIC EVENTS IN EARLY MOUSE EMBRYO DEVELOPMENT

1.2.1 PRE-IMPLANTATION EMBRYO MORPHOGENESIS

1.2.1.1 Compaction

The total embryo morphogenesis from single cell to the multi-layered and patterned structure at the time of gastrulation comes about by incremental complexity of morphogenetic events that build on top of each other. This begins at the 8-cell stage embryo where the process of compaction begins. Compaction is the increase of cell-cell surface area of contact between blastomeres which leads to the smooth outside appearance of the embryo. Aside from its effect on the appearance of the embryo, acquiring the spherical shape provides the optimal condition for internalisation of cells and thus ICM allocation (Maitre, 2017).

Achieving compaction involves the spreading of cell contacts and forces generated by the cytoskeleton (Maitre et al., 2012; Stirbat et al., 2013). During compaction, actomyosin is enriched on the contact-free portion of the 8-cell stage embryo whereas in the cell-contact areas actomyosin is inhibited by the presence of E-cadherin. Actomyosin contractility between blastomeres and filopodia projections from adjacent blastomeres promote pulling together of the blastomeres and transformation of the 8-cell stage embryo to a smooth spherical structure (Fierro-Gonzalez et al., 2013; Maitre et al., 2015; Stephenson et al., 2010; Turlier and Maitre, 2015; Zhu et al., 2017).

1.2.1.2 Cell internalisation

Concomitant with compaction, the 8-cell stage embryo starts to undergo another event of morphogenesis during its transition to a 16-cell embryo as well as during 16-32 cell transition. These two transitions have been associated with cell specification and allocation of cells to the trophectoderm or ICM lineages (Fleming, 1987; Morris et al., 2010; Pedersen et al., 1986). These transitions are not only associated with a doubling of blastomeres but also internalisation events. In particular, at the 8-cell stage, all 8 cells are identical in terms of their positional profile but upon initiation of the transition with the first cell division, some of the new cells produced will be internalised to go on and form the ICM at the blastocyst stage. This internalisation appears to be attributed to the asymmetry or symmetry of divisions. The general rule followed in cell division symmetry is that a division parallel to apico-basal axis of cell is a symmetric one, giving rise to two cells of equal potential (as both will inherit determinants that are differentially distributed along the apico-basal axis), whereas division perpendicular to the apicobasal axis will produce two cells with one inheriting determinants associated with the apical pole of the cell and the other with the basal pole having thus asymmetrically divided (Knoblich, 2010; Neumuller and Knoblich, 2009). An asymmetric division in the 8-cell stage embryo in this sense will produce two cells, one that will remain associated with the outside of the embryo and one that ends on the inside due to the plain of division (Skamagki et al., 2013). Adding to this model of cell allocation and

internalisation, it was shown that internalisation can be also attributed to the differential tension produced by the apical domain(Korotkevich et al., 2017; Maitre, 2017). The apical domain as mentioned above is less contractile by excluding actomyosin, thus a division along a plane that leads to asymmetric inheritance of the apical domain will lead to internalisation of the cell devoid of the apical domain because of its higher tension (Maitre et al., 2016; Sun et al., 2014). This is a more dynamic mode of internalisation that also explains observations of cells seen to actively move into the embryo interior after being produced on the outside.

1.2.1.3 Blastocyst formation

After these two rounds of cell divisions and internalisation, the compact spherical embryo starts to cavitate. This cavity is known as the blastocoel and this is the feature that gives the blastocyst its characteristic appearance (Garbutt et al., 1987). Forming an expanding cavity requires pumping of fluids by cells in the intercellular space. This requires that the structure being pumped with fluid to form the cavity maintains strong adhesion between its outside cells to avoid leaking or bursting (Casares et al., 2015; Niimura, 2003). Indeed, with initiation of cavity formation in the early blastocyst, the trophectoderm undergoes epithelialisation by enriching its tight junctions. Tight junctions serve a role to seal the blastocyst and maintain the integrity of the trophectoderm against the hydrostatic stresses generated by the pumping of the fluid into the blastocoel. There has been evidence recently that hydrostatic pressure may be triggering some mechanosensing process that leads to enrichment of tight junctions to prevent bursting (Chan, 2018).

1.2.2 *Peri- and post-implantation embryo morphogenesis*

1.2.2.1 Epiblast cavity

During implantation the embryo undergoes a major morphogenetic transformation which involves the hollowing of the Epi, the expansion of polar trophectoderm and the emergence of the ExE (Smith, 1985).

Initially, it was hypothesised that the cavity in the Epi emerged by cell death. According to this, as the Epi grows and increases in cell number, due to the limited space, cells accumulating in the centre of the Epi would die due to their failure to make contact with the underlying BM. The BM is known to be able to provide survival signals to cells, thus in the absence of such signals cell death is triggered leaving the centre of the Epi cavitated and filled with apoptotic cells (Coucouvanis and Martin, 1995, 1999) (**Figure 1.9A**). This was the predominant model for Epi cavitation despite the fact that the only supporting evidence for it came from experiments on embryoid bodies. While embryoid bodies can be a useful tool for understanding signalling mechanisms, in this case it was not the appropriate model as the number of cells making up an embryoid body compared to that of the implanting embryo are vastly different. The embryoid bodies are formed by aggregating many cells together to produce a structure with hundreds of cells forming its bulk and an outer layer that is separated from the rest by a BM. The highly crowded cells in the bulk of the embryoid body undergo apoptosis giving it a cavitated appearance (Li et al., 2003). However, this mechanism of cavitation is dependent on cell crowding and cell exclusion from BM

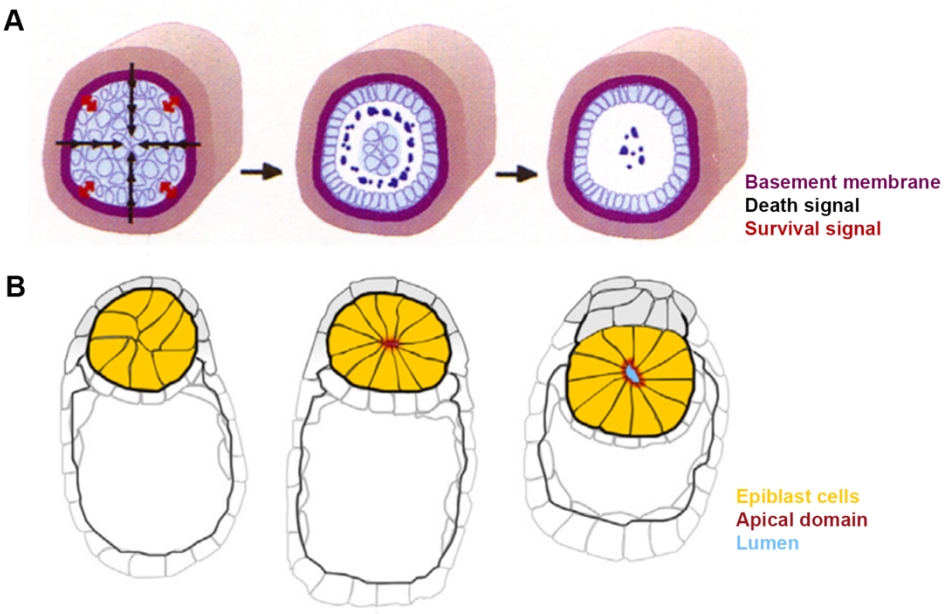

FIGURE 1.9: CAVITATION VERSUS HOLLOWING IN THE EPI

(A) The cavitation model proposes that the Epi cavity forms through apoptosis as a result of a death signal produced by the outside cells (VE) and counteracted only by the cells receiving a survival signal in direct contact with the basement membrane (Coucouvanis and Martin, 1995). (B) The hollowing model of Epi cavity formation proposes that the Epi cells apico-basally polarise forming a rosette structure which opens up by membrane separation through podocalyxin secretion (Bedzhov and Zernicka-Goetz, 2014; Ziomek and Johnson, 1980)

contact which is not the case in the implanting embryo (Martin-Belmonte et al., 2008).

This was finally demonstrated in 2014 by Bedzhov and Zernicka-Goetz who using an *in vitro* culture system that enables live imaging of embryos at the implantation stage demonstrated that the Epi cavity forms through a mechanism of hollowing. The updated model of Epi cavity formation stated that while the pre-implantation Epi cells are apolar and disorganised, shortly after and during the implanting stage, they become columnar and start to organise in a rosette structure. This structure then hollows in the middle where all the cells meet by means of membrane separation through polarised secretion of podocalyxin, a sialomucin that is highly negatively charged causing membrane repulsion (Bedzhov and Zernicka-Goetz, 2014; Meder et al., 2005; Orlando et al., 2001) (**Figure 1.9B**). This method of producing a cavity depends on establishing a strong apico-basal polarity firstly so as to be able to form the rosette structures and second to direct apical secretion of podocalyxin. The polarity cues stem from the forming BM that at this stage surrounds the Epi, activating integrin-β1 signalling (Bedzhov and Zernicka-Goetz, 2014). The ability of cells to organise into 3D structures when they are suspended in a 3D scaffold with polarisation signals has been demonstrated before with MDCK cells as well as with mouse embryonic stem cells (ESCs) which are more relevant to early mouse development as they represent the pluripotent Epi cells (O'Brien et al., 2001; Wang et al., 1990). Additionally, studies in MDCK cysts showed that the decision on the method of cavitation i.e. through apoptosis or rosette formation and hollowing, is dependent on the number of cells making up the cysts, providing further support to the model of Epi cavity formation through rosette resolution (Martin-Belmonte et al., 2008).

1.2.2.2 Extraembryonic ectoderm

Shortly after the formation of the Epi cavity the ExE emerges as an expanded polar trophectoderm along the PD axis (Smith, 1985). The polar trophectoderm is initially a flattened epithelium abutting the Epi, but during transformation of the blastocyst to the egg cylinder the cells become more cuboidal and appear to stack (Gardner, 1978). Despite this massive change in tissue morphology there are no studies examining the morphogenetic events of this transition. However, the specification of the ExE and the key players involved in ExE character acquisition is better understood. Namely, Elf5 has been identified as one of the critical factors in the absence of which, ExE establishment fails. Although these studies mainly focus on the markers that characterise the ExE rather than the cellular morphology of the polar trophectoderm, it seems that in the case of Elf5-/- there is no discernible expansion of the tissue at all but is unclear whether there is any change in the polar trophectoderm cellular morphology (Donnison et al., 2005; Donnison et al., 2015).

FGF signalling is the key player in formation of the ExE and maintenance of the trophoblast stem cell character. As mentioned above, the mechanism controlling changes in morphology and differentiation of cells towards ExE character is not yet determined. FGF ligands from the Epi bind to FGF receptors in the abutting polar trophectoderm which drives the trophoblast stem cell transcriptional network (Latos et al., 2015; Tanaka et

al., 1998). FGF, however, is also central in driving cell proliferation and epithelial-to-mesenchymal transition. These are two processes that may explain the morphogenetic transition from a flat epithelium to the stacked/expanded morphology of the nascent ExE. It has been shown before in the case of mouse lens epithelia that different dosages of bFGF control cell morphology, thus it is possible that the FGF signalling *per se* is driving this morphogenetic event in addition to its cell-specifying role (Wang et al., 2017a). Following the formation of the ExE, a slit-like cavity appears on the proximal-most part of the embryo in the ExE, the mechanism of morphogenesis of which has not been investigated so far. This is a feature that appears to be involved in the next morphogenetic step, the formation of the proamniotic cavity; the cavity that spans the egg cylinder in both embryonic and extraembryonic compartments.

1.2.2.3 Proamniotic cavity

A central feature of the egg cylinder is a central cavity that spans it and for the purposes of differentiating this from the Epi cavity established through rosette formation, this is termed the proamniotic cavity (**Figure 1.10**). While it is a well-known feature, the stages of its development and the mechanism of its formation are unknown, and this is evident from the variety of ways in which it is represented in the literature (which also holds true for the architecture of the ExE). In some cases, it has been presented as an extension of the Epi cavity at stages prior to gastrulation and in other cases shown to emerge much earlier. So, the timing of its emergence is not well-defined in the field. Additionally, the potential role of the ExE cavity in its emergence is almost completely ignored with only very few exceptions in the literature (Snell, 1966). Thus despite its significance in the formation of the extraembryonic membranes (Pereira et al., 2011) there is little understanding at this point how it forms.

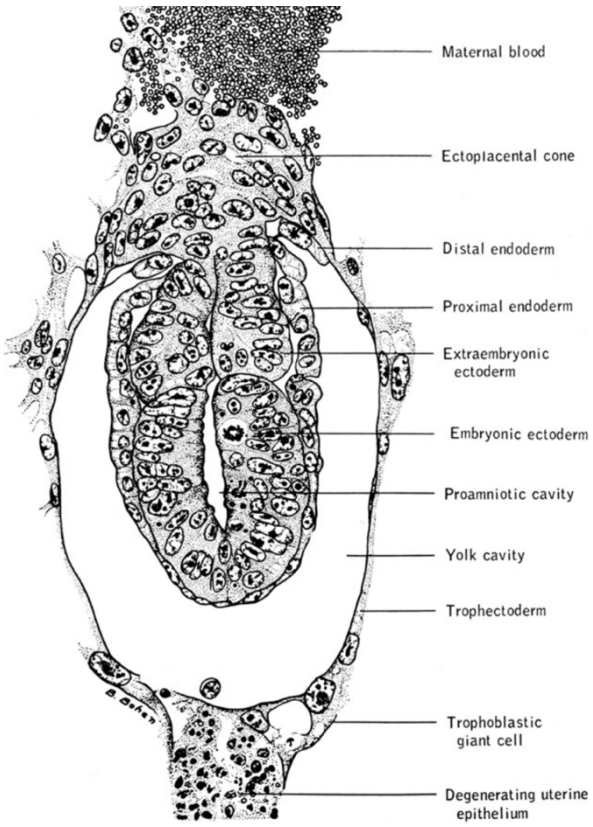

FIGURE 1.10: PROAMNIOTIC CAVITY IN THE EARLY POST-IMPLANTATION MOUSE EMBRYO

This is the first historical record of the proamniotic cavity spanning the egg cylinder. Drawn from histological section (Snell, 1966).

Following the formation of a hollowed egg cylinder, embryonic development enters the pre-gastrula stages characterised by an increase in size of the proamniotic cavity but with no other major morphogenetic changes (Snow, 1976). Patterning during these stages is down to

the molecular level, cell specification and preparation for gastrulation (Tam and Loebel, 2007).

1.2.2.4 Primitive streak Formation

The gastrula stage on the other hand, is a period of dramatic morphogenesis as the embryo becomes a trilaminar structure, forms a structure called the node which is important in patterning and the extraembryonic membranes are generated. The process of gastrulation begins with breaching of the BM at the proximo-posterior site of the Epi, forming the primitive streak (Tam et al., 1993; Williams et al., 2012). Dissolution of the extracellular matrix (ECM) facilitates epithelial-to-mesenchymal transition during which the epithelial Epi cells lose their apico-basal polarity and become mesenchymal. Both the removal of the physical barrier separating the underlying VE from the Epi as well as the acquisition of mesenchymal character allows the Epi cells on that site of the embryo to ingress in their epithelium and escape into the intercellular space underneath (Nakaya and Sheng, 2008) (**Figures 1.8, 1.11**). As they do this, they become migratory in a Rac1-dependent way and move away from the site of ingression and colonise the intended niches (Migeotte et al., 2011). The site of BM breaking and ingression of mesendodermal cells (Brachyury (T) – positive) is called the primitive streak and is the primary morphogenetic feature of early gastrulation.

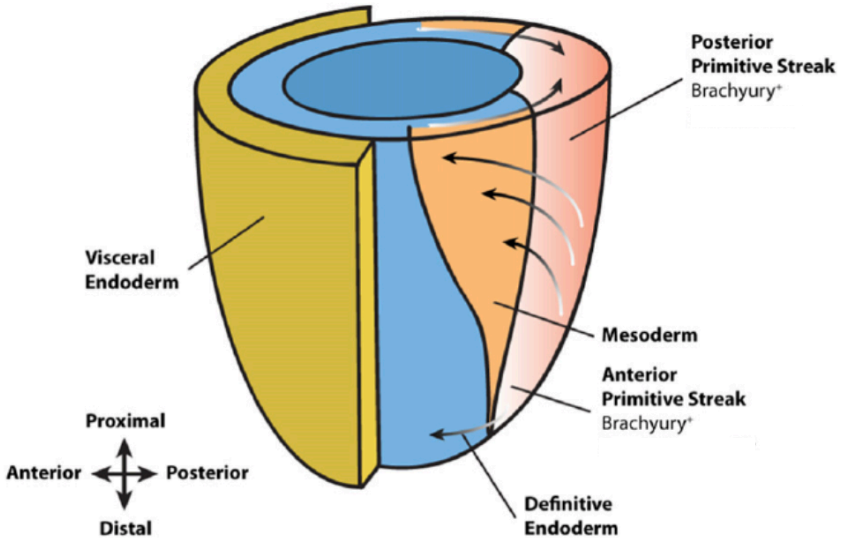

FIGURE 1.11: PRIMITIVE STREAK

A schematic showing the primitive streak forming at the posterior side characterised by expression of Brachyury (T), a mesendoderm factor. Arrows show the movement of cells from the Epi through the primitive streak followed by both lateral and anterior movement (Duelen and Sampaolesi, 2017).

1.2.2.5 Extraembryonic membranes

Cells ingressing first, which are closer to the posterior extraembryonic compartment, will migrate to proximo-posterior ExE to establish the extraembryonic mesoderm, important in allantois formation. The origin of the cells contributing to the allantois was challenged by Downs and colleagues who suggested the presence of an extraembryonic primitive streak through which cells migrate to form an allantoic core domain (Downs et al., 2009). This is one of the extraembryonic membranes that establish a connection between the embryo and the maternal tissues by fusing to the chorion; the chorioallantoic fusion (Downs and Gardner, 1995).

The allantois grows into the cavity known as the chorionic cavity flanked by the amnion and the chorion which is in turn dependent upon prior formation of the proamniotic cavity. The steps to forming the chorionic cavity, along with the flanking amniotic and ectoplacental cavities, have been described by Pereira and colleagues (2011). These cavities form by a different mechanism than those described in the literature as these depict the division of a pre-existing cavity; perhaps the only other example of this is the division of the primary yolk sac in human embryo development to give rise to the definitive yolk sac, although in this case the topology is different. The steps of cavity formation take place via a detachment of the posterior ExE and its subsequent movement to the anterior where it fuses with the epithelium (**Figure 1.12A-E**). By the end of this process three cavities emerge along the distal to proximal axis, the amniotic, chorionic and ectoplacental cavity. The cavity forming *de novo* by the detachment of the posterior ExE gives rise to the chorionic cavity whereas the other two cavities, amniotic and ectoplacental, share the same progenitor cavity (**Figure 1.12F-H**). The mechanics of this event i.e. from the detachment of the posterior ExE to the fusion of the membranes remain an open question. Although this process does coincide with extraembryonic mesoderm colonisation the link between them is not known. The significance of the emergence of these membranes has also been suggested to be

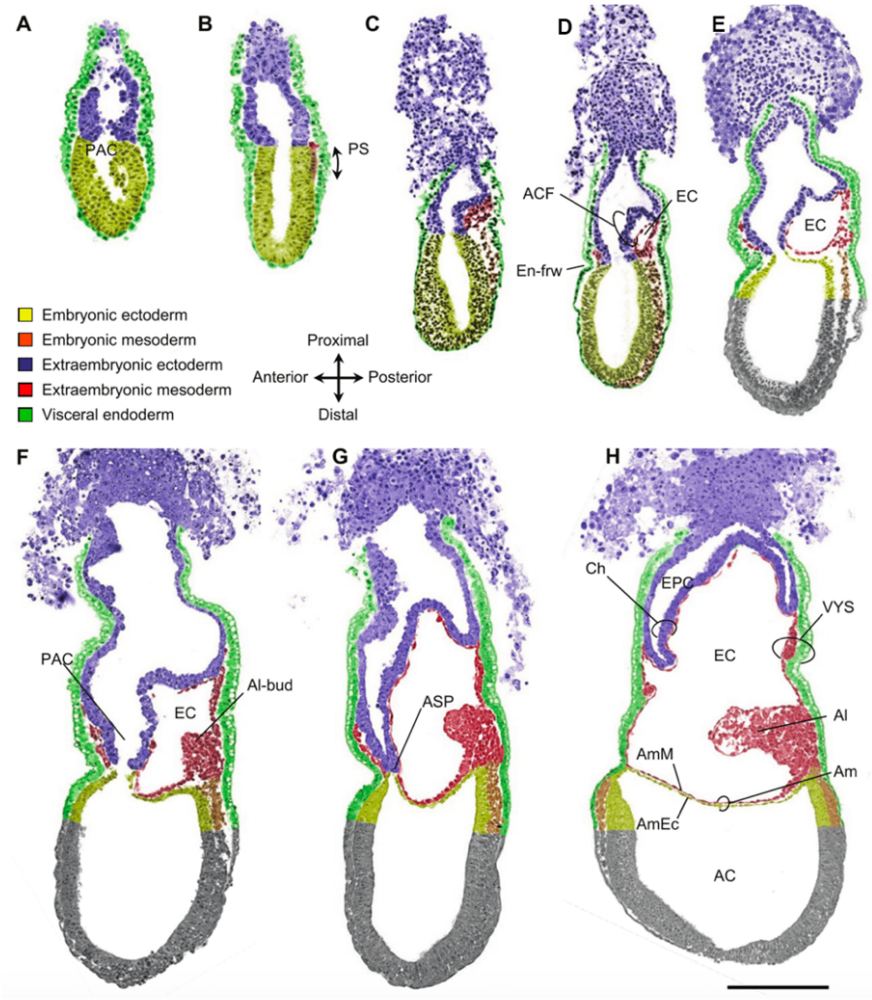

FIGURE 1.12: FORMATION OF THE EXTRAEMBRYONIC MEMBRANES

(A) E5.75 embryo with a proamniotic cavity (PAC). (B) Gastrulating embryo. (C-E) Detachment of posterior extraembryonic ectoderm and accumulation of extraembryonic mesoderm. (F-H) Fusion of the detached extraembryonic ectoderm to the anterior site creates two membranes, the amnion (Am) and the chorion (Ch). The allantois is formed during the same stages. PS = primitive streak, ACF = amniochorionic fold, En-frw = endodermal furrow, EC = exocoelomic cavity, Al-bud = allantoic bud, ASP = anterior separation point, AmM = amniotic mesoderm, AmEc = amniotic ectoderm, AC = amniotic cavity, VYS = visceral yolk sac, EPC = ectoplacental cavity. Scale bar = 200um (Pereira et al., 2011).

involved in promoting differentiation of the trophoblast stem cells by occluding the ectoplacental cavity from the FGF-producing Epi (Uy et al., 2002).

1.2.2.6 Node

Another structure that emerges at the time of gastrulation is the node. This is a specialised ciliated structure at the anterior primitive streak that is responsible for establishing the left-right axis of the embryo by creating an asymmetric Nodal flow perpendicular to the AP axis. The node forms at the anterior primitive streak and takes the form of a pit made up of a dorsal and a ventral compartment. The dorsal node is continuous to the Epi layer whereas the ventral layer is continuous to the underlying endoderm (Figure 1.13A). Both sides of the node are made up of columnar cells sharing a common basal side; essentially the same configuration of the Epi and VE in early stages of development (Lee and Anderson, 2008).

Studies following the stages of development of the node report a three-step process of the organ's assembly. Firstly, cells between the Epi and the endoderm at the site immediately anterior to the primitive streak (streak-derived cells) become the node precursor cells. The cell morphology of these cells is drastically different from that of either of the flanking tissues; the Epi and endoderm. More specifically, these cells acquire a reduced apical and ciliated surface. Following the node precursor cells' acquisition of said morphology, node morphogenesis proceeds to the second step. Here, the endoderm that covers the ventral node starts to exclude itself from the developing node domain; whether this is by means of cell movement or cell death remains unknown. Regardless, the removal of the endoderm from the anterior primitive streak exposes the ventral ciliated node to the yolk sac environment only covered by the Reichert's membrane. Following this, the third and final step begins. At this stage of node development, the node integrates itself into the endoderm (while maintaining its columnar morphology) making the endoderm and ventral node one continuous epithelium. By the end of its development, the node appears as a pit on the endodermal site surrounded by large squamous cells called the crown cells (Figure 1.13B). The node pit is covered by the Reichert's membrane creating a sealed cavity that contains the nodal flow (Lee and Anderson, 2008).

The node's development and anatomy provide a great example of how the morphogenetic strategy is decided based on the location, shape and cell morphology. In the case of the node, in order for the monocilium produced by the ventral node cells to create a flow and generate the asymmetry, a contained fluid-filled space is required. Morphogenesis here solves this problem by merging the middle layer of the trilaminar embryo with the bottom layer creating the indentation that the nodal flow requires for its generation. The emergence of this pit may also be dependent upon the cell morphology of the ventral node cells and particularly their significantly reduced apical surface (compared to the contiguous endoderm) (cyan endoderm vs purple ventral node cells in Figure 1.13B). The integration of the ventral node to the endoderm is an instrumental event in its morphogenesis as it provides the indented appearance of the node. This appears to involve fusion of the

two apposed tissues, but the mechanism is currently unknown. This is very reminiscent of the fusion of the detached posterior ExE to the anterior epithelium creating two separate membranes; the amnion and the chorion. Evidently, the fusion of membranes is not well understood at this point despite its significance in embryo development.

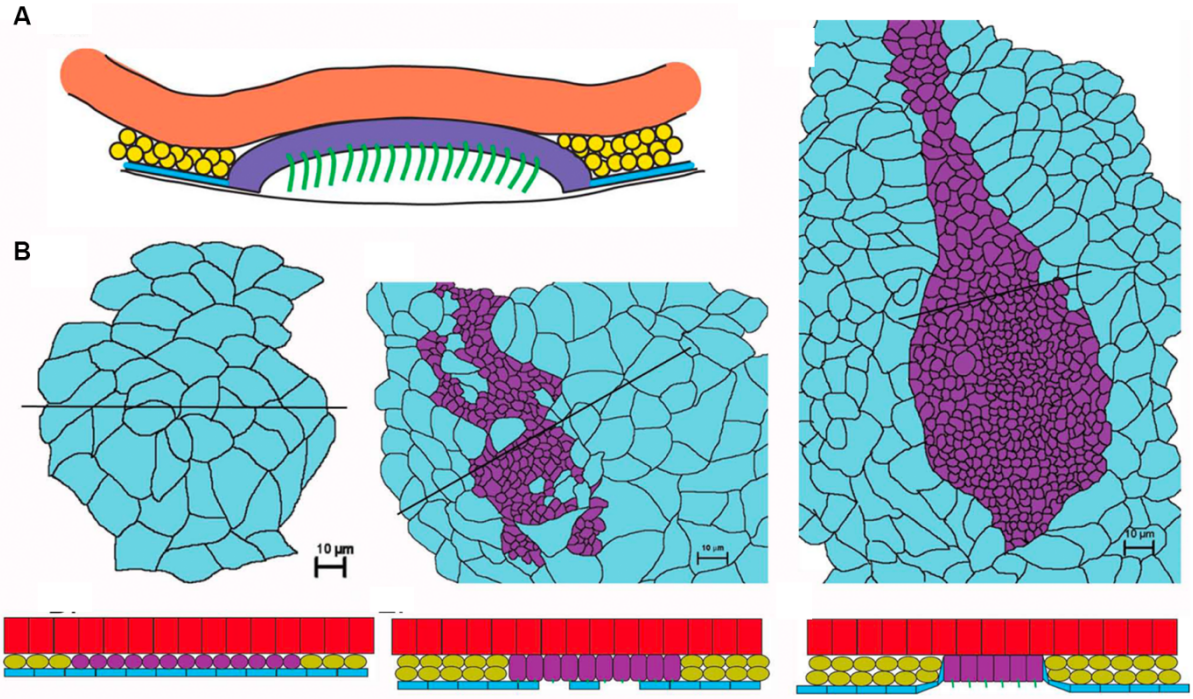

FIGURE 1.13: NODE MORPHOGENESIS

(A) Schematic of mouse node; red = embryonic ectoderm, yellow = mesoderm, cyan = endoderm, purple = node, green = cilia. (B) Node morphogenetic steps as seen from the ventral side. Cross sections of the side of node emergence shown at the bottom (Lee and Anderson, 2008).

1.3 CELL SPECIFICATION AND ASSOCIATED MORPHOGENETIC EVENTS

1.3.1 CELL SPECIFICATION IN PRE-IMPLANTATION DEVELOPMENT

1.3.1.1 Trophectoderm, inner cell mass and primitive endoderm decisions

The first segregation of cell lineages in mouse embryo development involves the acquisition of either a trophectoderm or ICM fate. The bias of cells to become one or the other has been shown to be initiated as early as the 4-cell stage of embryo development, which is of course prior to the first morphogenetic event described before, namely compaction. The four blastomeres of the 4-cell embryo have been independently sequenced and analysed to identify heterogeneities at the level of expression of major character-defining transcription factors involved in acquisition of trophectoderm or ICM fate. It was discovered that many targets of Oct4 and Sox2 (key ICM-associated markers) are heterogeneously expressed in the four blastomeres. One of these targets is Sox21 and cells expressing higher Sox21 levels preferentially contribute to the ICM lineage (Goolam et al., 2016) (**Figure 1.14**). Moreover, heterogeneous Oct4 kinetics and Sox2 DNA binding within the four blastomeres have also been demonstrated as a source of bias to lineage allocation (Plachta et al., 2011).

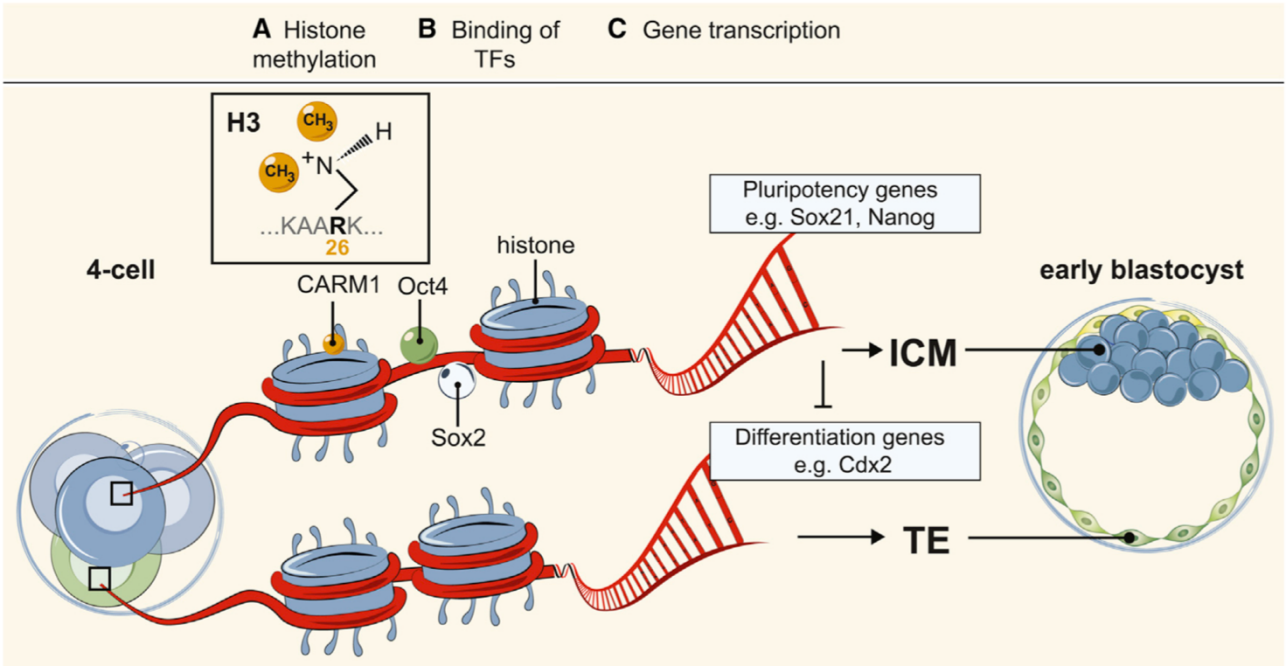

FIGURE 1.14: HETEROGENEITY AT 4-CELL STAGE BIASES ICM VS TE LINEAGE

CARM1 epigenetically regulates the transcription of pluripotency genes and is heterogeneously expressed in the four blastomeres of the 4-cell stage embryo. These differences in gene expression bias cell specification and the acquisition of either an ICM or a TE fate (Goolam et al., 2016).

While this bias in acquisition of fates seems to precede compaction and the subsequent internalisation waves described above, the geometrical positioning of the two lineages only happens at the 8-16- and 16-32-cell transitions. For the ICM cells to end up in the interior of the blastocyst they need to be internalised after compaction and this happens by means of asymmetrical cell division or cell engulfment. As shown before, the asymmetric divisions perpendicular to the apicobasal axis of cells creates daughter cells of different determinants, which in turn guide cell specification accordingly (Knoblich, 2008; Sutherland et al., 1990). More specifically, cell divisions separating the apical from the basal side of the blastomere leaves the basally-derived daughter cell lacking apical signals that inhibit Hippo signalling. In the presence of Hippo signalling the Lats kinase is activated which in turn phosphorylates Yap excluding it from the nucleus and thus restricting its ability to interact with Tead4, a transcription factor required to drive the trophectoderm lineage program (Nishioka et al., 2009). A Hippo-independent pathway was also discovered later that involves a membrane-localised Yap-binding protein, Angiomotin (Zhao et al., 2011). This protein's Yap-binding ability is inhibited by F-actin and polarity markers enriched in the apical domain. Thus, the exclusion of the apical domain during asymmetric divisions results in a daughter cell with Angiomotin which in turn is able to bind Yap and localise it to the membrane preventing it from nuclear translocation (Leung and Zernicka-Goetz, 2013) (**Figure 1.15**).

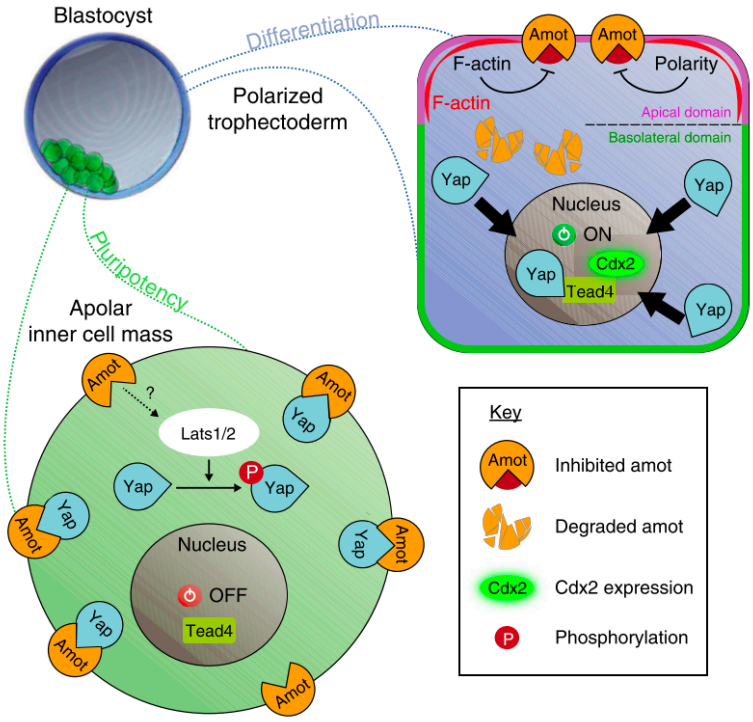

FIGURE 1.15: LINEAGE SEGREGATION BY ASYMMETRIC CELL DIVISION

In the apical domain-inheriting cell, angiomotin's (amot) binding to Yap is inhibited leaving Yap able to translocate into the nucleus and activate Cdx2 for TE specification. In the apolar cell Yap is sequestered by angiomotin at the membrane excluding it from the nucleus (Leung and Zernicka-Goetz, 2013).

Internalisation of the apical domain-excluded cells then takes place either due to the inherent positioning of the cell division plain (leaving the basal daughter cell in the interior), or due to the differential cortical tension between the apical and basolateral domains. However, more importantly, when it comes down to cell specification, the two rounds of divisions i.e. 8-16 and 16-32 and associated internalisation events have a different outcome in the segregation between the Epi

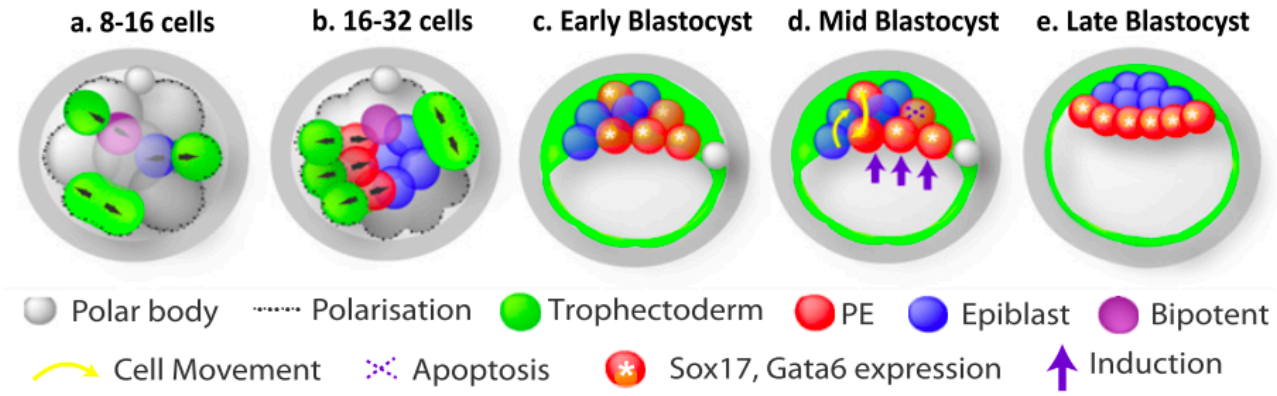

FIGURE 1.16: THE TWO WAVES OF ASYMMETRIC DIVISION BIAS SEGREGATION OF EPI VS PE LINEAGES

This model suggests that the first wave of division/cell internalisation biases cells towards the Epi fate, while second wave biases internalised cells towards the PE fate. Sorting of cells within the ICM takes place by cell movement, apoptosis and inductive signals (Morris et al., 2010).

and PE lineage in the ICM. It's been proposed that the decision on the ICM's cell fate – whether give rise to the Epi or the PE - is biased by the preceding waves of divisions during the 8-16 and 16-32-cell transitions. More specifically, the first wave gives rise to internalised cells that are biased towards contribution to the more pluripotent Epi cells whereas the second round of division biases cells towards the PE fate (Morris et al., 2010) (**Figure 1.16**). Upon reaching the stage of the early blastocyst, the two populations of cells arising from the previous two rounds of division, are distributed in the ICM in a salt and pepper fashion. While this is a model that supports lineage bias before blastocyst formation, it is likely that cells still retain enough plasticity and remain able to switch their fate to the other lineage to accommodate spatial segregation. To position the cells in their correct niche i.e. Epi cells flanked between the trophectoderm and the monolayer of PE, a process of cell sorting takes place. The cell sorting step in the ICM to spatially segregate the two lineages, involves the active migration of PE-biased cells to the outside of the ICM, switching of fate by positional cues (Wnt9a being one of the primary candidates) and apoptosis of mis-localised cells (Meilhac et al., 2009; Xenopoulos et al., 2012) (**Figure 1.16**).

1.3.2 CELL SPECIFICATION IN THE PERI- AND POST-IMPLANTATION DEVELOPMENT

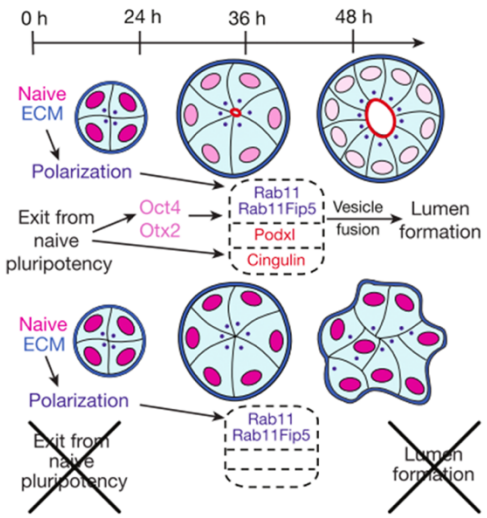

FIGURE 1.17: LUMENOGENESIS AND NAÏVE TO PRIMED PLURIPOTENCY TRANSITION

Cells manage to polarise regardless of their pluripotency state but fail to maintain epithelial character and form a central cavity (Shahbazi et al., 2017).

1.3.2.1 Naïve to primed pluripotency transition

During the peri-implantation stage of development concomitant with the major morphogenetic event of Epi lumenogenesis, is the change of the Epi cells' state of pluripotency from naïve to primed. The link between opening a cavity and this transition in the transcriptome has been recently established (Freedman et al., 2015; Shahbazi et al., 2017). Naïve pluripotency initiates polarisation of the Epi cells which acquire an apicobasal polarity but fail to undergo hollowing to give rise to the Epi cavity. Instead, when Epi morphogenesis is modelled *in vitro* by single cell suspensions in Matrigel (an exogenously provided ECM replacement), cells are locked in naïve pluripotency in pluripotency-maintaining conditions and culturing them further than the rosette stage leads to formation of disorganised cell clumps. Conversely, when cultured in the absence of pluripotency-maintaining conditions (permitting their exit from naïve pluripotency) the cells move past the rosette structure by opening up central lumens. This has been attributed to the upregulation of the sialomucin Podocalyxin and Cingulin as well as exocytosis factors like Rab11 upon exit from naïve pluripotency highlighting the coordination between morphogenesis and transcriptional networks regulating developmental potential (Shahbazi et al., 2017) (**Figure 1.17**).

1.3.2.2 Trophoblast stem cells establishment

Following Epi lumenogenesis, as outlined in the introduction of this chapter, the ExE forms from the polar trophectoderm, which is in direct apposition with the Epi cells. At this stage of development FGF signalling is required and Fgf ligands are secreted from the Epi (Tanaka et al., 1998). Specification of the ExE and acquisition of the trophoblast stem cell (TSC) character is dependent upon initiation of the core TSC transcriptional network. The main players maintaining TSC potency have been identified as the following: Cdx2, Eomes, Tfap2c, Gata3, Elf5, Ets2, Sox2 and Esrrb (Latos and Hemberger, 2014). Of these factors Cdx2 and Eomes are required in the preimplantation stages of development to maintain the trophectoderm character whereas other transcription factors of the core TSC network are required upon implantation for the establishment of the post-implantation ExE (Russ et al., 2000; Strumpf et al., 2005). In particular, knockouts of Elf5 and Ets2 have been previously found to lead to failure of ExE formation and establishment of TSCs (Donnison et al., 2005; Yamamoto et al., 1998). FGF signalling originating from the adjacent Epi drives expression of Elf5 to give

rise to the nascent ExE. Expression of Fgf4 in the Epi is in turn promoted by active Nodal. The polar trophectoderm responds to Fgf4 through Fgfr2 receptors which persist in the ExE and are required to maintain the TSC transcriptional network (Guzman-Ayala et al., 2004). The multipotency of the ExE is only lost later during its differentiation which gives rise to the invasive trophoblast (Adamson et al., 2002; Hemberger et al., 2004). Identification of the signalling factors required to maintain the TSC character *in vitro* has provided information of the signalling interactions *in vivo* between the Epi and ExE. Initially, TSCs were cultured *in vitro* in the presence of mouse embryonic fibroblasts (MEFs; or MEF-conditioned media) and Fgf4 with Heparin (facilitating binding of the ligand to the receptors) (Tanaka et al., 1998). Later, defined conditions were established that required TSCs to be cultured on an ECM substrate (Kubaczka et al., 2014; Ohinata and Tsukiyama, 2014). Regardless of the specific derivation and maintenance methods, FGF signalling is ubiquitously required to maintain TSC multipotency.

1.3.2.3 Segregation of embryonic and extraembryonic visceral endoderm

After, or possibly concomitant with initiation of ExE formation, the VE extends its monolayer proximally to cover the nascent ExE. The presence of VE in two separate niches, i.e. adjacent to the Epi or adjacent to the ExE, is also reflected in its transcriptional profile. The embryonic VE (emVE) and the extraembryonic VE (exVE) differentially express a set of genes confirming that the microenvironments provided by the Epi or ExE (or both) have an impact on the character of their adjacent tissues (Pfister et al., 2007). It's been shown that Nodal in the Epi and ExE signal/s are vital in driving the embryonic VE program, which has a subsequent impact on the establishment of specialised structures such as that of the AVE which establishes the anterior-posterior axis (Brennan et al., 2001; Mesnard et al., 2006) (Figure 1.18). Also, interestingly, the activity of Nodal in the Epi depends upon secretion of the pre-protein convertases Pace4 and Furin that cleave and activate pro-Nodal from the ExE. By extension, absence of these two enzymes leads to the failure of emVE character acquisition (Constam and Robertson, 2000; Mesnard et al., 2011). This provides a good indication of the three-way communication and interaction between the three lineages (VE, Epi and ExE) coordinating cell specification and morphogenesis. The emVE differs from the exVE not only in terms of transcriptional profile but also in appearance. While the emVE is made up of squamous cells, the exVE cells are largely cuboidal in shape (Reinius, 1965; Solter et al., 1970). The mechanism underlying their difference in appearance remains currently

unknown but could be potentially attributed to their difference in character as dictated by their exposure to Nodal.

1.3.2.4 Distal visceral endoderm specification

After establishment of the emVE, the emergence of a population of Cerberus-like and Lefty-expressing cells (both inhibitors of Nodal) at the distal tip of the emVE is observed (Bouwmeester et al., 1996; Thomas et al., 1997). This is called the distal VE (DVE), and when it starts to migrate on one side of the embryo to establish a Nodal activity gradient along an axis perpendicular to the PD axis, is referred to as the anterior VE (Thomas and Beddington, 1996; Thomas et al., 1998; Yamamoto et al., 2004). Its emergence is suggested to be dependent on the PD gradient of Nodal expression which is attributed to the ExE inductive signals and pre-protein convertases secretion, thus geometrical distance of the distal VE from the ExE could be a parameter contributing to correct embryo patterning (Brennan et al., 2001; Richardson et al., 2006; Rodriguez et al., 2005). Establishment of the DVE character (i.e. expression of Cerberus-like and Lefty) is also accompanied by

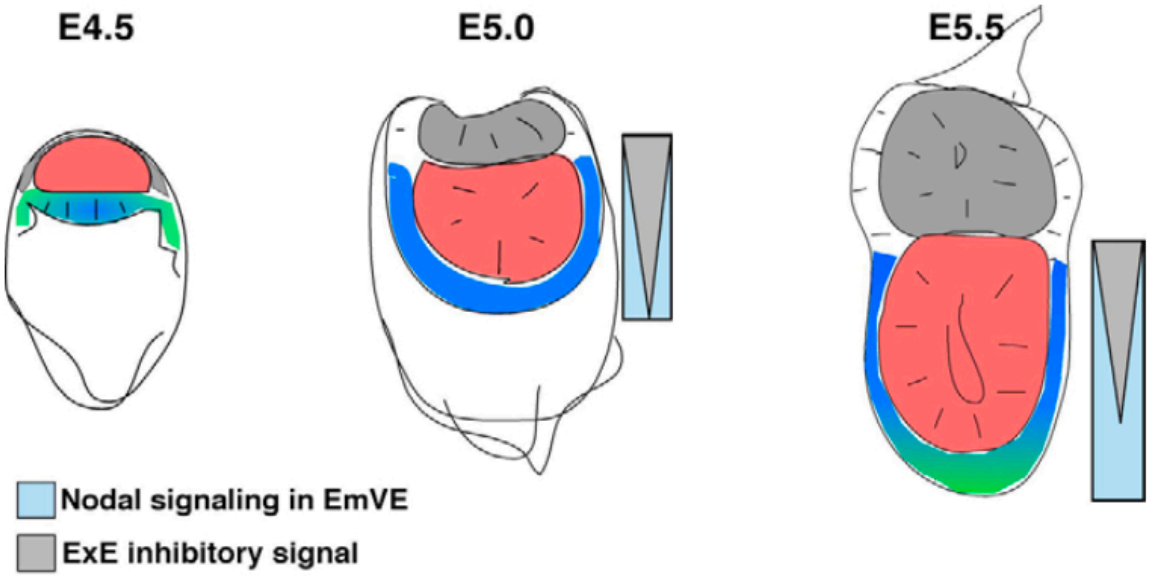

FIGURE 1.18: SEGREGATION PF EMBRYONIC AND EXTRAEMBRYONIC VISCERAL ENDODERM

Nodal signalling in embryonic portion of the embryo in combination with an inhibitory signal from the ExE promotes separation of the embryonic visceral endoderm (EmVE) from the extraembryonic visceral endoderm; blue/green = primitive endoderm/embryonic visceral endoderm, red = epiblast, grey = polar trophectoderm / extraembryonic ectoderm (Mesnard et al., 2006).

a morphological change of these cells. These cells undergo a squamous to columnar transition giving the distal tip of the embryo the appearance of a pointy edge which is termed VE thickening (VET) (Rivera-Perez et al., 2003) (**Figure 1.19A**). The mechanism and role of this transition in cell morphology has been suggested to be dependent on the ECM protein hensin based on studies with ES cells seeded on different substrates (Takito and Al-Awqati, 2004). Hensin is secreted as a monomer in the surrounding matrix which polymerises with

other proteins like galectin 3 to induce columnarisation of cells (Hikita et al., 2000). Its secretion seems to be dependent on the seeding density and only appears to induce the squamous to columnar transition at high density (Vijayakumar et al., 2006). This is quite interesting as columnarisation may be dependent on the embryo's geometry and thus the coordination of morphogenesis. Hensin is first expressed in the PE of the blastocyst, which is consistent with the observation that PE cells become columnar prior to implantation. Its expression is retained throughout the VE until its later restricted at the distal tip, again consistent with the formation of the VET (Vijayakumar et al., 2006) (**Figure 1.19B**). As stated earlier, Hensin secretion is dependent on cell density and thus it is possible that cell crowding at the distal tip of the VE monolayer that occurs due to the curvature of the embryo may act as a cue for cell columnarisation. Therefore, appearance of the VET could either be a direct result of DVE specification, a secondary effect of reduced Nodal at the distal tip or result of cell crowding. Of course, it could be a combination of all three possible explanations, but the exact mechanism is yet to be elucidated. Hensin however, remains a good candidate driver of this event. It is important to note here that differences in cellular morphology of emVE and exVE could also be attributed to differential exposure to hensin and if this is the case an unknown link between Nodal and hensin expression may exist.

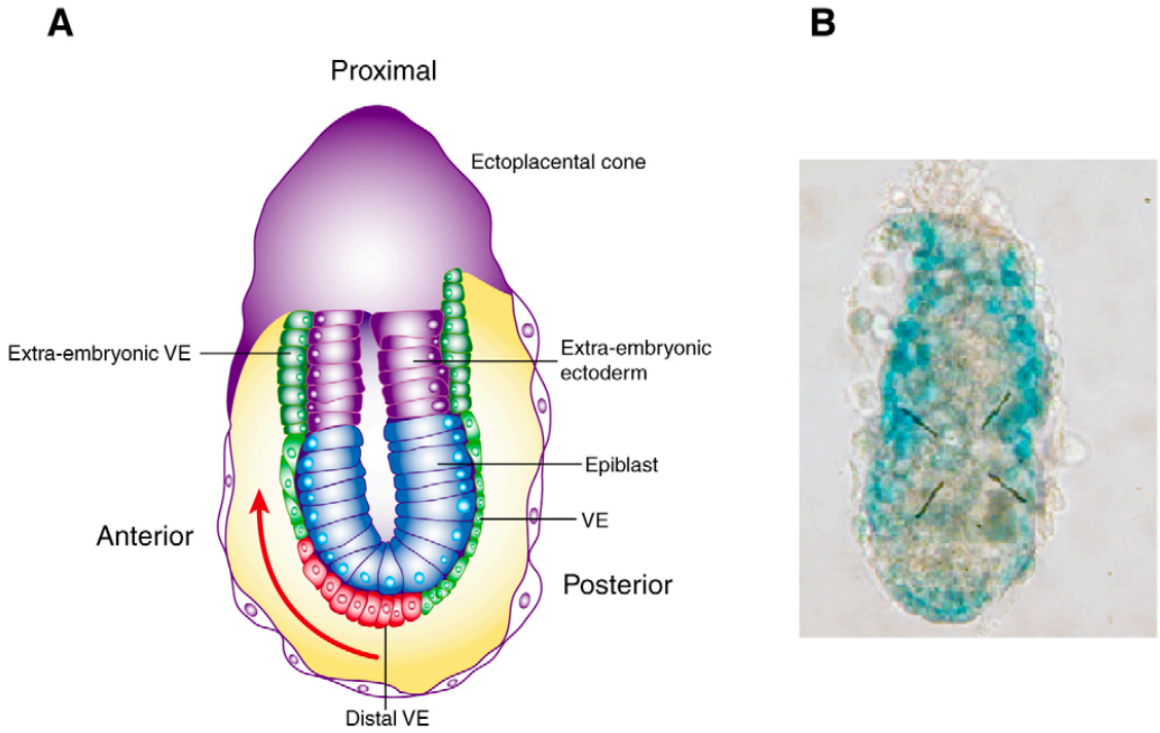

FIGURE 1.19: HENSIN AND VISCERAL ENDODERM MORPHOLOGY

(A) Schematic of a E5.5 embryo with an established DVE showing columnar morphology. (B) Hensin *in situ* revealing increased expression at the distal tip of the embryo and the extraembryonic visceral endoderm (Vijayakumar et al., 2006)

1.3.2.5 Anterior visceral endoderm establishment

Establishment of the *Cerberus-like* and *Lefty*-expressing DVE is followed by its migration to the site that will become anterior of the embryo and becomes known as the anterior VE (AVE). This migration has been both described to be active or passive by different studies; either through active collective migration guided by leader cells first emerging asymmetrically in the PE of blastocyst or Epi cell proliferation "pushing" AVE away from the future posterior (Morris et al., 2012; Stuckey et al., 2011). When it colonises one site of the embryo it forms a gradient of Nodal activity which is important in both specification of the anterior and the posterior (Thomas et al., 1998; Yamamoto et al., 2004). The DVE is considered to transform into the AVE upon the start of migration while new Lefty-expressing AVE cells emerge distally as the DVE migrates anteriorly (Takaoka et al., 2011; Trichas et al., 2012). While, there is little understanding of how the AVE decides to migrate (i.e. in which direction) and the signals involved, the players that make the DVE migratory and thus allow the transition to the AVE character have been studied. The columnar DVE cells acquire migratory morphology by generating basal projections (filopodia) that enable intercalation between adjacent VE cells, and by means of neighbour exchange they are progressively repositioned so as to move away from the distal site (Migeotte et al., 2010; Srinivas et al., 2004; Trichas et al., 2012). A central element in this is assembly of the WAVE complex through recruitment of Nap1 (Rakeman and Anderson, 2006). This complex drives Rho-GTPases to polymerise actin that in turn assembles the filopodial projections on the basal site of the cells. The cells polarise through the action of PTEN creating differential distribution along the planar axis leading to an increased localisation of PIP3 in the leading edge and increased localisation of PIP2 in the trailing edge (Stower and Srinivas, 2014). This polarisation within the cells directs them to migrate unilaterally and the actin dynamics are regulated by the active planar cell polarity (PCP) pathway through Frizzled and Dishivelled (DVL2) (Trichas et al., 2011) (**Figure 1.20**). To allow cells of the AVE to migrate collectively as

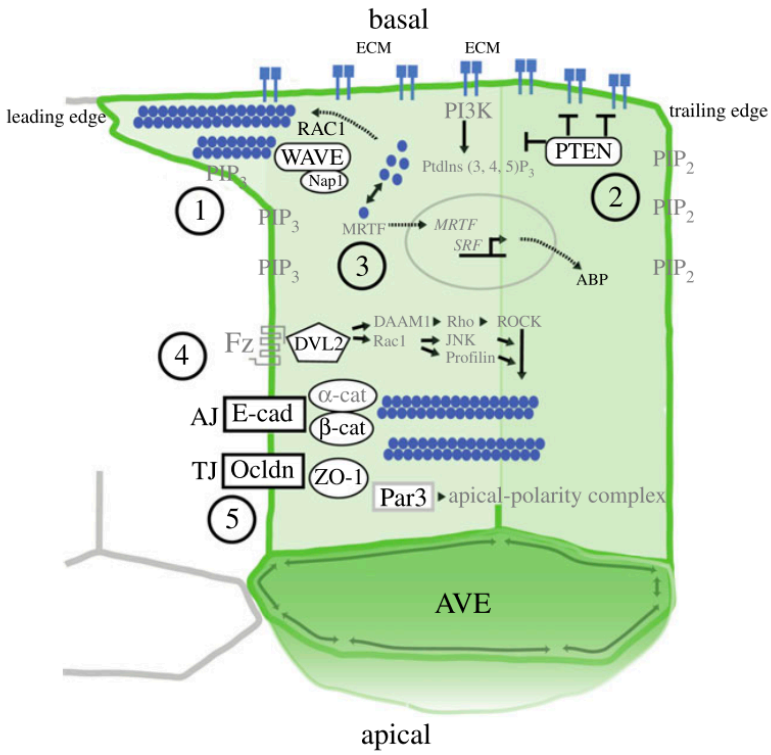

FIGURE 1.20: AVE MIGRATION PLAYERS

Summary of the different factors that drive established DVE cells to migrate and acquire the AVE character (Stower and Srinivas, 2014).

opposed to cell autonomously, PCP signalling in the VE promotes the formation of multicellular rosettes that counteract the reorganisation in the monolayer, a step necessary for AVE migration to take place (Trichas et al., 2012). Interestingly, as the initially columnar AVE migrates towards the proximal site of the embryo, it becomes squamous and stops its migration when it reaches the boundary of exVE (Trichas et al., 2011). The mechanism and signalling involved in achieving this tissue boundary remain unknown.

1.3.2.6 Mesendoderm specification and gastrulation initiation

AVE migration on one side has a very significant effect on embryo patterning and cell specification events, particularly important in initiation of gastrulation. As mentioned earlier, the AVE secretes the Nodal inhibitors Cerberus and Lefty creating a gradient of Nodal activity and expression (by abolishing the Nodal autoregulatory pathway) along an axis perpendicular to the PD axis (Brennan et al., 2001; Kumar et al., 2015). Additionally, the AVE secretes Dkk1, which is a Wnt inhibitor thus also inhibiting the adjacent ExE (which is a source of Wnt). Both Nodal and Wnt are posteriorising signals and as such their inhibition in the vicinity of the AVE, restricts the establishment of the posterior to the opposite side (Gadue et al., 2006). Direct anteriorisation of the Epi from the AVE has not been elucidated yet.

Wnt ligands are released from both the posterior ExE and the proximo-posterior VE. Activation of Wnt signalling leads to expression of Brachyury, a key transcription factor in mesendoderm specification, the precursor cells of mesoderm and endoderm upon gastrulation (Rivera-Perez and Magnuson, 2005) (**Figure 1.21**). However, gastrulation is a collection of cell-specifying and morphogenetic events that lead to formation of the trilaminar embryo. While mesendoderm specification is central to gastrulation initiation, the next step is for cells to be able to ingress in the Epi and reach the underlying VE and the space in between. For this to occur, breakage of the underlying BM is required, but the mechanism behind this is still not very well understood. Although it is likely to be dependent on the secretion of BM remodelling proteins like matrix metalloproteinases, in the chick embryo the BM at the primitive streak is dependent on loss of basally localised RhoA-Net1 in the overlying ectoderm cells (Nakaya et al., 2008; Williams et al., 2012). In the mouse embryo this could be dependent on Nodal or Wnt activity, but this has not yet been thoroughly investigated in this model. Along with BM breakdown and removal of the physical restriction of ingression, the cells lose their cell-cell adhesion through downregulation of E-cadherin by Eomes which is in turn upregulated by Nodal. The presence of Eomes and Nodal are also important in specifying both the definitive endoderm (DE) and the anterior primitive streak (Arnold et al., 2008; Ferrer-Vaquer et al., 2010). Nodal is also important in maintaining BMP4 in the ExE which in turn drives Wnt expression (Tam and Loebel, 2007).

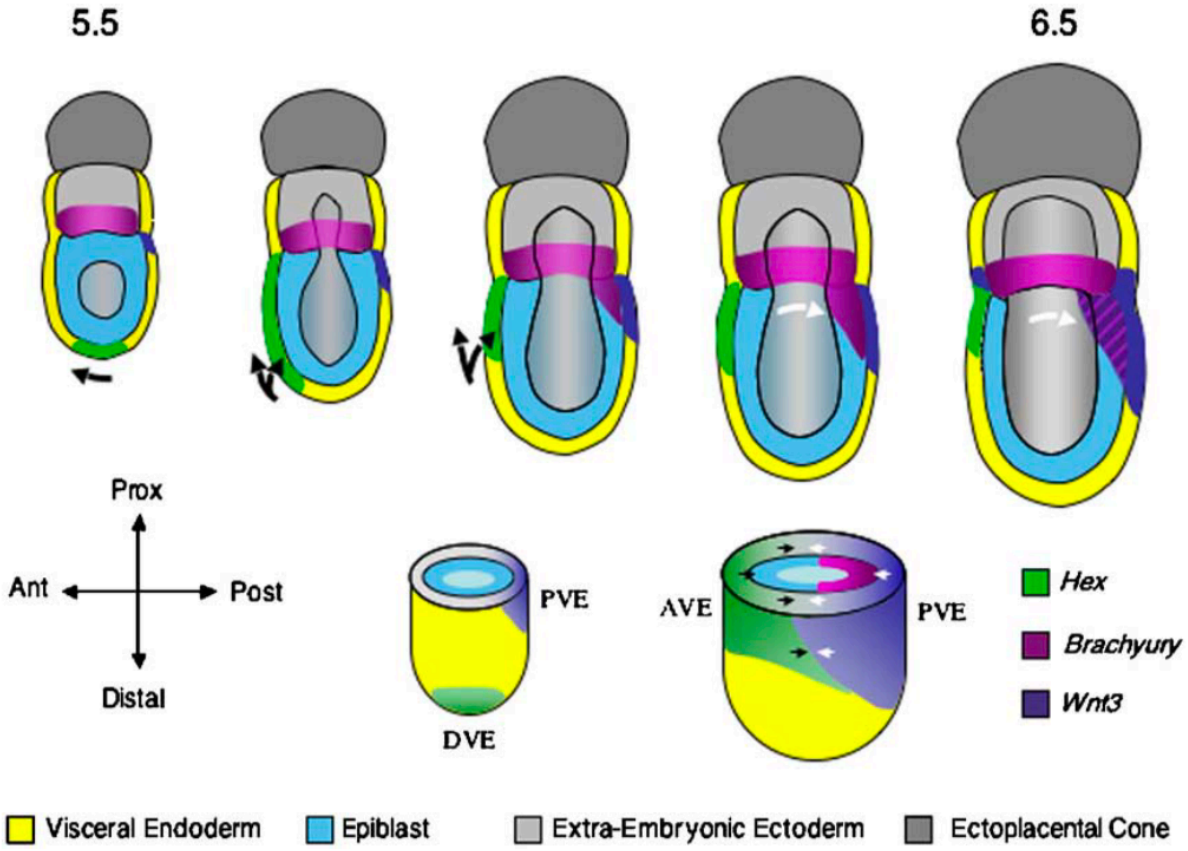

FIGURE 1.21: MESENDODERM SPECIFICATION

Schematic of changing patterns of expression during establishment of the posterior and specification of the mesendoderm. According to this model, Wnt3 from the proximo-posterior VE promotes expression of Brachyury in the adjacent Epi thus establishing the mesendoderm that will ingress through the primitive streak (Rivera-Perez and Magnuson, 2005).

1.4 PROJECT AIMS

The morphogenetic events shaping the early post-implantation mouse embryo are poorly described in the literature. Aiming to enrich the understanding of how the egg cylinder takes shape and develops its major features, the architecture of extraembryonic ectoderm was first characterised. Then its reorganisation was followed through by analysis of fixed samples, time-lapse movies and spatial transcriptomic analysis to elucidate the mechanism behind proamniotic cavity formation (Aim 1).

Finally, the project aimed to also understand the basement membrane dynamics during embryo expansion that accommodate growth as it enters the pre-gastrula stages. High resolution imaging, pharmacological and genetic approaches were implemented to reveal the mechanism controlling architecture of the basement membrane (Aim 2).

2 MATERIALS AND METHODS

2.1 EMBRYO RECOVERY AND CULTURE

Implantation stage embryos were recovered from wild type MF1 or CD1 females mated with mTmG (Muzumdar et al., 2007), LifeAct-GFP (Riedl et al., 2010) and wild type MF1 males. Nodal fl/fl:RCreT2 females were mated with Nodalfl/fl:RCreT2 males for experiments on role of Nodal an perforations (Kumar et al., 2015). RhoA fl/fl females (Melendez et al., 2011) were crossed with TTR-Cre; RhoA+/-; Hex-GFP males (Kwon and Hadjantonakis, 2009).Pre-implantation embryos were flushed out from the uteri by passing M2 through the uterine cavity with a 23G needle (BD Microlance 3). Post-implantation embryos were dissected out of the deciduae and transferred into IVC2 (Bedzhov et al., 2014b). After recovery, the embryos were transferred into drops of IVC2 (Advanced DMEM (Gibco, UK), L-glutamine (Gibco, UK), ITS-X (Gibco, UK), Pen/Strep (Gibco, UK), Knockout Serum Replacement (KSR; Life Technologies, UK), beta-estradiol (Sigma, Canada), progesterone (Sigma, Canada) and NAC (Sigma, Canada)) (1 embryo/drop) covered with mineral oil and cultured according to the experimental design.

2.2 PHARMACOLOGICAL TREATMENT OF EMBRYOS

For the enzymatic removal of the basement membrane, Collagenase IV (500ug/ml) was used for 3-5 hours in IVC2 and then replaced with 50ug/ml for overnight culture. For MMP-inhibited embryo culture a combination of MMP inhibitors NSC405020 (100uM) and Prinomastat hydrochloride (20uM) was used overnight (16 hours). For visualising cell death in MMP inhibitor-treated embryos in culture during live imaging the cleaved caspase live dye CellEvent Caspase-3/7 Green Detection Reagent was used at a concentration of 1uM. To induce deletion of Nodal in the Nodal fl/fl:RCreT2, recovered embryos were cultured in 2mM of (Z)-4-hydroxytamoxifen (ethanol). Embryos were cultured at 37^{o}C in 5% CO_2.

2.3 GENOTYPING

Single embryo genotyping was performed at the end of experiments using the Nodal fl/fl:RCreT2 and TTR-Cre;RhoA to confirm or select knockouts. To confirm *in vitro* Cre-induced deletion of Nodal and select VE-deleted RhoA embryos, a single embryo was lysed in 48.5ul of Viagen Direct PCR lysis buffer and 1.5ul of Proteinase K (Qiagen, UK) at 55^{o}C for 5 hours followed by 1 hour of neutralisation at 85^{o}C. From the lysates 2ul were used as template for the PCR reaction.

Genotyping of single embryos following conversion of Nodal fl/fl:RCreT2 was done using the primers for the floxed allele: Primer forward: 5'-ATGATTGTGGAGGAGTGTGGGTGC-3', Primer reverse: 5'-TCTCTGGCTTGGCAGGTCTAAG-3'.

For selecting RhoA VE-deleted knockouts, the sample was first genotyped for the presence of Cre using the primers: Primer forward: 5'-GCAGAACCTGAAGATGTTCGC-3', Primer reverse: 5'-AGGTATCTCTGACCAGAGTCA-3'. They were then genotyped for the presence of the floxed gene and absence of the wildtype gene using the primers: Primer forward: 5'-AGCCAGCCTCTTGACCGATTTA-3', Primer Reverse: 5'-TGTGGGATACCGTTTGAGCAT-3'.

Lysis of cells to extract DNA for genotyping MMP14-KO cells was performed using the following protocol: Medium was removed from the wells and replaced with 250ul of TNES (50uM Tris (pH7.4), 100uM EDTA (pH8.0), 400mM NaCl, 0.5% SDS) + 5ul of Proteinase K (Qiagen, UK). Cell were detached by pipetting up and down and transferred to a 1.5ml tube followed by incubation at 55^{o}C for 30 minutes. To precipitate cell membrane 75ul of 6M NaCl was added and vigorously shaken for 30 seconds before spinning for 10 minutes at maximum speed. A 1:1 volume of 100% ethanol was added to the supernatant and inverted ~20 times before spinning down for 5 minutes at maximum speed at 4^{o}C. The supernatant was then discarded, and the pellet was washed with 70% ethanol and span down again for 5 minutes at maximum speed at 4^{o}C. The supernatant was removed again and left the tubes to airdry for 10 minutes at room temperature. To dissolve the DNA pellet, 20ul of DNAse-free water was added and incubated at 65^{o}C for 20 minutes. From the resulting DNA sample, 2ul were used per PCR reaction.

For genotyping the primers used were: Primer forward: 5'-CAGTTCGCCGACTAAGCAGA- 3', Primer reverse: 5'-TACTTCGGGGCTGAAGTTGC-3'.

All PCR reactions were performed using the Fast Cycling PCR Buffer (Qiagen, UK).

2.4 IMMUNOSTAINING

Embryos were fixed in 4% paraformaldehyde (PFA) for 20 min at room temperature. Post-implantation embryos were permeabilized for ~12-20 min in 0.3% Triton X- 100 / 0.1M Glycin in PBS. The primary antibodies were then added to the blocking buffer (0.1% Tween-20 / 10% filtered FCS in PBS) and embryos incubated overnight at 4^{o}C. Embryos were then incubated for 3-4 hours at room temperature with secondary antibodies in blocking buffer. All washes were done in filtered PBS + 0.05% Tween-20 (PBST). Pre-implantation embryos were permeabilized in 0.5% Triton X-100 in PBS for 20 min at room temperature.

Primary antibodies were added in the blocking buffer (3% BSA in PBS + 0.1% Tween-20) and embryos incubated overnight at 4°C.

Primary antibodies used: ZO-1 (1:200; Thermofisher Scientific, 33-9100), E-cadherin (1:300; Thermofisher Scientific, 13-1900), aPKC (1:100; Santa Cruz Biotechnologies, sc-216), Oct4 (1:400; Santa Cruz Biotechnologies, sc-5279), GM130 (1:200; BD, 610822), Laminin (1:400; Sigma, L9393), Collagen IV (1:100; Millipore, AB769), HSPG2 (1:100; Millipore, MAB1948P), Otx2 (1:100; R&D Systems, AF1979), Cerberus (1:500; R&D Systems, MAB1986), MMP14 (1:100; Abcam, ab51074), Cdx2 (1:200; Biogenex, MU392A-UC), β1-integrin (1:50; Ha2/5; BD, 561796), active β1-integrin (1:50; 9EG7; BD, 553715), Ap2γ (1:300; Santa Cruz Biotechnologies, sc-8977), Eomes (1:400; Abcam, ab23345), Elf5 (1:400; Santa Cruz Biotechnologies, sc-9645), Podocalyxin (1:300; R&D systems, MAB1556), Pard6b (Santa Cruz Biotechnologies, sc-67393), pMLC (1:100; Cell Signalling Technologies, 3671P), cleaved Caspase-3 (1:200; Cell Signalling Technologies, 9664S), Rab11a (1:100; Cell Signalling Technologies, 2413S) Anxa2 (1:700; Abcam, ab41803), . Secondary antibodies in pre-implantation blocking buffer were then added to the embryos for ~2 hours at room temperature. Secondary antibodies used: Alexa 647 donkey anti-rabbit (1:500; Thermofisher Scientific, A31573), Alexa 594 donkey anti-rat (1:500; Thermofisher Scientific, A21209), Alexa 568 donkey anti-mouse (1:500; Thermofisher Scientific, A10037), Alexa 488 donkey anti-mouse (1:500; Thermofisher Scientific, A21202), Alexa 488 donkey anti-goat (1:500; Thermofisher Scientific, A11055), Phalloidin 488 (1:500; Thermofisher Scientific, A12379). All washes were done in PBS + 0.1% Tween-20. Nuclear staining: minimum 15 min incubation in DAPI + PBS (5mg/ml).

2.5 WESTERN BLOT

Protein lysates were recovered from cells in 2D cultures using RIPA Buffer (1M Tris-HCL, 1M NaCl, 0.5M EDTA, 10% TX-100, 10% Sodium Deoxycholate, 10% SDS) with protease inhibitor cocktail (cOmplete Mini; Roche; 11836153001) on ice. After spinning for 30 minutes at 4°C the supernatant was collected and quantified for protein using a BCA assay kit (Pierce BCA Protein Assay Kit; 23227). 20ug of the sample was boiled at 96 °C for 12 minutes in Laemmli buffer before being loaded in an 8% SDS-PAGE gel. After running and transfer on nitrocellulose paper (0.2um, BioRad; 160-0112), blotting was performed in 5% milk with the following antibodies: MMP2 (1:2000; abcam, ab92536), MMP14 (1:2000; abcam, ab51074), α-tubulin (1:10000; Sigma, T5168). HRP-conjugated antibodies: goat anti-rabbit (HRP) (1:10000; Stratech, 43C-CB1106-FIT), goat anti-mouse (HRP) (1:10000; Stratech, 43-GM30-FIT). HRP detection was performed using Clarity Western ECL Substrate (BioRad; 170-5060).

2.6 QUANTITATIVE PCR (QPCR)

To extract RNA from plated cells, the RNA extraction reagent TRIzol (Thermo, 15596010) was used according to manufacturer's protocol. For cDNA production from extracted RNA, 1ug of RNA was used for reverse transcription reaction with M-MuLV reverse transcriptase (New England BioLabs, M0253L), random primers (Promega, C1181), dNTPs (New England BioLabs, N0447S) and RNAse inhibitor (New England BioLabs, M0314L).

qPCR reaction was carried out using the Power SYBR Green PCR Master Mix (Thermo, 4368708). The program used on the Step One Plus Real-Time PCR machine (Applied Biosystems) was: 10 minutes at 95^{o}C and 40 cycles of 15 seconds at 95^{o}C and 1 minute at 60^{o}C. Primers used:

MMP2: FW = 5'-ACAAGTGGTCCGCGTAAAGT-3', RV = 5'-GTAAACAAGGCTTCATGGGGG-3'

MMP14: FW = 5'-CAGTATGGCTACCTACCTCCAG-3', RV = 5'-GCCTTGCCTGTCACTTGTAAA-3'

MMP25: FW = 5'-CCCTGACCTCCTCCAGACTT-3', RV = 5'-GACCTTCGCATCGGGATTCT-3'

For normalising expression, the housekeeping gene GAPDH was used in all experimental set ups. Primers used:
GAPDH: FW = 5'-AGGTCGGTGTGAACGGATTTG-3', RV = 5'-TGTAGACCATGTAGTTGAGGTCA-3
To calculate relative expression, the difference of quantification cycles (Cq) between GAPDH and gene of interest was first calculated for every replicate of the reaction (ΔCq; always done in triplicates). Then the average ΔCq expression (which is $2^{\Delta Cq}$) is calculated and divided by the ΔCq of the control (ΔΔCq). Relative gene expression is then calculated based on the differences of ΔΔCq between samples.

All primers were validated by performing qPCRs using different concentrations of sample and assessing linearity of C_q difference. Additionally, analysis of melting curves showed single amplicon production.

2.7 IMAGING

Fixed and stained embryos were imaged on a Leica SP5 or SP8 inverted confocal microscope at 20x, 40x or 63x depending on the resolution required for the analysis. For live imaging a multiphoton Leica SP8 was used. The wavelengths used for 2-photon excitation fluorescence (2PEF) when imaging mTmG (unconverted; Tomato) and LifeAct (GFP) were 1040nm and 910nm respectively.

2.8 IMAGE PROCESSING AND ANALYSIS

Images were acquired using the provided Leica software i.e. LASX for SP8 and LAS AF for SP5. Fiji image processing software was used for analysis while 3D reconstructions of cells were carried out on 3D Slicer software using manually segmented images from Fiji. Custom plugins that were installed on Fiji are Smart

Denoise (Dr. Richard Butler, Gurdon Institute, UK) and OrientationJ for vector map generation and perforation directionality (Biomedical Imaging Group, EPFL, Switzerland).

2.9 LASER ABLATION

Carried out on two-photon microscope (LaVision BioTec TriM Scope II). A multiphoton Insight DeepSee dual-line laser tuned to 920 nm was used to perform ablations. A region of interest was set to cell-cell interface and scanned at 3 different Z planes (1um) with the multiphoton laser set at 70% transmission with a pixel dwell time of 9.1µs. Images were taken immediately before, after and every 1 min following ablation.

2.10 CELL CULTURE

2.10.1 TROPHOBLAST STEM CELL CULTURE

Unconverted Confetti TSCs derived in defined conditions on fibronectin were used for TSCs aggregate experiments (provided by Jenny Nichols, Cambridge UK). TSCs were maintained and passaged under defined conditions on fibronectin (15ug/ml, Millipore)-coated wells as described previously (Ohinata and Tsukiyama, 2014). 1:1 v/v N2B27 (DMEM/F12 (GIBCO, UK) and Neurobasal A (without vitamin A; GIBCO, UK), 1% v/v B27 supplement (Thermo, UK), 0.5% v/v N2 (DMEM/F12 (GIBCO, UK), 2.5mg/ml Insulin (Sigma-Aldrich, I9287), 10mg/ml Apo-transferrin (Sigma-Aldrich, T1147), 0.75% v/v BSA Fraction V (Thermo, 15260037), 20um/ml Progesterone (Sigma-Aldrich, p8783), 1.6mg/ml Putrescine dihydrochloride (Sigma-Aldrich, P5780), 6ug/ml Sodium selenite (Sigma-Aldrich, S5261), 100uM beta-mercaptoethanol (GIBCO, UK), Penicillin/Streptomycin (GIBCO, UK), GlutaMAX (GIBCO, UK)) with 50ng/ml FGF2 (Stem Cell Institute, Cambridge, UK), 20ng/ml Activin A (Stem Cell Institute, Cambridge, UK), 10uM XAV939 (Sigma Aldrich, X3004), 5nM/ml Y-27632 (STEMCELL Technologies, 72304) (N2B27 + FAXY). Passaging was performed for 2-3 minutes with Accutase (Life Technologies) at 37^{o}C. Dissociation was stopped by adding 3x the amount of accutase in TS cell medium (RPMI, Penicillin/Streptomycin, 1mM Sodium Pyruvate (GIBCO, UK), 100uM beta-mercaptoethanol (GIBCO, UK), 2mM L-Glutamine (GIBCO, UK), 20% FBS (Stem Cell Institute, Cambridge, UK). The suspension was collected in 15ml falcon tubes and span at 1000g for 5 minutes and supernatant was removed. The cells were re-suspended in N2B27+FAXY and plated in fibronectin-coated dishes.

The cells were passaged when they reached ~70% confluency (normally once every three days) and medium was changed the day after passaging and then every other day. The cells were kept at 37^{o}C in 5% CO_2.

2.10.2 EMBRYONIC STEM CELL CULTURE

LifeAct-GFP ES cells were cultured on gelatin-coated dishes in feeder cell medium (DMEM (GIBCO, UK), 15% FBS (Stem Cell Institute, Cambridge, UK), Penicillin/Streptomycin (GIBCO, UK), GlutaMAX (GIBCO, UK), non-

essential aminoacids (GIBCO, UK), Sodium pyruvate (GIBCO, UK), 100UuM beta-mercaptoethanol (GIBCO, UK)) with 3uM GSK3 inhibitor CHIR99021 (Stem Cell Institute, Cambridge, UK), 1uM MEK inhibitor PD0325901 (Stem Cell Institute, Cambridge, UK) and 10ng/ml mouse LIF (Biochemistry Department, University of Cambridge) (FC + 2iLIF). E14 ES cells were also cultured in gelatin-coated dishes but 2iLIF was added to N2B27 (N2B27 + 2iLif).

Passaging was performed using 0.05% trypsin-EDTA (Invitrogen) for 3-4 minutes at 37°C when cells reached confluency. Trypsinisation was stopped by adding 3x the amount of trypsin in feeder cell medium. Cell suspension was collected in a 15ml falcon tube and span down at 1000g for 5 minutes. Supernatant was discarded and replaced with FC+2iLIF or N2B27+2iLIF before being plated back on gelatin-coated dishes.

The cells were passaged when they reached 70% confluency and medium was changed every other day. The cells were kept at 37°C in 5% CO_2.

2.11 STEM CELL AGGREGATES

TSCs were incubated for 2 min at 37°C in 0.05% trypsin- EDTA (Invitrogen) when they reached confluency. Trypsinization was stopped by adding TS medium (RPMI 1640 (Sigma), 20% FCS (GIBCO), penincillin/streptomycin (50um/ml) (GIBCO), Sodium pyruvate (1Mm) (GIBCO), β-mercaptoethanol (100uM), L-glutamine (2mM) (GIBCO)). The cell suspension was collected and spun down (1000 rpm for 5 min). The supernatant was discarded, and the pellet re-suspended as clumps in defined culture medium prior to plating in Matrigel (BD, 356230). Using a haemocytometer, the cell density was calculated, and then appropriate volume of cell suspension was aspirated to suspend ~20000 cells / Matrigel drop. The cell suspension was spun down (1000 rpm for 5 min) and supernatant removed. The TSCs in the pellet were gently re-suspended as clumps in a volume of Matrigel corresponding to 20ul / drop before plating each 20ul drop in one well of an ibiTreat microscopy plastic µ plate (Ibidi). After 2 min of incubation at 37°C to allow polymerization of the Matrigel, the media were added according to the designed experiment. The cells were kept at 37°C in 5% CO_2.

For ES cell aggregates the same method was used using the media for ES cells instead TS cells.

2.12 CRISPR-CAS9 MMP14 DELETION

The deletion of MMP14 was targeted to exon 1 at the translation initiation site. Two gRNAs to flank the initiation codon were designed using the online CRISPR Design Tool (http://tools.genome-engineering.org) by inputting the sequence for exon 1 of MMP14. From the list of possible gRNAs designed by the tool the following sequences were selected based on their position on the exon (to flank the initiation codon) and their score of inverse likelihood of off-target binding. The gRNAs selected to flank the initiation codon are:

gRNA1: 5'-GTGGATTCCTAGAGCGCGGT-3' , gRNA2: 5'-GGAGGCTGCGGGAGGGTCGA-3'

Each gRNA was cloned into the plasmid pSpCas9(BB)-2A-Puro (PX459) (deposited in Addgene by the Zhang lab) according to the published CRISPR-Cas9 protocol (Ran et al., 2013). Both gRNAs were co-transfected in LifeAct-GFP ESCs using the Lipofectamine 3000 transfection reagent (Thermo, L3000001) according to manufacturer's directions (250ng of each plasmid).

After two days of antibiotic selection using 2ug/ml Puromycin, the transfected cells were washed in fresh medium and allowed two more days to recover from the antibiotic treatment. To isolate individual clones, the remaining colonies surviving the antibiotic selection were trypsinised and plated at 1 cell/well in two 96-well plates. The plates were checked every day until colonies became visible. From 192 wells, 48 had a single colony growing. Each of the 48 wells was trypsinised and split into 3 new wells in 3 different 96-well plates to create triplicates of all clones. Once the colonies in the new plates became confluent, two plates were frozen down by first trypsinising and inactivating, followed by addition of equal volume of freezing medium (FBS + 20% DMSO). The cells in the remaining plate were allowed to grow for two more days before extracting DNA from each clone and genotyping as described in **2.3**. Deletion was confirmed by western blot described in **2.5**.

2.13 *IN VITRO* BASEMENT MEMBRANE DEGRADATION SYSTEM

To assess basement membrane degradation potential of Epi *in vitro*, ibiTreat microscopy plastic μ plates (Ibidi) were first coated with Poly-L-Lysine, followed by glutaraldehyde coating and finally fluorescent Cy3-Gelatin. The protocol and reagents were provided in the QCM Gelatin Invadopodia Assay (ECM671, Millipore). Once coated, ~5000 ESCs were counted and plated. They were allowed to recover for 24 hours in 2i+Lif conditions before starting the experiment.

Alternatively, ibiTreat microscopy plastic μ plates were coated with 100ug/ml of Laminin from Engelbreth-Holm-Swarm murine sarcoma basement membrane (L2020, Sigma-Aldrich) for ~2 hours at 37°C before plating cells as above. To visualise the laminin coat at the end of the experiment, it was immunostained using antibodies described in **2.4**.

2.14 GEO-SEQ

2.14.1 EMBRYO LASER CAPTURE MICRODISSECTION AND RNA ISOLATION:

The spatial transcriptome of embryos was obtained according to the Geo-seq method (Chen et al., 2017). In brief, E5.25, E5.5, E5.75 MF1 embryos in deciduas were embedded in OCT compound and cryosectioned serially at 15 μm along the proximodistal embryo axis. Serial sections were mounted on polyethylene terephthalate-coated slides. Frozen sections were allowed to thaw at room temperature and then dehydrated

in ice-cold 100% ethanol. Fixation was performed in 75% ethanol, then the slides were stained with 1% cresyl violet acetate solution (Sigma-Aldrich, prepared in 75% ethanol), dehydrated in a series of 75%, 95%, 100% ethanol (30 seconds for each step), and finally subjected to LCM on an MMI Cellcut Plus system (MMI, Zurich, Switzerland).

Approximately 20 cells in each section were harvested by LCM. Cell samples were lysed in 50 µl of 4 M guanidine isothiocyanate solution (GuSCN; Invitrogen, 15577-018) at 42°C for 10 min. The volume of the lysate was adjusted to 200 µl by nuclease-free water and was further concentrated by ethanol precipitation in the presence of 1/10 volume of acetate sodium (pH 5.7, 3 M; Ambion) and 2 µl of carrier glycogen (20 mg/ml; Roche). Total RNA pellets were dissolved in lysis solution and used as a template for low-cell number RNA-seq.

2.14.2 RNA-SEQ DATA PRE-PROCESSING:

Raw reads quality was evaluated with the FASTQC. Density distribution of gene expression for all samples were also plotted to assess whether there are inconsistent samples. Raw reads were mapped to mm10 version of mouse genome using Tophat2 v2.0.4 program (Trapnell et al., 2009). We calculated fragment per kilobase per million (FPKM) as expression level using Cufflinks v2.0.2 with default parameters (Kim et al., 2013). Genes with the FPKM > 1.0 in at least one sample across all samples were retained for further analysis. Finally, the expression levels were transformed to logarithmic space by using the $\log_2$(FPKM+1).

2.14.3 DIFFERENTIALLY EXPRESSED GENES (DEGS) ANALYSIS

Analysis between EPI and ExE were identified using RankProd (Hong et al., 2006) with P value < 0.05 and fold change > 1.5.

2.14.4 FUNCTIONAL ENRICHMENT ANALYSIS

Analysis of gene sets with different expression patterns was performed using the Database for Annotation, Visualization and Integrated Discovery v6.8 (DAVID v6.8) (Huang da et al., 2009).

2.14.5 GENE EXPRESSION VISUALISATION:

To visualize the genes expression patterns in each embryo section, we wrote a program for visualization in MATLAB (version: 2015a). To analyze the genes expression dynamics during development (E5.25, E5.5, E5.75), we normalized the three sequencing batches to the same standard using ComBat (Johnson et al., 2007), then ran the MATLAB program.

2.14.6 DATABASE AVAILABILITY:

RNA–seq data that support the findings of this study have been deposited in the Gene Expression Omnibus (GEO) under accession code GSE110808.

2.15 STATISTICS

For graphical statistics and statistical tests, GraphPad Prism 7 was used. For circular statistics Oriana software was used.

3 SEQUENTIAL FORMATION AND RESOLUTION OF MULTICELLULAR ROSETTES DRIVE PROAMNIOTIC CAVITY FORMATION

3.1 INTRODUCTION

Developing tissues can undergo multiple stages of morphogenesis until the adult structure is achieved. These stages are primarily achieved by cell proliferation, cell rearrangements and physical scaffolds that direct tissue shaping. While these cell behaviours take place at the cellular level, their effects manifest at the tissue level; several examples include branching, looping, cavitation and folding. Interestingly, these processes are characteristic of most of the morphogenetic events of embryo development. Just to mention a few, branching morphogenesis is seen in the lung, kidney, submandibular gland and pancreatic development (Bellusci et al., 1997; Majumdar et al., 2003; Villasenor et al., 2010; Wells et al., 2013). Looping primarily involves the looping and apposition of tubes, which is very well described in heart development (Goenezen et al., 2012). Folding involves sheets of tissues bending to create three-dimensional structures; this can be seen during development when the trilaminar embryo folds to generate a structure of a tube within a tube, which serves as the blueprint for the embryo's anatomy. Finally, and of particular relevance to this study, the process of cavitation (including hollowing) is a very frequent morphogenetic event employed in developmental programmes to generate epithelia or tubes (Girdler and Roper, 2014; Xu et al., 2011; Yang et al., 2013).

The generation of cavities through the organisation of adjacent cells to form an intercellular space can either be achieved by cell death, which clears the space between cells or by membrane separation. While these methods of cavity generation involve *in situ* rearrangement of cells, tubulogenesis employs a third method to do so which requires global tissue rearrangement. It does so by invagination of the tissue, guided by a subset of cells that "sink" into the epithelium, pulling the surrounding tissue with them and thus forming an elongated cavity. The developing tissue utilises these methods according to the context and the local architecture; there is evidence, however, that cavitation (i.e. creating space by apoptosis) or hollowing (i.e. creating space by membrane separation) can also compensate for one another (Martin-Belmonte et al., 2008).

Creating intercellular space is vital for primarily two reasons. Firstly, cavities may have a functional role in the adult tissue, for example, they allow lung tubules to be filled with air and the kidneys to be filled with waste filtered from the blood. The second role is a facilitative one, and that is to create space for other morphogenetic events to take place (Moriwaki et al., 2007) or create niches for morphogens (Shyer et al., 2015; Uy et al., 2002). A very striking example of this is the proamniotic cavity (PAC) which spans the mouse egg cylinder. The PAC is a fairly transient structure between E5.75 and E7.5 of mouse development. It should

be noted that the cavity does not collapse at this point but rather it ceases to be one unified cavity and becomes subdivided into three distinct membrane-separated cavities (Pereira et al., 2011).

Following the steps of PAC formation, it is evident that the previously multi-layered compact extraembryonic ectoderm (ExE) becomes a monolayer epithelium continuous to the epiblast (Epi). Immediately after this, the ExE detaches from the posterior site of the embryo and folds over, dividing the PAC into three cavities; the amniotic, chorionic and ectoplacental cavities. This is called the amniochorionic fold and requires the available space provided by the PAC to fold in this manner (Pereira et al., 2011).

While the PAC is a very prominent central cavity that spans the egg cylinder, the mechanisms of its formation are unclear. The general consensus is that it originates from the Epi cavity that precedes PAC formation. Indeed, even from brightfield images, the Epi cavity can be seen extending into the ExE (Rivera-Perez et al., 2003) but this extension has never been followed through to its completion and an understanding of the cell behaviours involved in achieving this is lacking. The Epi cavity does seem to be the primer for PAC formation but interestingly, the hollowing of the Epi and its extension into the ExE appear to be two separate processes. The formation of the Epi cavity has been described (based on studies with embryoid bodies) to result from apoptosis of cells that are not incorporated into the Epi epithelium (Coucouvanis and Martin, 1995). This model was later revisited, and it was demonstrated that this cavity is shaped through hollowing; this involves the Epi cells forming a rosette that opens a lumen in its centre (Bedzhov and Zernicka-Goetz, 2014). This thorough characterisation of the Epi cavity formation revealed that the cavity first forms as an isolated entity surrounded by Epi cells. This is important in trying to understand how the PAC forms as it excludes the classical tubulogenic model that supports one continuous *de novo* emergence of a cavity. In other words, PAC formation appears to consist of at least 2 separate steps as the Epi cavity is arranged through its own lumenogenesis programme. So, at first glance the PAC is a product of the extension of a pre-existing cavity into an adjacent tissue.

While the ExE appears to be a compact and multi-layered tissue, it also has a cavity of its own: the ExE cavity. This cavity has been rarely mentioned in literature (Bedzhov and Zernicka-Goetz, 2014; Snell, 1966) because this cavity is slit-like as opposed to the conspicuous lumen of the Epi, and thus it has been very difficult to observe by brightfield or confocal imaging (Beck et al., 2002; Bedzhov and Zernicka-Goetz, 2014; Donnison et al., 2015; Richardson et al., 2006; Shimokawa et al., 2011). Secreted podocalyxin (Podxl) between cells at the proximal site of the ExE shows that there is indeed intercellular space along the proximal-distal (PD) axis (Bedzhov and Zernicka-Goetz, 2014).

Based on these features of the pre-PAC embryo the formation of the PAC was hypothesized to include 4 separate processes i.e. formation of the Epi cavity, formation of the ExE cavity, extension of the Epi cavity and finally fusion of the two to form a unified cavity.

The morphogenetic events in question that are investigated in this study and introduced here are thus the following: 1) extension of cavities and 2) formation of slit-like cavities.

The extension of cavities into adjacent tissues to form elongated cavities has been studied in development previously in the context of kidney, pancreas, brain development and pharyngeal extension (Gutzman and Sive, 2010). Each of these examples presents a different way to extend cavities, as each of them has a different tissue architecture that needs to be remodelled accordingly.

In kidney development, the ureteric bud lumen eventually makes a connection with the lumen forming in the developing renal vesicle. In this case, the renal vesicle lumen forms in the centre of the renal vesicle cells resembling a rosette structure with a central cavity. The UB lumen formation precedes that of the RV lumen. After the appearance of the RV's lumen, the RV expands further, while maintaining its lumen. The cells lying between the RV lumen and the UB lumen start to rearrange into a tract leading to the UB forming a polarised tract. Eventually the tract reaches the UB bud fusing the two lumens together in the process (Yang et al., 2013).

In pancreatic plexus formation, fusion of multiple small lumens is the driving force of its morphogenesis (Azizoglu et al., 2017; Villasenor et al., 2010). In zebrafish hindbrain development, high actomyosin contractility keeps boundaries between cavitated ventricles together. During ventricle progression, the ventricle lumens expand by losing the actomyosin contractility and allowing the epithelium to relax and be "inflated" by fluid, fusing adjacent ventricles together in the process (Gutzman and Sive, 2010). This is possibly a strategy that is favoured in tissues that can employ significant hydrostatic forces and use actomyosin contractility as a regulator. At a smaller scale, the pharyngeal extension model in *C. elegans* heavily relies in dynamic rearrangement of surrounding cells. In this system the pharyngeal cells form a tube with a "dead end" (cap) which later extends into the surrounding mesenchymal tissues made up of arcane cells. To achieve this, both pharyngeal cells at the cap and the adjacent arcane cells reorient to form a tract continuous to the existing pharyngeal tube. This tract then opens and the arcane cells comprising the extended portion of the pharynx undergo epithelialisation (Portereiko and Mango, 2001).

It is evident that even though cavity extension is a process that happens frequently during development, it can be achieved in many different ways. The strategies selected for the different tissues to extend cavities largely depend on the architecture of the tissues in question and the ultimate function of the cavities. Therefore, while there is a wealth of literature studying these morphogenetic events in different systems, each one appears to have a unique way to achieve the same result. In terms of the size of the tissue and cavities involved,

the early post-implantation mouse embryo resembles the kidney development model described above. However, the precise architecture and cell organisation of the ExE (which in this system is the intervening tissue that needs to be remodelled during cavity extension) is not currently known, which is why in this study care was taken to characterise the ExE tissue itself before investigating the morphogenetic events that remodel it to promote PAC formation.

3.2 RESULTS

3.2.1 MACRO-CHARACTERISATION OF PROAMNIOTIC CAVITY FORMATION STAGES

Upon implantation of the mouse embryo and initiation of decidualisation, the processes for formation of the PAC commence. The key events for its formation can be listed as Epi cavity formation, extraembryonic cavity formation and tissue rearrangements between the cavities to promote final fusion. Based on this, 5 major steps (stages I – V) to PAC formation were identified and used as a reference for this study (**Figure 3.1A, B**).

The characterisation began right after implantation when the deciduas were still not fully formed but still discernible by the naked eye. The temporal stage of the embryos around this time was E5.0. Morphologically, this stage (stage I) had the following major features: a hollowed Epi and an expanded polar trophectoderm along the PD axis (nascent ExE) (**Figure 3.1A**). Epi cavity formation has been previously described to result from rosette formation and membrane separation during the stages of implantation through integrin-mediated signalling. The expansion of the ExE in the PD direction precedes the formation of the ExE cavity (Bedzhov and Zernicka-Goetz, 2014).

During the next step (stage II), the Epi cavity expanded, and the ExE tissue grew further. More strikingly at this stage, the ExE cavity emerged as a thin slit (visualized with the apical polarity marker aPKC) extending from the proximal-most part of the embryo to the middle of the ExE tissue (**Figure 3.1A)**. At this stage the embryonic-extraembryonic (Em-ExEm) boundary was still intact and with no evidence of reorganisation.

The Epi then reorganised at the interface with the ExE to expose the Epi cavity to the ExE tissue (stage III). The Epi cells at the boundary shifted from having their apico-basal axis aligned with the PD axis of the embryo to being perpendicular, overall transforming the spherical Epi to a cup-shaped structure (**Figure 3.1A, B & B'**). ExE cells were at this point exposed to the Epi cavity with their apical domain facing the cavity (white arrowhead in **Figure 3.1A**).

Once the Epi acquired the cup-shaped morphology, the Epi cavity extended into the ExE tissue (visualised with the apical polarity marker aPKC; dashed circle in **Figure 3.1A**). This invading cavity stage (stage IV) was the first reorganisation event in the ExE during PAC formation.

Finally, the extending Epi cavity and the ExE cavity met and fused with each other to form a unified cavity (stage V); the PAC (**Figure 3.1A, B)**. Moving from one stage to the next, the tissue became reorganised as described here, accompanied by the extension of cavities and a decrease of the distance between the two in a step-wise manner (**Figure 3.1C).**

The morphological characterisation of these stages of development proved to be a more precise, higher resolution method of staging, as it is evident from the variety of different PAC formation stages recovered from the same temporal stage. When recovering post-implantation embryos at E5.5, half of them (53.42%, n=73) were at PAC stage III, while the rest were either stage II (not reorganised Epi cells at the boundary) or stage IV (34.24% and 12.34% respectively, n=73) (Figure 3.1D). Out of the embryos recovered at E5.75, around a third of them (32.25%, n=31) had a formed PAC (stage V) while the remaining embryos were at stage IV with an extended Epi cavity into the ExE but with no fusion of cavities (67.75%, n=31) (Figure 3.1D).

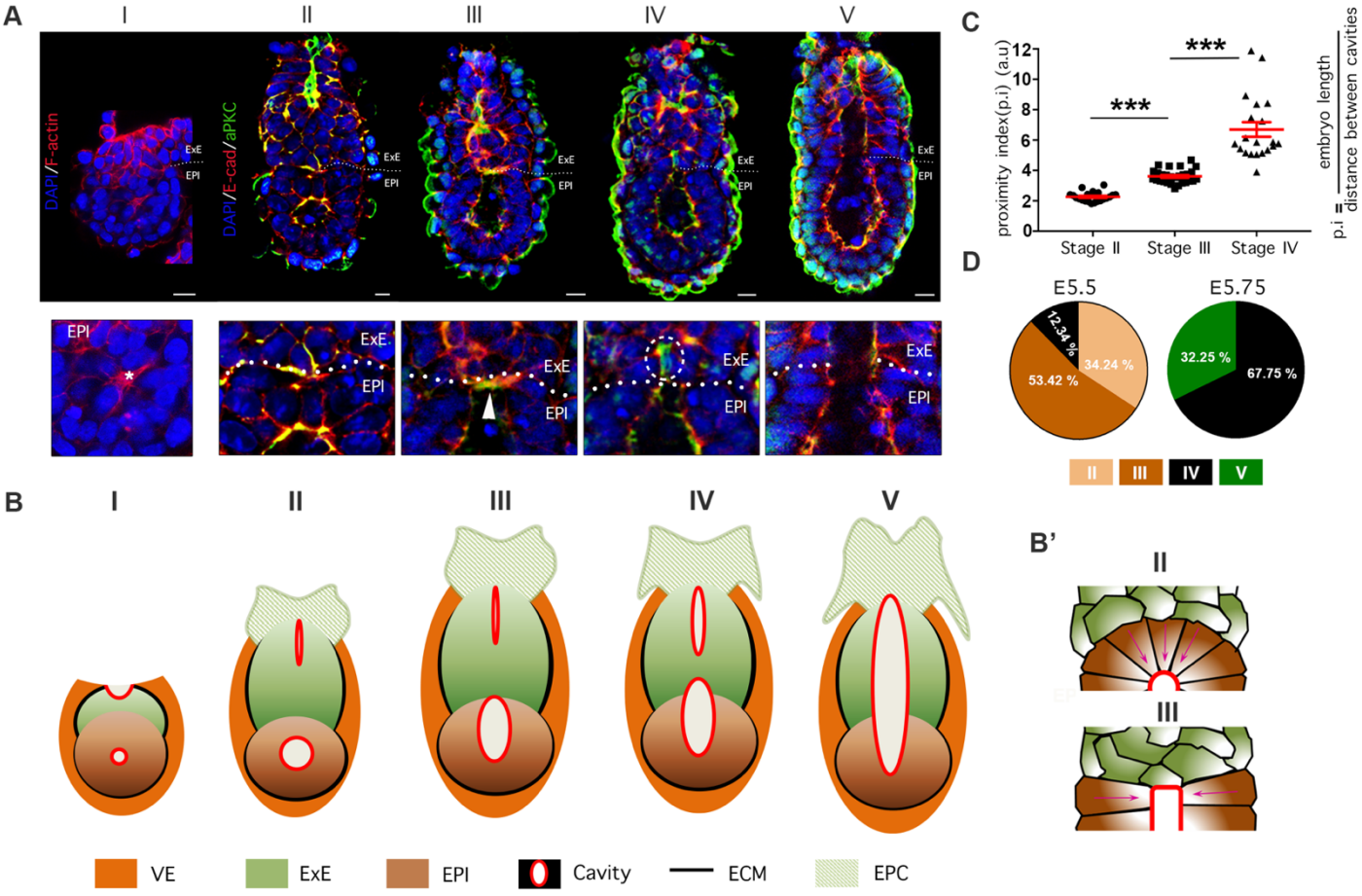

FIGURE 3.1: STAGES OF PROAMNIOTIC CAVITY FORMATION

(A) Morphological staging of the early post-implantation embryo from E5.25 to E5.75 based on the development of the PAC. Dashed lines across the embryos denote the Em-ExEm boundary; arrowhead points at the apical domain of ExE cells at the boundary after reorganisation of the epiblast; dashed circle highlights the invading epiblast cavity into the ExE; white star in zoomed in panel of stage I epiblast denotes the nascent epiblast cavity forming through rosette opening; scale bar =20um. (B) Schematic diagram of the morphological stages of PAC as interpreted from raw data. (B') Changes of epiblast boundary cells arrangement (magenta arrows) in relation to the proximal-distal axis during transition from stage II to stage III. (C) Quantification of proximity changes at different stages of PAC development; proximity index (p.i) calculated by dividing embryo length with the distance between Epi and ExE cavities; Stage II n=21, Stage III n=28, Stage IV n=20; unpaired student's t-test; ***<0.0001. (D) Quantification of embryos found in specific PAC formation stages when recovered at specific temporal stages (E5.5, n=73; E5.75, n=31). VE = visceral endoderm, ExE = extraembryonic ectoderm, EPI = epiblast, ECM = extracellular matrix, EPC = ectoplacental cone.

3.2.2 EXTRAEMBRYONIC ECTODERM CAVITY FORMATION

Between stage I and II, a slit-like cavity in the ExE emerged, that extended from the proximal-most site of the embryo into the bulk of the tissue (yellow asterisks in **Figure 3.2A**).

To characterise the steps that lead to formation of the ExE cavity, embryos were collected, fixed and stained in intermediate steps between stages I and II (between E5.0 and E5.25) (**Figure 3.2A)**. To avoid creating artefacts like enriching actomyosin due to a wound healing effect caused by dissecting the embryos out of the deciduas, deciduas were also recovered and fixed prior to embryo dissection **(Figure 3.2B)**.

In stage I of PAC formation the nascent ExE is a placode of cells; the proximal-most cells are enriched in apical markers (ZO-1) and adherens junctions (E-cadherin) (white and yellow arrowheads respectively in **Figure 3.2A**) and these same cells became elongated and apically constricted while maintaining their polarity. This cell shape change was followed by folding towards each other forming a crevice at the most-proximal site of the embryo (white dots and arrows in **Figure 3.2A**). By stage II a slit-like cavity formed at that site suggesting that this folding in of the proximal-most cells may be responsible for the formation of the ExE cavity.

To confirm this hypothesis and the sequence of events, the process was live imaged with a LifeAct-GFP (marking actin) mouse reporter line to track actin dynamics during this event (**Figure 3.2C**). Starting from an early stage I embryo, the cells of the nascent ExE formed the placode, as observed in the fixed samples. In the successive 45 minutes of development, these proximal-most cells enriched actin at their apical site and started to become apically constricted; this became more apparent 20 minutes later (red arrowheads in **Figure 3.2C**). By the end of this live imaging, these cells had undergone an invagination-like process, sinking in the tissue while surrounding cells moved around these "sinking" cells to line the forming slit cavity (**Figure 3.2C** in segmented 2D view: red cells are the cells apically constricting and "sinking" into the tissues, while green cells are the surrounding cells that move around them to form the cavity).

To visualise cellular dynamics at the apical site of the proximal-most cells, the movie was converted into a 3D reconstruction and re-recorded to monitor the apical site *en face.* The cells created an actin-enriched domain (red arrowheads in **Figure 3.2D**) on this site of the embryo, which eventually disappeared as the cells "sunk" into the tissue. Moreover, the cells that enriched actin on the apical site (red arrowheads in **Figure 3.2E**) underwent apical constriction (**Figure 3.2E**, segmented cells) further supporting the findings from the live imaging.

3.2.3 EXTRACELLULAR MATRIX ROLE ON POLARITY OF EXE CELLS

In the study by Bedzhov and Zernicka-Goetz, it was shown that basement membrane (BM) provision is important in activating integrin-mediated signalling which in turn polarises cells in the Epi to form a rosette (Bedzhov and Zernicka-Goetz, 2014). Indeed, similarly to the Epi cells, the ExE cells that are in direct contact with the underlying BM (dubbed 'outside cells') are both polarised (as it is apparent from the apical localisation of the golgi and the cell aspect ratio of these cells) and have an active integrin signalling pathway (**Figure 3.3A-C**).

To investigate the role of the niche provided by the underlying BM, a reduced system was implemented using trophoblast stem cells (TSCs) embedded in the extracellular matrix-rich 3D scaffold, Matrigel (**Figure 3.4A)**. Similar to the results of Bedzhov (2014) in embryonic stem cells (ESCs), when TSCs are embedded in Matrigel they organised into aggregates with the cells that are in direct contact with the Matrigel becoming polarised as revealed by the position of the golgi, the apically-localised tight junction protein ZO-1 and their cell aspect ratio. Conversely, TSCs are aggregated in suspension in the absence of Matrigel, failed to polarise (**Figure 3.4A**).

To remove the *in vivo* ligand of polarisation, collagenase IV (COLIV) was used to digest the BM providing the niche. The treatment with the enzyme removed both collagen and laminin as well as the heparan sulphate, Perlecan. Staining for active integrin revealed that integrin signalling became inactive and the outside cells (originally in direct contact with the BM) lost their polarised character. This was assessed based on the loss of their columnar shape and localisation of the tight junction protein ZO-1 (**Figure 3.4B-F**).

Similarly, to directly block the integrin pathway, an integrin-blocking antibody (Ha2/5) was used in TSCs embedded in Matrigel. Ha2/5 binds to integrin receptors and blocks integrin signalling and has been frequently used in studies perfomed on explants (Sakai et al., 2003). The model of choice here was once again the TSC model, since addition of the blocking antibody to embryos in culture led to antibody sequestration by the visceral endoderm (VE), thus preventing it from reaching the integrin receptors situated on the basal site of the outside cells. Indeed, adding Ha2/5 to the 3D culture led to loss of active integrin staining (also confirming the ability of the antibody to block the pathway), ZO-1 apical localisation as well as the columnar shape of the outside cells (based on cell aspect ratio) (**Figure 3.5**).

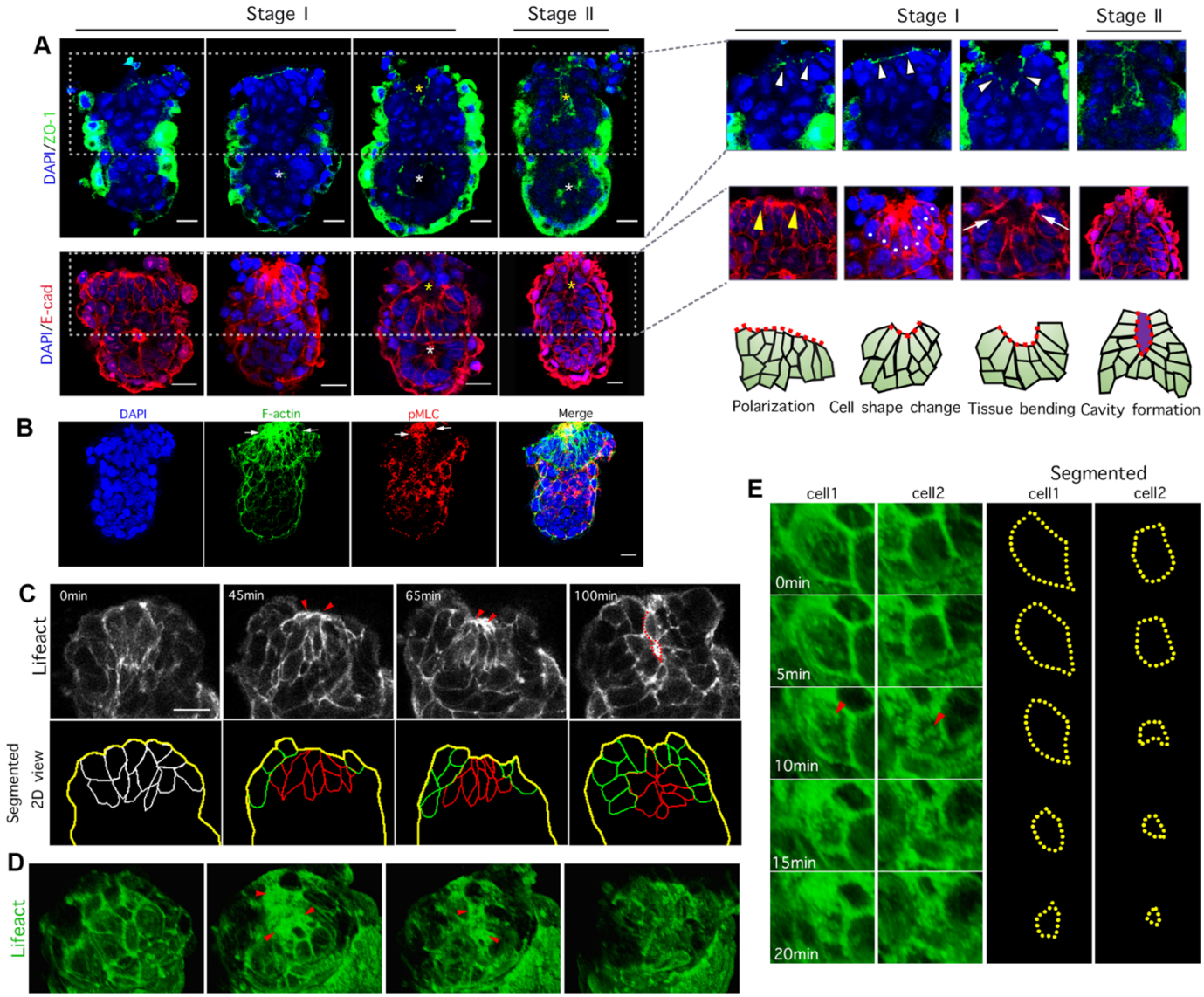

FIGURE 3.2: FORMATION OF THE EXTRAEMBRYONIC CAVITY

(A) Stages of extraembryonic cavity formation and polarity status of ExE cells. White asterisk denotes epiblast cavity and yellow asterisk denotes ExE cavity; white and yellow arrowheads point to apical domain of proximal-most cells of ExE; white dots annotate the cells undergoing cell shape changes i.e. apical constriction and elongation; white arrows point to the folding-in during invagination; scale bar = 20um. (B) Embryos fixed within the decidua prior to dissection and stained for actin and phosphorylated myosin light chain to ensure that cell shape change of proximal-most cells is not an artefact of the dissection or a wound healing response; scale bar = 20um. (C) Live imaging (5-minute time intervals) of LifeAct-GFP during transition from stage I to II; red arrowheads point to the actin-enriched domain and red-dotted line outlines the ExE cavity; red segmented cells are the cells undergoing shape changes while green cells are the surrounding cells moving around the point of invagination; scale bar = 20um. (D) Apical domain of proximal-most cells visualised *en face;* red arrowheads flank the actin-enriched domains. (E) Following the apical site of proximal-most cells during actin enrichment (red arrowheads) and segmented apical sites.

3.2.4 *Extracellular Matrix role in proamniotic cavity formation*

While the ECM has a key role in polarising the ExE cells and setting up the characteristic architecture described in the previous sections, it also appears to play a role in the formation of the PAC.

Treatment with COLIV as used previously to investigate the effect of BM on the polarity of ExE cells, also perturbed the formation of a unified cavity. Out of all the control embryos cultured overnight (~16 hours), 85.71% (n=21) of them had a unified cavity whereas 89.89% (n=27) COLIV-treated embryos failed to do so. Since COLIV digestion was sometimes partial as opposed to full, in the cases where only some of the BM was removed (3/27; 11.11%) the PAC formed normally (**Figure 3.6**).

3.2.5 *Multicellular rosettes form throughout the ExE*

The ExE tissue upon its expansion and formation of its cavity, appears to have a regular architecture, which as described in the previous sections involves the segregation of cells into the polarised, columnar outside cells and the apolar, more spherical inside cells (forming the bulk of the tissue). Further analysis of the microarchitecture of ExE revealed that multicellular rosette structures are formed during this period of development (**Figure 3.7A**).

Multicellular rosettes have been described before as a collection of polarised cells that contribute to a common central point. Rosettes can form in 2D monolayers or in 3D systems (e.g. MDCK cysts or the mouse embryo Epi). Staining for apical polarity markers (aPKC, ZO-1 and Par6) and active actomyosin contractility (pMLC) revealed foci in the ExE resulting from the contribution of multiple cells to a central common point (**Figure 3.7B**). Interestingly, these rosettes manifest as 3D structures in the tissue, and in contrast to the single 3D rosette that forms in the Epi required to form the cavity, in the ExE, multiple such rosettes were observed at the same time (**Figure 3.7C**). These rosette structures were identified throughout the ExE in a stage-dependent manner i.e. the average number of rosettes identified in stages IV and V was significantly reduced when compared to the previous stages (**Figure 3.7D**).

In ExE, 95% of these rosettes were made up of a combination of outside and inside cells. While normally inside cells were apolar with a fairly spherical morphology, upon contributing to rosettes they appeared polarised with an elongated shape (**Figure 3.8**).

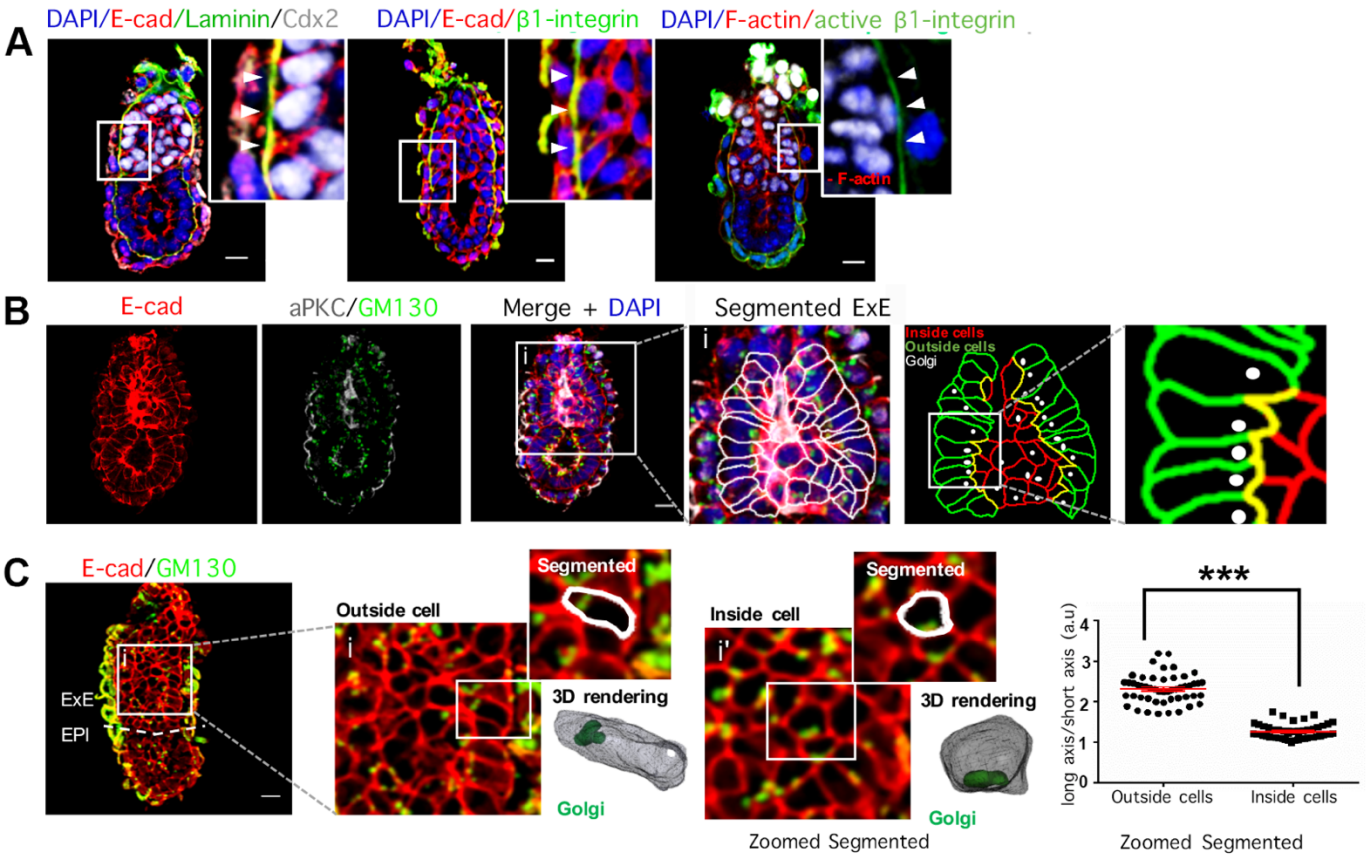

FIGURE 3.3:CHARACTERISATION OF EXE ARCHITECTURE

(A) Localisation of the BM (laminin) and active β1-integrin receptors (white arrowheads); E-cad = e-cadherin, adherens junctions' protein; Cdx2 = extraembryonic ectoderm marker. scale bar = 20um. (B) Image analysis of ExE architecture and the polarity status of outside and inside cells using golgi marker GM130 and apical polarity marker aPKC; scale bar = 20um. (C) Image analysis of outside and inside cell shape and quantification of cell aspect ratio (n=50, 6x E5.5 embryos) (unpaired student's t-test; ***<0.0001; scale bar =20um).

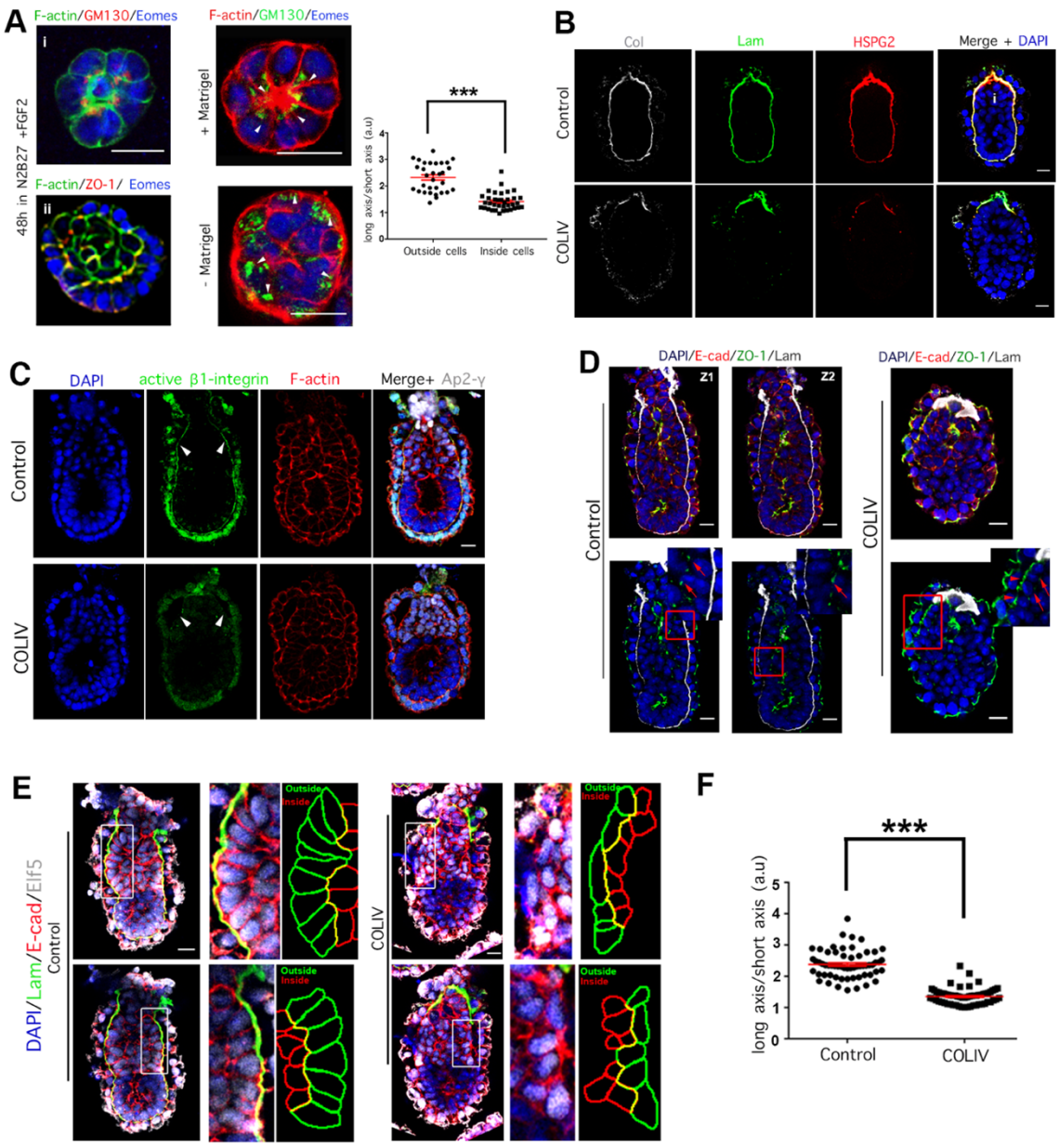

FIGURE 3.4: THE ROLE OF EXTRACELLULAR MATRIX ON POLARITY OF EXE CELLS

(A) TSCs suspended in Matrigel for 48 hours in N2B27 + FGF2 (example i and ii) and stained for polarity markers GM130 (golgi) and ZO-1 and cell aspect ratio quantification of outside cells; outside cells n=31, inside cells n=36; unpaired student's t-test; ***<0.0001; TSCs grown in Matrigel and the absence of Matrigel stained for golgi to assess polarity; TSCs also stained for Eomes, a TSC marker to confirm maintenance of TS stemness; white arrowhead points to the position of the golgi; scale bar = 20um. (B) Embryos treated with collagenase IV (COLIV) for 16 hours and stained for BM components; HSPG2 = perlecan; Lam = Laminin; scale bar 20um. (C) Collagenase IV-treated embryos and status of integrin activation (white arrowheads); AP2γ is a marker for ExE; scale bar =20um. (D) ZO-1 localisation of collagenase IV-treated embryos (red arrows); same embryos shown at 2 different z slices (z1 and z2); scale bar = 20um. (E) Embryos in the presence or absence of collagenase IV (COLIV) cultured from E5.5 for 16 hours and the morphology of outside cells; Elf5 = ExE marker; control n=12, COLIV n=13; scale bar = 20um. (F) Comparison of outside cells' aspect ratio (long axis/short axis) in control and COLIV-treated groups; ***<0.0001.

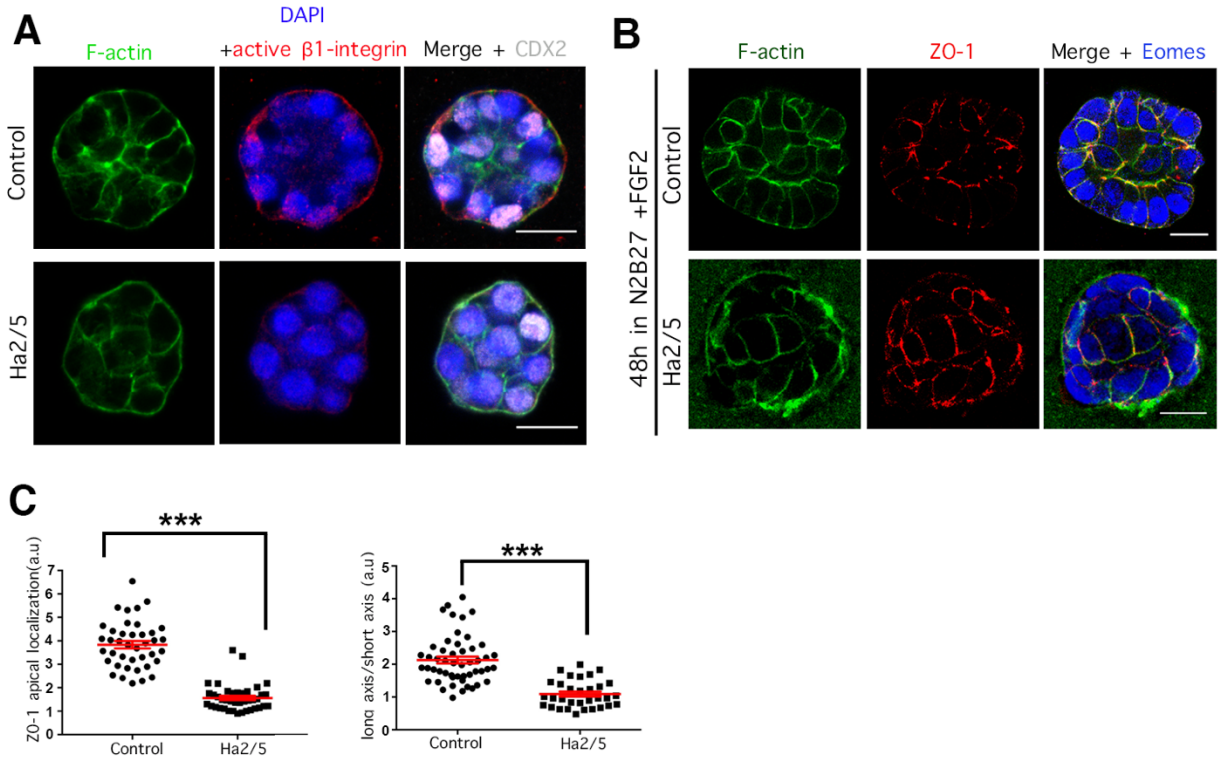

FIGURE 3.5: ROLE OF INTEGRIN SIGNALLING ON TSC AGGREGATES

(A) β-1 integrin signalling activation status in the presence and absence of the integrin function-blocking antibody; scale bar = 20um. (B) ZO-1 localisation in TSC aggregates after the addition of integrin function-blocking antibody 24 hours after plating; scale bar = 20um. (C) Comparison of ZO-1 apical localisation (apical ZO-1 average intensity / basolateral ZO-1 average intensity) and aspect ratio (long axis / short axis) of TSC aggregates' outside cells between control and Ha2/5-treated aggregates; ***<0.0001

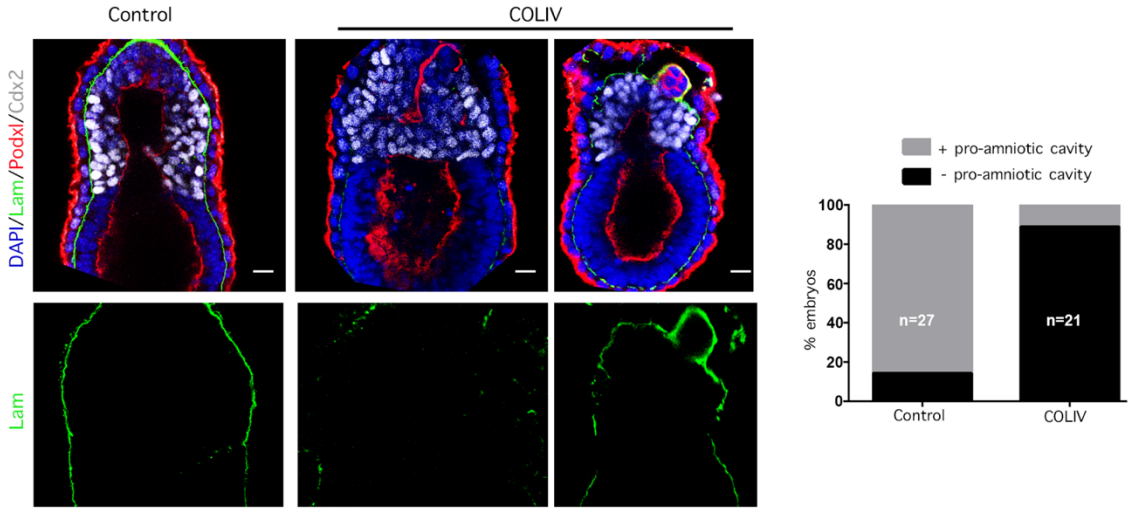

FIGURE 3.6: ROLE OF EXTRACELLULAR MATRIX ON PROAMNIOTIC CAVITY FORMATION

Full and partial digest of the surrounding BM through treatment with collagenase IV (COLIV) for 16 hours and quantification of percentage of embryos with a PAC in control and treated groups; scale bar = 20um

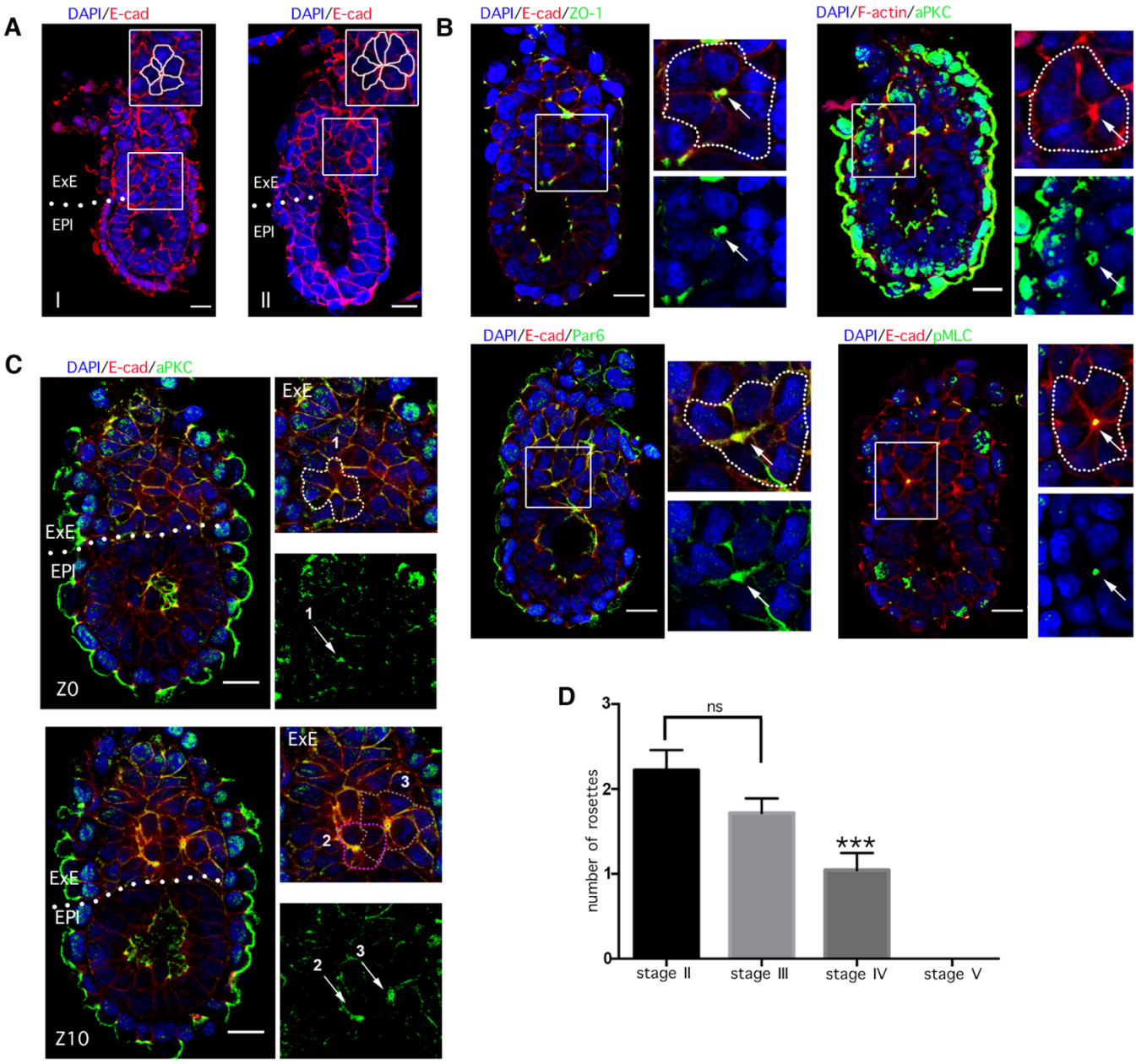

FIGURE 3.7: FORMATION OF ROSETTES IN THE EXE

(A) Two examples from different embryos (I and II) showing a rosette structure in each; scale bar = 20um. (B) Rosette structures (outlined with dashed lines) identified in embryos stained for different apical markers and pMLC, frequently observed in centres of rosettes; white arrows point to the middle of the rosettes; scale bar = 20um. (C) A representative example of an embryo with multiple rosette structures found in different planes (z0 and z10); arrows point to the middle of rosettes; scale bar = 20um. (D) Quantification of number of rosettes found per embryo based on the PAC staging system; ***<0.0001.

3.2.6 *CELLS IN ROSETTES CAN BE BIPOLAR*

The rosettes were seen to localise to different sites of the ExE and often were either adjacent to other rosettes or to either of the two cavities (annotated rosette "2" in **Figure 3.9; Figure 3.10A, 3.11A**). Detailed analysis of such rosettes showed that rosette cells can be bipolar, i.e. displaying two apical sites.

When two rosettes were found in close proximity to each other, quite often they were found to share at least one cell i.e. the shared cell contributed to the centre of both rosettes. Such cells displayed two apical sites and were thus dubbed 'bipolar' (**Figure 3.9**).

Similarly, rosettes adjacent to a cavity had at least one cell contributing to both the centre of the rosette as well as the cavity; again, displaying one apical site at the centre of the rosette and one at the site of the cavity (**Figure 3.9A**).

3.2.7 *ROSETTE FORMATION DEPENDS ON ECM/β1-INTEGRIN SIGNALLING*

Rosettes are made up of both outside and inside cells. As described in previous sections, the outside cells polarise through integrin-mediated signalling, activated by the underlying BM. Since inside cells only appear polarised when contributing to a rosette, it was hypothesized that the polarised outside cells provide the polarity cue for the inside cells to polarise in such a way so as to promote rosette formation. According to this hypothesis, the polarisation of the outside cells is instrumental in generating rosettes.

To test this, E5.5 embryos were freshly recovered from the mother and cultured for 5 hours in the presence of COLIV. At the end of the treatment, the BM was fully digested and as expected, the outside cells lost their polarisation (as also described in previous sections) (**Figure 3.10A**). Analysis of the treated embryos to identify rosette structures revealed that 92% of the COLIV-treated embryos had no rosettes (n=12); in contrast, all of the control embryos had rosettes (n=12)(**Figure 3.10B**).

These results suggested that ECM/β1-integrin signalling, required for the polarisation of the outside cells, is also required for the generation of rosettes within the ExE tissue. Potentially, some unidentified polarity cue stemming from the polarised outside cells directs the adjacent inside cells to polarise to contribute to rosette formation (**Figure 3.10C**).

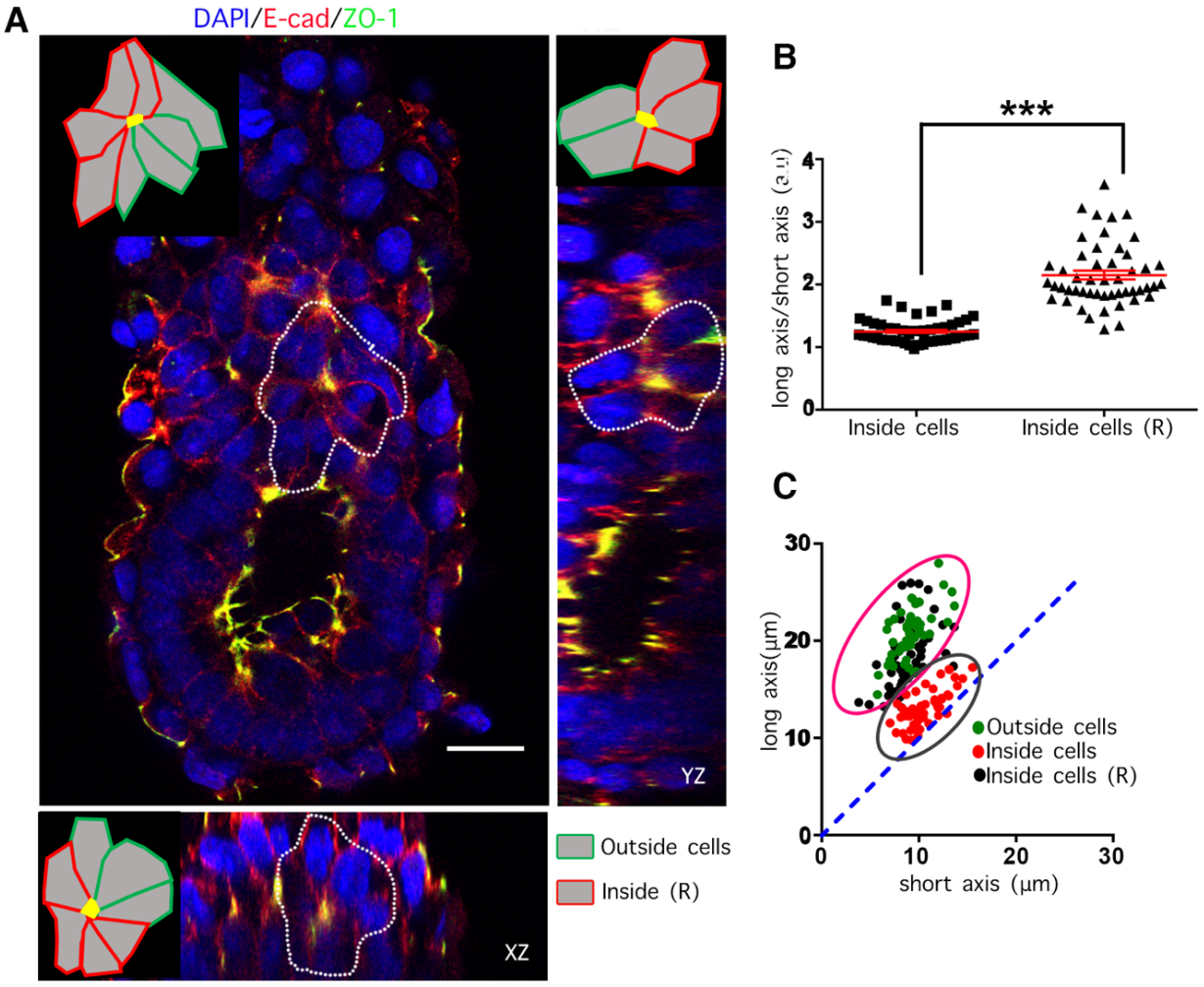

FIGURE 3.8: OUTSIDE AND INSIDE CELLS CONTRIBUTE TO EXE ROSETTES

(A) Representative example of an E5.5 embryos with a rosette made up of outside cells and inside cells (R = rosette); scale bar = 20um (B) Cell aspect ratio comparison of inside cells in rosettes (R) and inside cells with no contribution in rosette structures; ***<0.0001. (C) Plot of cell axes, colour coded to distinguish cells on the outside, inside and inside cells contributing to rosette; magenta circle highlights that outside and inside rosette cells have similar dimensions whereas inside cells cluster together near the y=x line (blue dashed line) which denotes a less columnar and more rounded morphology.

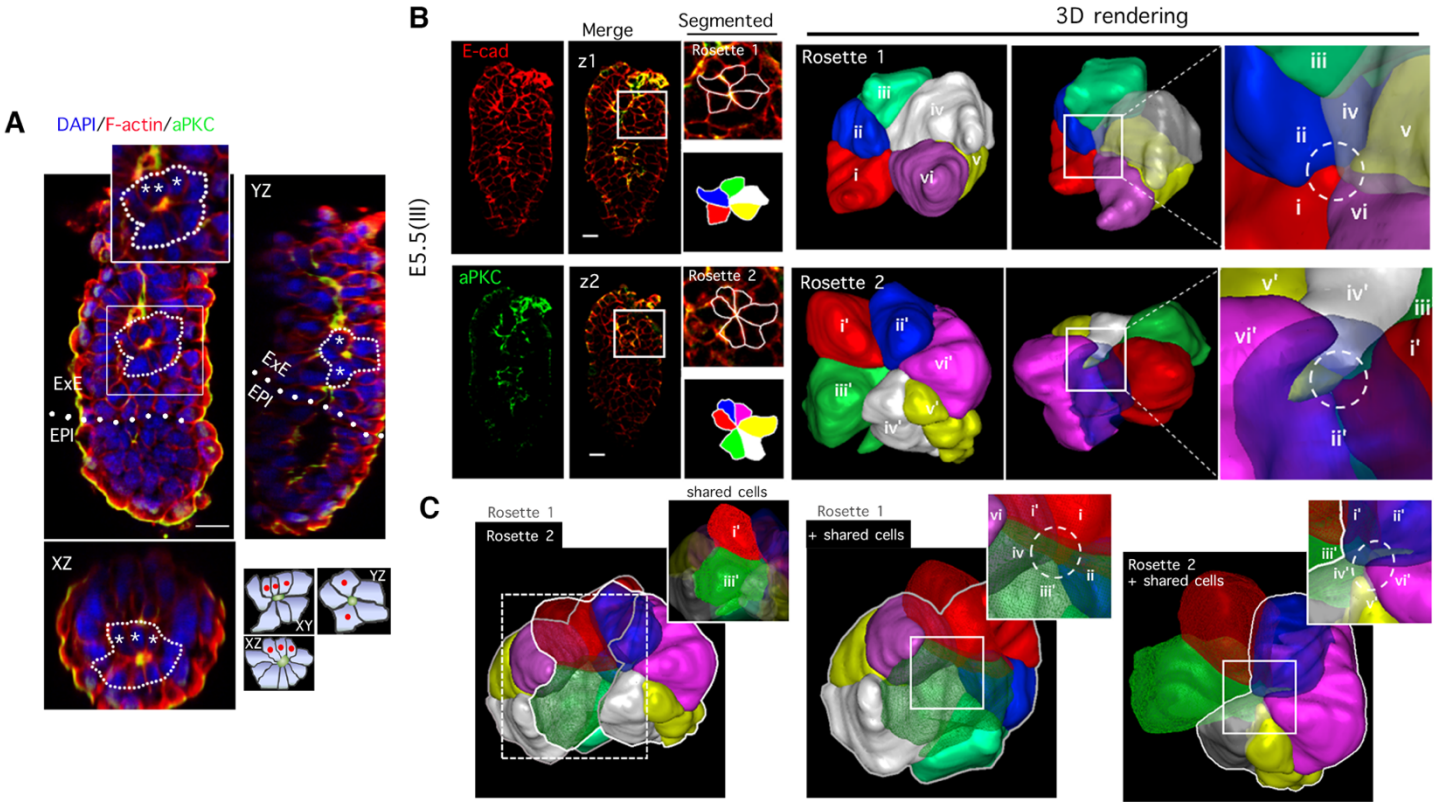

FIGURE 3.9: BIPOLARITY OF EXE CELLS CONTRIBUTING TO ROSETTES

(A) An example of a stage III E5.5 embryo with an ExE rosette with bipolar cells (white asterisks); segmentation at bottom right of panel; scale bar = 20um. (B) A stage III E5.5 embryo with two rosettes stacked on top of each other (z1 and z2 planes); cells of rosette 1 and 2 are arbitrarily coded for clarity and also annotated with latin numerals (i-vi; i'-vi'); scale bar = 20um. (C) Stacked rosettes from (B) put together to identify shared cells i.e. cells that contribute to both rosette centres.

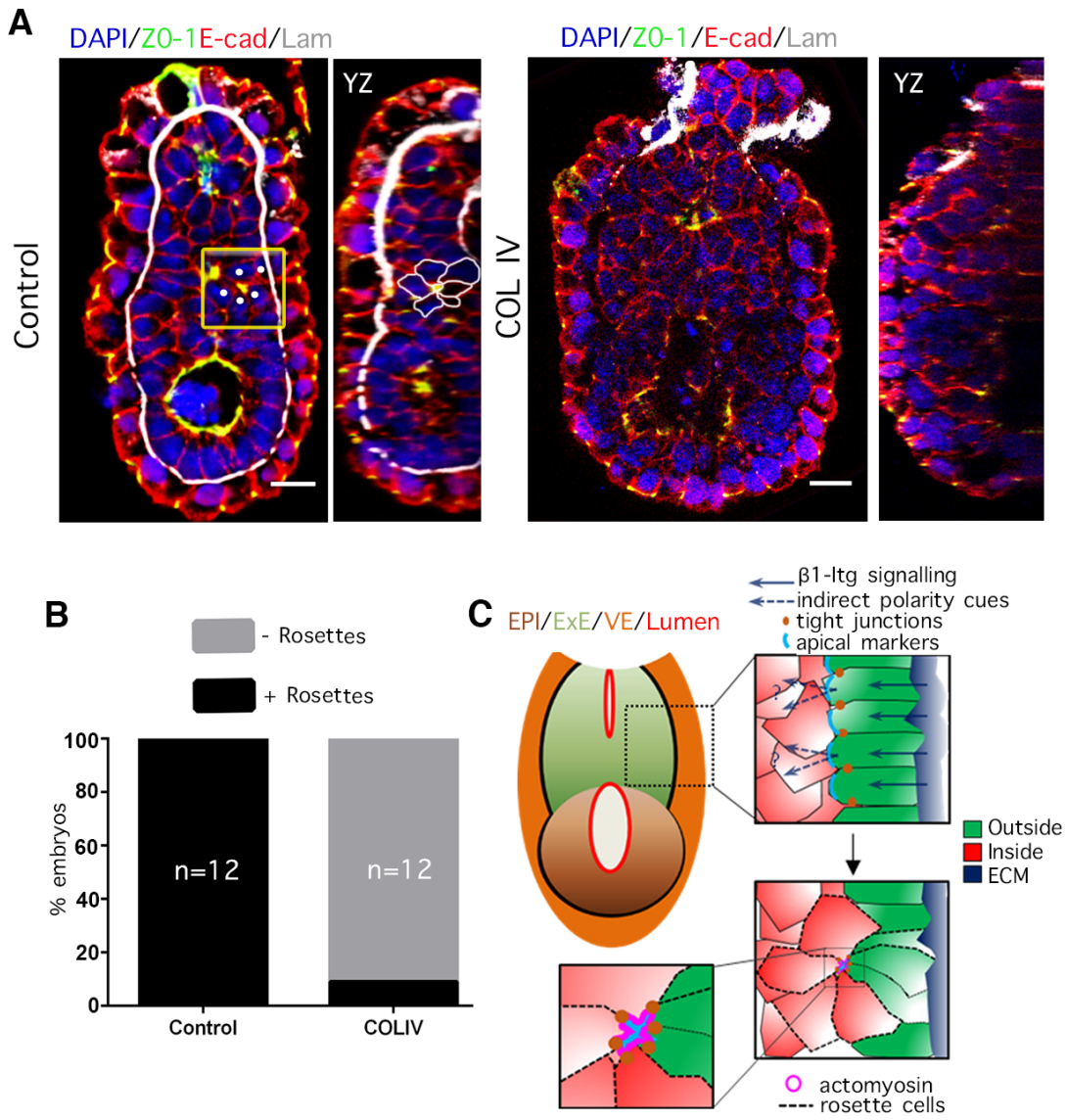

FIGURE 3.10: THE ROLE OF EXTRACELLULAR MATRIX IN ROSETTE FORMATION

(A) Collagenase IV (COLIV)- treated embryos assessed for rosette presence. The ExE appears disorganised with no apical marker foci characteristic of rosettes; scale bar = 20um. (B) Quantification of percentage of embryos with rosettes in control and COLIV-treated; n=12 for both groups. (C) Schematic for rosette formation through β1-integrin signalling from underlying ECM (extracellular matrix).

3.2.8 ROSETTE RESOLUTION DRIVES EPIBLAST REORGANISATION

The loss of PAC formation when disrupting the microarchitecture of the ExE tissue (i.e. the formation of rosettes), in turn suggested a possible role of the rosettes in the progression and fusion of cavities. While rosettes have been shown to be involved in branching morphogenesis in flat epithelia such as pancreatic explants, there are no current known systems in which 3D rosettes drive progression of cavities. To investigate

this possibility, freshly recovered, fixed and stained embryos were analysed at the different stages of PAC formation as described in previous sections.

At stage II, where the Epi has a spheroid morphology (and prior to Epi cavity progression), a rosette was identified at the Em-ExEm boundary composed of cells from both Epi and ExE; these types of rosettes were termed 'hybrid rosettes' (Figure 3.11A). Formation of this rosette was preceded by the breakdown of the BM that transiently forms between the polar trophectoderm and the Epi (Figure 3.11B).

Following this stage, the Epi reorganised into a cup-shaped epithelium and thus the rosette initially present at the boundary was lost. To test the hypothesis that the resolution of this hybrid itself is the driver of Epi reorganisation, embryos were analysed at intermediate stages between stages II and III (i.e. during Epi reorganisation at the boundary). This was achieved by examining both fixed preparations and live imaging movies of LifeAct-GFP embryos allowing for cell shape monitoring and actin dynamics (Figure 3.12A, B).

Analysis of the stages during reorganisation suggested that cells at the boundary had an 'open' rosette conformation (resolving rosette in Figure 3.12A). While Epi cells still contributed to a common central point with the adjacent ExE cells, their lateral membranes were separated; this was preceded by formation of a polarised tract along these membranes to the centre of the hybrid rosette (Figure 3.13A). The active actomyosin contractility in the centre of these resolving rosettes appeared reduced following this stage. The Epi cells at the boundary moved further apart and reset their apico-basal polarity perpendicular to the PD axis of the embryo (resolved rosette in Figure 3.12A).

To confirm this sequence of events, LifeAct-GFP (marking actin) embryos were recovered at early E5.5 just prior to stage III to capture this transient stage of hybrid rosette resolution. As suggested from the analysis of the fixed samples, the hybrid rosette at the boundary resolved by first losing the cell-cell adhesions on the lateral membranes of the Epi cells, followed by a decrease in actin enrichment at the centre of the rosette. The rosette then resolved, allowing Epi cells at the boundary to drift apart in opposite directions and reorganise the tissue (Figure 3.12B). It was interesting to note that during this process rosettes started to form in the ExE as well, adjacent to the site of hybrid rosette resolution (yellow outline in ExE rosette at 80 mins in Figure 3.12B).

To experimentally address the requirements for hybrid resolution i.e. loss of cell-cell adhesion on the lateral membranes and reduction in actomyosin contractility at the centre of the rosette, E5.25-E5.5 LifeAct-GFP embryos were recovered and laser ablated at the interface of the Epi lateral membranes in the hybrid rosette. This resulted in membrane separation allowing for cavity progression to the boundary (Figure 3.13B). By avoiding the ablation of the rosette centre the 'open' hybrid conformation was maintained. Interestingly, the actin enrichment at the centre of the rosette persisted for the duration of the 23 minutes of imaging after

ablation which contradicts the analysis of movies of natural hybrid resolution (**Figure 3.13B**). In natural resolution, the actin enrichment is lost in the same timeframe which may suggest that membrane separation and loss of the actomyosin contractility at the centre are normally coordinated.

3.2.9 Resolution of ExE rosettes drives proamniotic cavity formation

During resolution of the hybrid rosette as described above, rosettes are already forming within the ExE tissue. Quantification of the number of rosettes per stage of PAC formation revealed that on average 2 rosettes are present at any given time prior to progression of the cavity, whereas this decreased to 1 later on (**Figure 3.7D**).

This decrease in number of identifiable rosettes was accompanied by cavity progression into the ExE. This suggested that there could be a link between resolving rosettes and the embryo's progression to stage IV of PAC formation, conceptually extending the paradigm from hybrid rosette resolution and Epi reorganisation.

There are several studies investigating the role of 2D rosettes in branching morphogenesis, tissue shaping, organ development and even collective cell migration (Lecaudey et al., 2008; Shindo, 2018; Trichas et al., 2012; Villasenor et al., 2010). Rosettes appear to co-ordinate and organise tissue in small epithelial bundles that facilitate morphogenetic events. In the system described here, the rosettes assume a 3D profile (i.e. cells contribute to a central point from all axes as opposed to only the planar axis in 2D) as described in previous sections. This raised the question whether behaviours mediated by well-described 2D rosettes, also apply in this 3D context.

The most relevant systems that have been described in literature which involve morphogenesis and 3D rosette-mediated reorganisation include ESC rosettes (generated by suspending single ES cells in Matrigel) which resolve by membrane separation at the centre to form an expanding lumen (this is also a similar system to Matrigel-suspended MDCK rosettes) and *in vivo* tubulogenesis where cell membranes are separated at a common central point to allow for lumenogenesis at the centre of the developing tubule.

Initially a hypothesis was formulated to fit the model previously described for the formation of the pancreatic plexus. In that system, multiple rosettes form in the developing tissue. This is followed by cavitation at the centre of these rosettes and finally joining of the cavities through polarised tracts to form the plexus. Indeed, in the system described in this thesis, rosettes were found to be connected with the progressing cavities (Epi or ExE cavity) by the apical polarity markers aPKC and ZO-1 clusters giving the appearance of polarised tracts (**Figure 3.13A, 3.14**).

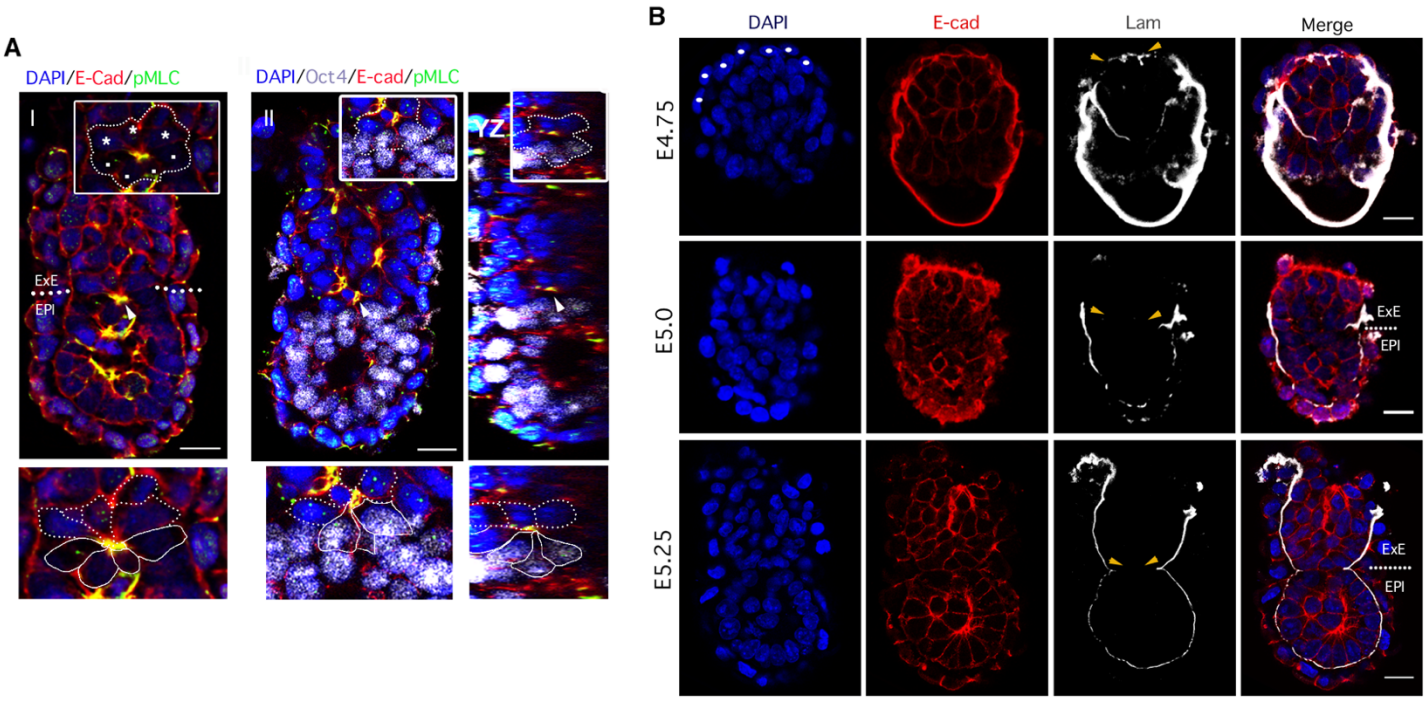

FIGURE 3.11: ROSETTE FORMATION AT THE EMBRYONIC-EXTRAEMBRYONIC BOUNDARY

(A) Two representative examples of rosette forming at the Em-ExEm boundary (hybrid) rosette (white arrowhead); white asterisks = ExE cells, white dots = Epi cells; dotted segmented cells = ExE cells, solid line segmented cells = Epi cells; scale bar = 20um. (B) Presence of BM (Laminin) between Epi and ExE (yellow arrowheads) prior and during presence of hybrid rosette; white dots = polar trophectoderm (cells that develop to ExE); scale bar = 20um

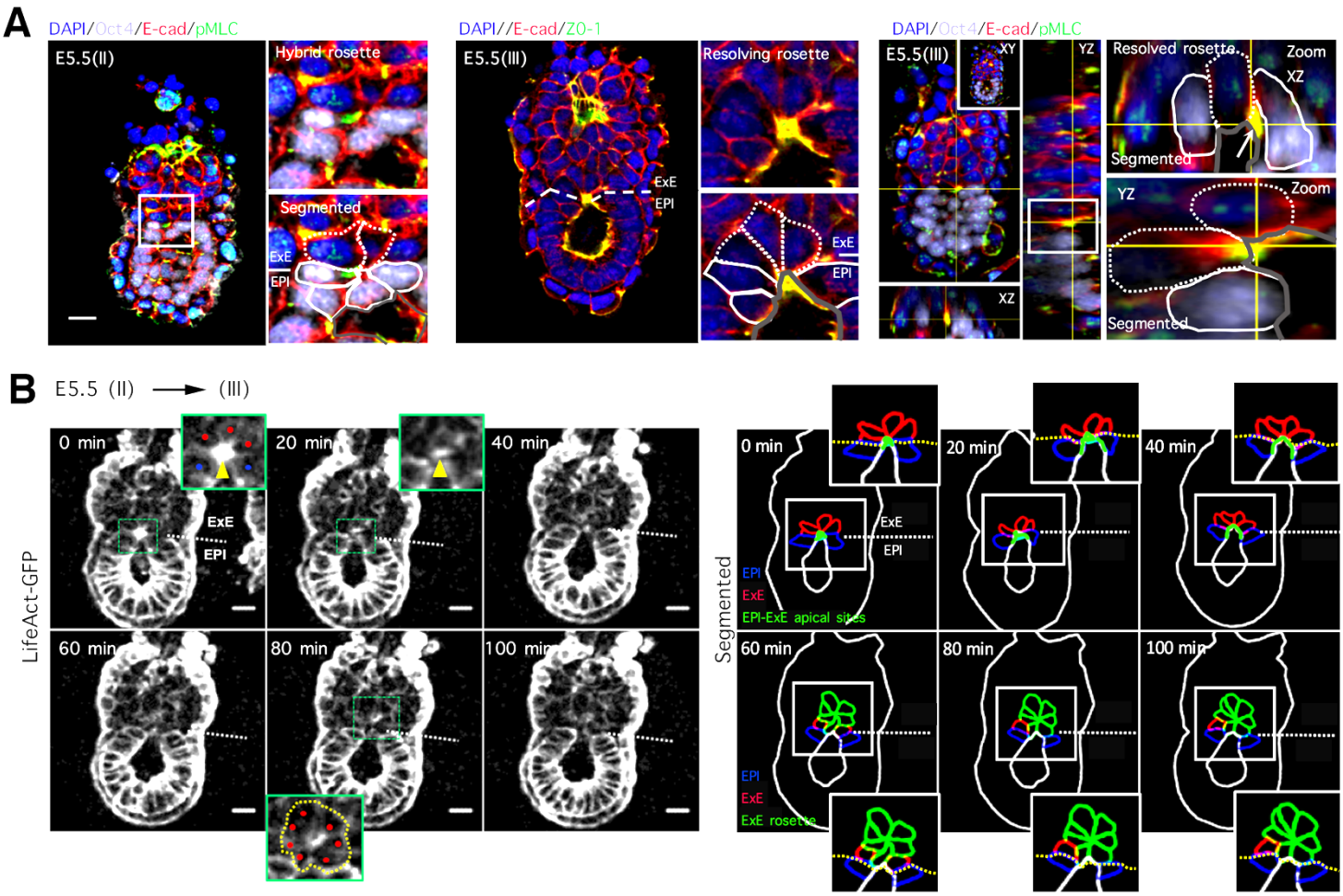

FIGURE 3.12: HYBRID ROSETTE RESOLUTION REORGANISES THE EPIBLAST

(A) Fixed samples from successive stages of hybrid rosette resolution (stage II and III); Zoomed panels focus on the hybrid rosette; white dotted line = ExE cells, white solid line = Epi cells; white arrow points to remnants of phosphomyosin enrichment that remains between Epi and ExE cells after resolution of the hybrid rosette; scale bar = 20um (B) Time-lapse imaging (20 min time intervals) of stage II LifeAct-GFP embryos going to stage III. A hybrid rosette is indicated by a yellow arrowhead evident from the actin enrichment which is lost upon its resolution. Soon after the resolution (at 80 mins) an ExE rosette appears adjacent to the resolved hybrid rosette (yellow dotted outline and red dots indicate the cells iof ExE rosette); blue dots = Epi cells, red dots = ExE cells; segmented version of the time-lapse movie on the right of the panel; scale bar = 20um.

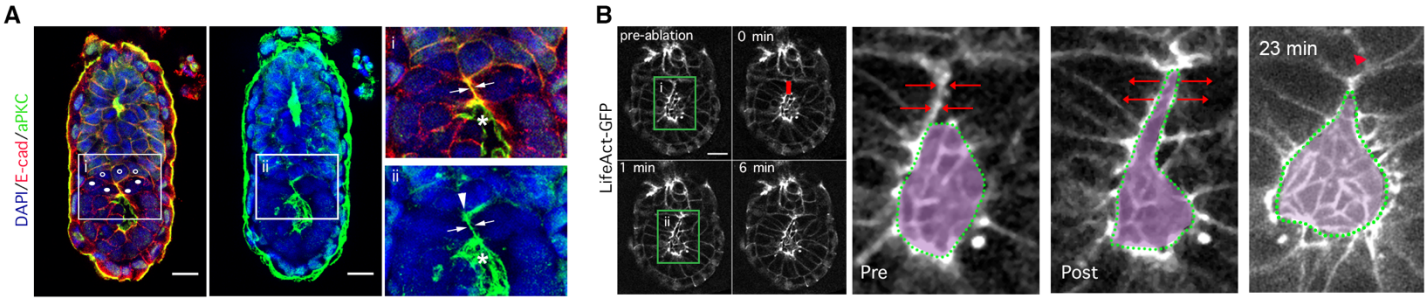

FIGURE 3.13: LATERAL MEMBRANES OF EPI CELLS SEPARATE TO RESOLVE HYBRID ROSETTE

(A) The lateral membranes of Epi cells in the hybrid rosette form a polarised tract indicated by the apical marker aPKC (white arrows) connecting the Epi cavity (white asterisk) with the rosette's centre (white arrowhead); white circles = Epi cells, open circles = ExE cells; scale bar = 20um. (B) Laser ablation at the interface of the Epi lateral membranes of the hybrid rosette; red bar indicates the site of ablation and red arrows indicate the trajectory of the lateral membranes just after ablation; red arrowhead = centre of hybrid rosette after ablation; purple mask = Epi cavity; scale bar = 20um

Similar to the analysis performed on the hybrid rosette, embryos were collected between stages III and IV (i.e. between the Epi reorganisation and the Epi cavity invasion into the ExE) to capture the different steps of ExE rosette resolution. In the late stage III the Epi cells at the boundary were reorganised to give the Epi its cup-shaped morphology but more importantly, adjacent to this most-proximal site of the Epi cavity, a rosette can be identified that has its centre joined to the Epi cavity via a polarised tract (ZO-1 cluster in between) (**Figure 3.14**).

In early stage IV a discernible thin cavity extension that leads to the centre of what can still be distinguished as a rosette (**Figure 3.14**). This was surprising as the membrane separation along the polarised tract observed at late stage III was not preceded by microlumen formation through opening of the rosette as shown in the pancreatic plexus model. This suggested that PAC formation was not a result of fusion of multiple microlumens but rather a progressive event.

To confirm the sequence of events and conclusions drawn from the fixed sample data, embryos during the stage III to IV transition were live imaged using the LifeAct-GFP reporter mouse line. Indeed, a rosette adjacent to the Epi cavity formed and resolved, while the cavity was extending into the ExE (**Figure 3.15A**). As revealed from the fixed sample data, the cells of the rosette directly abutting the Epi cavity lost their attachment to each other through lateral membrane separation resulting in an 'open' rosette conformation (as mentioned previously during hybrid rosette resolution). Moreover, this extension of cavities through rosette resolution is

not restricted to the Epi cavity but appears to take place in the ExE cavity as well (**Figure 3.15B**). As expected from the fixed sample data, there was no microlumen forming in the middle of the rosettes prior to resolution.

3.2.10 Spatiotemporal transcriptome during Proamniotic cavity formation

The morphogenetic events that reorganise and reshape the ExE to accommodate the extension and final fusion of the cavities to form the PAC are quite extensive. A combination of polarity acquisition and active cellular events drive the PAC formation as described in the previous sections. It was thus interesting to investigate whether there is some active regulation of these processes at the transcriptomic level.

To address this, a method of sample acquisition and sequencing was implemented as described in Chen et al., (2017), Peng et al., (2016) and 'Materials and Methods' section **2.14** of this thesis (**Figure 3.16A)**. Collected sample from stages E5.25, E5.5 and E5.75 was sent to collaborators at the Shanghai Institute of Biochemistry and Cell Biology (SIBCB; group of Jing Naihe) for processing. Slicing, sequencing and analysis was performed by the collaborators.

According to analysis correlating these three temporal stages to the PAC formation stages (as described in previous sections), they represent three major steps in the unification of cavities; E5.25 embryos are in stage I, E5.5 embryos are either stage II or III, E5.75 embryos are either stage IV or V (**Figure 3.1D**). The main events of PAC formation occur between stage III and IV, so it was expected that transcriptomic analysis between E5.25 and E5.75 as well as E5.5 and E5.75 would reveal differences that could help identify key regulators in ExE reorganisation.

Principal component analysis (PCA) provided by Ran Wang (Naihe group, SIBCB) showed that the ExE of E5.25 and E5.5 (i.e stages I-III) cluster together whereas E5.75 (i.e. stages IV and V) segregated (**Figure 3.16B**). This is in support of the initial hypothesis and consistent with the observation that the most dramatic cellular rearrangements in the ExE take place between stages III and IV-V. PCA was also used to cluster together the slices for each stage and confirm Epi segregation from ExE (**Figure 3.16C**). For further validation, specific Epi and ExE markers were checked on the generated corn plots (Cdx2 and Pou5f1 (Oct4)) (**Figure 3.16D**).

3D models of lumenogenesis as well as the mouse Epi model of rosette resolution during implantation have suggested that membrane separation involves exocytosis of Podxl, a highly charged protein that once secreted, remains associated with the apical membrane and promotes membrane separation by charge repulsion (Nielsen and McNagny, 2008). Gene ontology on the sequencing revealed that exocytosis factors like Rab11a, Stx3 and Snx18 are more differentially and highly expressed in stages E5.25 and E5.5 when

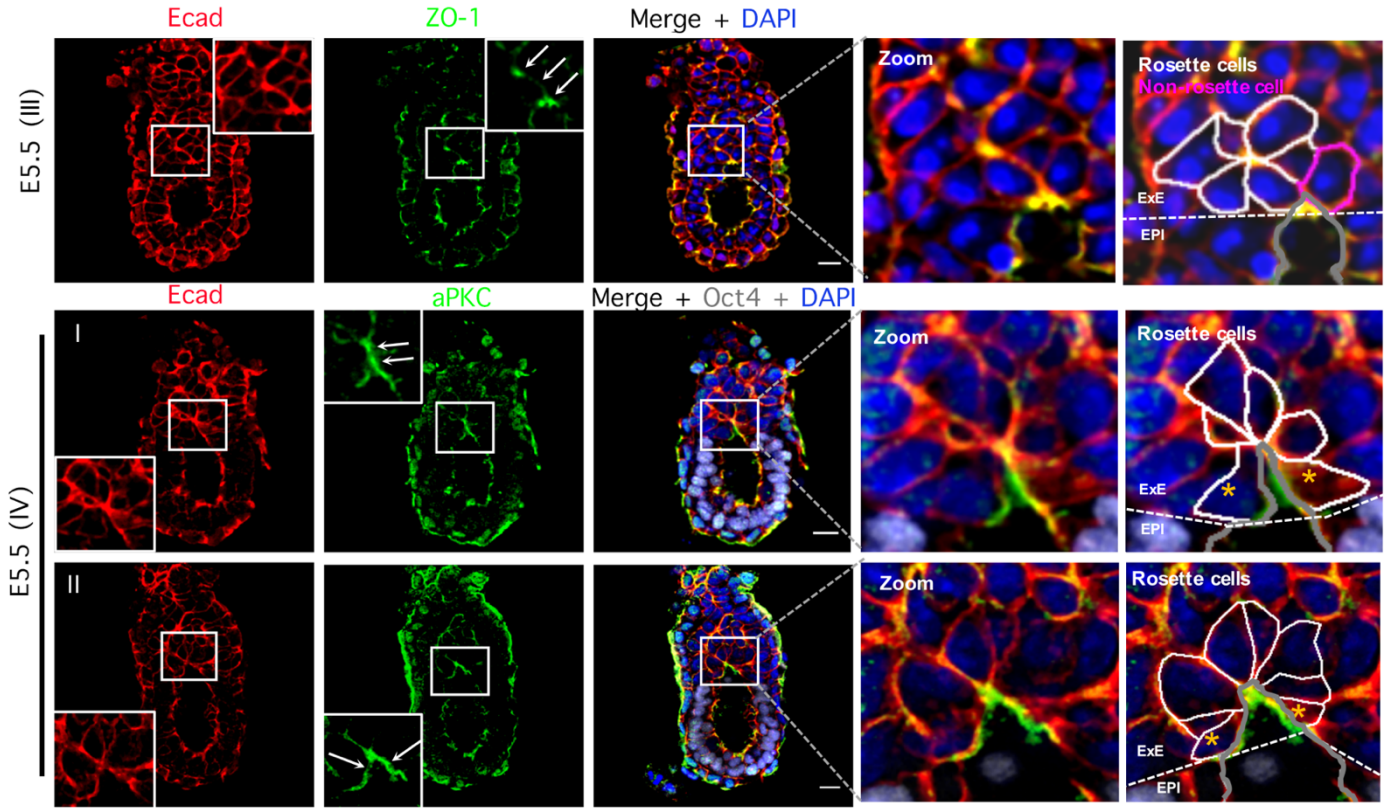

FIGURE 3.14: EXE ROSETTE RESOLUTION DRIVES EPI CAVITY PROGRESSION

Successive stages of ExE rosette resolution from stage III to stage IV. Polarised tracts = white arrows. At stage III the epiblast at the boundary is reorganised exposing the Epi cavity to the ExE while an ExE rosette is found directly adjacent to it (white segmented cells). Stage IV embryos shows the lateral membranes being separated driving the extension of the Epi cavity (orange asterisks); scale bar = 20um.

compared to E5.75. Very strikingly the exocytosis organiser Annexin a2 (Anxa2) is highly and differentially expressed at E5.25 and E5.5 whereas at E5.75, at which stage most of the PAC formation process is complete and rosettes have resolved, the expression of Anxa2 decreases.

Annexin was shown before in MDCK cysts to direct the polarised exocytosis of Podxl during lumenogenesis and is therefore very relevant to the mechanism suggested here (Martin-Belmonte et al., 2007). While Podxl involvement in membrane separation as described above would be expected to follow a similar transcriptomic profile as that of the exocytosis genes described above, the difference in Podxl expression between stages is only marginal. However, for the purposes of membrane separation the limiting factor is its secretion. Exocytosis genes involved in Podxl secretion are more highly expressed at stages E5.25 and E5.5.

Collectively, this data suggested that indeed regulation at the transcriptional level may be responsible for the resolution of rosettes and the process of cavity unification through expression of genes of the exocytotic pathway.

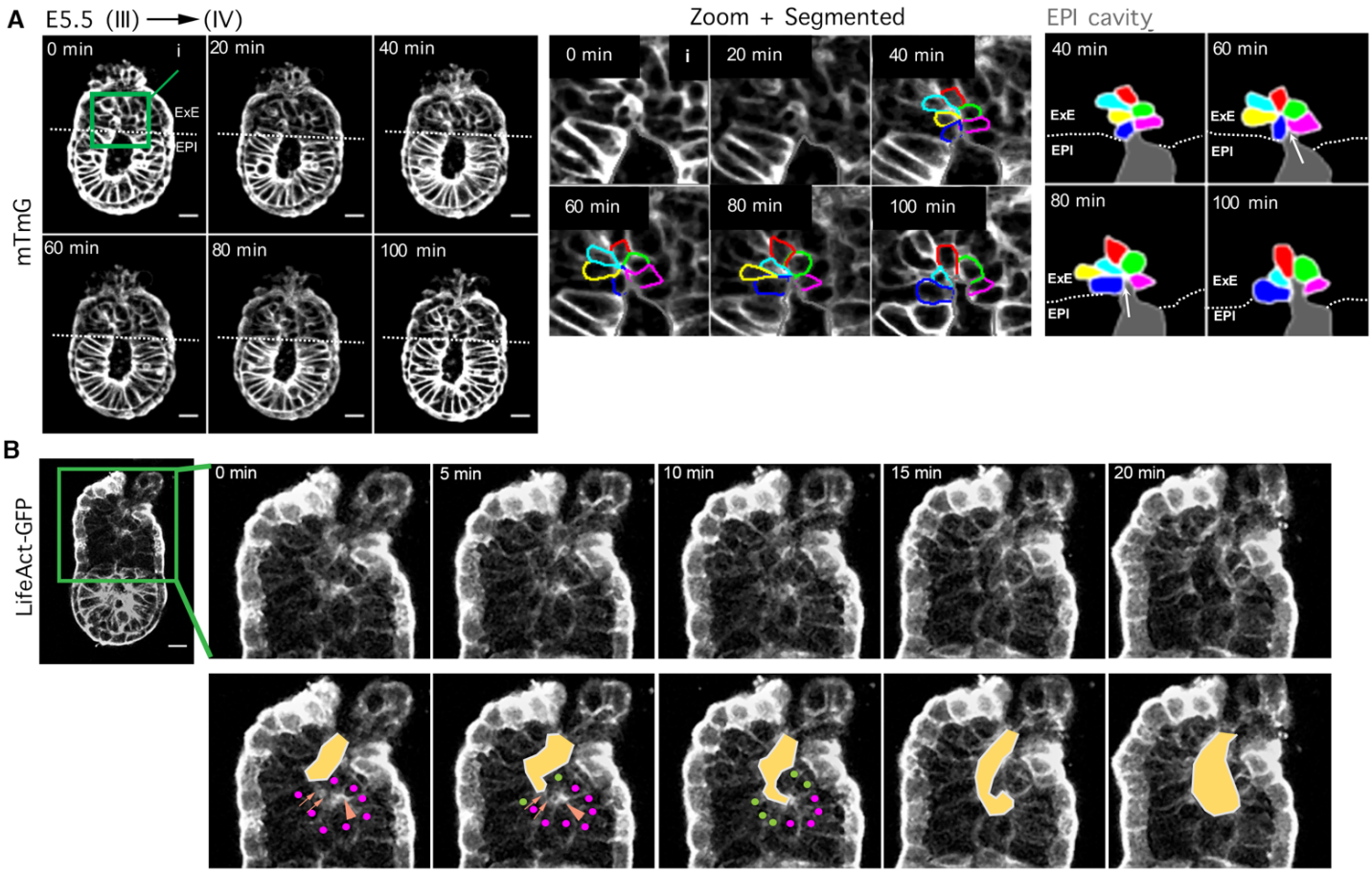

FIGURE 3.15: TIME-LAPSE MOVIES OF EXE ROSETTE RESOLUTION EXTENDING EPI AND EXE CAVITY

(A) Time-lapse images (20 min in intervals) of mTmG embryos progressing from stage III to IV. Segmented portion of the ExE where the ExE rosette adjacent to the Epi cavity resolves by separating the lateral membranes of cells in contact with the cavity and the rosette centre (white arrow; blue and magenta cells); scale bar = 20um. (B) ExE cavity extending to the centre of an adjacent ExE rosette (purple arrowhead; purple dots); green dots = ExE cells losing contact with each other to extend the cavity; ExE cavity coloured yellow; scale bar = 20um

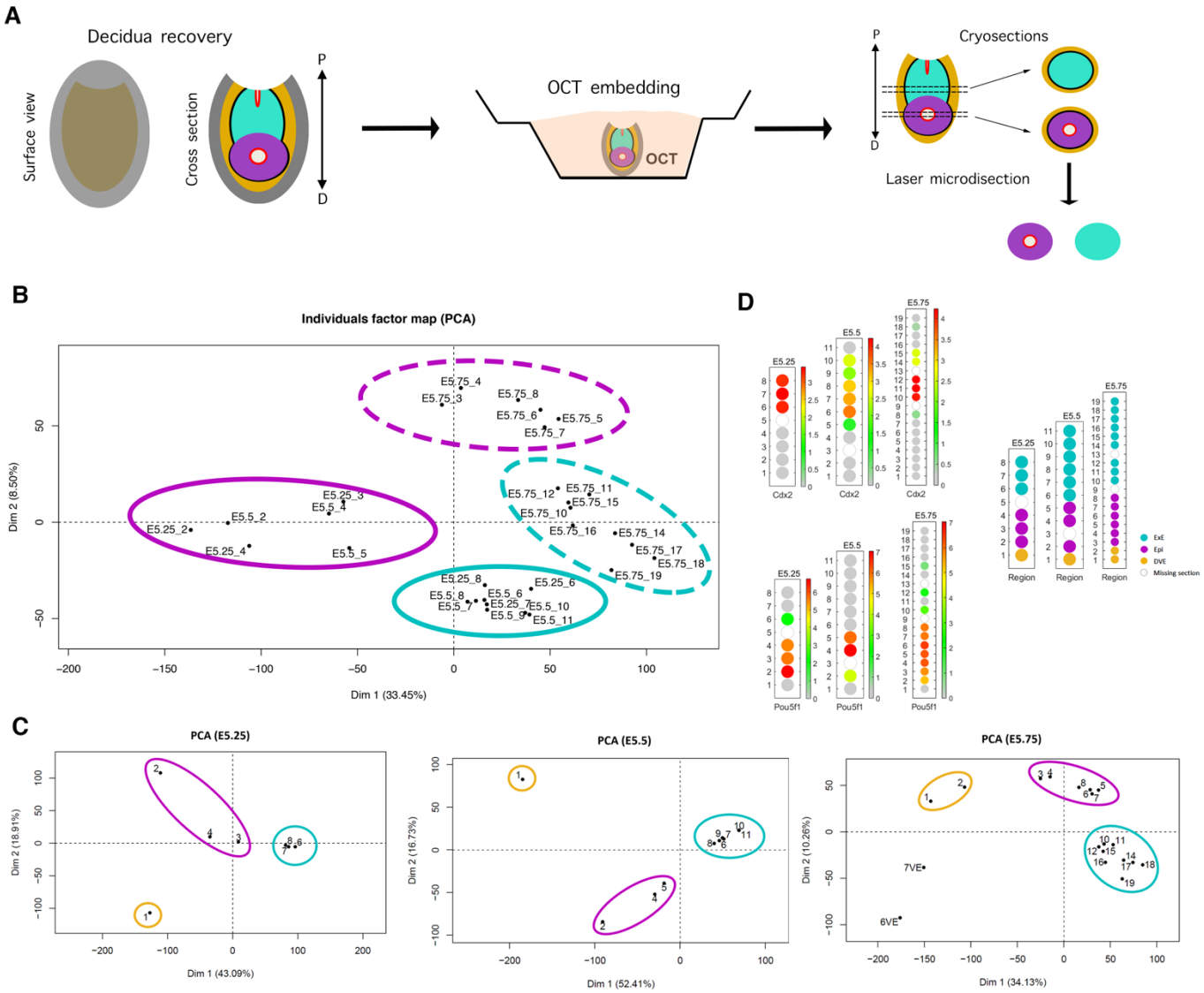

FIGURE 3.16: CONFIRMING SEQUENCING RESULTS

(A) Schematic of procedure to freeze recovered deciduas in OCT followed by laser capture microdissection along the proximo-distal axis; cyan = ExE, purple = Epi, yellow = VE P = proximal, D = distal. (B) PCA of all slices from all stages. E5.25 and E5.5 epiblast samples cluster together (solid purple circle); E5.25 and E5.5 ExE samples cluster together (solid cyan circle); E5.75 epiblast samples cluster away from epiblast samples of E5.25 and E5.5 (dashed purple circle); E5.75 ExE samples cluster away from the ExE sample of E5.25 and E5.5 (dashed cyan circle. (C) PCAs of the three different stages clustering the samples from the slices of epiblast (purple), ExE (cyan) and distal VE (yellow). (D) Corn-plots (graphical representations of relative gene expression between slices of the embryo) for Cdx2 and Pou5f1 (Oct4) confirming sequencing results of epiblast vs ExE. Colour coding represents $\log_2$(FPKM+1) values. PCA analysis and corn-plots generated by Ran Wang (Naihe group, SIBCB).

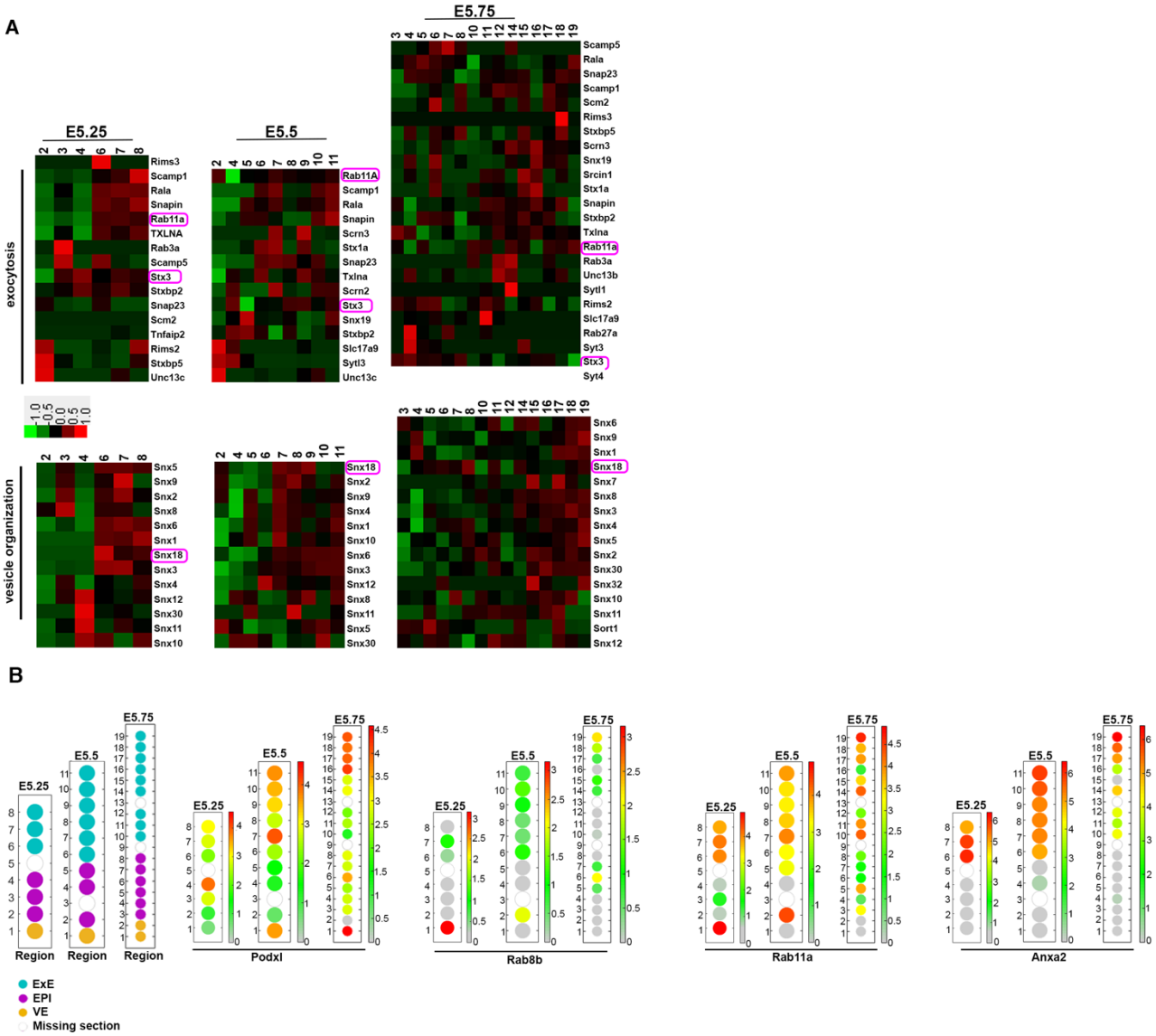

FIGURE 3.17: TRANSCRIPTOMIC ANALYSIS FOR EXOCYTOSIS-RELATED GENES

(A) Differential gene expression analysis heat maps for gene ontology terms: exocytosis, vesicle organization. E5.25: sections 2-4 EPI, sections 6-8 ExE; E5.5: sections 2,4,5 EPI, sections 6-11 ExE; E5.75 sections 3-8 EPI, sections 9-19 ExE. Purple outlines highlight genes previously reported to be involved in lumen formation. (B) Corn plots of selected genes involved in exocytosis and membrane separation during post-implantation development for the three sequenced temporal stages E5.25, E5.5 and E5.75; Colour coding of corn plots represents log2(FPKM+1) values (FPKM: fragment per kilobase per million); key for slice annotation presented on the left of the panel. Heat maps and corn-plots generated by Ran Wang (Naihe group, SIBCB).

3.2.11 PODCALYXIN-FILLED VESICLES ACCUMULATE AT THE INTERFACE OF POLARISED TRACTS PRIOR TO ROSETTE RESOLUTION

The data acquired from the sequencing results was very useful in pointing out the major players in the exocytotic pathway that are expressed concomitantly with the process of PAC formation. Having this data, it was important to confirm the results at the protein level and elucidate the localization of these in the context of the microarchitecture of the ExE described above.

To validate the sequencing data, the highly differentially expressed exocytotic organiser Anxa2 was confirmed by immunostaining. Indeed, as suggested by the sequencing results, Anxa2 is specifically expressed in the ExE (Figure 3.18A).

Rab11, which is an exocytotic vesicle protein and a major factor of exocytosis, was detected in the sequencing data as highly expressed in stages before E5.75. To confirm these results, embryos were co-stained for Rab11 and Podxl to test whether exocytotic vesicles were rich in Podxl. As expected, the ExE contains a high number of exocytotic vesicles filled with Podxl (Figure 3.18B).

Upon closer examination of stage III embryos, it was evident that these Podxl-filled vesicles accumulated at the lateral membranes of rosette cells, adjacent to the polarised tracts described above. This was true for both rosettes in the ExE as well as hybrid rosettes (Figure 3.18C, D).

Interestingly, even after cavity fusion (stage V), there was a significant number of cells that maintained Podxl-filled vesicles (Figure 3.19A). By this stage already, the vesicles accumulating at the polarised tract in rosettes had secreted their contents while the vesicles in other cells that hadn't contributed to the initial unification of cavities, remained. Though the scope of this study focuses on the progression and fusion of the cavities, it was important to examine the fate of these remaining cells. Indeed, when the PAC was fully formed, and the ExE had become a monolayer, the remaining cells had already deposited Podxl apically (Figure 3.19B).

Both live imaging and fixed samples revealed that the remaining cells in the PAC after initial fusion of the cavities are cleared through intercalation to form a pseudostratified monolayer (Figure 3.19C-F). Apoptosis was not the driver of this, as cleaved caspase staining revealed minimal levels of apoptosis that could not account for the number of cells required to be cleared (Figure 3.19G).

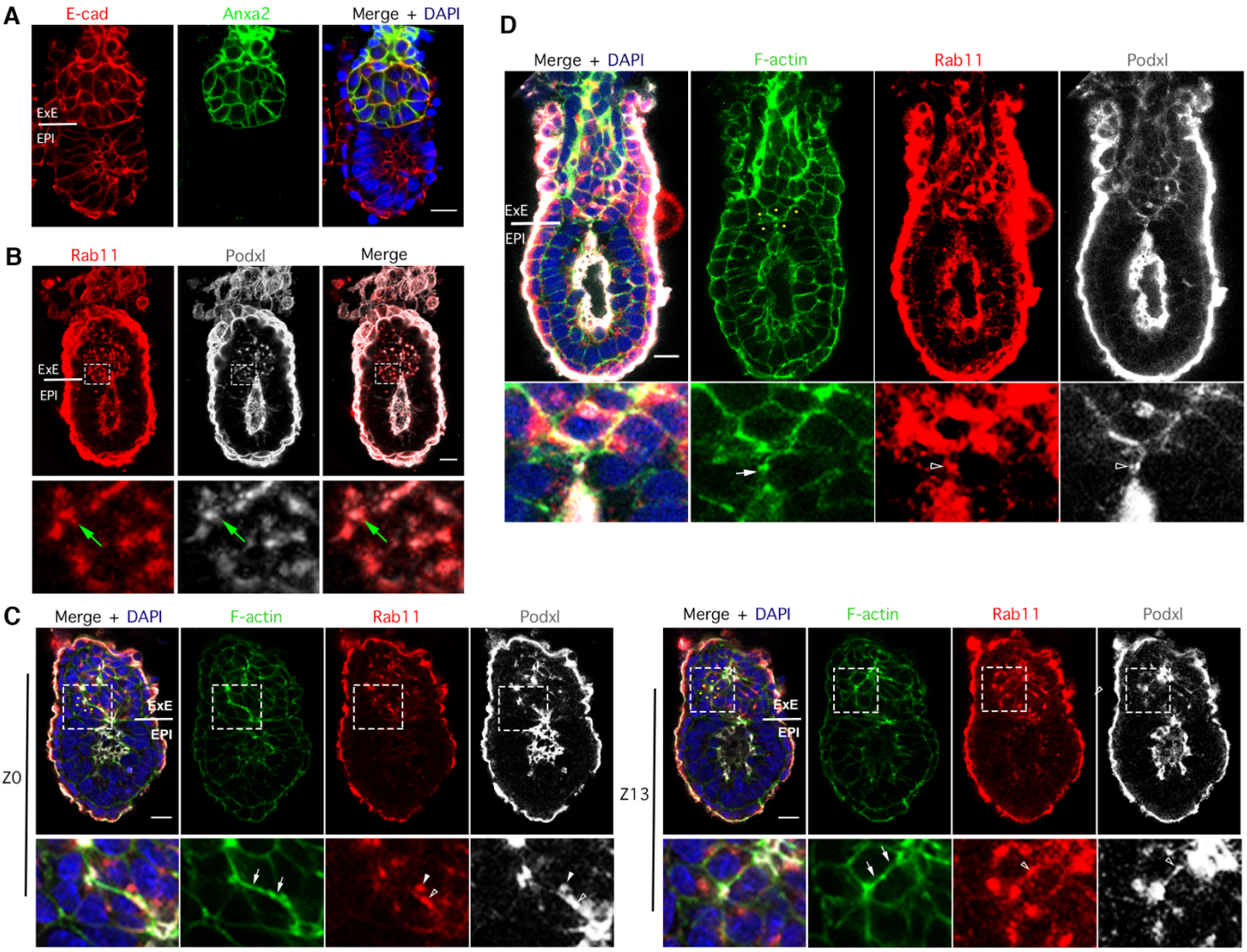

FIGURE 3.18: PODOCALYXIN VESICLE DOCKING AND SECRETION ALONG POLARISED TRACTS

(A) Immunostaining for Annexin A2 (Anxa2); scale bar = 20um. (B) Podxl vesicles' localisation in the ExE; green arrows point to Rab11/Podxl foci; scale bar = 20um. (C) Representative Z stacks in an embryo where Podxl secretion (hollow arrowhead) and Podxl vesicles (white arrowhead) docking along the polarised tracts (white arrows) is seen on both the side of extending Epi cavity and extending ExE cavity (white dots indicate the rosettes associated with the polarised tracts); scale bar = 20um. (D) Polarised docking of Podxl vesicles (hollow arrowhead) on polarised tracts (white arrow) in hybrid rosette (yellow dots); scale bar = 20um

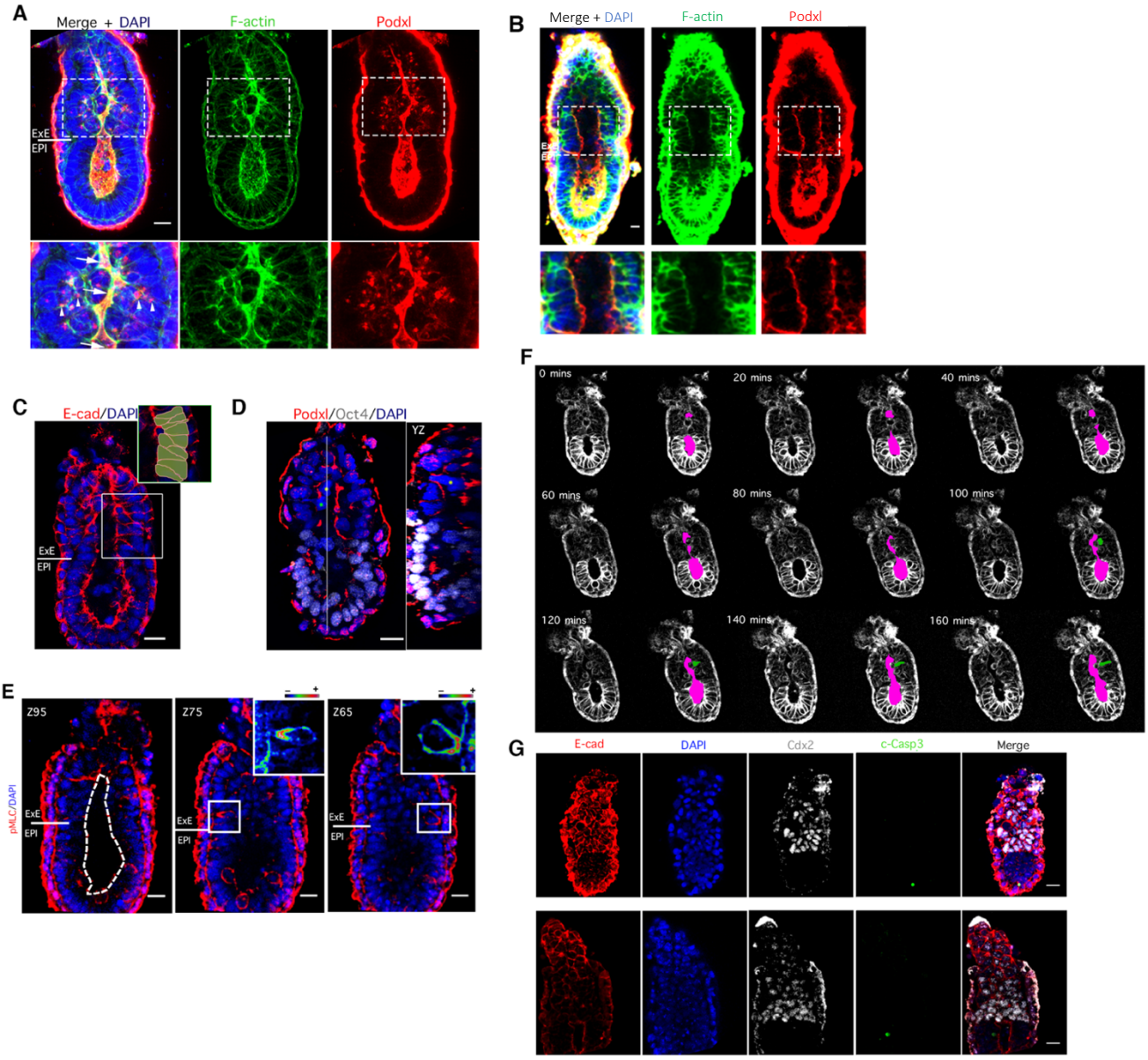

FIGURE 3.19: PROAMNIOTIC CAVITY FORMATION COMPLETED UPON INTERCALATION OF REMAINING CELLS IN EXE MONOLAYER

(A) Representative example of embryo at the initial unification of cavities stage. While there is a continuous nascent PAC lumen spanning the egg cylinder at this point (white arrows) there are still remaining cells in the bulk with Podxl vesicles (white arrowheads); scale bar = 20um. (B) E6.25 embryo i.e. after formation of PAC, the ExE becomes a monolayer with the cells having secreted Podxl on their apical site; scale bar =20um. (C) Pseudostratified appearance of the ExE monolayer after completion of the PAC formation; scale bar = 20um. (D) Representative embryo during clearing of remaining cells in the bulk by intercalation into the ExE monolayer (dots show the cells that appear to be intercalating back); scale bar = 20um. (E) Example of cells intercalating back with staining for phosphorylated myosin light chain (pMLC) being polarised towards the site of the ExE monolayer; scale bar = 20um. (F) Time-lapse movie of LifeAct-GFP during the unification of cavities (purple) showing a cell intercalating back (green). (G) Cleaved caspase 3 (c-Casp3) staining around the time of PAC formation shows minimal apoptosis; scale bar = 20um

3.2.12 A MODEL FOR PROAMNIOTIC CAVITY FORMATION

The events of cavity fusion and formation of the PAC were found here to begin from the early stages of implantation. As previously studied in Bedzhov and Zernicka-Goetz (2014), during embryo implantation into the uterine tissue, the Epi hollows to form the Epi cavity and demarcates the beginning of the dramatic morphogenetic transformation into an egg cylinder. Those findings are extended here to understand how the Epi cavity progresses into the nascent ExE to fuse with the ExE cavity and form the PAC. The model proposed from the data collected and analysed here is as follows (Figure 3.20):

1) Immediately after the stage of Epi rosette formation and Epi cavity emergence, the cells at the proximal site of the expanding ExE become elongated and apically constrict, driving an invagination-like process, creating a slit cavity.
2) The Epi cells at the boundary undergo reorganisation by reorienting their polarity to form a rosette structure with ExE cells at the boundary. This is followed by generation of a polarised tract along the lateral membranes of the Epi cells of this hybrid rosette leading to the centre of the rosette. A step later, the membranes of cells along this polarised tract separate, allowing reorganisation of the Epi from a spheroid structure into a cup-shaped epithelium. This is the first step of Epi cavity extension since at this point the Epi cavity is lined by both Epi and ExE cells.
3) More rosette structures, composed of ExE cells alone, then form and resolve in the same manner as the hybrid rosette. Polarised tracts extending either from the cavities or centres of other rosettes promote membrane separation in rosette cells thus extending and bringing the two cavities together until they finally fuse to create one unified PAC.

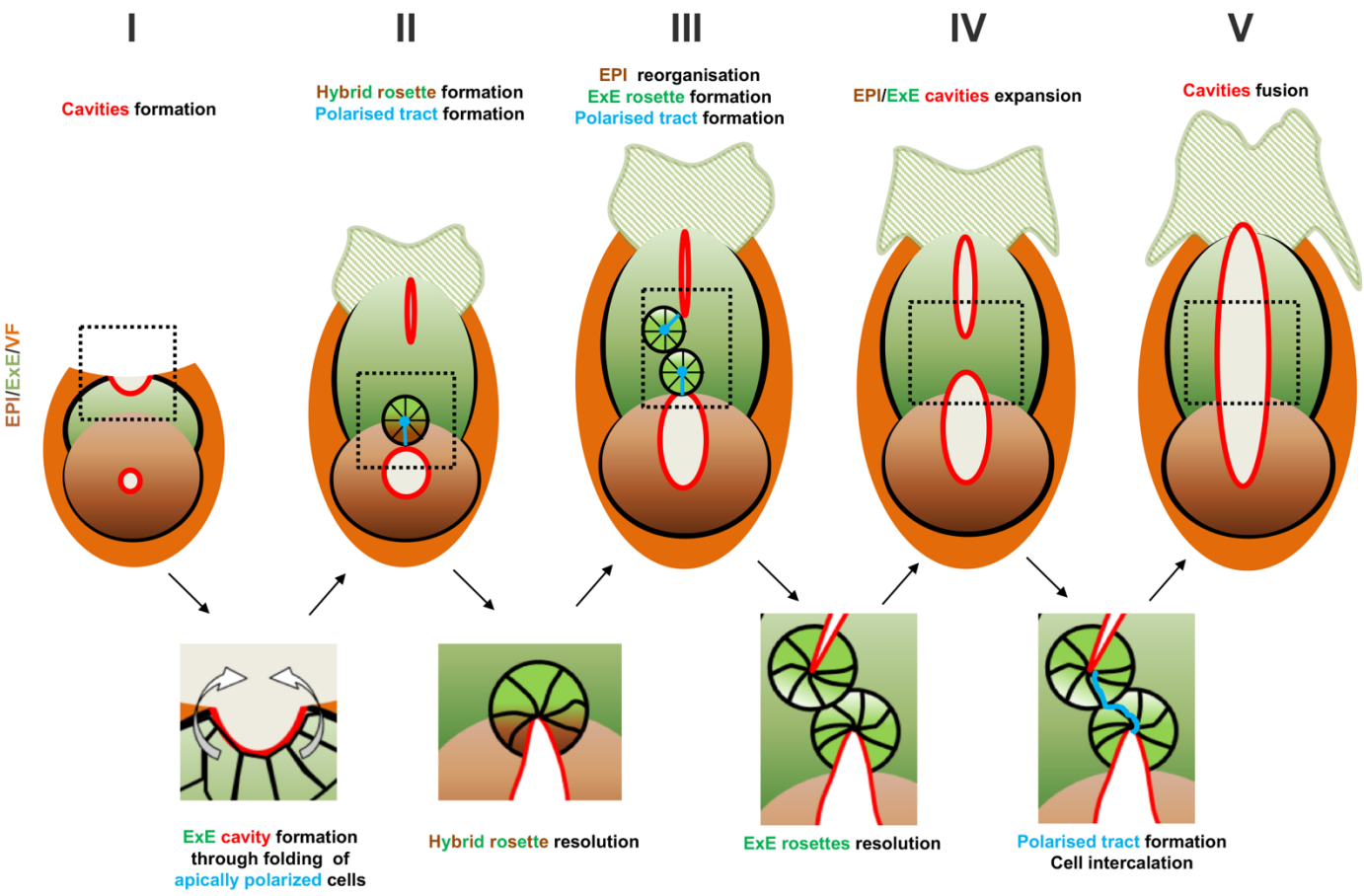

FIGURE 3.20: PROAMNIOTIC CAVITY FORMATION MODEL

Schematic representation of the different stages of PAC formation based on the data collected and interpreted in this study. Stage I begins once the epiblast cavity forms and prior to formation of the ExE cavity. Before moving to stage II, the ExE cavity forms by an invagination-like process of the proximal-most cells of the nascent ExE. At stage II a hybrid rosette forms at the Em-ExEm boundary which resolves along a polarised tract at the lateral membranes of the epiblast cells of the hybrid rosette. At this point the epiblast is reorganised from a spheroid to a cup-shaped structure. Stage III and IV are characterised by formation and resolution of rosettes in the ExE in the same manner as hybrid rosettes leading to progression of cavities. Finally, at stage V the cavities fuse forming the PAC.

3.3 DISCUSSION

The transformation of the blastocyst into the egg cylinder begins with the hollowing of the Epi during implantation. While this is the first morphogenetic event that contributes to the egg cylinder transition, the morphogenetic events that follow are not well studied or understood. This study focused on understanding the architecture of the expanded ExE and the cellular reorganisations that make the egg cylinder a cylinder (i.e. a hollowed structure). The major findings of this study can be summarised as follows:

1) The ExE cavity, which is the second cavity required for PAC generation, forms through a folding/invagination-like process on the proximal site of the implanting embryo.
2) The architecture of the ExE depends on ECM/β1-integrin signalling.
3) Rosette structures, both at the Em-ExEm boundary and the ExE, form and resolve to reorganise the Epi and ExE for PAC formation.
4) The PAC is a result of fusion of the Epi and ExE cavity (as opposed to expansion of a single cavity).

3.3.1 AN INVAGINATION-LIKE PROCESS DRIVES FORMATION OF THE EXE CAVITY

The ExE cavity has been an elusive structure in the mouse embryo development and has been frequently omitted in the literature (Beddington and Robertson, 1999; Rivera-Perez and Hadjantonakis, 2014; Rivera-Perez et al., 2003; Rossant, 2015; Sugimoto, 2014).

The key factor preventing the identification of the ExE cavity as a feature of the early egg cylinder has been its slit-like morphology. This is indeed a very thin cavity that cannot be identified through brightfield imaging, except on rare instances where this cavity appears a bit more laterally expanded than usual. While it can be easily confused for a cellular arrangement along the proximal midline, Podxl is clearly secreted in between the cells of what we identify as the ExE cavity, thus demonstrating a separation of the membranes. This is an arrangement very reminiscent of tubules during tubulogenesis, as they form elongated cavities prior to lumen expansion (Nedvetsky et al., 2014).

Tubulogenesis is a good analogy to understand formation of the slit-like cavity identified as the ExE cavity, as it provides multiple possible explanations from different systems on how a thin elongated lumen can arise. As reviewed before, there are four described ways in different models that explain the formation of a tubule (Hogan and Kolodziej, 2002). While all are equally possible, analysing the stages of cavity formation (i.e. E5.25 to E5.5) allowed us to conclude that this is more reminiscent of an invagination-like process as opposed to microlumen formation and fusion (Azizoglu et al., 2017; Villasenor et al., 2010), separation of apposed sheets

of cells (Bier, 2000; Hogan and Kolodziej, 2002) or cell canaliculisation (Buechner et al., 1999; Kamei et al., 2006; Nikolova and Metzstein, 2015).

Tubulogenesis through invagination has been described mainly in *Drosophila* salivary glands and mouse lung development and it begins with epithelial cells becoming increasingly columnar to form a placode. This placode drives invagination through apical constriction and "sinking" of the epithelial cells to form a tubule (Gelbart et al., 2012; Girdler and Roper, 2014). This is strikingly similar to the ExE cavity formation as described herein. The proximal-most cells in the ExE are epithelial as revealed by staining for ZO-1 and are very columnar/elongated in appearance when compared with other cells in the expanding ExE.

Following this, the apical site of these cells becomes enriched with actin and pMLC, denoting increased actomyosin contractility (which additionally explains the apical constriction of the cells). Such apical constriction of a subset of cells in a tissue has been described multiple times in the literature as a driver of tissue morphogenesis through deformation and shaping of tissues. The most striking example being the bottle cells in *Xenopus laevis* gastrulation in which the cells located at the blastopore apically constrict and pull the ectoderm inside (Hardin and Keller, 1988). Other examples include invagination of the *Drosophila* ventral furrow and, as mentioned earlier, in salivary gland tubulogenesis in *Drosophila* (Gelbart et al., 2012; Girdler and Roper, 2014).

Indeed, in the following step of ExE cavity formation the first stages of an invagination process is evident i.e. the apically constricted most-proximal cells appear to have "sunk" into the expanding ExE tissue forming a furrow. This is followed by the appearance of the slit-like cavity of the ExE. These steps are all consistent with an invagination-like process driven by a subset of cells that apically constrict, deforming the adjacent tissue in the process and shaping the cavity.

The mechanism of ExE cavity formation is markedly different to the Epi cavity formation as described before (Bedzhov and Zernicka-Goetz, 2014). In the case of the embryonic cavity, a central rosette forms in response to integrin signalling that is resolved by lumenogenesis through membrane separation at the centre. This is a well described mechanism, particularly in MDCK studies specifically investigating the methods by which epithelial cells are able to form cavities (Boehlke et al., 2013; Martin-Belmonte et al., 2008). While there are multiple examples of cavity formation through a tubulogenesis mechanism, this is the first time this has been described in the context of early mouse post-implantation development.

3.3.2 *ExE HAS A REGULAR ARCHITECTURE THAT IS DEPENDENT ON β1-INTEGRIN SIGNALLING*

Following the formation of the ExE cavity as described above, the ExE goes on to expand further and acquire a regular architecture. As described in the Results section, the ExE is surrounded by a BM (as is the Epi) and its cells are either in contact with this underlying ECM (outside cells) or not (inside cells). This type of architecture is very commonly seen in bud epithelia (lung, salivary, pancreatic buds) with the major difference between these systems and the one described here being the number of cells involved (Hsu et al., 2013; Patel et al., 2011; Villasenor et al., 2010). Interestingly, in many of these systems, cavitation ensues (as well as branching which is not directly relevant to this study) which suggests that tissues with this type of architecture generally undergo cavitation to form epithelia.

Characterising the process, the ExE is built, in terms of its different morphological components, suggested that the morphological differences of the cells may stem from a difference in their polarity status. The signalling capability of the BM to activate integrin signalling which in turn leads to acquisition of apico-basal polarity has often been described in other systems. (Klein et al., 1988; Lee and Streuli, 2014; O'Brien et al., 2001). This is the same signalling pathway responsible for polarity acquisition of both Epi cells in the mouse embryo during implantation as well as mouse ESCs (Bedzhov and Zernicka-Goetz, 2014; Shahbazi et al., 2017) and MDCK cysts when suspended in a BM-rich scaffold like Matrigel (O'Brien et al., 2001).

To functionally tackle the hypothesis that the underlying BM provides the polarity cues that give the outside cells their characteristic columnar shape, collagenase treatment was applied to dissolve the BM providing the niche for polarisation. This treatment was previously described in a study on the egg cylinder BM (Hiramatsu et al., 2013) and when applied it leads to severe disorganisation of the ExE. As the ECM is known to act as a ligand for integrin signalling (Calderwood et al., 1997; Jia et al., 2005; Nishiuchi et al., 2006) the next step was to inhibit integrin signalling to determine whether this phenocopies the digestion of the BM. In fact, this was essential to elucidate as the BM is also a physical scaffold of specific stiffness which may be affecting cell behaviour (Ladoux and Nicolas, 2012; Trichet et al., 2012). To address this, an integrin-blocking antibody was used that has been previously utilised in other systems (Daley et al., 2012; Liu et al., 2010). While a genetic approach would theoretically provide a cleaner assessment, several issues were taken into consideration in this case. Particularly, β1-integrin KO mice are embryonic lethal at around the time of implantation and therefore inaccessible for studying the formation of the PAC or the architecture of the ExE (Fassler and Meyer, 1995). A chimeric approach was attempted by aggregating β1-integrin KO 8-cell (floxed homozygous embryos treated with soluble Cre in culture medium) with LifeAct-GFP ES cells. The transferred chimeras were recovered at E5.5 and stained. Only 1 transferred embryo was reminiscent of an egg cylinder and while the

ExE appeared disorganised, the VE also failed to cover the ExE (possibly as a result of the absent integrin). This inhibited any further study as it is thus impossible to dissect the role of integrin from the BM-secreting VE (Bedzhov and Zernicka-Goetz, 2014).

Considering these issues, the blocking-antibody approach was taken to investigate integrin signalling. However, the delivery of the antibody is restricted to the VE when added to the culture medium, as a result of the presence of tight junctions sequestering it away from the basal site of the ExE cells. To circumvent this problem, TS cell aggregates embedded in Matrigel were used to recapitulate the ExE as previously partially described in the generation of synthetic ETS embryos (Harrison et al., 2017). As previously shown, integrin signalling from Matrigel perturbed by this class of antibodies, leads to loss of epithelial polarity (Daley et al., 2012; Sorokin et al., 1990). Moreover, TS aggregates generated in the absence of Matrigel, phenocopied the integrin-blocked Matrigel-embedded TS aggregates, suggesting that in the ExE the underlying BM provides the polarity cue to direct its architecture.

3.3.3 Formation and resolution of rosette-like structures drive reorganisation of Epiblast and proamniotic cavity progression

Rosette structures in epithelial morphogenesis are widely described and characterised as transient structures during junctional exchange between cells of an epithelium; reorganising cells in a way that drives tissue-wide morphogenesis (Blankenship et al., 2006; Kong et al., 2017; Lye and Sanson, 2011; Vichas and Zallen, 2011; Williams et al., 2014). Rosettes have also been observed in the VE of the E5.5 mouse embryo and have been suggested to play a role in collective cell migration of the AVE (Trichas et al., 2012). In both of these cases the rosettes involved form and operate on the planar axis and are regulated by planar cell polarity (PCP) pathways (Blankenship et al., 2006; Trichas et al., 2012; Williams et al., 2014). For all purposes, these rosettes can be described as 2D rosettes as their cells contribute to a common central point on only one axis (i.e. the planar axis).

A unique type of rosette is described in the zebrafish lateral line primordium development (Gompel et al., 2001; Lecaudey et al., 2008; Nechiporuk and Raible, 2008) in which unlike in the 2D rosettes, the centre of the rosette is made up of the apical site of the cells in the epithelium rather than the lateral adjoining membranes. This format creates an epithelial pocket which is filled with FGF, creating an important niche for the migration of the lateral line primordium (Lecaudey et al., 2008).

The last rosette format (also more relevant to this study) is the 3D rosette, in which, as the name suggests, cells contribute to a central point from all axes in a more spheroid-like conformation (Bedzhov and Zernicka-Goetz, 2014; O'Brien et al., 2001; Shahbazi et al., 2017). In development, examples of this include pancreatic branching, in which the rosettes form in the developing tissue and resolve centrally to create micro-lumens

that eventually fuse to generate the pancreatic plexus. Another example is the formation and resolution of the implanting Epi rosette in mouse development to create the Epi cavity (Bedzhov and Zernicka-Goetz, 2014; Villasenor et al., 2010).

As presented in the Results section, the ExE cells as well as the Epi cells at the boundary, form 3D rosette structures that create foci of enriched apical markers in the tissue. These rosettes are found close to a cavity or another rosette requiring sharing of cells and thus bipolarity. This bipolarity has been observed in other systems as well (Denker and Jiang, 2012) but is particularly similar in the case of the bipolar cells between rosettes during zebrafish gut development (Alvers et al., 2014). In this case, microlumens formed by rosettes in the developing gut are joined by expansion of the cavities and recycling of basolateral proteins at the cell interfaces between them. While this is similar to the model proposed in this study, in the ExE there are no microlumens forming but rather, foci are joined by polarised tracts (Villasenor et al., 2010). The interpretation of the data presented in this study suggests that polarised tracts connect the rosette centres to the progressing cavities. This is followed by secretion of the membrane-separating protein Podxl along these tracts that allows resolution of the rosettes and thus cavity progression. Such polarised tract formation and dissolution has been described in tubulogenesis of other systems (Cheng et al., 2015; Nedvetsky et al., 2014; Xu et al., 2011). Interestingly, while the architecture of tissues undergoing tubulogenesis requires extensive epithelial reorganisation through organisation of the tissue into polarised tracts (Villasenor et al., 2010), in the case of the ExE remodelling, rosettes form and resolve progressively along polarised tracts. Additionally, these polarised tracts are simply bipolar cells depositing apical marker along their lateral membranes rather than a collection of cells. This appears to be an adaptation of a tubulogenic programme to fit the much smaller tissue of the ExE.

Rosette formation and resolution as described above appear to be serving another similar yet distinct role in PAC formation. Before cavity progression, the Epi reorganises from a spheroid into a cup-shaped epithelium which is driven by formation and resolution of a hybrid rosette at the boundary comprised of both Epi and ExE cells. Upon resolution of this chimeric structure (in the way described above) the Epi cells at the boundary move apart to expose the Epi cavity to the ExE. This reorganisation of cells i.e. realigning of their apico-basal polarity to create the open end of the Epi has been reported previously in a different context. In *C. elegans* pharynx development, the pharyngeal cells create a tube with a cap surrounded by mesenchymal cells. Later the pharyngeal cells at the cap reorient to uncap and make a continuous tube with the mesenchymal cells (Portereiko and Mango, 2001). This is strikingly similar to the reorganisation event at the Em-ExEm boundary, however there is no characterised rosette structure acting as a transitory tool to reorient the apico-basal polarity of the pharyngeal cells as observed in the Epi cells. Additionally, unlike the case of the Epi reorientation, pharyngeal cap cells are surrounded by a BM that only breaks down moments before uncapping,

thus a chimeric rosette structure is unlikely to form. Thus, hybrid rosette formation as a tool to uncap an epithelium appears to be specific to the interaction between apposed epithelial tissues as is the case in Epi and ExE.

The formation of these rosettes, as stated earlier, appears to be dependent upon the underlying BM, since its pharmacological removal leads to disorganisation and loss of rosettes. This appears to be attributed to the inability of the outside cells to polarise, resulting in failure to organise neighbouring inside cells and form rosette structures. In a similar scenario, albeit a different context, the *C. elegans* pharynx forms through cyst formation as a result of PAR polarity acquisition at the midplane directed by cues from the underlying BM. The evidence on the mechanism by which cells of established polarity can organise neighbouring cells in the absence of any polarity cues comes from a laminin knockout (lam-1(-)) in *C. elegans.* In contrast to the ExE tissue, loss of BM signals causes reversal of polarity, positioning PAR polarity proteins between cells that have no other polarity cue. This causes cells (regardless of their original polarity status) to organise into rosette structures (Rasmussen et al., 2012). In another example, when ROCK1 is inhibited in the submandibular glands, there is random deposition of BM within the tissue. This causes local polarisation of cells which is enough to direct unpolarised cells around them to form rosette-like structures (Daley et al., 2012).

While the submandibular gland architecture appears to be very reminiscent of the ExE there are no reported rosettes forming. Evidently, similar architecture does not warrant identical cell behaviour; different cell types respond independently when arranged into discrete architectures. For example, when ES cells are aggregated to form embryoid bodies, the BM deposited by the cells on the outside provides a cell survival signal which causes the cells on the inside to die through programmed cell death (Murray and Edgar, 2000).

In conclusion, the evidence provided here suggest a sequential rosette formation and resolution-mediated mechanism for Epi and ExE remodelling. PAC formation follows a programme that is adapted for both the scale, the tissue architecture and the type of the cells.

4 BASEMENT MEMBRANE REMODELLING DURING EGG CYLINDER GROWTH AND PRE-PATTERNING OF THE PRIMITIVE STREAK

4.1 INTRODUCTION

During development, concerted cell behaviour involving cell shape changes and cellular rearrangements achieves a global change in tissue architecture which is instrumental in its function (Alvers et al., 2014; Blankenship et al., 2006; Martin and Goldstein, 2014). Such events have been extensively studied in developing epithelia in an effort to gain an understanding of tissue shaping events like bending, invagination and extension. While global tissue developmental dynamics are largely dependent on local cell behaviour that creates a tissue-wide effect, there are tissues that are "sculpted" by an underlying basement membrane (BM) through physical constraint and differential patterning (Chlasta et al., 2017; Crest et al., 2017; De Las Heras et al., 2018; Diaz-de-la-Loza et al., 2018; Haigo and Bilder, 2011; Harunaga et al., 2014). Although not all developing tissues are surrounded by a BM that can impose mechanical force, the early post-implantation mouse embryo is one of them. More specifically, a laminin and collagen-rich BM surrounds the egg cylinder covering both the embryonic and extraembryonic compartments during a highly proliferative phase of its development with no evidence of breakage (Gersdorff et al., 2005; Miner et al., 2004; Williams et al., 2012). BM breaching only becomes evident at the gastrula stage where the proximo-posterior BM is broken to allow ingression of embryonic ectoderm cells (Williams et al., 2012).

A compliant BM is an interesting subject in mechanobiology as it is a characteristic that can either be attributed to the composition of the BM or its architecture i.e. the way in which the BM components are laid down (Halfter et al., 2015). There are some very representative examples of how distensibility of the BM is controlled in the developmental context. These include bud growth/branching and *Drosophila* egg chamber extension (Daley and Yamada, 2013; Morrissey and Sherwood, 2015). The *Drosophila* egg chamber is one of the prime examples of how a BM completely surrounding an actively expanding tissue not only permits growth but does so in such a way so as to shape it into an elongated structure. A dense collagen IV BM surrounds the developing egg chamber during its expansion along the anterior-posterior (AP) axis without evidence of breaching during elongation (Chlasta et al., 2017; Crest et al., 2017; Haigo and Bilder, 2011). It has been shown that during the development of the egg chamber, the follicle cells on the outside revolve around the chamber depositing collagen fibres perpendicular to the AP axis (Haigo and Bilder, 2011). This arrangement of collagen fibrils acts as a molecular corset that promotes elongation of the tissue along the AP axis. It was also shown that

differential levels of the egg chamber BM components are important in this elongation suggesting that anisotropic tissue expansion is a result of differential BM stiffness (Crest et al., 2017).

More relevant to the architecture of the early post-implantation mouse embryo, a structure in which the BM has been described to be instrumental for morphogenesis through mechanical input, is the submandibular salivary gland. This model is widely used for understanding branching morphogenesis as the salivary gland develops robustly in a plate and inhibitors or function-blocking antibodies can be added to the *in vitro* culture. The salivary gland's main components include a surrounding mesenchyme and a bud made up of highly epithelial cells on the outside enclosed in a laminin and collagen-rich BM (Grobstein and Cohen, 1965; Harunaga et al., 2014; Larsen et al., 2006; Walker et al., 2008; Wells et al., 2013).

Studies on the BM composition of the salivary buds revealed that differential levels and types of BM components deposition are important in guiding branching morphogenesis (Grobstein and Cohen, 1965; Larsen et al., 2006; Nakanishi et al., 1988). Interestingly, high resolution 3D imaging of the BM during expansion and branching of the bud revealed that it is perforated, which permits growth (Harunaga et al., 2014). In this model, the underlying epithelial cells of the developing bud protrude through these perforations maintaining the perforated morphology. This indicates that the BM can act as a separate entity from the cellular component of the tissue and can establish a bidirectional relationship with the cells to control global tissue morphogenesis.

Perforations in the BM have also been reported in the Hydra (Shimizu et al., 2008). Similar to the submandibular gland described above, these perforations seem to be able to make the extracellular matrix (ECM) around the bud-forming areas more distensible for growth (Aufschnaiter et al., 2011). Additionally, the porous nature of the Hydra BM appears to be serving another role. While the BM maintains the tissue architecture in the budding hydra, concurrently it also creates a physical separation between the two cell layers on either side of it; the ectoderm and endoderm. The perforations create communication channels for ectoderm and endoderm cells to make contact (Aufschnaiter et al., 2011).

Another method of guiding morphogenesis is through the complete dissolution of the BM. One example of how removal of the BM can shape a tissue has been seen in the *Drosophila* wing and leg extensions (Diaz-de-la-Loza et al., 2018). Prior to their extension the wing and leg epithelia are completely covered, both apically and basally, by BMs. For the extension to initiate, the BM on both apical and basal site is dissolved by different proteases accompanied with convergent extension. This is an example of how BM remodelling becomes permissive for morphogenesis to take place as opposed to directly shaping the tissue.

Differential BM composition along a tissue can create differential stiffness profiles that promote the expansion of the tissue accordingly i.e. towards the weaker part of the BM. The salivary gland branching morphogenesis

has been the main model used for the study of this process. It was first proposed in 1965 that BM shapes the salivary gland by promoting branching. In that study they showed that "[Salivary epithelium] is "depatterned" midway in the morphogenetic course by a short exposure to a collagenase" and they suggested that collagen fibrils that were seen to accumulate to the clefts may act as stabilising agents to certain regions of the epithelium to create these clefts and promote branching (Grobstein and Cohen, 1965). These findings were later confirmed, and it was demonstrated that differential deposition of collagens along the salivary epithelium causes the cleft formation and thus initiates branching morphogenesis (Daley et al., 2017; Larsen et al., 2006; Nakanishi et al., 1988; Wang et al., 2017b). These seminal findings have established a strong basis on the role of BM-guided morphogenesis.

The *Drosophila* egg chamber, similar to the salivary gland, also exhibits differential BM component levels across its AP axis. This differential distribution of the collagen and perlecan creates a stiff BM in the central area of the egg chamber and weak poles. This, together with the architecture of the BM i.e. the collagen fibrils aligned perpendicular to the AP axis, promotes egg chamber elongation (Crest et al., 2017; Haigo and Bilder, 2011).

In both the *Drosophila* egg chamber and mouse salivary gland development, the differential deposition of BM components directs morphogenesis. However, the Hydra polyps model provides an alternative example in which differential levels of BM components guide morphogenesis without deposition. During budding of the Hydra polyps, while completely surrounded by laminin and collagen, the bud area BM becomes reduced in its composition of collagen-1 which allows stretching and extension of the growing bud (Aufschnaiter et al., 2011). Thus, in the case of the budding Hydra, evagination of the buds is more dependent on the remodelling of the existing BM as opposed to the deposition of its components.

In conclusion, the BM constitutes a physical scaffold that has a role not only in maintaining the integrity of the tissue and preventing ectopic transmigration events but also in shaping the tissue. The early post-implantation mouse embryo has an elongated cylindrical shape surrounded by a BM that grows rapidly for nearly 48 hours before the first evidence of breaching (during gastrulation) (Williams et al., 2012). This study focused on understanding how the composition/architecture of the BM permits growth during these stages of rapid tissue expansion and how this is regulated and co-ordinated with other concurrent morphogenetic events.

4.2 Results

4.2.1 *Basement membrane under the epiblast is perforated in the early post-implantation stages*

In order to visualise the 3D architecture of the BM of the early post-implantation mouse embryo in detail, high resolution and dense z-stacks were acquired from fixed embryos and stained for BM proteins such as laminin, collagen and perlecan (**Figure 4.1A**). This revealed that the BM is perforated. These perforations were evenly distributed in the Epi during the early stages (E5.25 – E5.75) and then asymmetrically accumulated to one side of the embryo, perpendicularly to its proximal-distal (PD) axis (**Figure 4.2**).

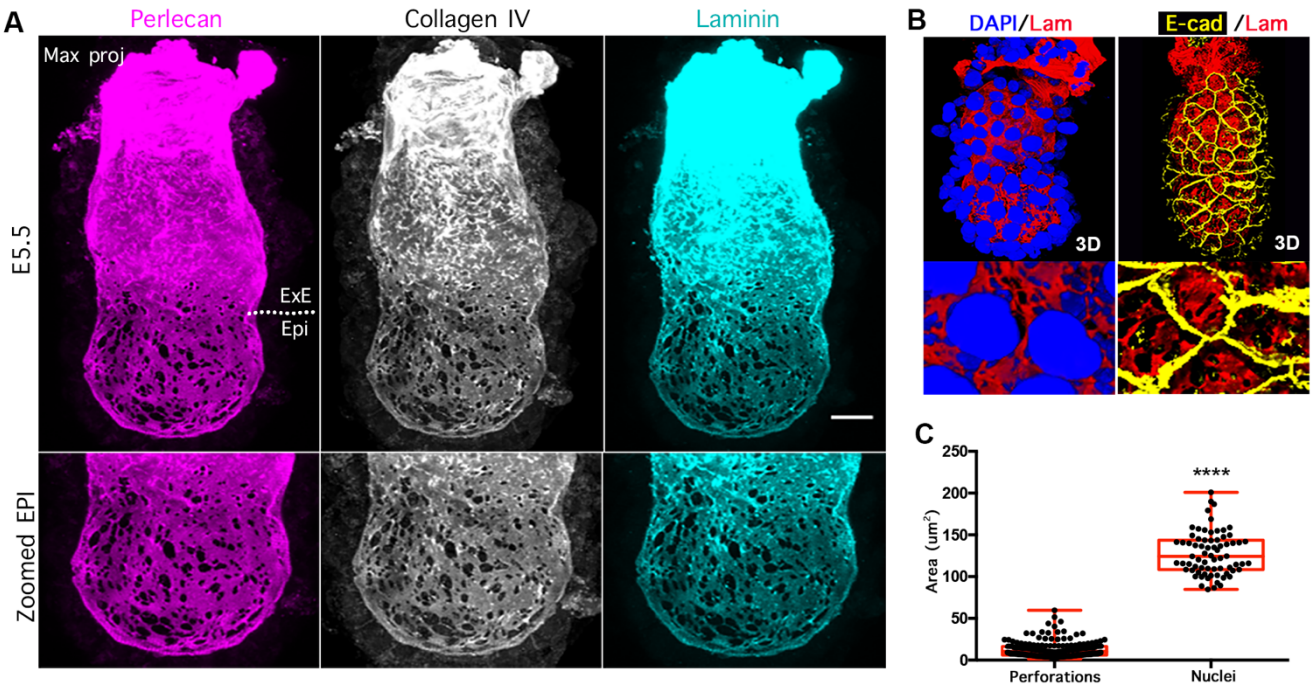

FIGURE 4.1: THE EPIBLAST BASEMENT MEMBRANE IS PERFORATED

(A) Representative E5.5 mouse embryo recovered directly from the mother and stained for three different BM components. Z-stacks were maximally projected. (B) Close up of 3D-reconstructed BMs with overlying VE nuclei or membrane. (C) Comparison of size of perforations with size of nuclei. Unpaired student's t-test ****<0.0001. Scale bar = 20um

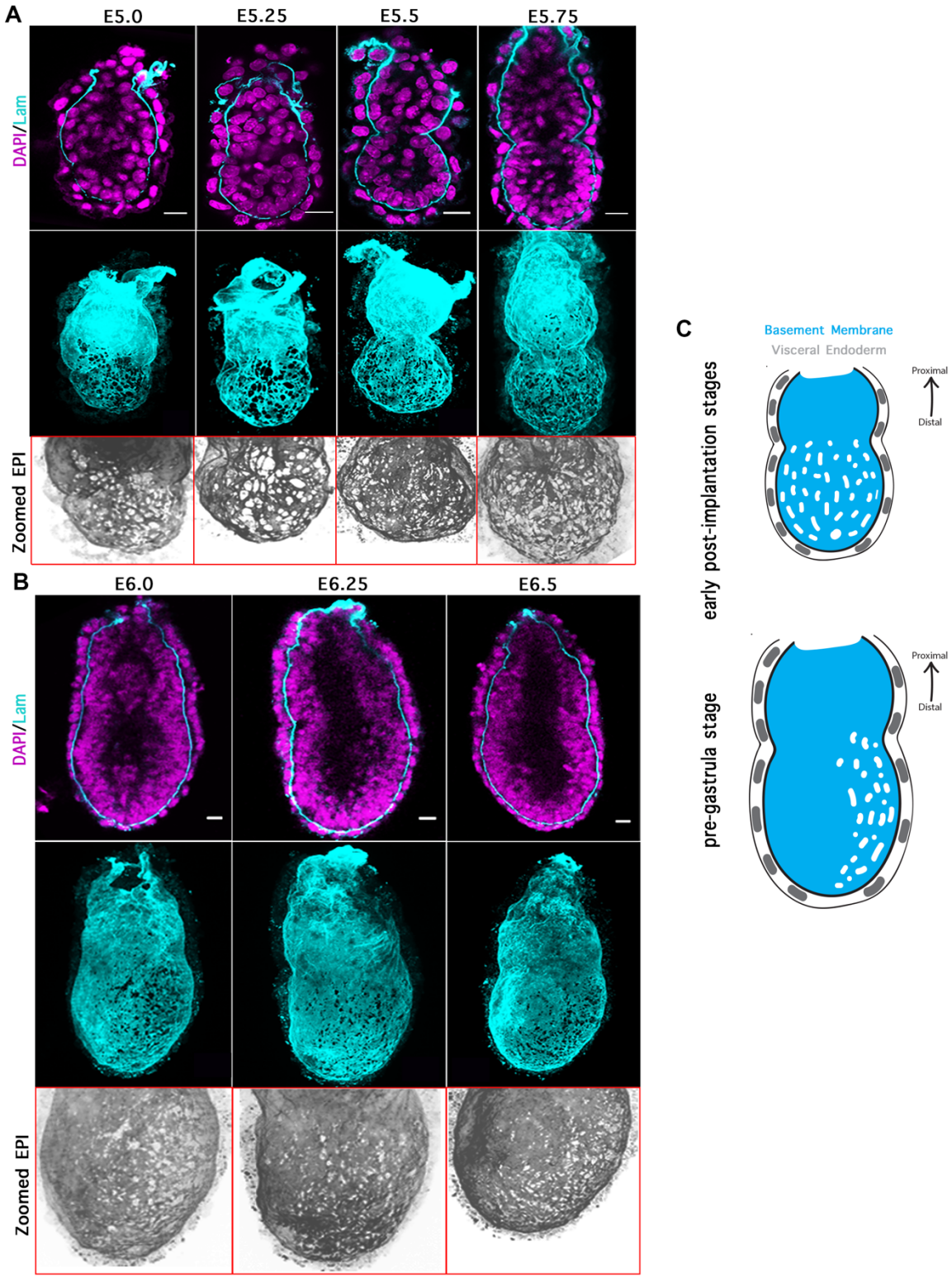

FIGURE 4.2: PERFORATIONS REDISTRIBUTION IN PRE-GASTRULA STAGES

(A) Early post-implantation embryo perforations (E5.25 – E5.75). (B) Pre-gastrula stages perforations asymmetrically accumulate on one side (E6.0 – E6.5). (C) Schematic of perforations distribution in early post-implantation and pre-gastrula stages. Scale bar = 20um

These perforations ranged in size from 1um to 70um. In some cases, multiple perforations fused together to form larger clearings. The size of cells on either side of the BM (i.e. either VE or Epi) was significantly larger than the perforations, with their nuclei ranging from 100um to 200um. Thus, the BM while perforated, still provided a physical separation between the Epi and the VE (**Figure 4.1B, C)**.

Together, these results suggest that the BM enveloping the Epi develops perforations with a dynamic distribution in the early stages of post-implantation development. Although, some perforations were also visible in the ExE, they disappeared at the pre-gastrula stages (E6.0 – E6.5).

4.2.2 THE EPIBLAST ACTIVELY REMODELS THE UNDERLYING BASEMENT MEMBRANE

The development of perforations in the BM could be explained in two distinct ways. One way would be the loss of integrity as a result of failed cellular support i.e. loss of ECM stabilisation. Alternatively, cells may be actively remodelling it by locally breaking it down. To experimentally determine the manner in which perforations may develop, an *in vitro* system was used to assess the ability of cells resembling the Epi to remodel an exogenously supplied ECM (mimicking the Epi-BM micro-environment), that is not reliant on stabilisation by the cells it is in contact with. This is a frequently used experimental setup in cancer studies employed to assess changes in invasion potential of treated cancer cells. It consists of a fluorescent substrate on an optical slide with cells seeded on top. The embryonic BM counterpart was modelled *in vitro* by coating optical slides with either Cy3-Gelatin or laminin. To model the interaction between the BM and Epi cells, the coated plates were plated with embryonic stem cells (ESCs) for 48 hours in the absence of the pluripotency-maintenance factors 2i (CHIR99021 and PD0325901) and mouse LIF. A 48-hour period of differentiation has been reported to lead to cells acquiring a cell fate representative of post-implantation Epi cells (Kalkan et al., 2017; Shahbazi et al., 2017). After 48 hours, the Cy3-Gelatin or immunostained laminin were scanned to assess the level of ECM remodelling by identifying regions of cleared substrate. When compared to undifferentiated cells (more reminiscent of pre-implantation Epi cells), differentiated cells were more potent in ECM remodelling. This suggested an active mechanism of BM remodelling as opposed to a passive mechanism mediated by BM stabilisation (**Figure 4.3A, B**).

Interestingly, in many cases there was an overlap of the perforations observed on the exogenous ECM with actin foci formed at the basal site of the differentiated cells (**Figure 4.3C**). This was very reminiscent of invadopodia formation and local BM remodelling often seen in invasive cells. Invadopodias are transient local protrusions forming on the basal site of cells that are rich in actin and matrix metalloproteinases (Artym et al., 2006; Sherwood and Plastino, 2018).

This observation further suggested an active role of Epi cells in producing these BM perforations. To check whether this might be the case in the embryo as well, staining for pMLC (marker of the active formation of protrusions) and BM revealed that some perforations overlapped with pMLC foci on the basal site of Epi cells (**Figure 4.4**). Since invadopodias are transient structures, it was not possible to observe them in all perforations and live imaging of actin with BM is not currently available as there are no mouse fluorescent BM reporter lines (Morris et al., 2018). Alternatively, these invadopodia-like structures may be more reminiscent of the protrusions observed in the submandibular gland BM perforations (Harunaga et al., 2014).

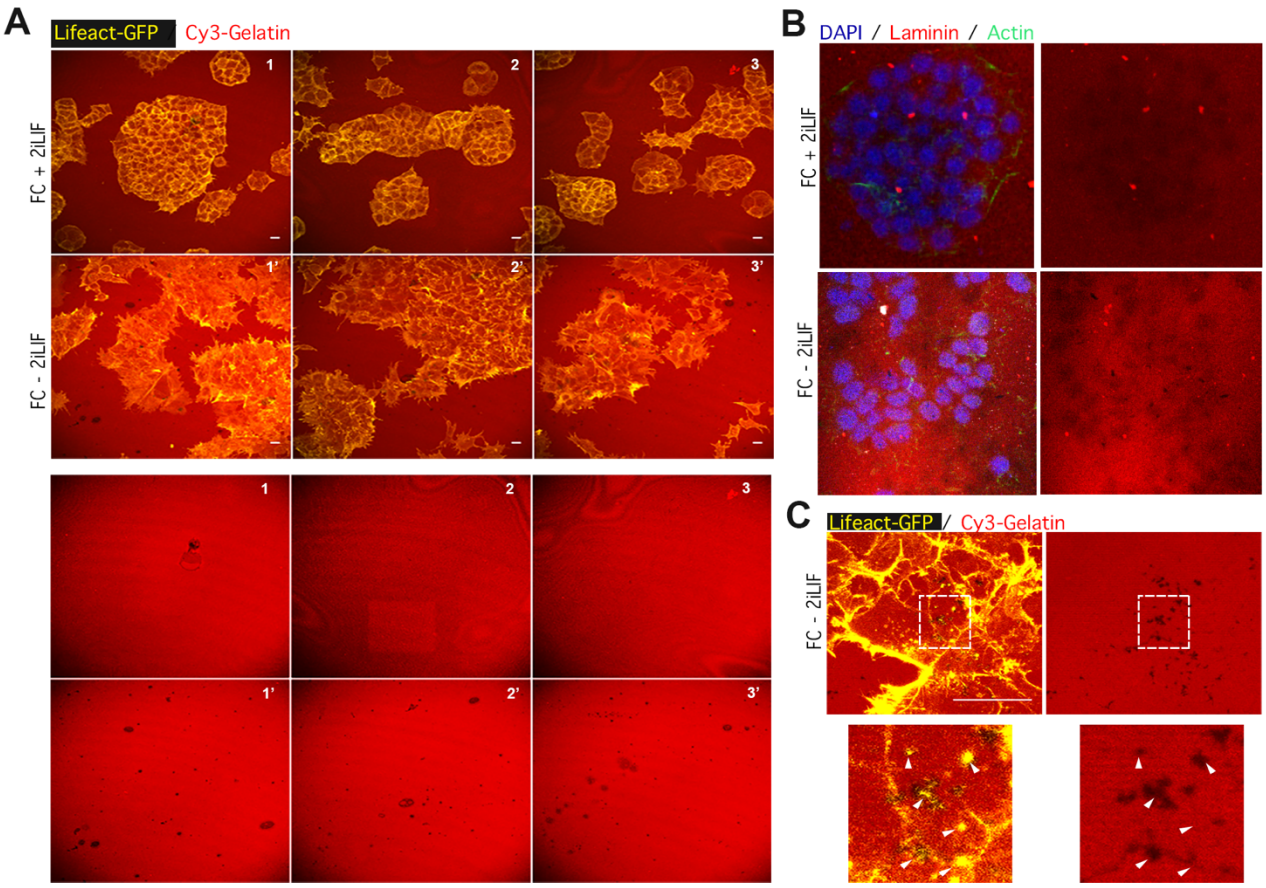

FIGURE 4.3: BASEMENT MEMBRANE REMODELLING IN UNDIFFERENTIATED AND DIFFERENTIATED ESCS

(A) Lifeact-GFP ESCs plated on fluorescent Cy3-Gelatin for 48 hours in feeder cell (FC) medium in the presence of 2iLIF (+2iLIF) or in the absence of 2iLIF (-2iLIF). (B) ESCs plated on laminin-coated dishes in the presence or absence of 2iLIF for 48 hours. (C) Co-localisation of actin enrichments and perforations in the Cy3-Gelatin (white arrowheads). Scale bar = 20um

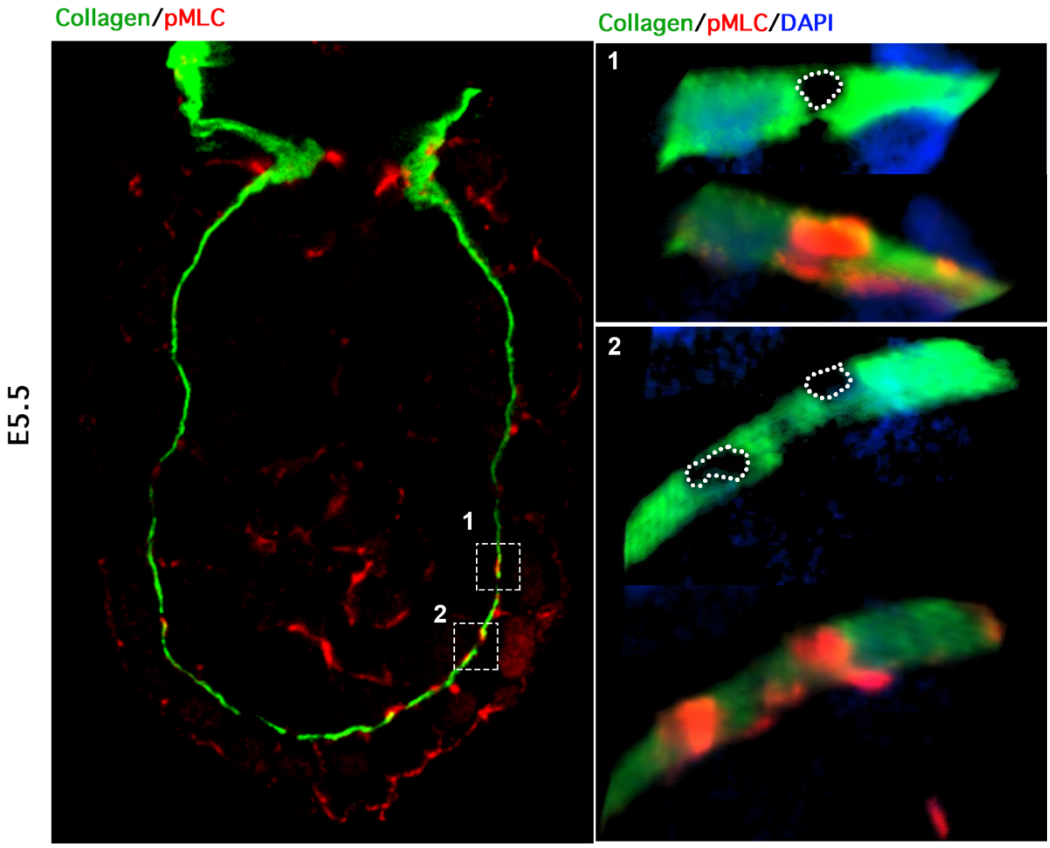

FIGURE 4.4: FOCI OF ACTIVE ACTOMYOSIN CONTRACTILITY ON THE BASAL SITE OF CELLS CO-LOCALISES WITH PERFORATIONS

A representative E5.5 embryo stained for the active actomyosin contractility marker pMLC and the BM protein collagen IV. 3D reconstruction of a few z slices at the basal site of cells reveals a co-localisation of perforations (outlined with white dotted line) and pMLC foci.

4.2.3 *REDISTRIBUTION OF PERFORATIONS IN THE PRE-GASTRULA STAGES IS CONTROLLED BY THE ANTERIOR VISCERAL ENDODERM*

During the characterisation of the BM architecture in the early stages of post-implantation development it was evident that while the perforations were initially evenly distributed in the BM under the Epi, upon entering the pre-gastrula stages (E6.0) they asymmetrically accumulated on one side of the embryo on an axis perpendicular to the PD axis.

Concomitant with this redistribution, the AP axis is established by migration of a population of VE cells (anterior visceral endoderm; AVE) that originate at the distal tip to one side of the embryo perpendicular to the PD axis. Since the perforations also accumulated along an axis perpendicular to the PD axis, the next step was to establish whether there was a correlation between the AP axis establishment and the side of perforations.

To address this, several stages of the AVE migration were collected and stained for the AVE marker *Cerberus-like* (or the Cerberus-GFP mouse line was used) and laminin to visualise the BM. There was an inverse correlation between AVE position and perforation domain at all stages of migration, culminating in the accumulation of perforations in the future posterior. This suggested that the AVE actively elicits a response from the tissues surrounding the BM to remodel it (Figure 4.5 and 4.6).

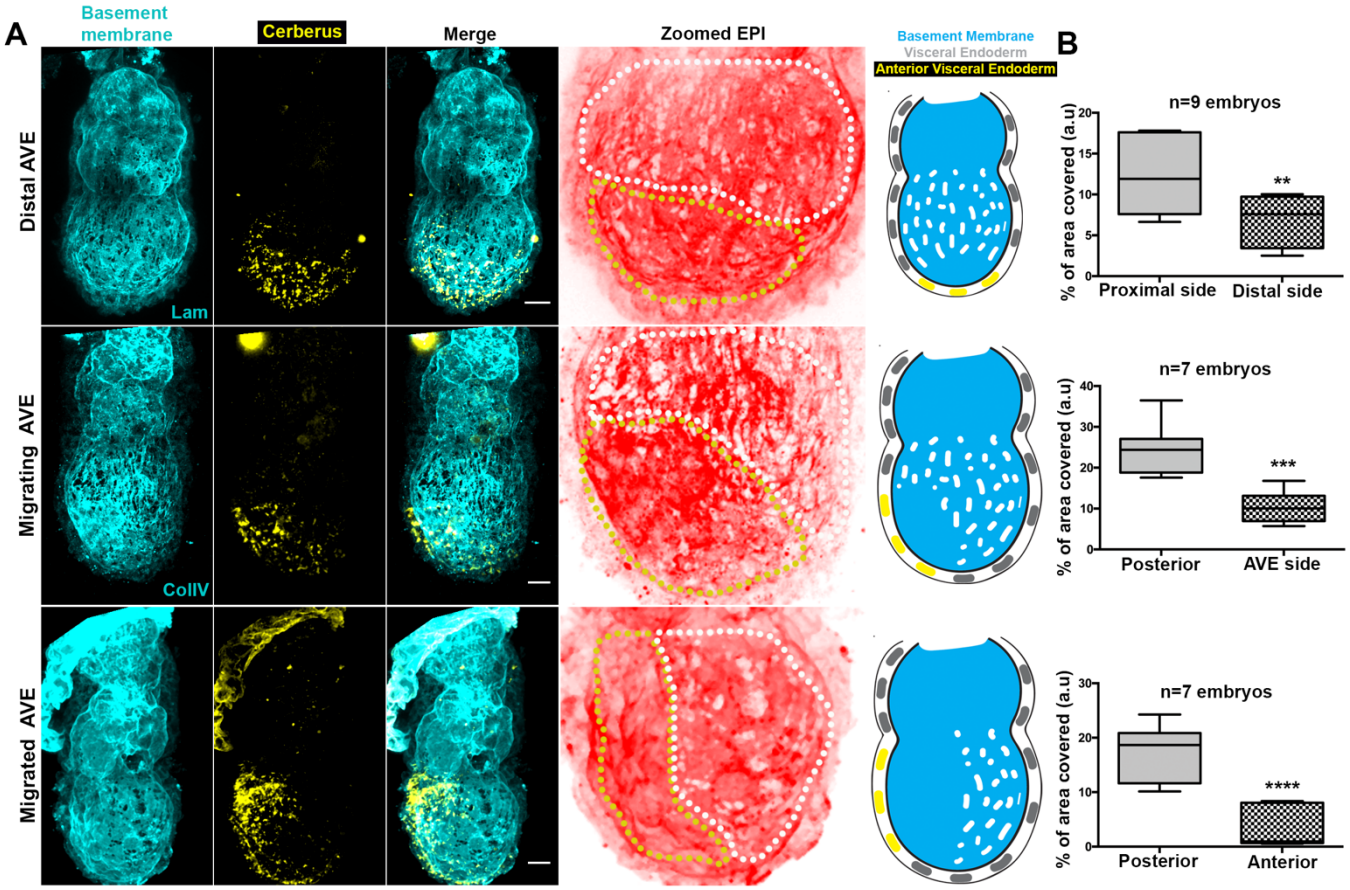

FIGURE 4.5: AVE POSITION CORRELATION AND DISTRIBUTION OF PERFORATIONS

(A) Three different stages in AVE migration (distal, migrating and migrated) stained for the AVE marker Lefty and the BM components laminin or collagen IV. Zoomed Epi BM is outlined with the AVE domain (yellow dotted line) and the domain away from the AVE (white dotted line). Schematic on the right of each AVE migration stage shows relative position of perforations with the AVE position. (B) Quantification of percentage of area covered by perforations in the different domains as dictated by the position of AVE. Paired student's t-test; **<0.01, ***<0.001, ****<0.0001. Scale bar = 20um

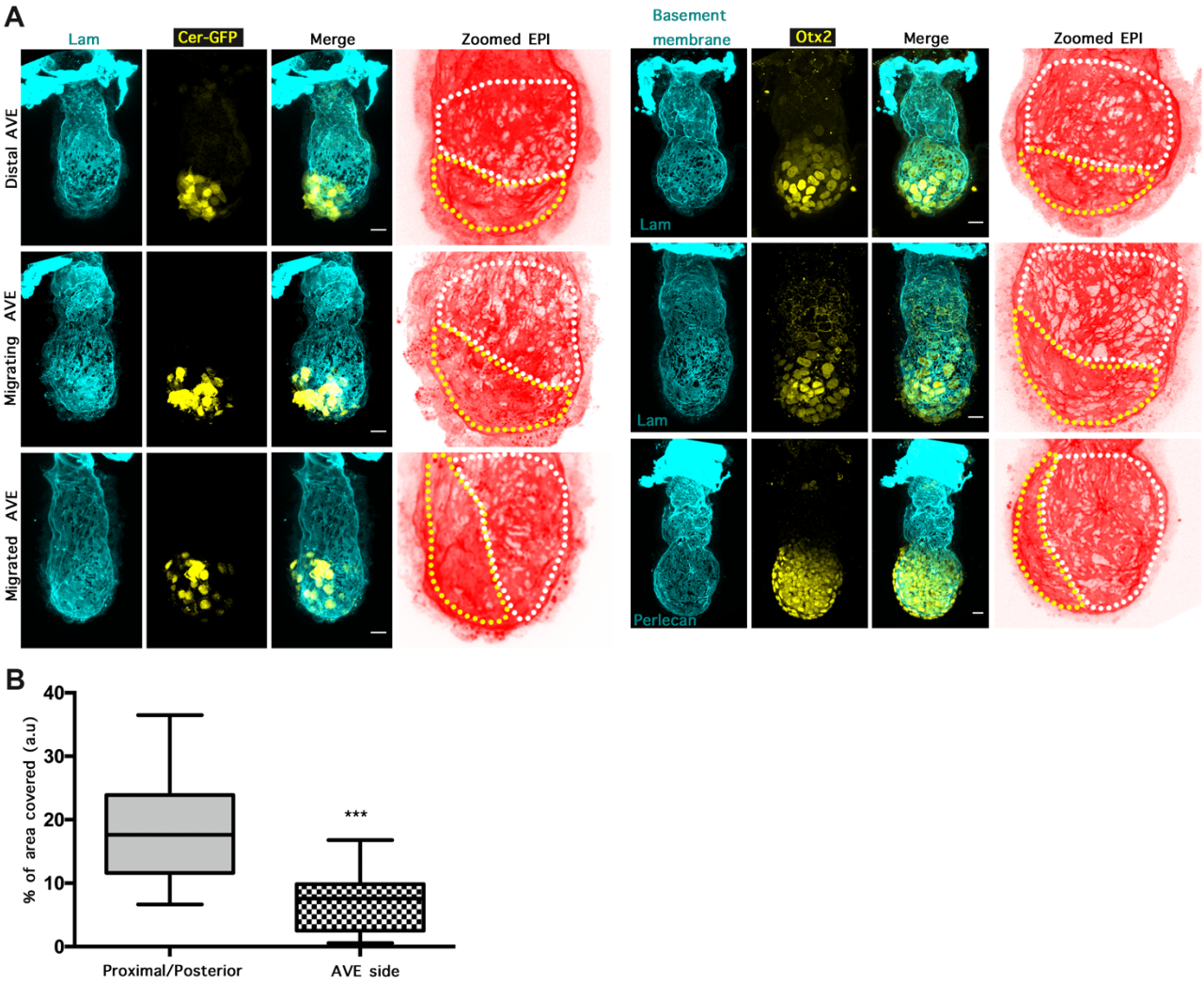

FIGURE 4.6: CORRELATION OF OTHER AVE MARKERS WITH POSITION OF PERFORATIONS

(A) Cerberus-GFP transgenic embryos recovered fresh from the mother and stained with laminin at different stages of AVE migration. Wildtype embryos stained for Otx2 and BM components laminin or perlecan. (B) Quantification of the BM area covered by perforations at regions away or close to AVE population with embryos from different AVE migration stages pooled together. Paired student's t-test: ***p<0.001. Yellow outlines: AVE region. White outlines: region away from AVE. Scale bar = 20um

To functionally assess this observation, it was essential to manipulate the positioning of the AVE and assess the effect of these presumptive anterior cells on the perforation redistribution. The AVE is a signalling centre (which is how it establishes the AP axis), and therefore it was important to make sure that the manipulation of the AVE positioning would not affect its signalling role. Since AVE migration depends on collective cell migration, proteins like RhoA, Rac1, Nckap1 and other WAVE complex components could be targeted to specifically affect positioning (Stower and Srinivas, 2014). However, the role of such proteins extends beyond just AVE migration during early embryo development and thus a total KO of any of these proteins would potentially create artefacts. To address this, a collaboration with Dr. Isabelle Migeotte was established, who provided a VE-specific RhoA-KO. Embryos were generated by crossing RhoA $^{fl/fl}$ with ttr:Cre; RhoA$^{+/-}$; Hex-GFP and fixed at E6.25-E6.5 (at which point perforations were asymmetrically distributed towards the future posterior). The embryos were then permeabilized and stained for the AVE marker *Cerberus-like*, and laminin. Then they were assessed in the same way wild type embryos were when establishing the correlation between the position of the AVE and site of perforations. From 3 independent experiments, 7 embryos were confirmed by single embryo genotyping to be complete KOs of RhoA in the VE and all 7 had a distal, although slightly expanded, AVE/DVE. In those embryos, the perforations were located proximally and excluded only from the distally located AVE area (*Cerberus-like* or Hex-GFP-positive area) (**Figure 4.7**). This supported the hypothesis of a role of the AVE in the distribution of the perforations at these stages of development.

The accumulation of the perforations in the future posterior was followed by initiation of gastrulation. The first hallmark of gastrulation initiation is the breakage of the BM at the proximo-posterior site of the Epi. Then, ingression of cells from the Epi through the breached BM, accompanied by mesendoderm specification, eventually gives rise to the trilaminar embryo. Interestingly, the accumulated perforations on the posterior site persisted along the future primitive streak site even after its formation and extension. The extension took place along the perforations' domain progressively suggesting that they may play role during gastrulation (**Figure 4.8 A-C**). Pre-patterning the BM by weakening it along the AP axis, suggested it may be priming gastrulation initiation and progression to take place specifically opposite the AVE. The weakening of the BM in combination with cell proliferation prior to BM breaching could be driving the formation and extension of the primitive streak. To examine how cell proliferation before gastrulation correlates with the perforations domain, E6.5-6.75 embryos were stained for BM and phospho-histone 3 (PH3) to mark cell proliferation. These immunostainings revealed a co-localisation of the two, suggesting that the weakened posterior BM in combination with the expanding Epi may be promoting progressive BM breaking and extension of the primitive streak (n=7; **Figure 4.8D**).

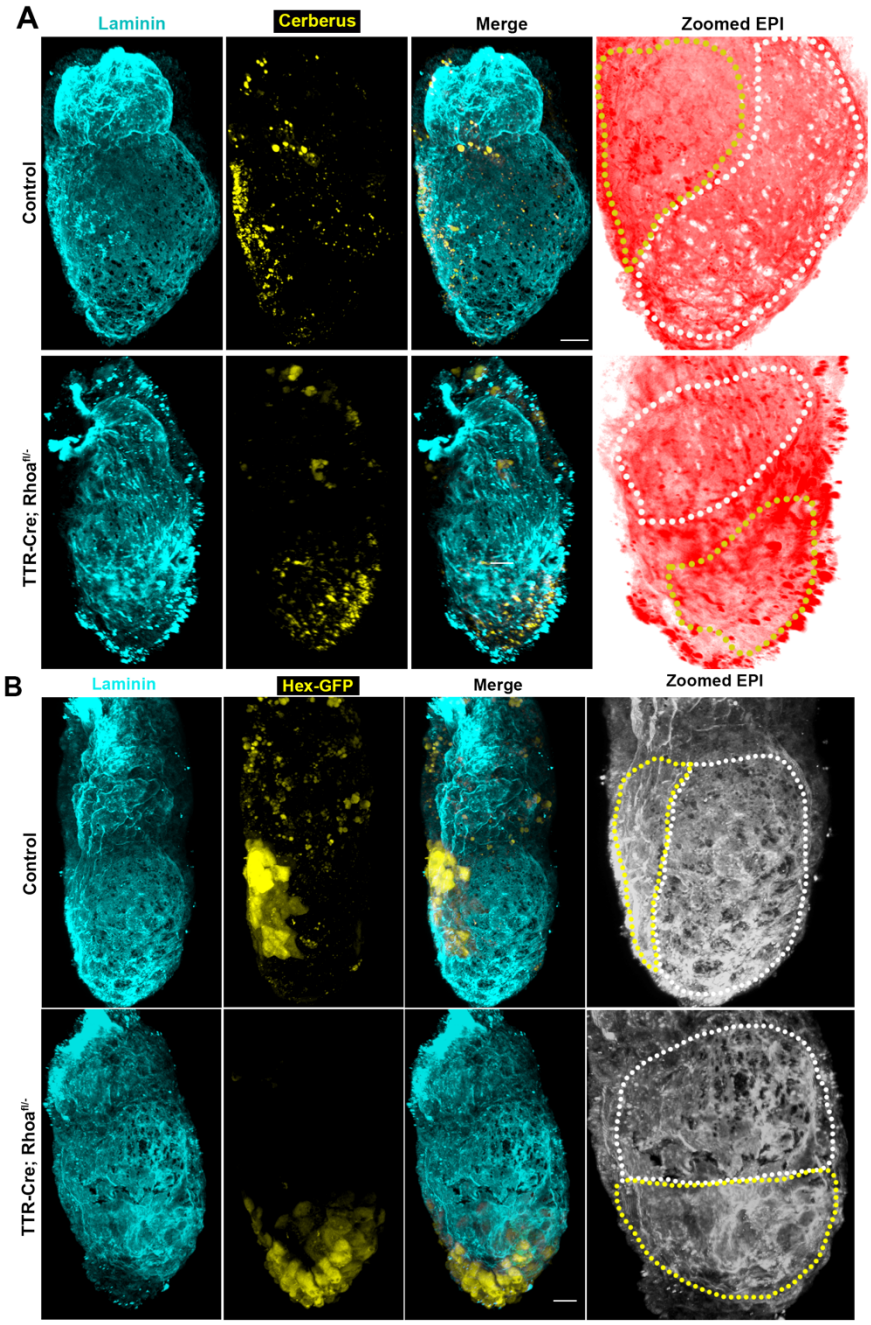

FIGURE 4.7: AVE MIGRATION INHIBITION PERTURBS PERFORATION DISTRIBUTION

(A) Embryos with deleted RhoA in the VE stained for Cerberus to assess the position of the AVE and laminin to visualise perforations. (B) Hex-GFP-positive embryos directly indicate the position of the AVE in both control and VE-deleted RhoA embryos. Yellow dotted line: AVE domain; White dotted line: Domain away from AVE. Scale bar = 20um

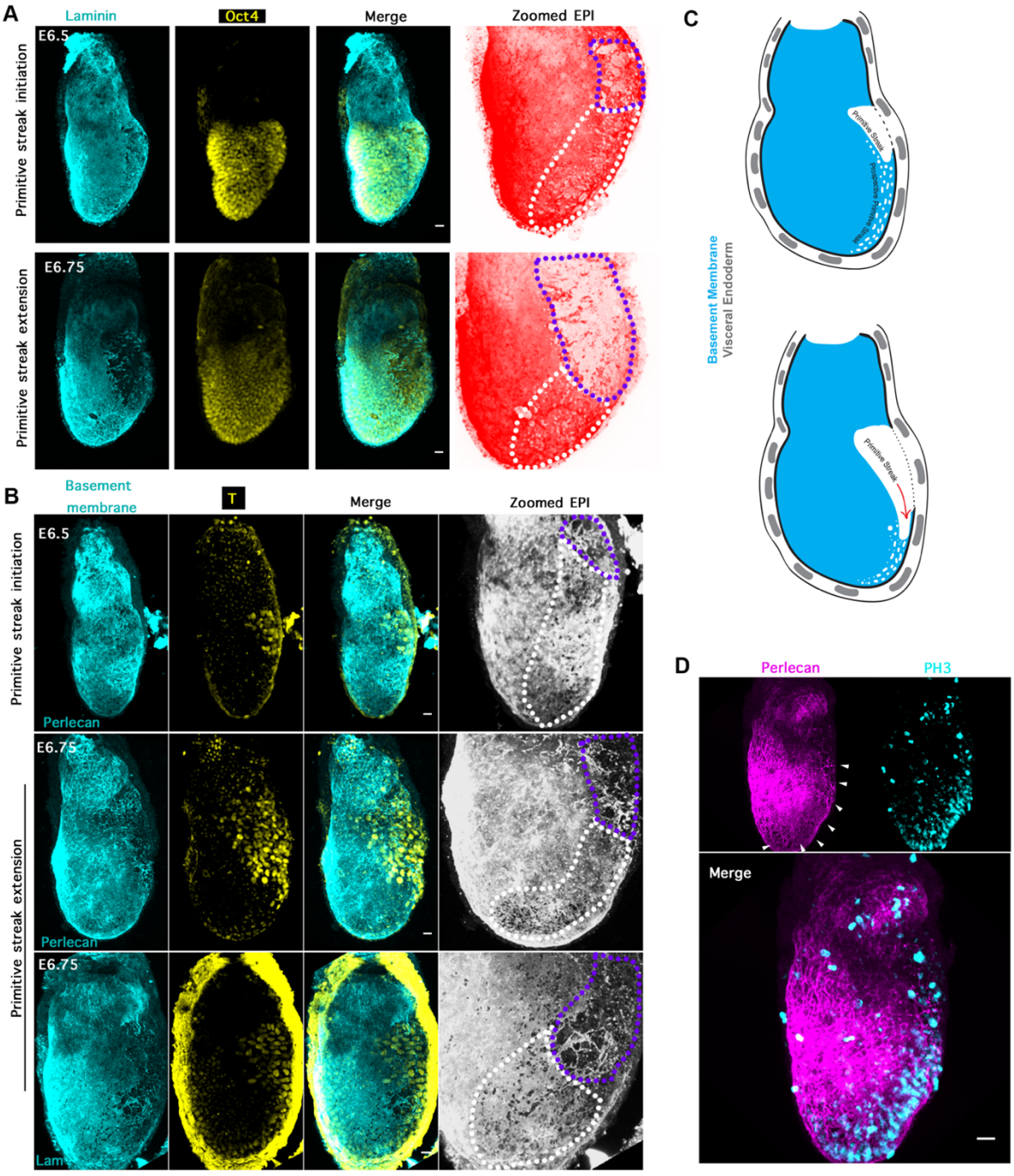

FIGURE 4.8: PERFORATION ACCUMULATION AND BASEMENT MEMBRANE BREACHING AT THE POSTERIOR

(A) Representative embryos stained for laminin and Oct4 at the initiation and extension of the primitive streak. Higher levels of Oct4 on one side denote the anterior. (B) Representative embryos at primitive streak initiation and extension and position of the mesendoderm-specified cells (T). Purple dotted line: breached BM; White dotted line: perforations lining the future primitive streak. (C) Schematic of primitive streak initiation and extension in relation to the position of accumulated perforations. (D) Immunostaining of E6.5 embryo with perlecan and phospho-histone 3 (PH3) for cell proliferation. White arrowheads point to the posterior perforations domain. Scale bar = 20um

4.2.4 *THE ROLE OF NODAL IN PERFORATION GENERATION*

The role of the AVE in perforation distribution revealed a previously unknown link between AP axis establishment and a change in the mechanical components of mouse embryo development. More importantly it provided evidence that the AVE controls this redistribution.

The signalling role of the AVE in embryo development has been extensively studied as it is the most instrumental event in AP establishment. In particular, the AVE secretes the Nodal inhibitors, *Cerberus-like and Lefty1,* which create a gradient of Nodal activity across the Epi. When the AVE migrates to one side of the embryo, a Nodal activity gradient is established along an axis perpendicular to the PD axis (**Figure 4.9A**). In turn Nodal promotes mesendodermal specification on one side of the embryo establishing the AP axis. Since Nodal elicits a response in the Epi for cell specification it was hypothesised that it could also promote Epi cells to remodel the underlying BM. To put this hypothesis to the test, a tamoxifen-inducible Nodal-KO line (Nodal fl/fl:RCreT2) was used to delete Nodal in the post-implantation stages. The BM appearance was then assessed.

Nodal fl/fl:RCreT2 embryos at E5.75 were recovered and cultured in the presence or absence of (Z)-4-hydroxytamoxifen for 16 hours to allow embryos to enter the pre-gastrula stages. The cultured embryos were then fixed and stained with laminin and assessed for the presence of perforations. In the Nodal-deleted embryos (confirmed by genotyping) the BM did not have any perforations (17/17). Moreover, they had accumulated speckled and stranded laminin throughout the embryo. On the other hand, most controls (7/10) had perforations and the BM was smooth with the exception of the BM under the AVE (where laminin appeared to be accumulating) (**Figure 4.9B, C**).

Upon deletion of Nodal, the AVE failed to be maintained, as revealed when staining for *Cerberus-like* in the Nodal-deleted embryos (**Figure 4.9B** white arrowhead). Thus, the absence of Nodal and not the AVE *per se* led to the phenotype of the BM. If the AVE provided some other factor that was important in maintaining integrity of the underlying BM, a dense and unperforated BM would not have been observed. This further supported the hypothesis that the AVE's role in setting up a Nodal activity gradient is key in the shifting of perforation distribution.

To further support the hypothesis that this Nodal-mediated BM remodelling in the embryo is attributed to the Epi cells, it was necessary to investigate how ESCs remodel gelatin in the presence of Nodal inhibition. For this, ESCs were plated on Cy3-Gelatin and allowed to differentiate for 48 hours in the presence of the Nodal inhibitor SB431542 before the plate was scanned to assess remodelling of gelatin. Indeed, inhibition of Nodal perturbed the cells' ability to create perforations in the gelatin coat, thus suggesting that the Epi requires Nodal (**Figure 4.9D**).

Together, the experiments described here suggest that Nodal promotes the Epi cells to create perforations and the redistribution of the perforations is a result of patterned Nodal activity as instructed by the AVE position.

4.2.5 *IDENTIFICATION OF CANDIDATE MMPS RESPONSIBLE FOR THE PERFORATIONS*

The experiments described up to this point revealed a requirement for Nodal for the embryo to achieve the perforated BM under the Epi. To identify the downstream effectors of BM remodelling we looked at the family of matrix metalloproteinases (MMPs) that are known for their role in degrading the BM and are highly expressed in the Epi at the early post-implantation stages (Boroviak et al., 2015; Page-McCaw et al., 2007).

Sequencing studies of the pre and post-implantation mouse Epi showed a significant upregulation of MMP2, 14 and 25 upon implantation (Boroviak et al., 2015). The expression and Epi specificity of these candidates was confirmed by Geo-Seq data produced in collaboration with the lab of Dr. Naihe Jiang. Additionally, the expression of MMP2, 14 and 25 was highly upregulated in Epi-like cells (EpiLC cells) when compared to undifferentiated ESCs (Acampora et al., 2016) (**Figure 4.10A-D**).

To establish whether these MMPs are downstream of the Nodal pathway, ESCs were allowed to differentiate for 48 hours to switch on expression of the MMPs in the presence or absence of the Nodal inhibitor SB451342 (40uM). The cells were harvested, and cDNA was prepared for qPCR. The expression of the candidate MMPs was significantly reduced in the presence of the Nodal inhibitor which was in accordance with the literature (Costello et al., 2009; Huang et al., 2017). The effect of Nodal inhibition on MMP2 and 14 was confirmed at the protein level as well by western blot (commercially available MMP25 antibodies were not compatible with western blot) (**Figure 4.10E-H**). The presence of MMP14 was also confirmed directly in the embryo with immunostaining (commercially available MMP2 antibodies were not compatible with immunostainings for these stages of development). In the E5.5 embryos, MMP14 was found everywhere in the Epi only (**Figure 4.11A**) and then (E6.25 – E6.5) its localisation shifted posteriorly lining the site of perforations and the domain of expression of the invadopodia marker Sh3pxd2a (Tks5) (Murphy and Courtneidge, 2011) (**Figure 4.11B-C**). The co-localisation of the MMP14 and Sh3pxd2a domains of expression was supportive of an invadopodia-mediated degradation at the pre-gastrula stages (E6.25 – E6.5). Geo-seq data from the early post-implantation stages (E5.25 – E5.75), however, showed no expression of Sh3pxd2a suggesting that there is no invadopodia-mediated generation of perforations at the earlier stages.

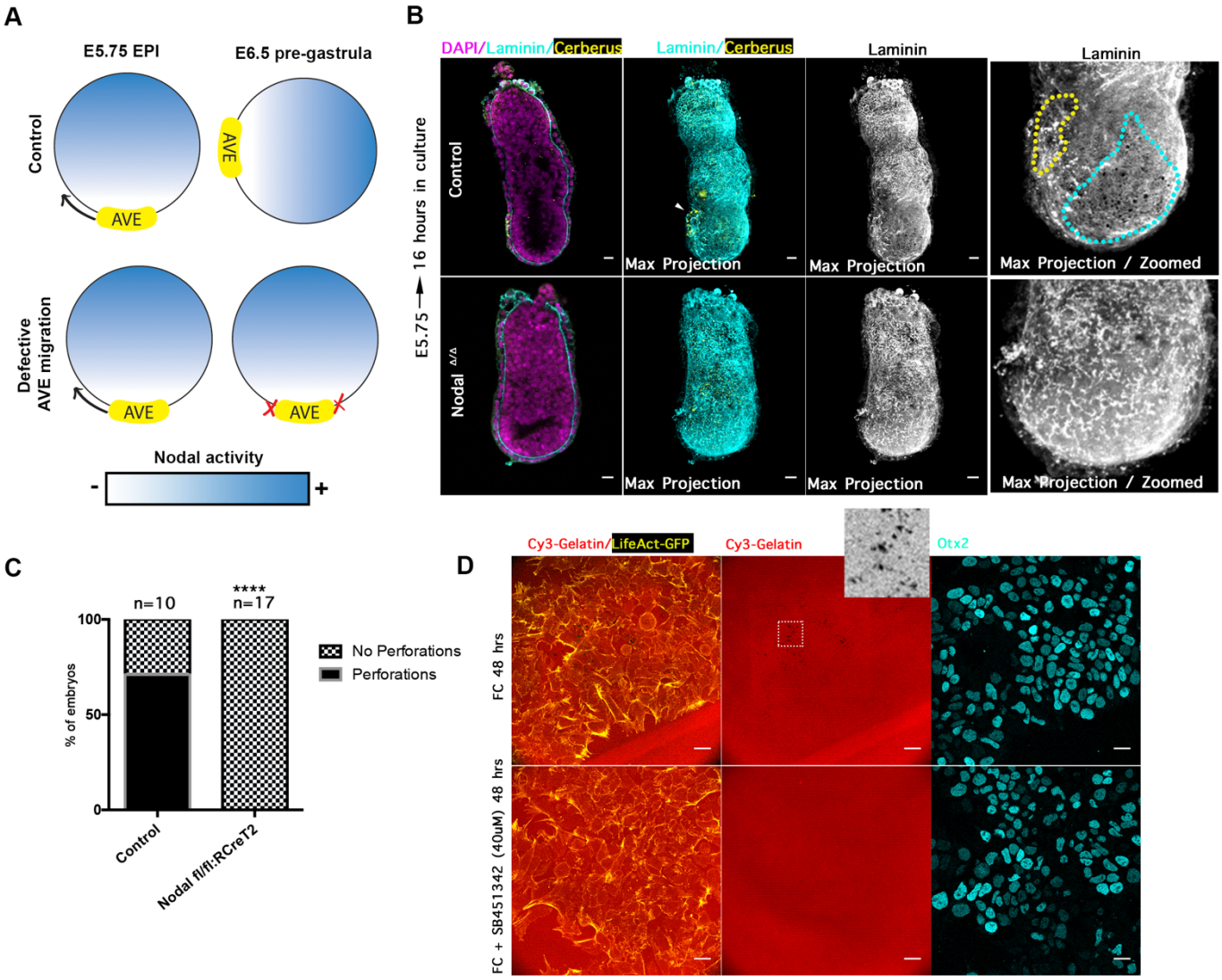

FIGURE 4.9: THE EFFECT OF NODAL ON PERFORATIONS

(A) Schematic of Nodal activity gradient established in Epi in normal and perturbed AVE migration. (B) Nodal fl/fl:RCreT2 embryos recovered at E5.75 and cultured in the absence (Control) or presence of tamoxifen (Nodal $^{\Delta/\Delta}$) stained for laminin and Cerberus. AVE is not maintained in the Nodal-deleted embryos in contrast to the control embryos (white arrowhead). Yellow dotted line = AVE position; Cyan dotted line = perforation domain (C) Quantification of percentage of embryos in control and Nodal-deleted embryos with and without perforations. Unpaired student's t-test. ****<0.0001. (D) Lifeact-GFP ESCs differentiated (feeder cell medium (FC) in the absence of 2iLif) for 48 hours in the presence or absence of SB451342 (40uM) plated on fluorescent gelatin (Gelatin-Cy3). Staining for Otx2 shows that treatment with Nodal inhibitor does not affect differentiation. Scale bar = 20um.

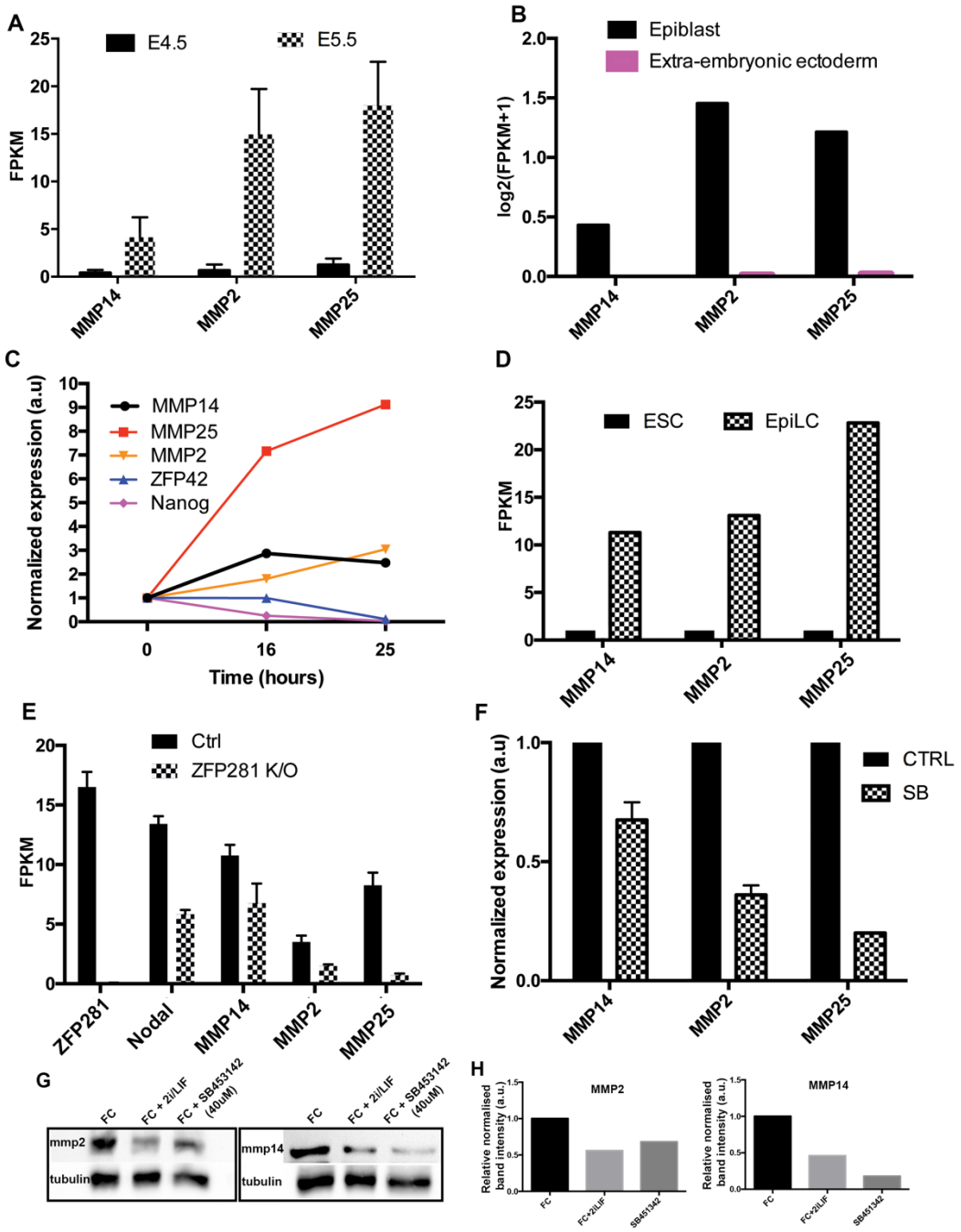

FIGURE 4.10: EXPRESSION OF CANDIDATE MMPS IN POST-IMPLANTATION EMBRYOS AND ESCS AND RESPONSE TO NODAL

(A) MMPs expression in the Epi in E4.5 and E5.5 stages (Boroviak et al., 2015). MMPs expression is higher in the E5.5 (differentiated) Epi. (B) MMPs expression in the Epi and extra-embryonic ectoderm. MMPs are specifically expressed in the Epi. (C) MMPs expression during ESCs differentiation (Kalkan et al., 2017). MMPs expression starts to increase when ESCs start to differentiate. (D) MMPs expression in ESCs and EpiLC (Acampora et al., 2016). (E) Nodal and MMPs expression levels in ZFP281 KO mice (Huang et al., 2017). (F) qPCR data from control and Nodal inhibited treated ESCs. (G) Western blot for MMP2 and MMP14 in differentiated (FC), undifferentiated (FC + 2iLif) and differentiated in presence of Nodal inhibitor (FC + SB451342 (40 uM). (H) Quantification of Western Blot bands intensity normalised to tubulin first and then FC.

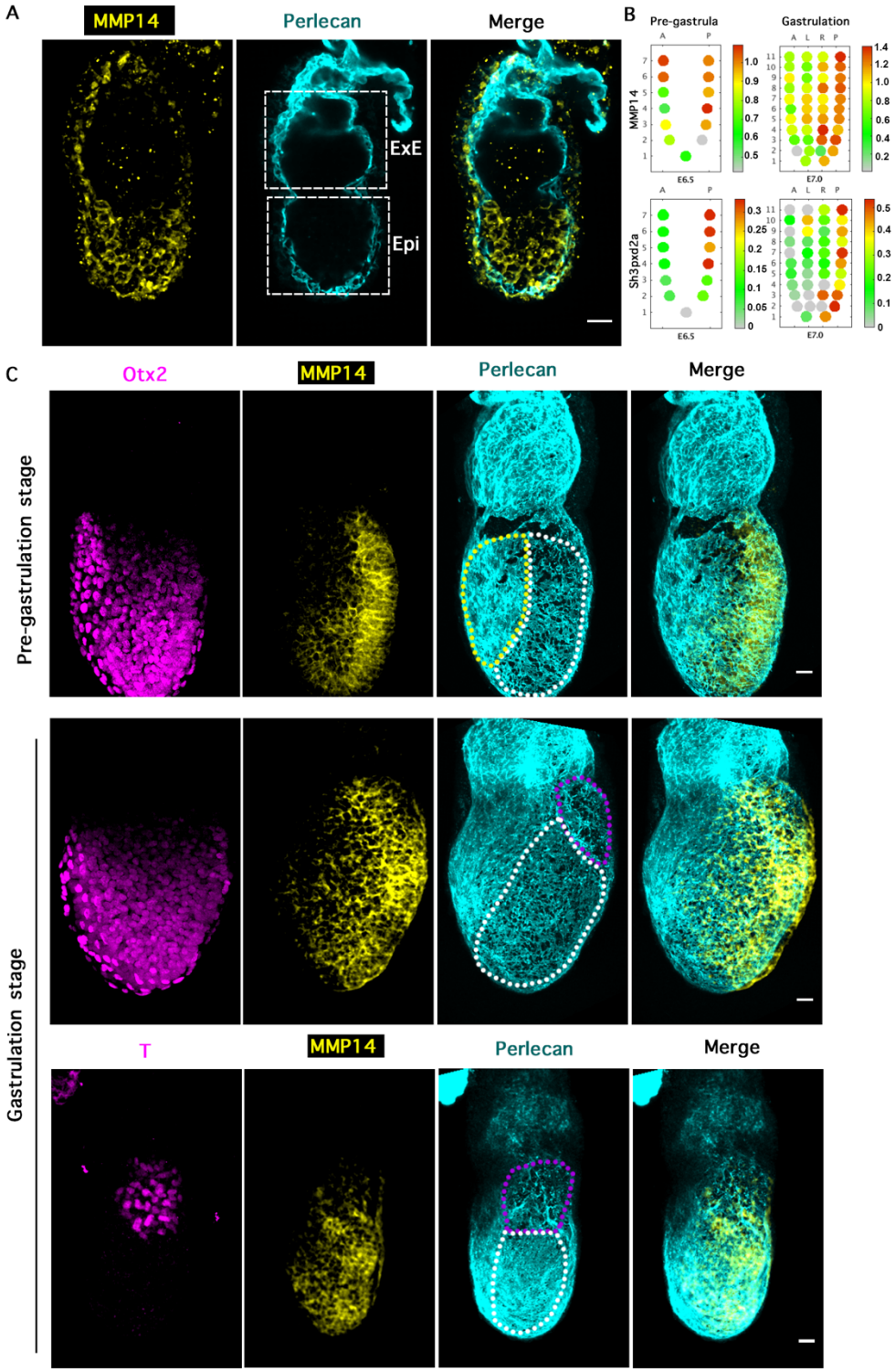

FIGURE 4.11: MMP14 LOCALISATION IN POST-IMPLANTATION DEVELOPMENT

(A) Immunostaining for MMP14 in early post-implantation embryo reveals uniform Epi-specific expression/secretion. (B) Spatial transcriptome for MMP14 and invadopodia marker Sh3pxd2a in pre-gastrula (E6.5) and gastrulation stages (E7.0). A=anterior, P=posterior, L=left, R=right. Data provided by Ran Wang (Naihe Jiang group) (C) MMP14 localisation after AP axis establishment and during gastrulation. Co-localisation with domain of perforations. Scale bar = 20um

To genetically address the effect of loss of MMP activity on the ability of cells to remodel the underlying ECM, MMP14 was targeted for knockout as it is also important in the activation of MMP2. For this the CRISPR/Cas9 technology was implemented to delete a region spanning the initiation codon (ATG) in exon 1 of MMP14 to perturb its translation. To achieve this, two gRNAs were generated using the online tool provided by Zhang and colleagues to flank the ATG codon in exon1 and cloned into the plasmid PX459 containing the Cas9 sequence and gRNA scaffold sequence (1 gRNA per plasmid). The two plasmids carrying the two gRNAs were co-transfected in LifeAct-GFP cells and selected over the course of 48 hours (**Figure 4.12A)**. Clones were isolated by serial dilutions and positive clones were detected by genotyping using the primers described in Materials and Methods (**Figure 4.12B**). Loss of protein was confirmed by western blot (**Figure 4.12C**).

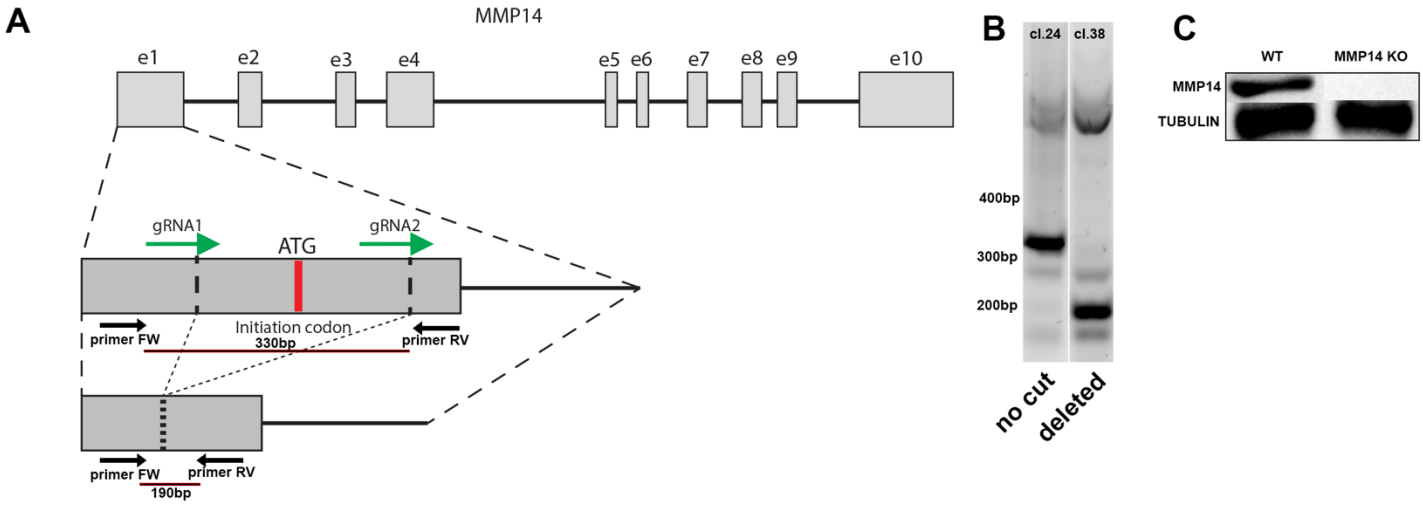

FIGURE 4.12: GENERATION OF MMP14-KO ESCS

(A) Schematic of the KO strategy using a combination of two gRNAs flanking the initiation codon in exon 1. Resulting exon does not have the initiation codon and is 140bp shorter than the wildtype allele. (B) Identification of positive clones using genotyping with primers flanking a 330bp region that contains the portion of the gene targeted for deletion. Clone 38 was the clone selected to be used in further studies. (C) Confirmation of MMP14 KO by western blot.

When the MMP14-KO cells were plated on Cy3-Gelatin to assess their BM remodelling potential as before, the cells failed to remodel the underlying gelatin. This indicated that in the cell model, abrogating the effect of MMP14 was sufficient to perturb BM remodelling (**Figure 4.13**). MMP14-KO cells' reduced ability to degrade underlying ECM further supported the role of MMPs in BM remodelling by the Epi.

To address the effect of MMP inhibition on BM perforations in the embryo, E5.75 wildtype embryos were recovered and cultured for 16 hours to enter pre-gastrula stages, in the presence or absence of the MMP

inhibitors NSC405020 (100uM; MMP14 specific inhibitor) + Prinomastat hydrochloride (20uM; broad spectrum inhibitor; IC_{50} =5pM for MMP2). Embryos cultured in the presence of the inhibitors developed a dense BM with absent perforations (16/18). Control embryos had perforations and a smooth BM (9/13) (Figure 34A, B). A fraction (2/20) of the MMP inhibitor-treated embryos had a breached BM at the distal site (**Figure 4.14C**).

In summary, the experiments and literature suggest that the candidate MMPs are expressed in the post-implantation Epi, are downstream of Nodal and are responsible for the perforations and smooth appearance of the BM.

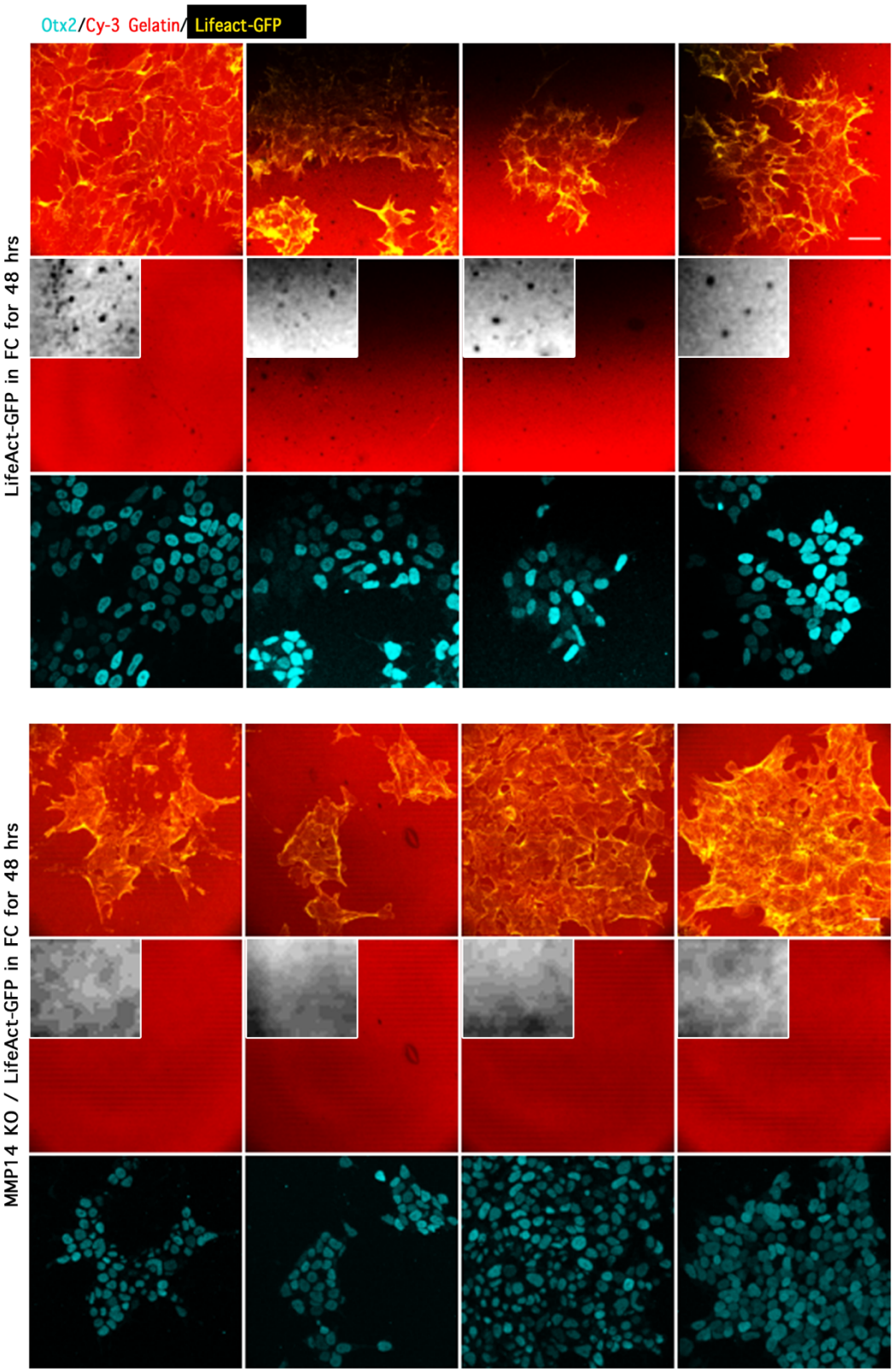

FIGURE 4.13: MMP14-KO ESCS HAVE REDUCED BASEMENT MEMBRANE REMODELLING ABILITY

Wildtype Lifeact ESCs and MMP14 KO ESCs differentiated for 48 hours and plated on fluorescent gelatin Gelatin-Cy3 and assessed for remodelling. Perforations were rarely observed under the MMP14 KO colonies.

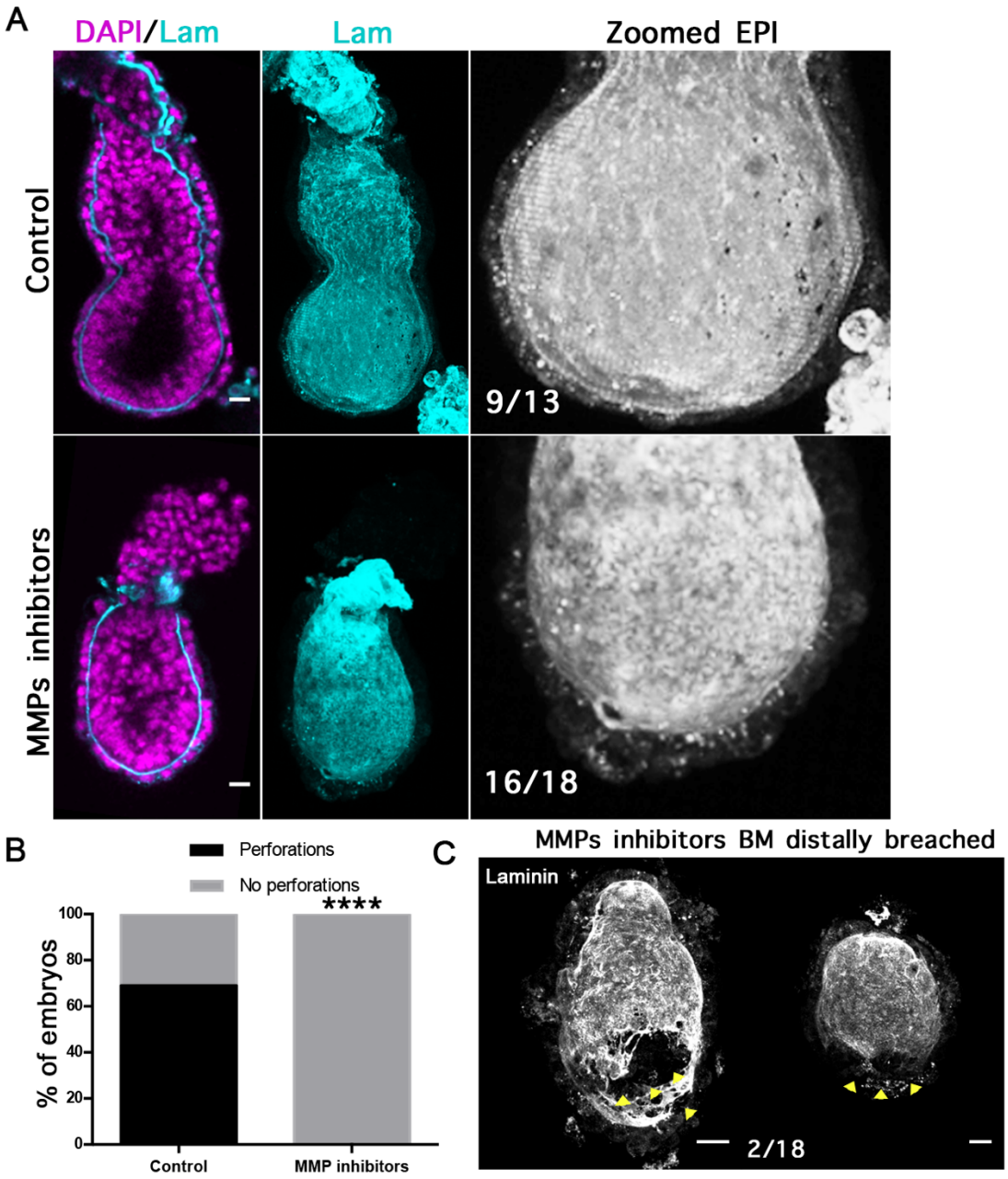

FIGURE 4.14: MMP INHIBITION IN CULTURED EMBRYOS ABOLISHES PERFORATED MORPHOLOGY

(A) Embryos recovered at E5.75 and cultured for 16 hours in a combination of MMPs inhibitor (Prinomastat (20uM) and NSC405020 (100uM)), fixed and stained for laminin. (B) Quantification of embryos with and without perforations in the presence or absence of MMP inhibitors. Chi-squared test, ****<0.0001. (C) Only 2 out of 18 MMP inhibitor-treated embryos showed distal breaching (yellow arrowhead) not included in the analysis. Scale bar = 20um

4.2.6 *MMP ACTIVITY IS REQUIRED FOR EGG CYLINDER GROWTH*

The above experiments demonstrated that Nodal is required in driving MMP expression in the Epi, which in turn generate perforations in the BM. The next question to be addressed was that of the role of perforations in egg cylinder development and growth.

To address this, embryos cultured in MMP inhibitors were quantified for the presence of perforations (as described in the previous section), their size at the end of the culture and their growth rate. The size of MMP inhibitor-treated embryos was significantly reduced by the end of the culture and the Epi appeared very crowded with a collapsed proamniotic cavity (**Figure 4.15A, B**). The growth rate of the egg cylinders when measured along the PD axis from the most proximal to the most distal point of the embryo, appeared to level after 8-9 hours in culture. Once the embryo started stalling in growth, the Epi started to show increased apoptosis (**Figure 4.15A**). By the end of the experiment, the treated embryos only increased in size by a factor of 1.2 as opposed to the control embryos which increased in size by a factor of 1.8 (**Figure 4.15C, D**).

To further understand the dynamics of growth in an environment that cannot be remodelled, a 3D cell culture system was used to mimic the expanding Epi surrounded by the BM. To do this, ESCs were suspended in Matrigel and allowed to grow for 60 hours in total. The Matrigel provides both the signalling required to polarise the cells but also a physical scaffold that needs to be remodelled by the cells to accommodate growth. First, the ESCs were suspended in Matrigel for 48 hours in the absence of 2i+Lif to acquire the Epi morphology and character (Shahbazi et al., 2017). At this point, the combination of MMP inhibitors (NSC405020 and Prinomastat) were added for a further 12 hours before fixation and staining of the spheroids. 60 hours in total after plating, ESCs formed spheroids of an average area of 2100um^3 which was significantly greater than ESCs treated with the combination of MMP inhibitors (900um^3) at 48 hours after plating (**Figure 4.16A, B**).

To monitor MMP activity in this system, Matrigel was mixed with DQ collagen (a MMP activity reporter). This is a molecule that is cleaved by the MMPs to produce fluorescence. Since fluorescence persists after cleaving the DQ collagen, it was not possible to use it to monitor MMP activity in the system where ESC spheroids are inhibited for 48 hours, as fluorescence from the cleaved molecule also reported MMP activity prior to the addition of inhibitors. However, when used in experiments where MMP inhibitors were added from the time of plating (i.e. day 0) and cultured for 60 hours, there was no detectable fluorescence from DQ collagen, confirming the effectiveness of the MMP inhibitors. Strikingly, when ESCs were subjected to MMPs inhibition from day 0 (at which point they were single cells), they failed to progress past the first cell division (**Figure 4.16C**).

Single cells in Matrigel in the absence of MMP activity halted their proliferation due to their inability to remodel the surrounding ECM. However, spheroids left to grow for 48 hours prior to MMP inhibition induced apoptosis to cope with the abrupt handicap in remodelling the Matrigel (**Figure 4.16D**). This was reminiscent of the embryo Epi observed in embryos cultured in the presence of MMP inhibitors.

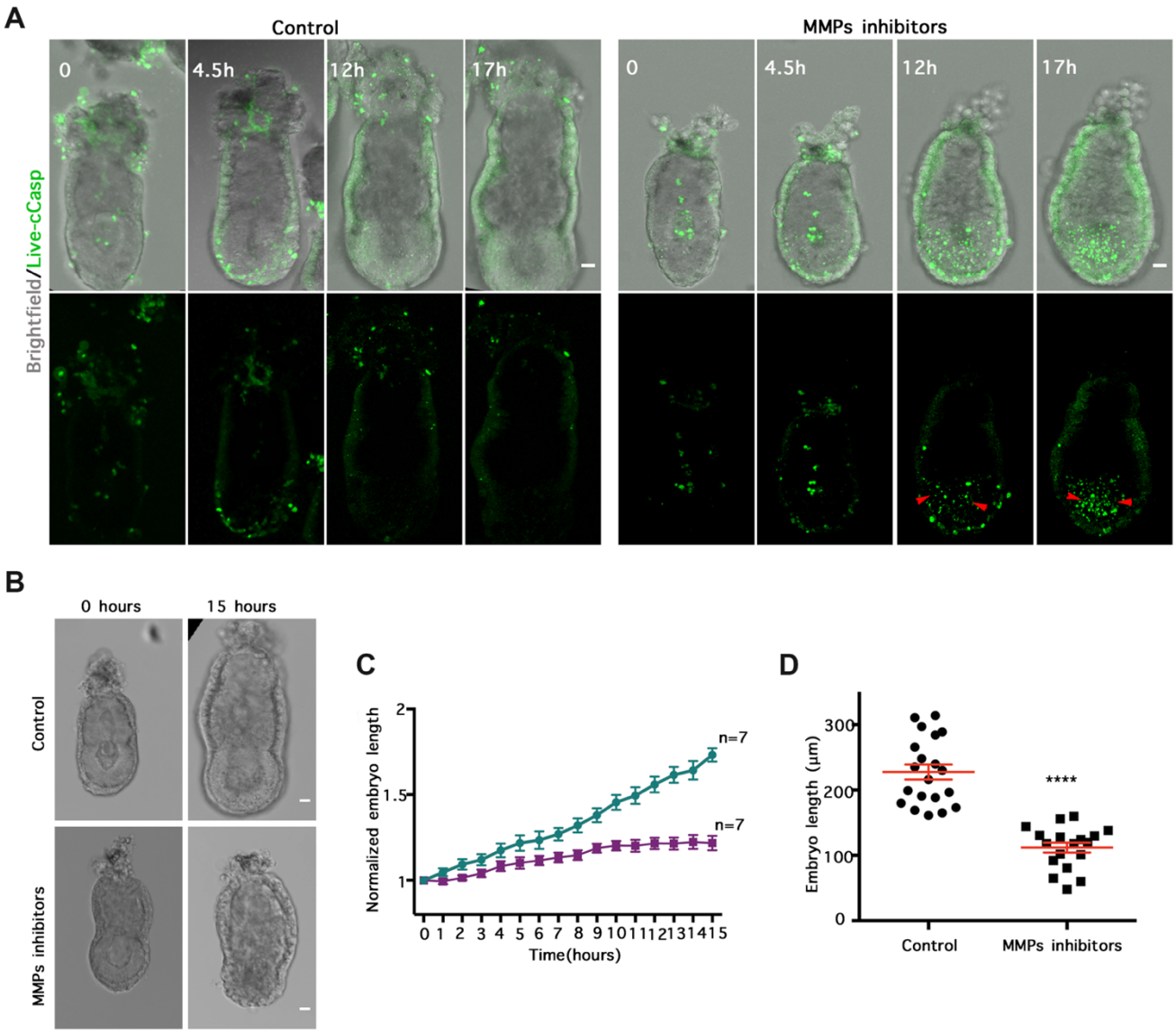

FIGURE 4.15: MMP INHIBITION ON EGG CYLINDER GROWTH

(A) Live imaging of embryos treated in MMP inhibitors (combination of Prinomastat (20uM) and NSC405020 (100uM) in c-Casp live dye to monitor cell death. c-Casp signal becomes enriched in the Epi during the course of the culture in the MMP inhibitor-treated embryos (red arrowheads). (B) Egg cylinder appearance by the end of the culture in the presence of the MMP inhinitors. Epi appears collapsed. (C) Increase in embryo length (from tip of ExE to tip of Epi) during culture in the presence or absence of MMP treatment in relation to starting size. (D) Final size comparison of embryos in control and MMP inhibitor treatment. Paired student's t-test; ****<0.0001. Scale bar = 20um

To test whether in the reduced spheroid system MMP14 deletion would be sufficient to affect the growth of the spheroids, MMP14-KO spheroids were grown in Matrigel for 60 hours. The spheroids exhibited reduced growth, reproducing the results of MMP-inhibited spheroids (**Figure 4.16E, F**).

In conclusion, here the experiments provide evidence of the embryo's requirement of MMPs for egg cylinder growth and the effects of the absence of such BM remodelling on both size and cell survival.

4.2.7 PERFORATIONS DEFORM IN RELATION TO THE DIRECTION OF EGG CYLINDER GROWTH

While the MMP requirement is evident for the growth of the egg cylinder, how this physically manifests can only be determined through observation of the BM during this growth. The hypothesis of the physical role of perforations in making the BM more flexible is their ability to deform along the direction of growth without the need for BM breaking or extra BM deposition.

According to this hypothesis it was expected that during growth, these perforations would be deformed along the PD axis as this is the direction of egg cylinder growth (Copp, 1978). Since there is no available mouse fluorescent BM reporter line and tagged antibodies for collagen are sequestered in the VE, it was not possible to dynamically observe the shape of perforations during growth. To address this, embryos at E5.0 – 5.25 (a stage before egg cylinder growth) and embryos at E5.5 – 5.75 (stages during egg cylinder growth) were recovered and stained for a BM marker. The maximum intensity projected images were then thresholded to create a binary image and a vector map analysis was applied. In this analysis, vectors are generated in an overlaid grid on the image. The angle of vectors is automatically determined to follow the trending direction of the perforations' deformation; generally following the long axis of the perforations (**Figure 4.17A, B**). This created an unbiased collection of vector angles from 10 E5.0 – 5.25 and 10 E5.5 – 5.75 embryos that were added to a histogram to assess the distribution. Comparing the two samples, revealed a significant skew in the distribution of vector angles in the E5.5 – 5.75 group towards being aligned with the PD axis; the direction of growth (**Figure 4.17C, D**).

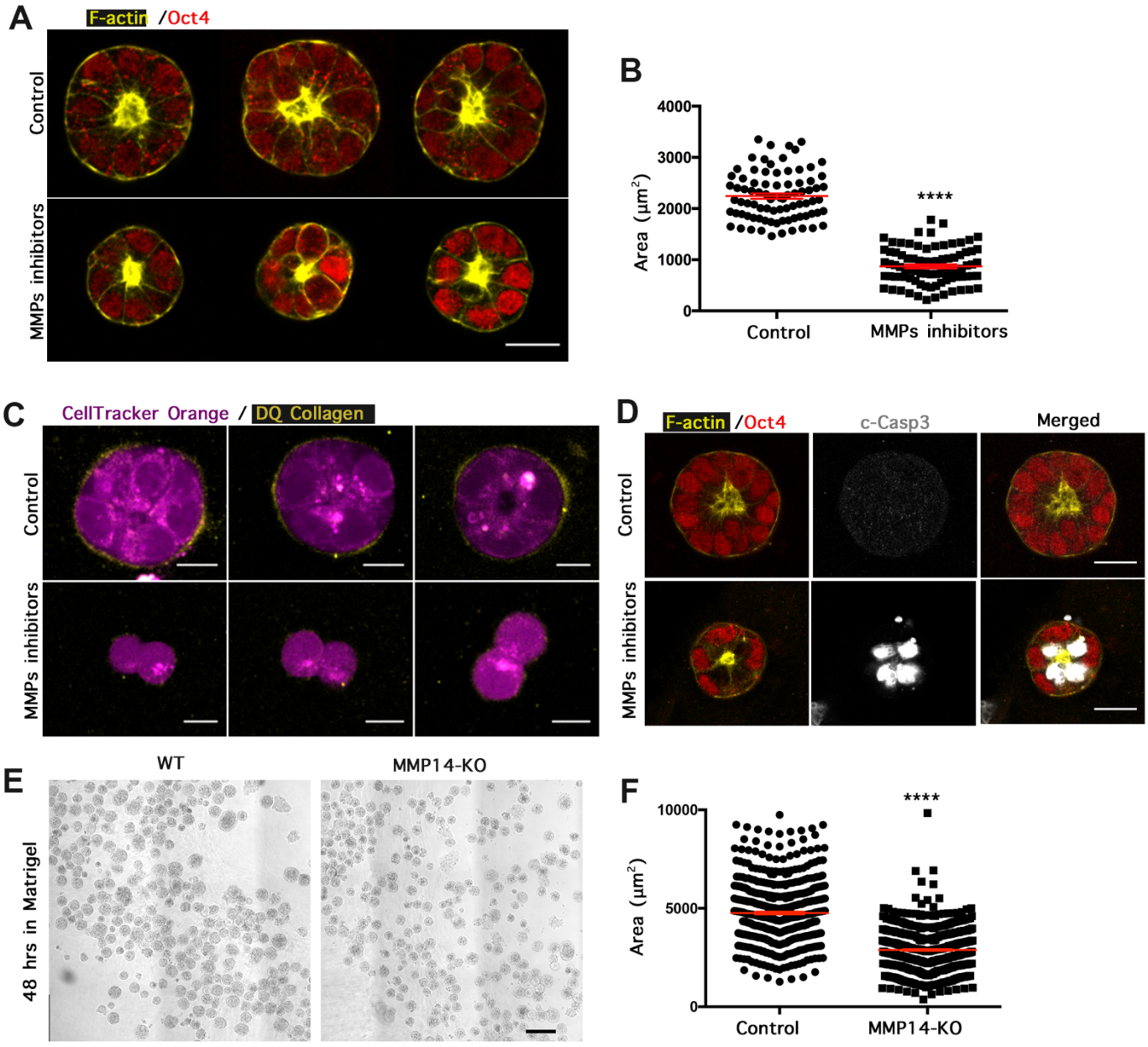

FIGURE 4.16: *IN VITRO* MODELLING OF EPIBLAST GROWTH IN ABSENCE OF MMP ACTIVITY

(A) ESCs suspended in Matrigel for 48 hours and MMP inhibitors introduced 24 hours after plating. (B) Quantification of size of ESC spheroids in the presence or absence of MMP inhibitors (Prinomastat 20uM + NSC405020 (100uM)). Unpaired student's t-test. ****<0.0001. (C) ESCs embedded in DQ-collagen/Matrigel and MMPs introduced at the time of plating. Notice the failure of cells to divide more than once and absent DQ-collagen signal indicating absent MMP activity. (D) ESCs suspended in Matrigel for 60 hours with MMP inhibitors introduced 48 hours after plating. Spheroids are stained for c-Casp3 to assess apoptosis. Notice increased cell death in treated cells. (E) Wildtype and MMP14-KO cells embedded in Matrigel for 48 hours to assess extent of growth. (F) Quantification of ESC spheroid size in wildtype and MMP14-KO spheroids. Unpaired student's t-test. ****<0.0001. Scale bar = 20um

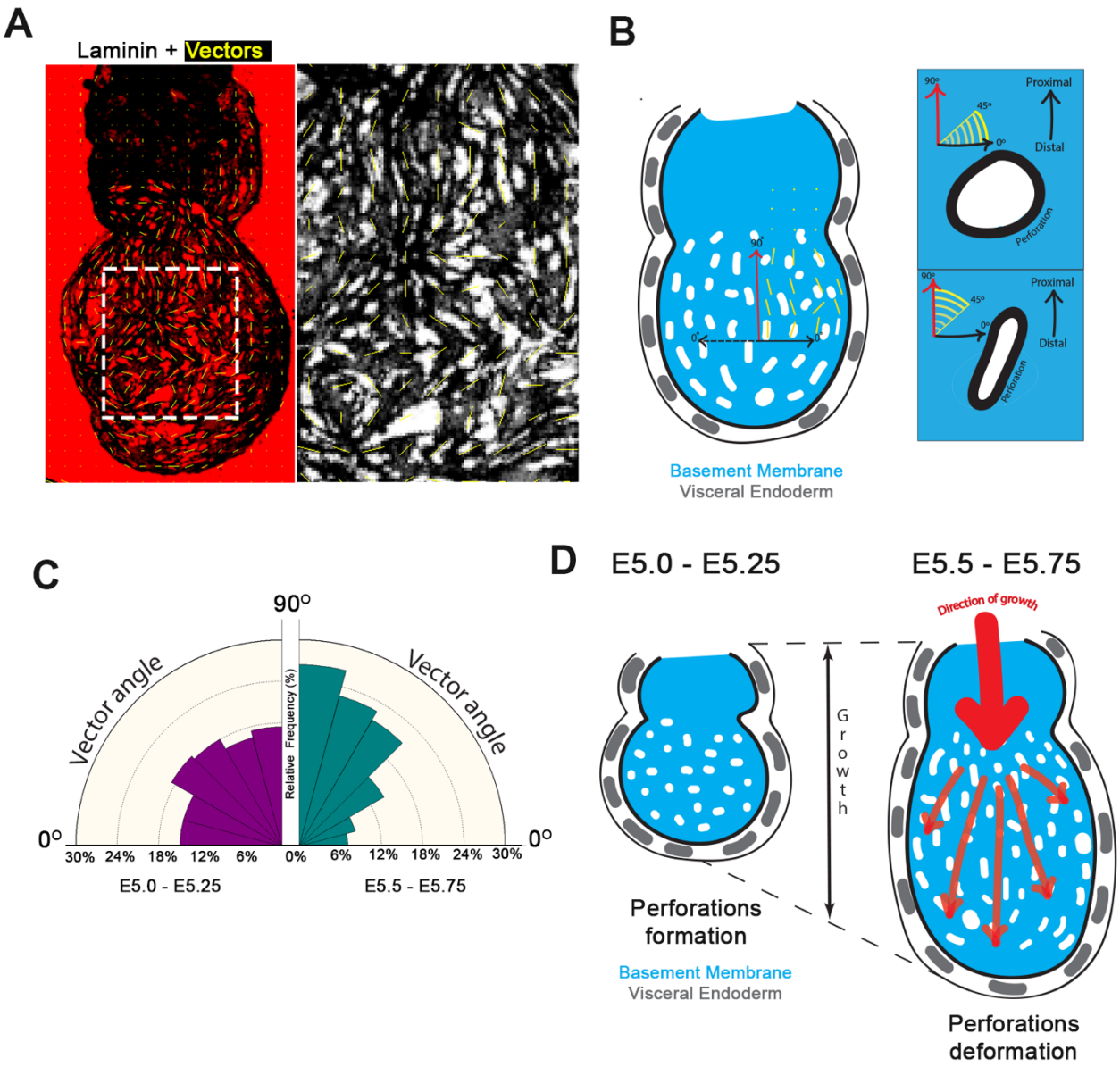

FIGURE 4.17: PERFORATIONS DEFORM IN THE DIRECTION OF THE EMBRYO GROWTH

(A) Maximum projection of laminin in an E5.75 embryo, manually thresholded with vector mapping applied. (B) Schematic of how vectors align in response to the shape of perforations. Orientation of the vectors in relation to an axis as shown in the diagram. (C) Distribution of vector angles with 90° -angled vectors being aligned to the proximal-distal axis and 0° -angled vectors perpendicular to the proximal-distal axis. (D) Schematic of how perforations deform as the embryo grows along the proximal-distal axis.

4.2.8 *A model for Basement Membrane remodelling in the early post-implantation mouse embryo*

The experiments described in the previous sections, revealed a novel morphogenetic event involving the architecture and patterning of the BM under the Epi that takes place during egg cylinder growth and extends to the gastrula stages. This event is involved in egg cylinder growth and by extension Epi cell survival and has a potential role in primitive streak extension during gastrulation. The sequence of events in patterning the BM as described above can be summarised below and in Figure 4.18:

1) Upon implantation and formation of the nascent egg cylinder (corresponding to E5.0) the BM under the Epi exhibits a perforated appearance as opposed to the BM under the ExE that appears continuous and unperforated.
2) At AVE induction, the AVE inhibits Nodal activity in its proximity by secretion of the Nodal antagonists *Cerberus-like* and *Lefty1*. Absence of Nodal activity in turn leads to downregulation of MMPs that are required to create perforations that accommodate growth of the embryo along the PD axis.
3) When the AVE colonises the anterior site of the embryo, the perforations accumulate to the opposite site which is the future posterior due to the restricted MMP expression as dictated by the Nodal activity gradient along the AP axis.
4) Following accumulation of perforations on the future posterior, the primitive streak (PS) initiates on the proximo-posterior site of the embryo by breaching the BM. The perforations persist along the domain of the future extended PS. As the PS extends it does so along the perforations track suggesting a role of the AP-patterned BM in PS extension.

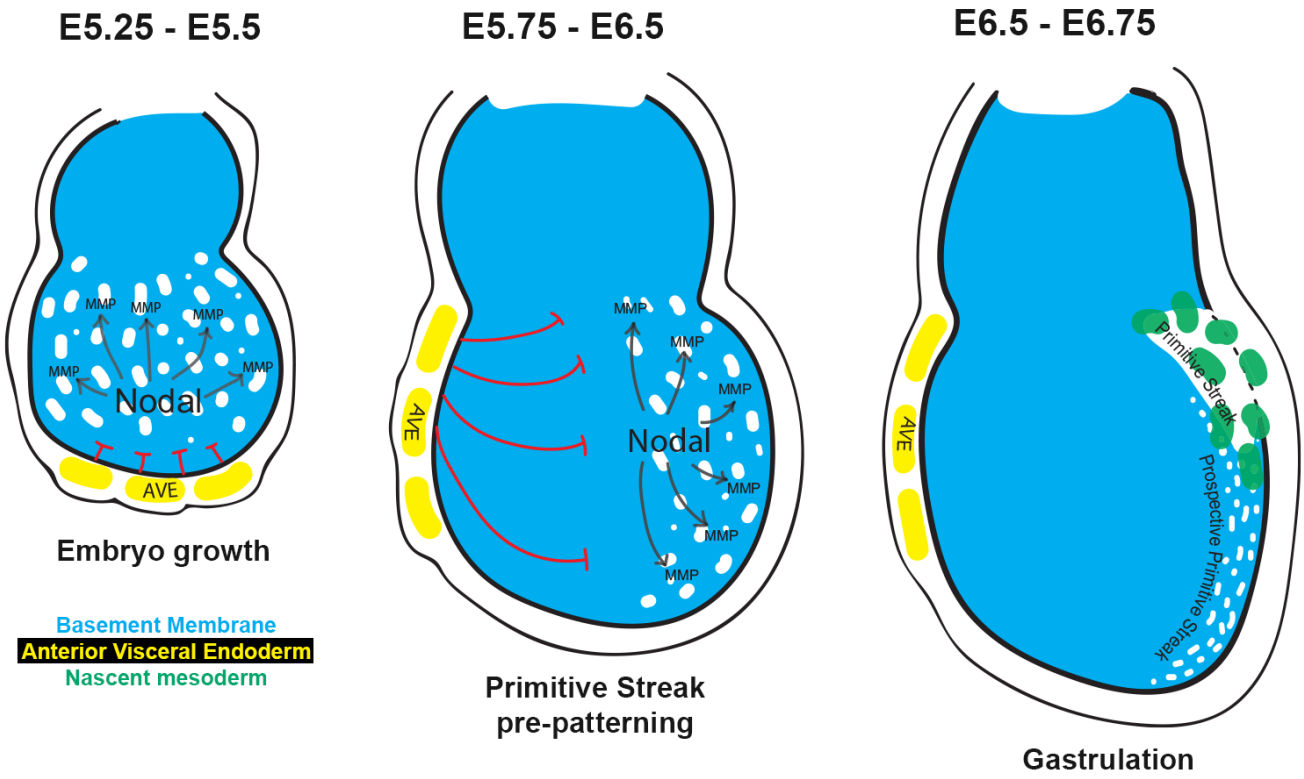

FIGURE 4.18: A MODEL FOR BASEMENT MEMBRANE REMODELLING IN THE EARLY POST-IMPLANTATION MOUSE EMBRYO

Initially the perforations are present uniformly everywhere in response to Nodal, which drives MMP expression from the Epi. The embryo grows along the proximal-distal axis during these stages as permitted by the deformation of the perforations. The AVE migrates anteriorly setting up a Nodal activity gradient along the anterior-posterior axis which in turn drives MMP expression asymmetrically towards the posterior and perforation accumulation in the future primitive streak. Upon initiation of gastrulation the BM is breached proximo-posteriorly and the breach extends along the perforations domain that persist after their redistribution.

4.3 DISCUSSION

In this study, the physical role of the BM was investigated in the context of egg cylinder elongation during the early post-implantation stages up to the stage of gastrulation. Tampering with the BM architecture during these stages revealed the importance of patterning of the BM and demonstrated a previously unknown mechanism of BM regulation that is controlled by Nodal and the established AP axis. In summary the data provided in the described experiments led to the formulation of a model of BM patterning regulation that begins as early as E5.0; upon implantation of the embryo to the uterine tissue and initiation of the egg cylinder transformation. The main findings can be summarised in the list of points below:

1) Upon Epi cell differentiation, they start to express MMPs that can remodel the underlying nascent BM.
2) Perforations form throughout the Epi BM and are distributed evenly as a result of MMPs expression.
3) Growth of the egg cylinder is permitted along the direction of growth (proximo-distally) only in the presence of these perforations.
4) Establishment of the AVE and migration creates a Nodal activity pattern that inhibits the region of the Epi close to the AVE from expressing MMPs, which manifests in "filling up" of the holes close to the anterior and their accumulation at the posterior.
5) Once the perforations colonise the posterior, they persist even during gastrulation and line the future primitive streak, suggesting a role of PS BM pre-patterning in gastrulation progression.

4.3.1 MMPS ARE EXPRESSED IN THE POST-IMPLANTATION EPIBLAST

The role of MMP activity in the growing egg cylinder is not well documented in the literature. There is only one study, by Hiramatsu and colleagues (2013), investigating the expression of MMPs and their activity in the context of Epi to VE transmigration. More specifically, *in situ* and MMP activity reporters revealed that there is no MMP activity in the embryo (Hiramatsu et al., 2013). However, in this paper, the *in situ* zymography reagents used to detect MMP activity were likely not properly delivered to the site of activity as they were intravenously injected in pregnant mice or added to the medium of *in vitro* developing embryos (Hiramatsu et al., 2013). These results are in contrast to the data collected in this study. All sequencing databases and microarray data indicate that there are MMPs expressed during these stages (Acampora et al., 2016; Boroviak et al., 2015; Kalkan et al., 2017). Additionally, the effect of MMP inhibitors on the BM appearance and the immunostaining of MMP14 suggest that MMPs are present during early post-implantation stages and are active in their role of BM remodelling (Acampora et al., 2016; Boroviak et al., 2015; Kalkan et al., 2017). The data presented here are also supported by the phenotype of Smad4 and Smad2 knockout mice (Costello et

al., 2009; Weinstein et al., 1998). In both cases the size of the knockout embryos is greatly decreased and in the case of Smad4 KOs, microarray data of embryoid bodies revealed a downregulation of MMP14.

The perforations that were observed in the Epi BM appeared as local remodelling events reminiscent of active BM degradation observed in invasive cancer cells. Surprisingly, in both the *in vitro* and *in vivo* data it appears that perforations may be formed through an invadopodia-mediated process (Artym et al., 2006). Invadopodias are basal projections in cells that are formed by enriching actin and cortactin as well as invadopodia-specific scaffolding proteins like Sh3pxd2a (Tks5) (Murphy and Courtneidge, 2011; Paz et al., 2014). They are responsible for releasing MMP14 and membrane-bound MMP2 to break down the BM locally around the invadopodia area. This process creates perforations that in the context of cancer progression, are important in delamination of cells from the primary tumour and metastasis (Eckert and Yang, 2011; Jacob and Prekeris, 2015; Leong et al., 2014). Interestingly, invadopodias have been described also in the developmental context in the case of *C. elegans* development. The anchor cell generates invadopodias on its basal site and degrades the underlying BM by producing a hole that expands through which other cells can migrate and colonise the intended niches (Lohmer et al., 2014; Sherwood and Plastino, 2018).

In the model described here, basal projections of actin and pMLC foci have indeed been observed and in many cases these co-localised with the perforations underneath. However, Sh3pxd2a expression, an invadopodia-specific scaffolding protein, only co-localises with the site of perforations and MMP14 in the pre-gastrula stages (Artym et al., 2006). In earlier stages (E5.25 – E5.75) there is no detectable Sh3pxd2a. This may suggest that there are different mechanisms of production of perforations depending on the stage of development. In pre-gastrula stages perforations may be formed by an invadopodia-mediated mechanism whereas in the earlier stages, basal protrusions observed may be similar to those described in salivary gland buds (Harunaga et al., 2014)

Regardless of the MMP delivery method to the BM, the *in vitro* model of the Epi-BM microenvironment revealed that indeed post-implantation Epi cells are capable of creating perforations in the BM, attributed to their ability to upregulate MMPs such as MMP14. While, the MMP14-KO differentiated ESCs fail to generate perforations in the *in vitro* system, MMP14-KO mice are viable and only develop post-natal symptoms (Beertsen et al., 2002; Holmbeck et al., 1999; Holmbeck et al., 2003; Oblander et al., 2005; Zhou et al., 2000). The viability of MMP14-KO mice can be attributed to a compensatory mechanism due to enzymatic redundancy by other members of the MMP family (Page-McCaw et al., 2007).

4.3.2 THE ROLE OF PERFORATIONS AND EGG CYLINDER ELONGATION

During these stages the egg cylinder undergoes a significant increase in size and elongation along the PD axis. The growth of the mouse post-implantation embryo along this axis was postulated by Andrew Copp and with

the advent of microscopy and *in vitro* culture of embryos it became evident that the direction of growth is along this axis (Copp, 1978). The perforations during this period of growth are deformed to oval-shaped holes with the majority of them having their long axis aligned with the PD axis. Deformation of perforation in the BM in response to growth has been described before in Hydra polyps during bud evagination (Aufschnaiter et al., 2011). As mentioned in the introduction, Hydra polyps have a porous BM that has two roles; one is to maintain direct cellular connection between ectoderm and endoderm cells that are found on opposite sides of the BM and the second is to facilitate bud expansion. The perforations around the area of bud initiation are deformed along the direction of growth.

The ability of the perforations to deform in response to mechanical forces together with the decreased BM density, may be what provides the increased distensibility of the BM as suggested before (Harunaga et al., 2014). Indeed, AFM studies on perforated versus unperforated BMs in the retina demonstrated that perforated membranes are less stiff (Halfter et al., 2015). In the experiments presented here, MMP inhibition results in the absence of perforations during this period of growth. This resulted in a significantly decreased growth of the egg cylinder and increased apoptosis in the mechanically constrained Epi.

Programmed cell death in physically restricted expanding tissue was also confirmed using the ESC spheroid model in the presence of MMPs inhibitors. The Matrigel in this spheroid system provides an "infinite", non-physiological polymerised ECM that does not depend on cellular support for its stabilisation (Bedzhov and Zernicka-Goetz, 2014; Harrison et al., 2017; Hughes et al., 2010). When 48-hour differentiated spheroids were exposed to these inhibitors, their overall size 12 hours after treatment was significantly smaller than the control counterpart but also had increased levels of apoptosis. Contrary to this result, when single cells suspended in Matrigel were exposed to these inhibitors from day 0, they were able to divide once and then halted further development. While these experiments suggested a MMP-dependent spheroid growth (Carey et al., 2017; Das et al., 2017; Guzman et al., 2017; Simian et al., 2001), it also raised an intriguing question as to how physical constraints can affect a collection of cells i.e. tissues, as opposed to single cells. Mechanically constraining cells spatially growing on 2D substrates has been shown before to have a negative effect on cell cycle progression (Simian et al., 2001; Streichan et al., 2014). However, it has also been shown that mechanical forces can trigger apoptosis in systems like human fibroblasts (Grinnell et al., 1999). While both mechanisms of tissue homeostasis have been described before there are no examples in the literature in which a cell type selects a specific strategy depending on whether it's single cell or part of a tissue. This result could potentially establish the ESC spheroids and the mouse Epi as models for investigating tissue homeostasis regulation in response to physical confinement.

The effect of the BM on tissue growth has been described in other models as well. As briefly mentioned in the introduction of this chapter, the BM can restrict growth as part of the physiological process of morphogenesis

as in the case of wing and leg extension in *Drosophila* development. Also, restricting growth differentially in the tissue directs shape acquisition as in the case of bud development and egg chamber elongation (Crest et al., 2017; Diaz-de-la-Loza et al., 2018; Haigo and Bilder, 2011).

In these examples, the BM achieves this by its remodelling, differential deposition and architecture. In the model described here, the directional growth of the egg cylinder together with the differential BM architecture between the ExE BM and Epi BM (i.e. intact/stiff continuous BM in the extraembryonic compartment and elastic/perforated embryonic BM), may be directing tissue shaping. As suggested by the other models, in the case of isotropic growth of the tissue, the tissue will preferentially grow towards the direction of the least stiffness (or the weaker part of the BM) (Moore et al., 2005). Thus, growth on the very proximal site of the embryo will "push" the rest of the embryo distally due to the mechanical constraints as directed by the BM (with the weaker part of the embryo BM being on the embryonic/distal site) (Copp, 1978; Matsuo and Hiramatsu, 2017).

The growth along the PD axis, possibly due to the differential BM architecture in Epi and ExE, does not cause a tear in the embryonic part of the BM because of the perforations' ability to deform (thus increasing distensibility). In all the embryos recovered and stained for BM components, tearing of the BM was a very rare event and was usually attributed to experimental handling during embryo recovery. In a study investigating the effect of decidual mechanical forces on the embryo it was observed that forces applied to the lateral sides of the embryo, caused the distal BM to break allowing transmigration of Epi cells to the VE layer (Hiramatsu et al., 2013). Distal breakage of BM is something that was never observed from freshly-recovered and fixed embryos in the course of this study.

However, distal BM breakage was observed experimentally in some embryos treated with MMP inhibitors. Embryos that had their BM stiffened by this treatment, either remained small and triggered apoptosis in the compressed Epi or the distal BM teared. This phenomenon can be attributed to the geometrical curvature of the distal tip of the egg cylinder, which makes it the weakest part of the BM and thus most prone to breakage (Matsuo and Hiramatsu, 2017).

4.3.3 The role of Nodal in MMP expression and BM patterning

The role of Nodal in embryo patterning is very well studied in the context of AP axis patterning and during left-right asymmetry and it achieves this at the level of cell specification (Brennan et al., 2001; Collignon et al., 1996; Hirokawa et al., 2006; Morris et al., 2012; Stower and Srinivas, 2014). Here, it was shown that the role of Nodal goes beyond cell specification by eliciting a response from the Epi cells to remodel the underlying BM to accommodate growth and pre-patterning of the primitive streak.

Downregulation of the candidate MMPs as identified from the literature, appears to be consistent with a downregulation of Nodal as shown in ZFP281-KO embryos (Huang et al., 2017). ZFP281 is an epigenetic factor that controls the expression of Nodal and in ZFP281 knockouts the embryos remain compact and small. Although the relation between size and the decrease in Nodal in this paper is not explicitly linked to MMPs and/or BM architecture, the Smad4 (which is the downstream effector of Nodal signalling) knockouts have a thick BM and downregulate MMP14. This is consistent with the association that was made in this study (Costello et al., 2009). This was confirmed using both the Nodal-KO mice which exhibited a thickened BM with loss of the perforated morphology, and the Nodal-inhibited ES cells on fluorescent gelatin that failed to remodel the underlying ECM while also downregulating MMP14 and MMP2.

The identification of Nodal as the effector of the BM morphology came about by the observation that the perforation distribution is skewed towards the future posterior. Establishing this correlation of the position of the perforations in the pre-gastrula stages with the AP axis suggested a possible role of the AP-establishing key player Nodal on the expression of MMPs. The other possible explanation of the observed correlation between the position of the AVE and perforation distribution could be its ability to stabilise the underlying BM. It was shown before that the AVE expresses FLRT3, a transmembrane basal protein that maintains BM integrity (Egea et al., 2008). While this may be true of the AVE's role in establishing this AP patterning of the BM, it is not sufficient as revealed by the Nodal-KO mice. Loss of Nodal results in failure of AVE maintenance while the BM becomes thicker and stabilised. Assuming that the AVE's role in stabilising the underlying BM was sufficient to create the patterning of the BM, then the absence of the AVE (which is the case in Nodal-KO embryos) should result in the maintenance of the perforations. However, BM under the AVE appears thicker which could support its role in contributing to the patterning. While not experimentally addressed, it appears that secreted laminin surrounds the AVE cells which may suggest that deposition increases around those cells.

A TGFbeta link to BM stiffness has been shown recently in the *Drosophila* egg chamber. In this model, the BM stiffness depends on the effect of TGFbeta on the BM architecture at the level of collagen fibril stiffness. This is different to the effect of Nodal on the MMP expression seen in the model described in this study but there seems to be some conserved mechanism across different species where TGFbetas regulate BM remodelling (Chlasta et al., 2017). Also, TGFbeta has been associated with invasiveness and EMT in tumours and has been suggested to be key in endometrial carcinoma invasion, likened to embryo implantation behaving in an unregulated manner (Muinelo-Romay et al., 2011). The data provided in this study along with the studies showing a connection between TGFbetas and BM remodelling create a strong basis of our understanding of how cell specification and the ECM niche can be linked to co-ordinate a bidirectional communication that bring morphogenesis and cell differentiation together.

Moreover, MMP activity also has a signalling potential by generating collagen fragments (NC1) that act as signalling molecules (Rebustini et al., 2009). This could be providing a way to co-ordinate morphogenesis and signalling events of cell specification.

4.3.4 *PRE-PATTERNING THE PRIMITIVE STREAK AND POTENTIAL SIGNIFICANCE IN GASTRULATION*

With the AVE migration to the future anterior, the MMP expression is restricted to the future posterior as revealed by the MMP14 immunostainings at the pre-gastrula stages. This, perhaps together with increased deposition of BM components or stabilisation by the AVE itself, causes the perforations to accumulate in the future posterior. The position of this perforation domain is the true posterior as revealed by stainings at gastrulation stages when Brachyury-positive cells co-localise with this site. This also constitutes the earliest posterior feature of the mouse embryo as it precedes Brachyury expression which is generally considered the earliest indication of posterior identity acquisition (Rivera-Perez and Magnuson, 2005).

Upon close examination of the perforations during gastrulation, the breached BM through which the nascent mesendodermal cells delaminate is situated on the most proximal site of the posterior and is followed by the perforation domain. This perforation domain persists even with the extension of the breached BM which suggests that primitive streak extension follows this site and opens up progressively. This is an interesting hypothesis as it is complementary and supportive of the widely accepted model of *in situ* extension of the primitive streak during gastrulation (Williams et al., 2012). In this model, the BM is suggested to break *in situ* in a progressive manner although the mechanism behind it is not investigated. With the current data and the status of the BM prior to and during the primitive streak extension we can suggest a model in which the BM is breached progressively as a result of the cell movements and proliferation that take place at the site of gastrulation. A thinned-out BM lining the future primitive streak creates a differential stiffness pattern that makes the posterior the preferred direction of growth and thus that under the most tension. What was evident from analysing the maximum projections of the BM prior to and during gastrulation was that the posterior apart from being covered with perforations, was also bulging out when compared to the anterior giving the appearance of having a posterior hunch. This is possibly the result of the more elastic part of the BM being pushed outwards by the dividing cells and increasingly crowded cell population underneath as revealed by the PH3 immunostainings. Eventually, that part of the BM breaks which initiates the primitive streak and upon start of delamination and continuous proliferation, the BM continues to break proximo-distally along this track of perforations like a 'run in the stocking'.

The 'run in the stocking' proposal was first proposed in the paper by Moore and colleagues, where the effect of the build-up of tension by the underlying cells facilitates the thinning of the BM as it's being stretched out (Moore et al., 2005). This suggests that the combination of differential BM stiffness across the tissue with

increasing tension due to tissue growth may be responsible for the initial breakage at gastrulation initiation and the progression of the breakage along the posterior perforation domain. The mechanical forces generated during delamination and ingression of the Epi cells through the breached BM may be making the perforated BM adjacent to the breached BM the weakest part and thus the most prone to breakage. Moreover, this model of gastrulation initiation/progression is further supported by the observation reported before by M.H.L Snow in 1976 and Patrick Tam in 1993 that at gastrulation onset there is great cell proliferation in the Epi and the cell number is critical for its initiation (Power and Tam, 1993; Snow, 1976).

In conclusion, the perforations constitute a novel morphogenetic feature of the early post-implantation mouse embryo that is accompanied by their dynamic redistribution during AP axis establishment. This is achieved through regulation of MMPs, that locally degrade the BM, by Nodal activity which is in turn spatially controlled by the AVE. The role of the perforations was shown in this dissertation to be in guiding and permitting egg cylinder growth at the stages E5.25 – E5.75. It was also postulated here that the redistribution of perforations towards the future posterior may be instrumental in gastrulation initiation and progression. Overall, the BM dynamics appear to be important in normal embryo development and further study will be required especially focusing on its role in shaping the egg cylinder and priming gastrulation.

5 CONCLUSIONS AND FUTURE DIRECTIONS

Embryo morphogenesis is a complex multi-faceted collection of processes that integrates biological responses and biophysical interactions to establish the correct shape, compartmentalisation and cell character in the adult mouse. This complexity has an additive effect as morphogenesis happens progressively in development and through the construction of transient structures. Therefore, for a global understanding of embryo morphogenesis, it is critical to discern how separate structures are built, as well as how these structures, in turn, inform further morphogenesis. Early post-implantation mouse development precedes the formation of complex structures like organs, and morphogenesis aims to lay down the basic architecture of the embryonic and placental components. While there is little complexity at this stage of development in terms of tissue shaping when compared to later stages, there is still very little understanding of how the different features of the mouse egg cylinder are generated. The transition from blastocyst to egg cylinder has only been made amenable for morphogenetic studies in recent years with the advent of a live-imaging, compatible with *in vitro* culture system for peri-implantation development. This will hopefully aid our understanding of the way in which the extraembryonic ectoderm develops from the flattened polar trophectoderm and it is then covered by the visceral endoderm (VE). (Bedzhov et al., 2014b; Morris et al., 2012).

However, post-implantation *in vitro* culture has been available for years and while it was used to examine anterior visceral endoderm (AVE) migration and the establishment of the AP axis, the morphogenesis of the ExE has been largely ignored, to the point that even a description of the cellular organisation within this tissue was lacking. Its significance in embryo patterning and the further development of placental structures had been reported but its dynamicity during development had not been described (Pereira et al., 2011). In terms of embryo morphogenesis, the ExE “cavitates” to give the egg cylinder its hollow character, a prerequisite to further morphogenesis of the extraembryonic membranes (and possibly to coordinate chorionic ectoderm formation and its differentiation). A full understanding of the mechanisms behind the reorganisation of the tissue, required a characterisation of the starting architecture and assembly of cells within the ExE.

In this study, evidence is provided that the nascent ExE undergoes an invagination-like process that gives rise to a slit-like cavity (the ExE cavity) through apical constriction of the proximal-most ExE cells. The trigger of this process, however, is currently not known. An attractive theory postulates that the maternal microenvironment promotes this morphogenetic event in the embryo. However, the formation of the ExE cavity has been observed in embryos cultured *in vitro* from blastocyst stage and thus it is unlikely to be dependent upon maternal tissues. The same applies for any biophysical effects from the surrounding decidua

as *in vitro* cultured embryos are grown in free-floating conditions (Bedzhov et al., 2015). Formation of the ExE cavity coincides with ExE character acquisition (i.e. Elf5, Ets2 expression) and cell shape change from squamous to columnar at the tip. To gain further understanding of the development of the post-implantation embryo it would be interesting to investigate the link between the change in cellular appearance, FGF-dependent ExE character acquisition and invagination of the tip cells. It is likely that ExE cavity formation initiates as a combination of the aforementioned events or as a secondary effect of cell shape change, topology (situated at the far-end of the embryo with no cell-cell contacts on the apical side) and concomitant cell proliferation in the rest of the ExE tissue.

The same morphogenetic process that seems to be driving the formation of the ExE cavity, is likely to be also responsible for the ExE architecture described in this study. The segregation of inside and outside cells in the ExE remains one of the new questions emerging from this study. Is the symmetry of divisions in the nascent ExE important to the way in which inside and outside cells are produced? Is differential tension as important here as seems to be important in blastomere internalisation prior to compaction in the pre-implantation embryo? Are all cells in the nascent ExE the same until β1-integrin signalling becomes active to drive apico-basal polarity acquisition in the cells in direct contact with the underlying BM?

More importantly, a bigger question arising from the description of the ExE architecture, is the relative potency of inside and outside cells in the production of trophoblast stem cells (TSCs). While staining for the core TSC transcription network factors did not reveal a distinct pattern, staining for pERK, and thus FGF activity, was more heterogeneous. There is preliminary evidence that pERK is more prominent in outside cells rather than inside cells, and there seems to be a pattern of pERK localisation being notably absent (or decreased) in cells adjacent to the tip of the ExE cavity (Yang et al., 2006). The differential response to FGF ligands from the epiblast (Epi) suggests that cells in the ExE may be expressing different levels or types of FGF receptors, or the underlying ECM has a role in FGF response (Hemberger et al., 2004). For instance, heparan sulphate, is an ECM protein that is required in FGF response and is enriched at the basal side of ExE outside cells (Shimokawa et al., 2011). Dissecting the two populations followed by RNA sequencing may reveal important differences in the transcriptional profiles of outside and inside cells. This would be important in understanding the origins of these differences and determine the contribution of the ECM and asymmetric cell divisions during the establishment of the ExE. Furthermore, following these sequencing studies TSC lines could be derived from the two populations and assess their differences in potency.

FGF signalling's role in maintaining the TSC character *in vitro* is well established (Hemberger and Cross, 2001; Hemberger et al., 2004; Kubaczka et al., 2014; Ohinata and Tsukiyama, 2014). *In vitro* inhibition of FGF signalling using the SU5402 inhibitor, leads to the loss of the major factors of the TSC network in the ExE, with the exception of Tfap2c, and it is also accompanied by a failure in proamniotic cavity (PAC) formation

(preliminary data). This is possibly attributed to perturbed polarisation in the ExE as revealed by aPKC staining. This introduces an interesting new link between PAC cavity formation and differentiation of TSCs; the equivalent event takes place in the Epi during lumenogenesis and the transition from naïve to primed pluripotency (Shahbazi et al., 2017). Elucidating the link between TSC character and PAC formation is a daunting task as it requires the dissection of the effect of FGF signalling on the ExE. FGF signalling has a role in both polarisation and TSC character acquisition. In turn polarisation (as shown in this study) has an instrumental role in PAC formation. What remains to be understood at this point is if and how the TSC character may be affecting the ExE architecture as the FGF inhibition experiments suggest.

Morphogenesis in different organisms is not only dependent on cellular rearrangements but also on biophysical events such as tissue tension and physical constraints imposed by the ECM (Crest et al., 2017; Diaz-de-la-Loza et al., 2018; Gutzman and Sive, 2010; Haigo and Bilder, 2011). Tissue tension is likely to play a role in PAC formation as suggested by actin enrichment in the ExE and the actomyosin contractility brought about by the formation of rosettes (pMLC enrichment at the centres of rosettes). The multiple foci of pMLC in the ExE tissue may facilitate an accumulation of tension which is released upon resolution of rosettes promoting opening and expansion of the developing PAC as previously shown in brain ventricle opening in zebrafish (Gutzman and Sive, 2010). Abolishing tension from the tissue by perturbing phosphorylation of myosin light chain can lead to artefacts as it is likely to be affecting other processes like cell division. Thus, a more targeted approach (as opposed to a pharmacological treatment) would be required to study the contribution of tension in morphogenesis. An optogenetic method could be implemented to deplete myosin specifically from the foci in the centre of the rosettes (Yi et al., 2014). This would require continuous monitoring during the stages of PAC formation with live imaging and the manual targeting of the foci.

The BM surrounding the developing early post-implantation mouse embryo imposes mechanical constraints on its growth. As the data in this study suggest, patterned architecture of the BM is important in allowing/directing embryo growth along the PD axis in preparation for the gastrula stages. As shown here, the BM is highly perforated at the Epi site that is deformed during growth to accommodate its expansion. These perforations are dependent on MMP activity. However, BM homeostasis is not only dependent on its remodelling but also on its rate of deposition/polymerisation. While Nodal modulates MMP expression in the Epi (as revealed by the embryonic stem cell (ESC) model), it does not affect expression of laminin (preliminary data). This finding contradicts the enrichment of laminin on the anterior site observed upon redistribution of perforations. It is likely that the VE plays a physiological role in BM architecture regulation and more specifically in laminin deposition. This is also supported by embryoid bodies composed of Smad4 -/- ESCs. In these structures laminin expression, which is attributed to the VE-like layer that naturally forms upon aggregate

formation, is affected (Costello et al., 2009). To address this in the embryo, qPCR for the different BM components can be performed on Nodal-KO embryos where the VE has been dissected.

As shown here, the BM appears to pre-pattern the primitive streak to weaken the posterior and facilitate progressive breaking. The current hypothesis of the role of perforations in this pre-patterning is that the differential stiffness of the BM across the anterior-posterior axis in combination with cell proliferation and movement in the Epi causes the tearing of the posterior BM. This has been partially addressed through a correlation of the site of perforations with PH3-positive cells. This demonstrated that the weakened BM can be stretched out to the point of breaching possibly as a result of the increased cell proliferation underneath. This can be further examined with the use of EdU which allows longer tracking of cell proliferation prior to gastrulation. Inhibition of cell proliferation during the extension of the primitive streak could contribute towards understanding the effect of cell crowding on a non-uniformly stiff BM. The expected result would be a failure of streak extension along the posterior. This in combination with computational modelling could provide a better idea of the biophysical aspect of gastrulation and the importance of pre-patterning. A live marker for BM would be a critical tool to examine these dynamics. However, currently there is no available mouse reporter line for the study of these stages of development.

In summary, in this work two new morphogenetic events shaping the egg cylinder in mouse post-implantation development have been described. While the PAC is a well-documented feature of the early mouse embryo, its mechanism of formation has not been investigated. Furthermore, in this dissertation, the morphogenetic process generating this cavity was described revealing a 3D rosette-guided strategy. Moreover, this work has described a second morphogenetic event of the early post-implantation mouse development involving patterning of the underlying BM. A connection between this patterning event and the establishment of the AP axis was established, enriching the field of BM mechanics and dynamics in early mammalian development. Additionally, the morphogenetic processes described here can potentially establish the early murine post-implantation embryo as an attractive model for the fields of tubulogenesis, cell polarisation, mechanobiology and more broadly, biophysics.

6 REFERENCES

Acampora, D., Omodei, D., Petrosino, G., Garofalo, A., Savarese, M., Nigro, V., Di Giovannantonio, L.G., Mercadante, V., and Simeone, A. (2016). Loss of the Otx2-Binding Site in the Nanog Promoter Affects the Integrity of Embryonic Stem Cell Subtypes and Specification of Inner Cell Mass-Derived Epiblast. Cell Rep *15*, 2651-2664.

Adamson, S.L., Lu, Y., Whiteley, K.J., Holmyard, D., Hemberger, M., Pfarrer, C., and Cross, J.C. (2002). Interactions between trophoblast cells and the maternal and fetal circulation in the mouse placenta. Dev Biol *250*, 358-373.

Alvers, A.L., Ryan, S., Scherz, P.J., Huisken, J., and Bagnat, M. (2014). Single continuous lumen formation in the zebrafish gut is mediated by smoothened-dependent tissue remodeling. Development *141*, 1110-1119.

Arnold, S.J., Hofmann, U.K., Bikoff, E.K., and Robertson, E.J. (2008). Pivotal roles for eomesodermin during axis formation, epithelium-to-mesenchyme transition and endoderm specification in the mouse. Development *135*, 501-511.

Artym, V.V., Zhang, Y., Seillier-Moiseiwitsch, F., Yamada, K.M., and Mueller, S.C. (2006). Dynamic interactions of cortactin and membrane type 1 matrix metalloproteinase at invadopodia: defining the stages of invadopodia formation and function. Cancer Res *66*, 3034-3043.

Aufschnaiter, R., Zamir, E.A., Little, C.D., Ozbek, S., Munder, S., David, C.N., Li, L., Sarras, M.P., Jr., and Zhang, X. (2011). In vivo imaging of basement membrane movement: ECM patterning shapes Hydra polyps. J Cell Sci *124*, 4027-4038.

Azizoglu, D.B., Braitsch, C., Marciano, D.K., and Cleaver, O. (2017). Afadin and RhoA control pancreatic endocrine mass via lumen morphogenesis. Genes Dev *31*, 2376-2390.

Beck, S., Le Good, J.A., Guzman, M., Ben Haim, N., Roy, K., Beermann, F., and Constam, D.B. (2002). Extraembryonic proteases regulate Nodal signalling during gastrulation. Nat Cell Biol *4*, 981-985.

Beddington, R.S., and Robertson, E.J. (1999). Axis development and early asymmetry in mammals. Cell *96*, 195-209.

Bedzhov, I., Bialecka, M., Zielinska, A., Kosalka, J., Antonica, F., Thompson, A.J., Franze, K., and Zernicka-Goetz, M. (2015). Development of the anterior-posterior axis is a self-organizing process in the absence of maternal cues in the mouse embryo. Cell Res *25*, 1368-1371.

Bedzhov, I., Graham, S.J., Leung, C.Y., and Zernicka-Goetz, M. (2014a). Developmental plasticity, cell fate specification and morphogenesis in the early mouse embryo. Philos Trans R Soc Lond B Biol Sci *369*.

Bedzhov, I., Leung, C.Y., Bialecka, M., and Zernicka-Goetz, M. (2014b). In vitro culture of mouse blastocysts beyond the implantation stages. Nat Protoc *9*, 2732-2739.

Bedzhov, I., and Zernicka-Goetz, M. (2014). Self-organizing properties of mouse pluripotent cells initiate morphogenesis upon implantation. Cell *156*, 1032-1044.

Beertsen, W., Holmbeck, K., Niehof, A., Bianco, P., Chrysovergis, K., Birkedal-Hansen, H., and Everts, V. (2002). On the role of MT1-MMP, a matrix metalloproteinase essential to collagen remodeling, in murine molar eruption and root growth. Eur J Oral Sci *110*, 445-451.

Bellusci, S., Grindley, J., Emoto, H., Itoh, N., and Hogan, B.L. (1997). Fibroblast growth factor 10 (FGF10) and branching morphogenesis in the embryonic mouse lung. Development *124*, 4867-4878.

Bergstrom, S. (1971). Surface ultrastructure of human amnion and chorion in early pregnancy: a scanning electron microscope study. Obstet Gynecol *38*, 513-524.

Bier, E. (2000). Drawing lines in the Drosophila wing: initiation of wing vein development. Curr Opin Genet Dev *10*, 393-398.

Blankenship, J.T., Backovic, S.T., Sanny, J.S., Weitz, O., and Zallen, J.A. (2006). Multicellular rosette formation links planar cell polarity to tissue morphogenesis. Dev Cell *11*, 459-470.

Boehlke, C., Kotsis, F., Buchholz, B., Powelske, C., Eckardt, K.U., Walz, G., Nitschke, R., and Kuehn, E.W. (2013). Kif3a guides microtubular dynamics, migration and lumen formation of MDCK cells. PLoS One *8*, e62165.

Boroviak, T., Loos, R., Lombard, P., Okahara, J., Behr, R., Sasaki, E., Nichols, J., Smith, A., and Bertone, P. (2015). Lineage-Specific Profiling Delineates the Emergence and Progression of Naive Pluripotency in Mammalian Embryogenesis. Dev Cell *35*, 366-382.

Bouwmeester, T., Kim, S., Sasai, Y., Lu, B., and De Robertis, E.M. (1996). Cerberus is a head-inducing secreted factor expressed in the anterior endoderm of Spemann's organizer. Nature *382*, 595-601.

Brennan, J., Lu, C.C., Norris, D.P., Rodriguez, T.A., Beddington, R.S., and Robertson, E.J. (2001). Nodal signalling in the epiblast patterns the early mouse embryo. Nature *411*, 965-969.

Buechner, M., Hall, D.H., Bhatt, H., and Hedgecock, E.M. (1999). Cystic canal mutants in Caenorhabditis elegans are defective in the apical membrane domain of the renal (excretory) cell. Dev Biol *214*, 227-241.

Cai, K.Q., Capo-Chichi, C.D., Rula, M.E., Yang, D.H., and Xu, X.X. (2008). Dynamic GATA6 expression in primitive endoderm formation and maturation in early mouse embryogenesis. Dev Dyn *237*, 2820-2829.

Calderwood, D.A., Tuckwell, D.S., Eble, J., Kuhn, K., and Humphries, M.J. (1997). The integrin alpha1 A-domain is a ligand binding site for collagens and laminin. J Biol Chem *272*, 12311-12317.

Carey, S.P., Martin, K.E., and Reinhart-King, C.A. (2017). Three-dimensional collagen matrix induces a mechanosensitive invasive epithelial phenotype. Sci Rep *7*, 42088.

Casares, L., Vincent, R., Zalvidea, D., Campillo, N., Navajas, D., Arroyo, M., and Trepat, X. (2015). Hydraulic fracture during epithelial stretching. Nat Mater *14*, 343-351.

Chan, C.J., Costanzo, M., Ruiz-Herrero, T., Monke, G., Petrie, R., Mahadevan, L., Hiiragi, T. (2018). Hydraulic control of embryo size, tissue shape and cell fate. bioRxiv.

Chen, J., Suo, S., Tam, P.P., Han, J.J., Peng, G., and Jing, N. (2017). Spatial transcriptomic analysis of cryosectioned tissue samples with Geo-seq. Nat Protoc *12*, 566-580.

Cheng, C.N., Verdun, V.A., and Wingert, R.A. (2015). Recent advances in elucidating the genetic mechanisms of nephrogenesis using zebrafish. Cells *4*, 218-233.

Chlasta, J., Milani, P., Runel, G., Duteyrat, J.L., Arias, L., Lamire, L.A., Boudaoud, A., and Grammont, M. (2017). Variations in basement membrane mechanics are linked to epithelial morphogenesis. Development *144*, 4350-4362.

Collignon, J., Varlet, I., and Robertson, E.J. (1996). Relationship between asymmetric nodal expression and the direction of embryonic turning. Nature *381*, 155-158.

Constam, D.B., and Robertson, E.J. (2000). SPC4/PACE4 regulates a TGFbeta signaling network during axis formation. Genes Dev *14*, 1146-1155.

Copp, A.J. (1978). Interaction between inner cell mass and trophectoderm of the mouse blastocyst. I. A study of cellular proliferation. J Embryol Exp Morphol *48*, 109-125.

Costello, I., Biondi, C.A., Taylor, J.M., Bikoff, E.K., and Robertson, E.J. (2009). Smad4-dependent pathways control basement membrane deposition and endodermal cell migration at early stages of mouse development. BMC Dev Biol *9*, 54.

Coucouvanis, E., and Martin, G.R. (1995). Signals for death and survival: a two-step mechanism for cavitation in the vertebrate embryo. Cell *83*, 279-287.

Coucouvanis, E., and Martin, G.R. (1999). BMP signaling plays a role in visceral endoderm differentiation and cavitation in the early mouse embryo. Development *126*, 535-546.

Crest, J., Diz-Munoz, A., Chen, D.Y., Fletcher, D.A., and Bilder, D. (2017). Organ sculpting by patterned extracellular matrix stiffness. Elife *6*.

Daley, W.P., Gervais, E.M., Centanni, S.W., Gulfo, K.M., Nelson, D.A., and Larsen, M. (2012). ROCK1-directed basement membrane positioning coordinates epithelial tissue polarity. Development *139*, 411-422.

Daley, W.P., Matsumoto, K., Doyle, A.D., Wang, S., DuChez, B.J., Holmbeck, K., and Yamada, K.M. (2017). Btbd7 is essential for region-specific epithelial cell dynamics and branching morphogenesis in vivo. Development *144*, 2200-2211.

Daley, W.P., and Yamada, K.M. (2013). ECM-modulated cellular dynamics as a driving force for tissue morphogenesis. Curr Opin Genet Dev *23*, 408-414.

Das, A., Monteiro, M., Barai, A., Kumar, S., and Sen, S. (2017). MMP proteolytic activity regulates cancer invasiveness by modulating integrins. Sci Rep *7*, 14219.

De Las Heras, J.M., Garcia-Cortes, C., Foronda, D., Pastor-Pareja, J.C., Shashidhara, L.S., and Sanchez-Herrero, E. (2018). The Drosophila Hox gene Ultrabithorax controls appendage shape by regulating extracellular matrix dynamics. Development *145*.

Denker, E., and Jiang, D. (2012). Ciona intestinalis notochord as a new model to investigate the cellular and molecular mechanisms of tubulogenesis. Semin Cell Dev Biol *23*, 308-319.

Diaz-de-la-Loza, M.D., Ray, R.P., Ganguly, P.S., Alt, S., Davis, J.R., Hoppe, A., Tapon, N., Salbreux, G., and Thompson, B.J. (2018). Apical and Basal Matrix Remodeling Control Epithelial Morphogenesis. Dev Cell *46*, 23-39 e25.

Donnison, M., Beaton, A., Davey, H.W., Broadhurst, R., L'Huillier, P., and Pfeffer, P.L. (2005). Loss of the extraembryonic ectoderm in Elf5 mutants leads to defects in embryonic patterning. Development *132*, 2299-2308.

Donnison, M., Broadhurst, R., and Pfeffer, P.L. (2015). Elf5 and Ets2 maintain the mouse extraembryonic ectoderm in a dosage dependent synergistic manner. Dev Biol *397*, 77-88.

Downs, K.M., and Gardner, R.L. (1995). An investigation into early placental ontogeny: allantoic attachment to the chorion is selective and developmentally regulated. Development *121*, 407-416.

Downs, K.M., Inman, K.E., Jin, D.X., and Enders, A.C. (2009). The Allantoic Core Domain: new insights into development of the murine allantois and its relation to the primitive streak. Dev Dyn *238*, 532-553.

Duelen, R., and Sampaolesi, M. (2017). Stem Cell Technology in Cardiac Regeneration: A Pluripotent Stem Cell Promise. EBioMedicine *16*, 30-40.

Eckert, M.A., and Yang, J. (2011). Targeting invadopodia to block breast cancer metastasis. Oncotarget *2*, 562-568.

Egea, J., Erlacher, C., Montanez, E., Burtscher, I., Yamagishi, S., Hess, M., Hampel, F., Sanchez, R., Rodriguez-Manzaneque, M.T., Bosl, M.R.*, et al.* (2008). Genetic ablation of FLRT3 reveals a novel morphogenetic function for the anterior visceral endoderm in suppressing mesoderm differentiation. Genes Dev *22*, 3349-3362.

Fassler, R., and Meyer, M. (1995). Consequences of lack of beta 1 integrin gene expression in mice. Genes Dev *9*, 1896-1908.

Ferrer-Vaquer, A., Viotti, M., and Hadjantonakis, A.K. (2010). Transitions between epithelial and mesenchymal states and the morphogenesis of the early mouse embryo. Cell Adh Migr *4*, 447-457.

Fierro-Gonzalez, J.C., White, M.D., Silva, J.C., and Plachta, N. (2013). Cadherin-dependent filopodia control preimplantation embryo compaction. Nat Cell Biol *15*, 1424-1433.

Fleming, T.P. (1987). A quantitative analysis of cell allocation to trophectoderm and inner cell mass in the mouse blastocyst. Dev Biol *119*, 520-531.

Frankenberg, S., Smith, L., Greenfield, A., and Zernicka-Goetz, M. (2007). Novel gene expression patterns along the proximo-distal axis of the mouse embryo before gastrulation. BMC Dev Biol *7*, 8.

Freedman, B.S., Brooks, C.R., Lam, A.Q., Fu, H., Morizane, R., Agrawal, V., Saad, A.F., Li, M.K., Hughes, M.R., Werff, R.V.*, et al.* (2015). Modelling kidney disease with CRISPR-mutant kidney organoids derived from human pluripotent epiblast spheroids. Nat Commun *6*, 8715.

Fujiwara, H., Hayashi, Y., Sanzen, N., Kobayashi, R., Weber, C.N., Emoto, T., Futaki, S., Niwa, H., Murray, P., Edgar, D.*, et al.* (2007). Regulation of mesodermal differentiation of mouse embryonic stem cells by basement membranes. J Biol Chem *282*, 29701-29711.

Gadue, P., Huber, T.L., Paddison, P.J., and Keller, G.M. (2006). Wnt and TGF-beta signaling are required for the induction of an in vitro model of primitive streak formation using embryonic stem cells. Proc Natl Acad Sci U S A *103*, 16806-16811.

Garbutt, C.L., Chisholm, J.C., and Johnson, M.H. (1987). The establishment of the embryonic-abembryonic axis in the mouse embryo. Development *100*, 125-134.

Gardner, R.L. (1978). The Relationship Between Cell Lineage and Differentiation in the Early Mouse Embryo. In Genetic Mosaics and Cell Differentiation, W.J. Gehring, ed. (Berlin, Heidelberg: Springer Berlin Heidelberg), pp. 205-241.

Gardner, R.L. (2000). Flow of cells from polar to mural trophectoderm is polarized in the mouse blastocyst. Hum Reprod *15*, 694-701.

Gelbart, M.A., He, B., Martin, A.C., Thiberge, S.Y., Wieschaus, E.F., and Kaschube, M. (2012). Volume conservation principle involved in cell lengthening and nucleus movement during tissue morphogenesis. Proc Natl Acad Sci U S A *109*, 19298-19303.

Gersdorff, N., Muller, M., Otto, S., Poschadel, R., Hubner, S., and Miosge, N. (2005). Basement membrane composition in the early mouse embryo day 7. Dev Dyn *233*, 1140-1148.

Girdler, G.C., and Roper, K. (2014). Controlling cell shape changes during salivary gland tube formation in Drosophila. Semin Cell Dev Biol *31*, 74-81.

Goenezen, S., Rennie, M.Y., and Rugonyi, S. (2012). Biomechanics of early cardiac development. Biomech Model Mechanobiol *11*, 1187-1204.

Gompel, N., Cubedo, N., Thisse, C., Thisse, B., Dambly-Chaudiere, C., and Ghysen, A. (2001). Pattern formation in the lateral line of zebrafish. Mech Dev *105*, 69-77.

Goolam, M., Scialdone, A., Graham, S.J.L., Macaulay, I.C., Jedrusik, A., Hupalowska, A., Voet, T., Marioni, J.C., and Zernicka-Goetz, M. (2016). Heterogeneity in Oct4 and Sox2 Targets Biases Cell Fate in 4-Cell Mouse Embryos. Cell *165*, 61-74.

Grinnell, F., Zhu, M., Carlson, M.A., and Abrams, J.M. (1999). Release of mechanical tension triggers apoptosis of human fibroblasts in a model of regressing granulation tissue. Exp Cell Res *248*, 608-619.

Grobstein, C., and Cohen, J. (1965). Collagenase: effect on the morphogenesis of embryonic salivary epithelium in vitro. Science *150*, 626-628.

Gutzman, J.H., and Sive, H. (2010). Epithelial relaxation mediated by the myosin phosphatase regulator Mypt1 is required for brain ventricle lumen expansion and hindbrain morphogenesis. Development *137*, 795-804.

Guzman, A., Sanchez Alemany, V., Nguyen, Y., Zhang, C.R., and Kaufman, L.J. (2017). A novel 3D in vitro metastasis model elucidates differential invasive strategies during and after breaching basement membrane. Biomaterials *115*, 19-29.

Guzman-Ayala, M., Ben-Haim, N., Beck, S., and Constam, D.B. (2004). Nodal protein processing and fibroblast growth factor 4 synergize to maintain a trophoblast stem cell microenvironment. Proc Natl Acad Sci U S A *101*, 15656-15660.

Haigo, S.L., and Bilder, D. (2011). Global tissue revolutions in a morphogenetic movement controlling elongation. Science *331*, 1071-1074.

Halfter, W., Oertle, P., Monnier, C.A., Camenzind, L., Reyes-Lua, M., Hu, H., Candiello, J., Labilloy, A., Balasubramani, M., Henrich, P.B.*, et al.* (2015). New concepts in basement membrane biology. FEBS J *282*, 4466-4479.

Hardin, J., and Keller, R. (1988). The behaviour and function of bottle cells during gastrulation of Xenopus laevis. Development *103*, 211-230.

Harrison, S.E., Sozen, B., Christodoulou, N., Kyprianou, C., and Zernicka-Goetz, M. (2017). Assembly of embryonic and extraembryonic stem cells to mimic embryogenesis in vitro. Science *356*.

Harunaga, J.S., Doyle, A.D., and Yamada, K.M. (2014). Local and global dynamics of the basement membrane during branching morphogenesis require protease activity and actomyosin contractility. Dev Biol *394*, 197-205.

Hemberger, M., and Cross, J.C. (2001). Genes governing placental development. Trends Endocrinol Metab *12*, 162-168.

Hemberger, M., Hughes, M., and Cross, J.C. (2004). Trophoblast stem cells differentiate in vitro into invasive trophoblast giant cells. Dev Biol *271*, 362-371.

Hikita, C., Vijayakumar, S., Takito, J., Erdjument-Bromage, H., Tempst, P., and Al-Awqati, Q. (2000). Induction of terminal differentiation in epithelial cells requires polymerization of hensin by galectin 3. J Cell Biol *151*, 1235-1246.

Hiramatsu, R., Matsuoka, T., Kimura-Yoshida, C., Han, S.W., Mochida, K., Adachi, T., Takayama, S., and Matsuo, I. (2013). External mechanical cues trigger the establishment of the anterior-posterior axis in early mouse embryos. Dev Cell *27*, 131-144.

Hirokawa, N., Tanaka, Y., Okada, Y., and Takeda, S. (2006). Nodal flow and the generation of left-right asymmetry. Cell *125*, 33-45.

Hogan, B.L., and Kolodziej, P.A. (2002). Organogenesis: molecular mechanisms of tubulogenesis. Nat Rev Genet *3*, 513-523.

Holmbeck, K., Bianco, P., Caterina, J., Yamada, S., Kromer, M., Kuznetsov, S.A., Mankani, M., Robey, P.G., Poole, A.R., Pidoux, I.*, et al.* (1999). MT1-MMP-deficient mice develop dwarfism, osteopenia, arthritis, and connective tissue disease due to inadequate collagen turnover. Cell *99*, 81-92.

Holmbeck, K., Bianco, P., Chrysovergis, K., Yamada, S., and Birkedal-Hansen, H. (2003). MT1-MMP-dependent, apoptotic remodeling of unmineralized cartilage: a critical process in skeletal growth. J Cell Biol *163*, 661-671.

Hong, F., Breitling, R., McEntee, C.W., Wittner, B.S., Nemhauser, J.L., and Chory, J. (2006). RankProd: a bioconductor package for detecting differentially expressed genes in meta-analysis. Bioinformatics *22*, 2825-2827.

Hsu, J.C., Koo, H., Harunaga, J.S., Matsumoto, K., Doyle, A.D., and Yamada, K.M. (2013). Region-specific epithelial cell dynamics during branching morphogenesis. Dev Dyn *242*, 1066-1077.

Huang da, W., Sherman, B.T., and Lempicki, R.A. (2009). Systematic and integrative analysis of large gene lists using DAVID bioinformatics resources. Nat Protoc *4*, 44-57.

Huang, X., Balmer, S., Yang, F., Fidalgo, M., Li, D., Guallar, D., Hadjantonakis, A.K., and Wang, J. (2017). Zfp281 is essential for mouse epiblast maturation through transcriptional and epigenetic control of Nodal signaling. Elife *6*.

Hughes, C.S., Postovit, L.M., and Lajoie, G.A. (2010). Matrigel: a complex protein mixture required for optimal growth of cell culture. Proteomics *10*, 1886-1890.

Inoue, S., Leblond, C.P., and Laurie, G.W. (1983). Ultrastructure of Reichert's membrane, a multilayered basement membrane in the parietal wall of the rat yolk sac. J Cell Biol *97*, 1524-1537.

Jacob, A., and Prekeris, R. (2015). The regulation of MMP targeting to invadopodia during cancer metastasis. Front Cell Dev Biol *3*, 4.

Jia, W., Li, H., and He, Y.W. (2005). The extracellular matrix protein mindin serves as an integrin ligand and is critical for inflammatory cell recruitment. Blood *106*, 3854-3859.

Jin, J.Z., Zhu, Y., Warner, D., and Ding, J. (2016). Analysis of extraembryonic mesodermal structure formation in the absence of morphological primitive streak. Dev Growth Differ *58*, 522-529.

Johnson, W.E., Li, C., and Rabinovic, A. (2007). Adjusting batch effects in microarray expression data using empirical Bayes methods. Biostatistics *8*, 118-127.

Kalkan, T., Olova, N., Roode, M., Mulas, C., Lee, H.J., Nett, I., Marks, H., Walker, R., Stunnenberg, H.G., Lilley, K.S.*, et al.* (2017). Tracking the embryonic stem cell transition from ground state pluripotency. Development *144*, 1221-1234.

Kamei, M., Saunders, W.B., Bayless, K.J., Dye, L., Davis, G.E., and Weinstein, B.M. (2006). Endothelial tubes assemble from intracellular vacuoles in vivo. Nature *442*, 453-456.

Kim, D., Pertea, G., Trapnell, C., Pimentel, H., Kelley, R., and Salzberg, S.L. (2013). TopHat2: accurate alignment of transcriptomes in the presence of insertions, deletions and gene fusions. Genome Biol *14*, R36.

Klein, G., Langegger, M., Timpl, R., and Ekblom, P. (1988). Role of laminin A chain in the development of epithelial cell polarity. Cell *55*, 331-341.

Knoblich, J.A. (2008). Mechanisms of asymmetric stem cell division. Cell *132*, 583-597.

Knoblich, J.A. (2010). Asymmetric cell division: recent developments and their implications for tumour biology. Nat Rev Mol Cell Biol *11*, 849-860.

Kojima, Y., Tam, O.H., and Tam, P.P. (2014). Timing of developmental events in the early mouse embryo. Semin Cell Dev Biol *34*, 65-75.

Kong, D., Wolf, F., and Grosshans, J. (2017). Forces directing germ-band extension in Drosophila embryos. Mech Dev *144*, 11-22.

Korotkevich, E., Niwayama, R., Courtois, A., Friese, S., Berger, N., Buchholz, F., and Hiiragi, T. (2017). The Apical Domain Is Required and Sufficient for the First Lineage Segregation in the Mouse Embryo. Dev Cell *40*, 235-247 e237.

Kubaczka, C., Senner, C., Arauzo-Bravo, M.J., Sharma, N., Kuckenberg, P., Becker, A., Zimmer, A., Brustle, O., Peitz, M., Hemberger, M.*, et al.* (2014). Derivation and maintenance of murine trophoblast stem cells under defined conditions. Stem Cell Reports *2*, 232-242.

Kumar, A., Lualdi, M., Lyozin, G.T., Sharma, P., Loncarek, J., Fu, X.Y., and Kuehn, M.R. (2015). Nodal signaling from the visceral endoderm is required to maintain Nodal gene expression in the epiblast and drive DVE/AVE migration. Dev Biol *400*, 1-9.

Kwon, G.S., and Hadjantonakis, A.K. (2009). Transthyretin mouse transgenes direct RFP expression or Cre-mediated recombination throughout the visceral endoderm. Genesis *47*, 447-455.

Ladoux, B., and Nicolas, A. (2012). Physically based principles of cell adhesion mechanosensitivity in tissues. Rep Prog Phys *75*, 116601.

Larsen, M., Wei, C., and Yamada, K.M. (2006). Cell and fibronectin dynamics during branching morphogenesis. J Cell Sci *119*, 3376-3384.

Latos, P.A., Goncalves, A., Oxley, D., Mohammed, H., Turro, E., and Hemberger, M. (2015). Fgf and Esrrb integrate epigenetic and transcriptional networks that regulate self-renewal of trophoblast stem cells. Nat Commun *6*, 7776.

Latos, P.A., and Hemberger, M. (2014). Review: the transcriptional and signalling networks of mouse trophoblast stem cells. Placenta *35 Suppl*, S81-85.

Lawson, K.A., Dunn, N.R., Roelen, B.A., Zeinstra, L.M., Davis, A.M., Wright, C.V., Korving, J.P., and Hogan, B.L. (1999). Bmp4 is required for the generation of primordial germ cells in the mouse embryo. Genes Dev *13*, 424-436.

Lecaudey, V., Cakan-Akdogan, G., Norton, W.H., and Gilmour, D. (2008). Dynamic Fgf signaling couples morphogenesis and migration in the zebrafish lateral line primordium. Development *135*, 2695-2705.

Lee, J.D., and Anderson, K.V. (2008). Morphogenesis of the node and notochord: the cellular basis for the establishment and maintenance of left-right asymmetry in the mouse. Dev Dyn *237*, 3464-3476.

Lee, J.L., and Streuli, C.H. (2014). Integrins and epithelial cell polarity. J Cell Sci *127*, 3217-3225.

Leong, H.S., Robertson, A.E., Stoletov, K., Leith, S.J., Chin, C.A., Chien, A.E., Hague, M.N., Ablack, A., Carmine-Simmen, K., McPherson, V.A*., et al.* (2014). Invadopodia are required for cancer cell extravasation and are a therapeutic target for metastasis. Cell Rep *8*, 1558-1570.

Leung, C.Y., and Zernicka-Goetz, M. (2013). Angiomotin prevents pluripotent lineage differentiation in mouse embryos via Hippo pathway-dependent and -independent mechanisms. Nat Commun *4*, 2251.

Li, S., Edgar, D., Fassler, R., Wadsworth, W., and Yurchenco, P.D. (2003). The role of laminin in embryonic cell polarization and tissue organization. Dev Cell *4*, 613-624.

Liu, S., Yamashita, H., Weidow, B., Weaver, A.M., and Quaranta, V. (2010). Laminin-332-beta1 integrin interactions negatively regulate invadopodia. J Cell Physiol *223*, 134-142.

Lohmer, L.L., Kelley, L.C., Hagedorn, E.J., and Sherwood, D.R. (2014). Invadopodia and basement membrane invasion in vivo. Cell Adh Migr *8*, 246-255.

Lye, C.M., and Sanson, B. (2011). Tension and epithelial morphogenesis in Drosophila early embryos. Curr Top Dev Biol *95*, 145-187.

Maitre, J.L. (2017). Mechanics of blastocyst morphogenesis. Biol Cell *109*, 323-338.

Maitre, J.L., Berthoumieux, H., Krens, S.F., Salbreux, G., Julicher, F., Paluch, E., and Heisenberg, C.P. (2012). Adhesion functions in cell sorting by mechanically coupling the cortices of adhering cells. Science *338*, 253-256.

Maitre, J.L., Niwayama, R., Turlier, H., Nedelec, F., and Hiiragi, T. (2015). Pulsatile cell-autonomous contractility drives compaction in the mouse embryo. Nat Cell Biol *17*, 849-855.

Maitre, J.L., Turlier, H., Illukkumbura, R., Eismann, B., Niwayama, R., Nedelec, F., and Hiiragi, T. (2016). Asymmetric division of contractile domains couples cell positioning and fate specification. Nature *536*, 344-348.

Majumdar, A., Vainio, S., Kispert, A., McMahon, J., and McMahon, A.P. (2003). Wnt11 and Ret/Gdnf pathways cooperate in regulating ureteric branching during metanephric kidney development. Development *130*, 3175-3185.

Martin, A.C., and Goldstein, B. (2014). Apical constriction: themes and variations on a cellular mechanism driving morphogenesis. Development *141*, 1987-1998.

Martin-Belmonte, F., Gassama, A., Datta, A., Yu, W., Rescher, U., Gerke, V., and Mostov, K. (2007). PTEN-mediated apical segregation of phosphoinositides controls epithelial morphogenesis through Cdc42. Cell *128*, 383-397.

Martin-Belmonte, F., Yu, W., Rodriguez-Fraticelli, A.E., Ewald, A.J., Werb, Z., Alonso, M.A., and Mostov, K. (2008). Cell-polarity dynamics controls the mechanism of lumen formation in epithelial morphogenesis. Curr Biol *18*, 507-513.

Matsuo, I., and Hiramatsu, R. (2017). Mechanical perspectives on the anterior-posterior axis polarization of mouse implanted embryos. Mech Dev *144*, 62-70.

McRae, A.C., and Church, R.B. (1990). Cytoplasmic projections of trophectoderm distinguish implanting from preimplanting and implantation-delayed mouse blastocytes. J Reprod Fertil *88*, 31-40.

Meder, D., Shevchenko, A., Simons, K., and Fullekrug, J. (2005). Gp135/podocalyxin and NHERF-2 participate in the formation of a preapical domain during polarization of MDCK cells. J Cell Biol *168*, 303-313.

Meilhac, S.M., Adams, R.J., Morris, S.A., Danckaert, A., Le Garrec, J.F., and Zernicka-Goetz, M. (2009). Active cell movements coupled to positional induction are involved in lineage segregation in the mouse blastocyst. Dev Biol *331*, 210-221.

Melendez, J., Stengel, K., Zhou, X., Chauhan, B.K., Debidda, M., Andreassen, P., Lang, R.A., and Zheng, Y. (2011). RhoA GTPase is dispensable for actomyosin regulation but is essential for mitosis in primary mouse embryonic fibroblasts. J Biol Chem *286*, 15132-15137.

Mesnard, D., Donnison, M., Fuerer, C., Pfeffer, P.L., and Constam, D.B. (2011). The microenvironment patterns the pluripotent mouse epiblast through paracrine Furin and Pace4 proteolytic activities. Genes Dev *25*, 1871-1880.

Mesnard, D., Guzman-Ayala, M., and Constam, D.B. (2006). Nodal specifies embryonic visceral endoderm and sustains pluripotent cells in the epiblast before overt axial patterning. Development *133*, 2497-2505.

Migeotte, I., Grego-Bessa, J., and Anderson, K.V. (2011). Rac1 mediates morphogenetic responses to intercellular signals in the gastrulating mouse embryo. Development *138*, 3011-3020.

Migeotte, I., Omelchenko, T., Hall, A., and Anderson, K.V. (2010). Rac1-dependent collective cell migration is required for specification of the anterior-posterior body axis of the mouse. PLoS Biol *8*, e1000442.

Miner, J.H., Li, C., Mudd, J.L., Go, G., and Sutherland, A.E. (2004). Compositional and structural requirements for laminin and basement membranes during mouse embryo implantation and gastrulation. Development *131*, 2247-2256.

Moore, K.A., Polte, T., Huang, S., Shi, B., Alsberg, E., Sunday, M.E., and Ingber, D.E. (2005). Control of basement membrane remodeling and epithelial branching morphogenesis in embryonic lung by Rho and cytoskeletal tension. Dev Dyn *232*, 268-281.

Moriwaki, K., Tsukita, S., and Furuse, M. (2007). Tight junctions containing claudin 4 and 6 are essential for blastocyst formation in preimplantation mouse embryos. Dev Biol *312*, 509-522.

Morris, J.L., Cross, S.J., Lu, Y., Kadler, K.E., Lu, Y., Dallas, S.L., and Martin, P. (2018). Live imaging of collagen deposition during skin development and repair in a collagen I - GFP fusion transgenic zebrafish line. Dev Biol *441*, 4-11.

Morris, S.A., Grewal, S., Barrios, F., Patankar, S.N., Strauss, B., Buttery, L., Alexander, M., Shakesheff, K.M., and Zernicka-Goetz, M. (2012). Dynamics of anterior-posterior axis formation in the developing mouse embryo. Nat Commun *3*, 673.

Morris, S.A., Teo, R.T., Li, H., Robson, P., Glover, D.M., and Zernicka-Goetz, M. (2010). Origin and formation of the first two distinct cell types of the inner cell mass in the mouse embryo. Proc Natl Acad Sci U S A *107*, 6364-6369.

Morrissey, M.A., and Sherwood, D.R. (2015). An active role for basement membrane assembly and modification in tissue sculpting. J Cell Sci *128*, 1661-1668.

Muinelo-Romay, L., Colas, E., Barbazan, J., Alonso-Alconada, L., Alonso-Nocelo, M., Bouso, M., Curiel, T., Cueva, J., Anido, U., Forteza, J.*, et al.* (2011). High-risk endometrial carcinoma profiling identifies TGF-beta1 as a key factor in the initiation of tumor invasion. Mol Cancer Ther *10*, 1357-1366.

Murphy, D.A., and Courtneidge, S.A. (2011). The 'ins' and 'outs' of podosomes and invadopodia: characteristics, formation and function. Nat Rev Mol Cell Biol *12*, 413-426.

Murray, P., and Edgar, D. (2000). Regulation of programmed cell death by basement membranes in embryonic development. J Cell Biol *150*, 1215-1221.

Muzumdar, M.D., Tasic, B., Miyamichi, K., Li, L., and Luo, L. (2007). A global double-fluorescent Cre reporter mouse. Genesis *45*, 593-605.

Nakanishi, Y., Nogawa, H., Hashimoto, Y., Kishi, J., and Hayakawa, T. (1988). Accumulation of collagen III at the cleft points of developing mouse submandibular epithelium. Development *104*, 51-59.

Nakaya, Y., and Sheng, G. (2008). Epithelial to mesenchymal transition during gastrulation: an embryological view. Dev Growth Differ *50*, 755-766.

Nakaya, Y., Sukowati, E.W., Wu, Y., and Sheng, G. (2008). RhoA and microtubule dynamics control cell-basement membrane interaction in EMT during gastrulation. Nat Cell Biol *10*, 765-775.

Nechiporuk, A., and Raible, D.W. (2008). FGF-dependent mechanosensory organ patterning in zebrafish. Science *320*, 1774-1777.

Nedvetsky, P.I., Emmerson, E., Finley, J.K., Ettinger, A., Cruz-Pacheco, N., Prochazka, J., Haddox, C.L., Northrup, E., Hodges, C., Mostov, K.E.*, et al.* (2014). Parasympathetic innervation regulates tubulogenesis in the developing salivary gland. Dev Cell *30*, 449-462.

Neumuller, R.A., and Knoblich, J.A. (2009). Dividing cellular asymmetry: asymmetric cell division and its implications for stem cells and cancer. Genes Dev *23*, 2675-2699.

Nielsen, J.S., and McNagny, K.M. (2008). Novel functions of the CD34 family. J Cell Sci *121*, 3683-3692.

Niimura, S. (2003). Time-lapse videomicrographic analyses of contractions in mouse blastocysts. J Reprod Dev *49*, 413-423.

Nikolova, L.S., and Metzstein, M.M. (2015). Intracellular lumen formation in Drosophila proceeds via a novel subcellular compartment. Development *142*, 3964-3973.

Nishioka, N., Inoue, K., Adachi, K., Kiyonari, H., Ota, M., Ralston, A., Yabuta, N., Hirahara, S., Stephenson, R.O., Ogonuki, N.*, et al.* (2009). The Hippo signaling pathway components Lats and Yap pattern Tead4 activity to distinguish mouse trophectoderm from inner cell mass. Dev Cell *16*, 398-410.

Nishiuchi, R., Takagi, J., Hayashi, M., Ido, H., Yagi, Y., Sanzen, N., Tsuji, T., Yamada, M., and Sekiguchi, K. (2006). Ligand-binding specificities of laminin-binding integrins: a comprehensive survey of laminin-integrin interactions using recombinant alpha3beta1, alpha6beta1, alpha7beta1 and alpha6beta4 integrins. Matrix Biol *25*, 189-197.

O'Brien, L.E., Jou, T.S., Pollack, A.L., Zhang, Q., Hansen, S.H., Yurchenco, P., and Mostov, K.E. (2001). Rac1 orientates epithelial apical polarity through effects on basolateral laminin assembly. Nat Cell Biol *3*, 831-838.

Oblander, S.A., Zhou, Z., Galvez, B.G., Starcher, B., Shannon, J.M., Durbeej, M., Arroyo, A.G., Tryggvason, K., and Apte, S.S. (2005). Distinctive functions of membrane type 1 matrix-metalloprotease (MT1-MMP or MMP-14) in lung and submandibular gland development are independent of its role in pro-MMP-2 activation. Dev Biol *277*, 255-269.

Ohinata, Y., and Tsukiyama, T. (2014). Establishment of trophoblast stem cells under defined culture conditions in mice. PLoS One *9*, e107308.

Orlando, R.A., Takeda, T., Zak, B., Schmieder, S., Benoit, V.M., McQuistan, T., Furthmayr, H., and Farquhar, M.G. (2001). The glomerular epithelial cell anti-adhesin podocalyxin associates with the actin cytoskeleton through interactions with ezrin. J Am Soc Nephrol *12*, 1589-1598.

Page-McCaw, A., Ewald, A.J., and Werb, Z. (2007). Matrix metalloproteinases and the regulation of tissue remodelling. Nat Rev Mol Cell Biol *8*, 221-233.

Passey, R.J., Williams, E., Lichanska, A.M., Wells, C., Hu, S., Geczy, C.L., Little, M.H., and Hume, D.A. (1999). A null mutation in the inflammation-associated S100 protein S100A8 causes early resorption of the mouse embryo. J Immunol *163*, 2209-2216.

Patel, N., Sharpe, P.T., and Miletich, I. (2011). Coordination of epithelial branching and salivary gland lumen formation by Wnt and FGF signals. Dev Biol *358*, 156-167.

Paz, H., Pathak, N., and Yang, J. (2014). Invading one step at a time: the role of invadopodia in tumor metastasis. Oncogene *33*, 4193-4202.

Pedersen, R.A., Wu, K., and Balakier, H. (1986). Origin of the inner cell mass in mouse embryos: cell lineage analysis by microinjection. Dev Biol *117*, 581-595.

Pereira, P.N., Dobreva, M.P., Graham, L., Huylebroeck, D., Lawson, K.A., and Zwijsen, A.N. (2011). Amnion formation in the mouse embryo: the single amniochorionic fold model. BMC Dev Biol *11*, 48.

Pfister, S., Steiner, K.A., and Tam, P.P. (2007). Gene expression pattern and progression of embryogenesis in the immediate post-implantation period of mouse development. Gene Expr Patterns *7*, 558-573.

Plachta, N., Bollenbach, T., Pease, S., Fraser, S.E., and Pantazis, P. (2011). Oct4 kinetics predict cell lineage patterning in the early mammalian embryo. Nat Cell Biol *13*, 117-123.

Portereiko, M.F., and Mango, S.E. (2001). Early morphogenesis of the Caenorhabditis elegans pharynx. Dev Biol *233*, 482-494.

Power, M.A., and Tam, P.P. (1993). Onset of gastrulation, morphogenesis and somitogenesis in mouse embryos displaying compensatory growth. Anat Embryol (Berl) *187*, 493-504.

Rakeman, A.S., and Anderson, K.V. (2006). Axis specification and morphogenesis in the mouse embryo require Nap1, a regulator of WAVE-mediated actin branching. Development *133*, 3075-3083.

Ran, F.A., Hsu, P.D., Wright, J., Agarwala, V., Scott, D.A., and Zhang, F. (2013). Genome engineering using the CRISPR-Cas9 system. Nat Protoc *8*, 2281-2308.

Rasmussen, J.P., Reddy, S.S., and Priess, J.R. (2012). Laminin is required to orient epithelial polarity in the C. elegans pharynx. Development *139*, 2050-2060.

Rebustini, I.T., Myers, C., Lassiter, K.S., Surmak, A., Szabova, L., Holmbeck, K., Pedchenko, V., Hudson, B.G., and Hoffman, M.P. (2009). MT2-MMP-dependent release of collagen IV NC1 domains regulates submandibular gland branching morphogenesis. Dev Cell *17*, 482-493.

Reinius, S. (1965). Morphology of the mouse embryo, from the time of implantation to mesoderm formation. Z Zellforsch Mikrosk Anat *68*, 711-723.

Richardson, L., Torres-Padilla, M.E., and Zernicka-Goetz, M. (2006). Regionalised signalling within the extraembryonic ectoderm regulates anterior visceral endoderm positioning in the mouse embryo. Mech Dev *123*, 288-296.

Riedl, J., Flynn, K.C., Raducanu, A., Gartner, F., Beck, G., Bosl, M., Bradke, F., Massberg, S., Aszodi, A., Sixt, M.*, et al.* (2010). Lifeact mice for studying F-actin dynamics. Nat Methods *7*, 168-169.

Rivera-Perez, J.A., and Hadjantonakis, A.K. (2014). The Dynamics of Morphogenesis in the Early Mouse Embryo. Cold Spring Harb Perspect Biol *7*.

Rivera-Perez, J.A., Mager, J., and Magnuson, T. (2003). Dynamic morphogenetic events characterize the mouse visceral endoderm. Dev Biol *261*, 470-487.

Rivera-Perez, J.A., and Magnuson, T. (2005). Primitive streak formation in mice is preceded by localized activation of Brachyury and Wnt3. Dev Biol *288*, 363-371.

Rodriguez, T.A., Srinivas, S., Clements, M.P., Smith, J.C., and Beddington, R.S. (2005). Induction and migration of the anterior visceral endoderm is regulated by the extra-embryonic ectoderm. Development *132*, 2513-2520.

Rossant, J. (2015). Mouse and human blastocyst-derived stem cells: vive les differences. Development *142*, 9-12.

Russ, A.P., Wattler, S., Colledge, W.H., Aparicio, S.A., Carlton, M.B., Pearce, J.J., Barton, S.C., Surani, M.A., Ryan, K., Nehls, M.C.*, et al.* (2000). Eomesodermin is required for mouse trophoblast development and mesoderm formation. Nature *404*, 95-99.

Sakai, T., Larsen, M., and Yamada, K.M. (2003). Fibronectin requirement in branching morphogenesis. Nature *423*, 876-881.

Shahbazi, M.N., Scialdone, A., Skorupska, N., Weberling, A., Recher, G., Zhu, M., Jedrusik, A., Devito, L.G., Noli, L., Macaulay, I.C*., et al.* (2017). Pluripotent state transitions coordinate morphogenesis in mouse and human embryos. Nature *552*, 239-243.

Sherwood, D.R., and Plastino, J. (2018). Invading, Leading and Navigating Cells in Caenorhabditis elegans: Insights into Cell Movement in Vivo. Genetics *208*, 53-78.

Shimizu, H., Aufschnaiter, R., Li, L., Sarras, M.P., Jr., Borza, D.B., Abrahamson, D.R., Sado, Y., and Zhang, X. (2008). The extracellular matrix of hydra is a porous sheet and contains type IV collagen. Zoology (Jena) *111*, 410-418.

Shimokawa, K., Kimura-Yoshida, C., Nagai, N., Mukai, K., Matsubara, K., Watanabe, H., Matsuda, Y., Mochida, K., and Matsuo, I. (2011). Cell surface heparan sulfate chains regulate local reception of FGF signaling in the mouse embryo. Dev Cell *21*, 257-272.

Shindo, A. (2018). Models of convergent extension during morphogenesis. Wiley Interdiscip Rev Dev Biol *7*.

Shyer, A.E., Huycke, T.R., Lee, C., Mahadevan, L., and Tabin, C.J. (2015). Bending gradients: how the intestinal stem cell gets its home. Cell *161*, 569-580.

Simian, M., Hirai, Y., Navre, M., Werb, Z., Lochter, A., and Bissell, M.J. (2001). The interplay of matrix metalloproteinases, morphogens and growth factors is necessary for branching of mammary epithelial cells. Development *128*, 3117-3131.

Skamagki, M., Wicher, K.B., Jedrusik, A., Ganguly, S., and Zernicka-Goetz, M. (2013). Asymmetric localization of Cdx2 mRNA during the first cell-fate decision in early mouse development. Cell Rep *3*, 442-457.

Smith, K.K., and Strickland, S. (1981). Structural components and characteristics of Reichert's membrane, an extra-embryonic basement membrane. J Biol Chem *256*, 4654-4661.

Smith, L.J. (1985). Embryonic axis orientation in the mouse and its correlation with blastocyst relationships to the uterus. II. Relationships from 4 1/4 to 9 1/2 days. J Embryol Exp Morphol *89*, 15-35.

Snell, G.D., Stevens, L.C. (1966). Early embryology in biology of the laboratory mouse. In, E.L. Green, ed. (New York: McGraw-Hill Book Co.), pp. 205-245.

Snow, M.H.L. (1976). Embryo growthduring the immediate postimplantation period. In Embryogenesis in Mammals, M.O.C. Katherine Elliott, ed.

Solter, D., Damjanov, I., and Skreb, N. (1970). Ultrastructure of mouse egg-cylinder. Z Anat Entwicklungsgesch *132*, 291-298.

Sorokin, L., Sonnenberg, A., Aumailley, M., Timpl, R., and Ekblom, P. (1990). Recognition of the laminin E8 cell-binding site by an integrin possessing the alpha 6 subunit is essential for epithelial polarization in developing kidney tubules. J Cell Biol *111*, 1265-1273.

Sozen, B., Amadei, G., Cox, A., Wang, R., Na, E., Czukiewska, S., Chappell, L., Voet, T., Michel, G., Jing, N*., et al.* (2018). Self-assembly of embryonic and two extra-embryonic stem cell types into gastrulating embryo-like structures. Nat Cell Biol *20*, 979-989.

Srinivas, S., Rodriguez, T., Clements, M., Smith, J.C., and Beddington, R.S. (2004). Active cell migration drives the unilateral movements of the anterior visceral endoderm. Development *131*, 1157-1164.

Stephenson, R.O., Yamanaka, Y., and Rossant, J. (2010). Disorganized epithelial polarity and excess trophectoderm cell fate in preimplantation embryos lacking E-cadherin. Development *137*, 3383-3391.

Stirbat, T.V., Mgharbel, A., Bodennec, S., Ferri, K., Mertani, H.C., Rieu, J.P., and Delanoe-Ayari, H. (2013). Fine tuning of tissues' viscosity and surface tension through contractility suggests a new role for alpha-catenin. PLoS One *8*, e52554.

Stower, M.J., and Srinivas, S. (2014). Heading forwards: anterior visceral endoderm migration in patterning the mouse embryo. Philos Trans R Soc Lond B Biol Sci *369*.

Streichan, S.J., Hoerner, C.R., Schneidt, T., Holzer, D., and Hufnagel, L. (2014). Spatial constraints control cell proliferation in tissues. Proc Natl Acad Sci U S A *111*, 5586-5591.

Strumpf, D., Mao, C.A., Yamanaka, Y., Ralston, A., Chawengsaksophak, K., Beck, F., and Rossant, J. (2005). Cdx2 is required for correct cell fate specification and differentiation of trophectoderm in the mouse blastocyst. Development *132*, 2093-2102.

Stuckey, D.W., Clements, M., Di-Gregorio, A., Senner, C.E., Le Tissier, P., Srinivas, S., and Rodriguez, T.A. (2011). Coordination of cell proliferation and anterior-posterior axis establishment in the mouse embryo. Development *138*, 1521-1530.

Sugimoto, M. (2014). Developmental genetics of the mouse t-complex. Genes Genet Syst *89*, 109-120.

Sun, Q., Luo, T., Ren, Y., Florey, O., Shirasawa, S., Sasazuki, T., Robinson, D.N., and Overholtzer, M. (2014). Competition between human cells by entosis. Cell Res *24*, 1299-1310.

Sutherland, A.E., and Calarco-Gillam, P.G. (1983). Analysis of compaction in the preimplantation mouse embryo. Dev Biol *100*, 328-338.

Sutherland, A.E., Speed, T.P., and Calarco, P.G. (1990). Inner cell allocation in the mouse morula: the role of oriented division during fourth cleavage. Dev Biol *137*, 13-25.

Takaoka, K., Yamamoto, M., and Hamada, H. (2011). Origin and role of distal visceral endoderm, a group of cells that determines anterior-posterior polarity of the mouse embryo. Nat Cell Biol *13*, 743-752.

Takito, J., and Al-Awqati, Q. (2004). Conversion of ES cells to columnar epithelia by hensin and to squamous epithelia by laminin. J Cell Biol *166*, 1093-1102.

Tam, P.P., and Behringer, R.R. (1997). Mouse gastrulation: the formation of a mammalian body plan. Mech Dev *68*, 3-25.

Tam, P.P., and Loebel, D.A. (2007). Gene function in mouse embryogenesis: get set for gastrulation. Nat Rev Genet *8*, 368-381.

Tam, P.P., Williams, E.A., and Chan, W.Y. (1993). Gastrulation in the mouse embryo: ultrastructural and molecular aspects of germ layer morphogenesis. Microsc Res Tech *26*, 301-328.

Tanaka, S., Kunath, T., Hadjantonakis, A.K., Nagy, A., and Rossant, J. (1998). Promotion of trophoblast stem cell proliferation by FGF4. Science *282*, 2072-2075.

Thomas, P., and Beddington, R. (1996). Anterior primitive endoderm may be responsible for patterning the anterior neural plate in the mouse embryo. Curr Biol *6*, 1487-1496.

Thomas, P., Brickman, J.M., Popperl, H., Krumlauf, R., and Beddington, R.S. (1997). Axis duplication and anterior identity in the mouse embryo. Cold Spring Harb Symp Quant Biol *62*, 115-125.

Thomas, P.Q., Brown, A., and Beddington, R.S. (1998). Hex: a homeobox gene revealing peri-implantation asymmetry in the mouse embryo and an early transient marker of endothelial cell precursors. Development *125*, 85-94.

Trapnell, C., Pachter, L., and Salzberg, S.L. (2009). TopHat: discovering splice junctions with RNA-Seq. Bioinformatics *25*, 1105-1111.

Trichas, G., Joyce, B., Crompton, L.A., Wilkins, V., Clements, M., Tada, M., Rodriguez, T.A., and Srinivas, S. (2011). Nodal dependent differential localisation of dishevelled-2 demarcates regions of differing cell behaviour in the visceral endoderm. PLoS Biol *9*, e1001019.

Trichas, G., Smith, A.M., White, N., Wilkins, V., Watanabe, T., Moore, A., Joyce, B., Sugnaseelan, J., Rodriguez, T.A., Kay, D*., et al.* (2012). Multi-cellular rosettes in the mouse visceral endoderm facilitate the ordered migration of anterior visceral endoderm cells. PLoS Biol *10*, e1001256.

Trichet, L., Le Digabel, J., Hawkins, R.J., Vedula, S.R., Gupta, M., Ribrault, C., Hersen, P., Voituriez, R., and Ladoux, B. (2012). Evidence of a large-scale mechanosensing mechanism for cellular adaptation to substrate stiffness. Proc Natl Acad Sci U S A *109*, 6933-6938.

Turlier, H., and Maitre, J.L. (2015). Mechanics of tissue compaction. Semin Cell Dev Biol *47-48*, 110-117.

Uy, G.D., Downs, K.M., and Gardner, R.L. (2002). Inhibition of trophoblast stem cell potential in chorionic ectoderm coincides with occlusion of the ectoplacental cavity in the mouse. Development *129*, 3913-3924.

Vichas, A., and Zallen, J.A. (2011). Translating cell polarity into tissue elongation. Semin Cell Dev Biol *22*, 858-864.

Vijayakumar, S., Takito, J., Gao, X., Schwartz, G.J., and Al-Awqati, Q. (2006). Differentiation of columnar epithelia: the hensin pathway. J Cell Sci *119*, 4797-4801.

Villasenor, A., Chong, D.C., Henkemeyer, M., and Cleaver, O. (2010). Epithelial dynamics of pancreatic branching morphogenesis. Development *137*, 4295-4305.

Walker, J.L., Menko, A.S., Khalil, S., Rebustini, I., Hoffman, M.P., Kreidberg, J.A., and Kukuruzinska, M.A. (2008). Diverse roles of E-cadherin in the morphogenesis of the submandibular gland: insights into the formation of acinar and ductal structures. Dev Dyn *237*, 3128-3141.

Wang, A.Z., Ojakian, G.K., and Nelson, W.J. (1990). Steps in the morphogenesis of a polarized epithelium. II. Disassembly and assembly of plasma membrane domains during reversal of epithelial cell polarity in multicellular epithelial (MDCK) cysts. J Cell Sci *95 (Pt 1)*, 153-165.

Wang, D., Wang, E., Liu, K., Xia, C.H., Li, S., and Gong, X. (2017a). Roles of TGFbeta and FGF signals during growth and differentiation of mouse lens epithelial cell in vitro. Sci Rep *7*, 7274.

Wang, S., Sekiguchi, R., Daley, W.P., and Yamada, K.M. (2017b). Patterned cell and matrix dynamics in branching morphogenesis. J Cell Biol *216*, 559-570.

Weinstein, M., Yang, X., Li, C., Xu, X., Gotay, J., and Deng, C.X. (1998). Failure of egg cylinder elongation and mesoderm induction in mouse embryos lacking the tumor suppressor smad2. Proc Natl Acad Sci U S A *95*, 9378-9383.

Wells, K.L., Gaete, M., Matalova, E., Deutsch, D., Rice, D., and Tucker, A.S. (2013). Dynamic relationship of the epithelium and mesenchyme during salivary gland initiation: the role of Fgf10. Biol Open *2*, 981-989.

Williams, M., Burdsal, C., Periasamy, A., Lewandoski, M., and Sutherland, A. (2012). Mouse primitive streak forms in situ by initiation of epithelial to mesenchymal transition without migration of a cell population. Dev Dyn *241*, 270-283.

Williams, M., Yen, W., Lu, X., and Sutherland, A. (2014). Distinct apical and basolateral mechanisms drive planar cell polarity-dependent convergent extension of the mouse neural plate. Dev Cell *29*, 34-46.

Xenopoulos, P., Kang, M., and Hadjantonakis, A.K. (2012). Cell lineage allocation within the inner cell mass of the mouse blastocyst. Results Probl Cell Differ *55*, 185-202.

Xu, K., Sacharidou, A., Fu, S., Chong, D.C., Skaug, B., Chen, Z.J., Davis, G.E., and Cleaver, O. (2011). Blood vessel tubulogenesis requires Rasip1 regulation of GTPase signaling. Dev Cell *20*, 526-539.

Yamamoto, H., Flannery, M.L., Kupriyanov, S., Pearce, J., McKercher, S.R., Henkel, G.W., Maki, R.A., Werb, Z., and Oshima, R.G. (1998). Defective trophoblast function in mice with a targeted mutation of Ets2. Genes Dev *12*, 1315-1326.

Yamamoto, M., Saijoh, Y., Perea-Gomez, A., Shawlot, W., Behringer, R.R., Ang, S.L., Hamada, H., and Meno, C. (2004). Nodal antagonists regulate formation of the anteroposterior axis of the mouse embryo. Nature *428*, 387-392.

Yang, W., Klaman, L.D., Chen, B., Araki, T., Harada, H., Thomas, S.M., George, E.L., and Neel, B.G. (2006). An Shp2/SFK/Ras/Erk signaling pathway controls trophoblast stem cell survival. Dev Cell *10*, 317-327.

Yang, Z., Zimmerman, S., Brakeman, P.R., Beaudoin, G.M., 3rd, Reichardt, L.F., and Marciano, D.K. (2013). De novo lumen formation and elongation in the developing nephron: a central role for afadin in apical polarity. Development *140*, 1774-1784.

Yi, J.J., Wang, H., Vilela, M., Danuser, G., and Hahn, K.M. (2014). Manipulation of endogenous kinase activity in living cells using photoswitchable inhibitory peptides. ACS Synth Biol *3*, 788-795.

Zhao, B., Li, L., Lu, Q., Wang, L.H., Liu, C.Y., Lei, Q., and Guan, K.L. (2011). Angiomotin is a novel Hippo pathway component that inhibits YAP oncoprotein. Genes Dev *25*, 51-63.

Zhou, Z., Apte, S.S., Soininen, R., Cao, R., Baaklini, G.Y., Rauser, R.W., Wang, J., Cao, Y., and Tryggvason, K. (2000). Impaired endochondral ossification and angiogenesis in mice deficient in membrane-type matrix metalloproteinase I. Proc Natl Acad Sci U S A *97*, 4052-4057.

Zhu, M., Leung, C.Y., Shahbazi, M.N., and Zernicka-Goetz, M. (2017). Actomyosin polarisation through PLC-PKC triggers symmetry breaking of the mouse embryo. Nat Commun *8*, 921.

Ziomek, C.A., and Johnson, M.H. (1980). Cell surface interaction induces polarization of mouse 8-cell blastomeres at compaction. Cell *21*, 935-942.

7 APPENDIX: ORIGINAL PUBLICATIONS

Harrison, S.E., Sozen, B., Christodoulou, N., Kyprianou, C., and Zernicka-Goetz, M. (2017). Assembly of embryonic and extraembryonic stem cells to mimic embryogenesis in vitro. Science *356*.

Christodoulou, N.C.*, Kyprianou, C.*, Weberling, A., Wang, R., Cui, G.,Peng, G., Jing, N., and Zernicka-Goetz, M. (2018). Sequential formation and resolution of multiple rosettes drives embryo remodelling after implantation. Nat Cell Biol. *In Press.*

*These authors contributed equally